COUPLED FINITE-DISCRETE ELEMENT ANALYSIS OF SOIL-PIPE INTERACTION

By

Masood Meidani

Department of Civil Engineering and Applied Mechanics

McGill University

Montreal, Quebec, Canada

July 2018

A thesis submitted to McGill University in partial fulfillment of the requirements for the degree of Doctor of Philosophy

ABSTRACT

Buried pipes are safe and economical method of transporting natural resources. Failure of these infrastructures poses significant damage to the environment and people safety. Permanent ground deformation is one of the major causes of buried pipe failure. It was reported that axial force on pipes buried in dense granular material obtained using the current guidelines can be significantly smaller than the measured values. Standard finite element methods are known to be efficient in studying soil-structure interaction problems, however, modeling soil-structure interaction involving granular material and large deformation is challenging, particularly at the particle scale level. On the other hand, the discrete element method has proven its capability in capturing the response of granular material at the microscopic scale. However, the method has some limitation in modeling flexible structural elements. Coupling the discrete and finite elements methods is a promising approach that takes advantage of the two methods. In this thesis, the response of buried pipes subject to axial and lateral ground movements are evaluated using three-dimensional discrete and coupled discrete-finite element methods.

The research results have been published in refereed journals and presented in seven chapters that comprises this manuscript-based thesis. The behavior of rigid pipe buried in dense sand under axial ground movement is first evaluated using discrete element method. The input parameters of the model are obtained using a precise calibration procedure and numerical results are validated using experimental data. Results indicated that, for the rigid pipes buried in dense sand, current equations may not properly consider the dilative behavior of the soil and underestimate the soil axial resistance. The numerical approach has proven to be efficient in modeling pipelines subjected to relative soil movement. The created model is then used to conduct a comprehensive parametric study to develop a new expression that estimates the earth pressure coefficient and the soil axial resistance acting on the rigid pipe.

A three-dimensional coupled finite-discrete element framework has been developed and used to investigate the response of a (medium density polyethylene) MDPE pipe under axial and lateral relative ground movements. The pipe is modeled using finite elements while the surrounding soil is modeled using discrete elements. Interface elements are used to transfer forces between these two domains. The response of the soil at microscale level was analyzed and the deformations and strains developing in the MDPE pipe were investigated. Results showed that caution must be considered

when using current methods in the analysis of MDPE pipes. Conclusions and recommendations have been made on the pipe-soil interactions under soil movement.

RESUME

Les tuyaux enterrés sont une méthode sûre et économique de transport des ressources naturelles. La défaillance de ces infrastructures entraîne des dommages importants pour l'environnement et la sécurité des personnes. La déformation permanente du sol est l'une des principales causes de rupture des conduites enterrées. Il a été rapporté que la force axiale sur les tuyaux enfouis dans un matériau granulaire dense obtenu en utilisant les lignes directrices actuelles peut être significativement plus petite que les valeurs mesurées. Les méthodes standard d'éléments finis sont connues pour être efficaces dans l'étude des problèmes d'interaction sol-structure, cependant, la modélisation de l'interaction sol-structure impliquant un matériau granulaire, une grande déformation est difficile, particulièrement au niveau de l'échelle des particules. D'autre part, la méthode des éléments discrets a prouvé sa capacité à capturer la réponse du matériau granulaire à l'échelle microscopique. Cependant, la méthode présente certaines limites dans la modélisation d'éléments structural flexibles. Le couplage des méthodes des éléments discrets et des éléments finis est une approche prometteuse qui tire parti des deux méthodes. Dans cette thèse, la réponse de tuyaux enterrés soumis à des mouvements de terrain axiaux et latéraux est évaluée à l'aide de méthodes d'éléments discrets discrets et couplés-éléments finis couplés.

Les résultats de la recherche ont été publiés dans des revues à comité de lecture et présentés dans sept chapitres qui comprennent cette thèse basée sur un manuscrit. Le comportement des tuyaux rigides enfouis dans du sable dense soumis à un mouvement axial du sol est d'abord évalué à l'aide de la méthode des éléments discrets. Les paramètres d'entrée du modèle sont obtenus en utilisant une procédure d'étalonnage précise et les résultats numériques sont validés en utilisant des données expérimentales. Les résultats indiquent que, pour les tuyaux rigides enfouis dans du sable dense, les équations de courant peuvent ne pas tenir compte du comportement dilutif du sol et sous-estimer la résistance axiale du sol. L'approche numérique s'est révélée efficace dans la modélisation de pipelines soumis à des mouvements de sol relatifs. Le modèle créé est ensuite utilisé pour mener une étude paramétrique complète afin de développer une nouvelle expression qui estime le coefficient de pression de la terre et la résistance axiale du sol agissant sur le tuyau rigide.

Un cadre d'éléments finis-discrets couplés tridimensionnels a été développé et utilisé pour étudier la réponse d'un tube MDPE sous des mouvements de masse axiaux et latéraux relatifs. Le tube est modélisé en utilisant des éléments finis tandis que le sol environnant est modélisé en utilisant des éléments discrets. Les éléments d'interface sont utilisés pour transférer des forces entre ces deux domaines. La réponse du sol à l'échelle microscopique a été analysée et les déformations et déformations se développant dans le tube MDPE ont été étudiées. Les résultats ont montré que des précautions doivent être prises lors de l'utilisation des méthodes actuelles dans l'analyse des tuyaux en MDPE. Des conclusions et des recommandations ont été faites sur les interactions tuyau-sol dans le mouvement du sol.

ACKNOWLEDGMENTS

First, I wish to express my great gratitude to my supervisors Prof. Mohamed Meguid and Prof. Luc Chouinard for their guidance, support and understanding throughout the years. I am truly indebted to both for their motivating enthusiasm and leading me to a stimulating research program.

Special thanks to Dr. Viet Tran for his kind help and advice during this research.

Many thanks to my colleagues in the geotechnical group at McGill University who directly or indirectly have contributed to the accomplishment of this thesis.

Special thanks are due to the Technical Staff of the Department of Civil Engineering and Applied Mechanics at McGill University, notably Dr. Bill Cook and Mr. Jorge Sayat.

I would like to acknowledge the financial support of the McGill Engineering Doctoral Award.

Above all, I would like to express my gratitude to my wife, Kimiya for her love, patience, and encouragement during my studies. I owe deep appreciation and thanks to my parents, Mrs. Vida Eftekhari and Mr. Karim Meidani, and my sister, Mrs. Mina Meidani for their prolonged understanding, support and dedications.

PUBLICATIONS TO DATE

Journal papers

[J1] Meidani, M., Meguid, M.A. and Chouinard L.E. (2017). Evaluation of soil–pipe interaction under relative axial ground movement, ASCE Journal of Pipeline Systems Engineering and Practice, 8(4), 1-10.

[J2] Meidani, M., Meguid, M.A. and Chouinard, L.E. (2018). Estimating earth loads on buried pipes under axial loading condition: insights from 3D discrete element analysis. International Journal of Geo-Engineering, 9(1), 1-20.

[J3] Meidani, M., Meguid, M.A. and Chouinard, L.E. (2018). A finite-discrete element approach for modeling polyethylene pipes subjected to axial ground movement. International Journal of Geotechnical Engineering, 1-13.

[J4] Meidani, M., Meguid, M.A. and Chouinard, L.E. (2018). A finite-discrete element approach for modeling polyethylene pipes subjected to lateral ground movement. Submitted to International Journal of Geomechanics.

Conference papers

[C1] Meidani, M. Chouinard, L.E. and Meguid, M.A. (2016). Finite-discrete element analysis of interface shear damage to HDPE geomembrane in contact with gravel drainage layer. The 7th International Conference on Discrete Element Methods, Dalian, China, 9 pages.

[C2] Meidani, M. Chouinard, L.E. and Meguid, M.A. (2016). A calibration procedure for modeling HDPE geomembrane using discrete element method. GeoVancouver, B.C., Canada, 7 pages.

[C3] Meidani, M. Chouinard, L.E. and Meguid, M.A. (2017). Analyzing HDPE geomembrane wrinkle using a finite-discrete element framework. GeoOttawa, Ottawa, Ontario, Canada, 7 pages.

TABLE OF CONTENTS

LIST OF FIGURES

LIST OF TABLES

Chapter 1. **Introduction**

1.1 Introduction

In the last few decades, buried pipelines have become one of the most economical and safe methods to transport natural resources such as oil, natural gas and water. Failures of these systems can cause significant impact on businesses, environment and can pose safety threats if flammable contents ignite in populated areas.

Failure causes can be related to material corrosion, excavation damage and incorrect operation, however, natural hazardous such as earthquake and landslides are also major contributing factors. One of the major risks to buried pipelines arises from permanent ground deformation (PGD) where soil movement can induce potentially unacceptable high strains and stresses in the pipe. Permanent ground movement might result from creeping ground, landslides, slope instability, and earthquake. The 10th report of the European Gas Pipeline Incident Data Group (2018) has indicated that ground movement represents the fourth major cause of gas pipeline failure in Europe where almost half of them resulted in pipe rupture. Although it is recommended to avoid areas with potential permanent ground movement, sometimes, because of land availability and other environmental constraints, it is unavoidable that major pipelines need to be routed through these areas.

The response of pipes to slope movement depends on the orientation of the pipeline with respect to the moving slope. Figure 1-1 presents an example of two conditions where soil and pipe interact with each other. In the first condition, when the pipe axis is parallel to the direction of the sliding soil, the pipe is subjected to longitudinal (axial) strains and the different sections of the pipe will experience either tensile or compressive stresses. The second condition occurs when the axis of the pipe is normal to the soil movements, the soil applies lateral loads to the pipe resulting in bending moment and shear loads on different sections of the pipe. It should be noted that a pipe subjected to slope movement may experience one or more of the above conditions.

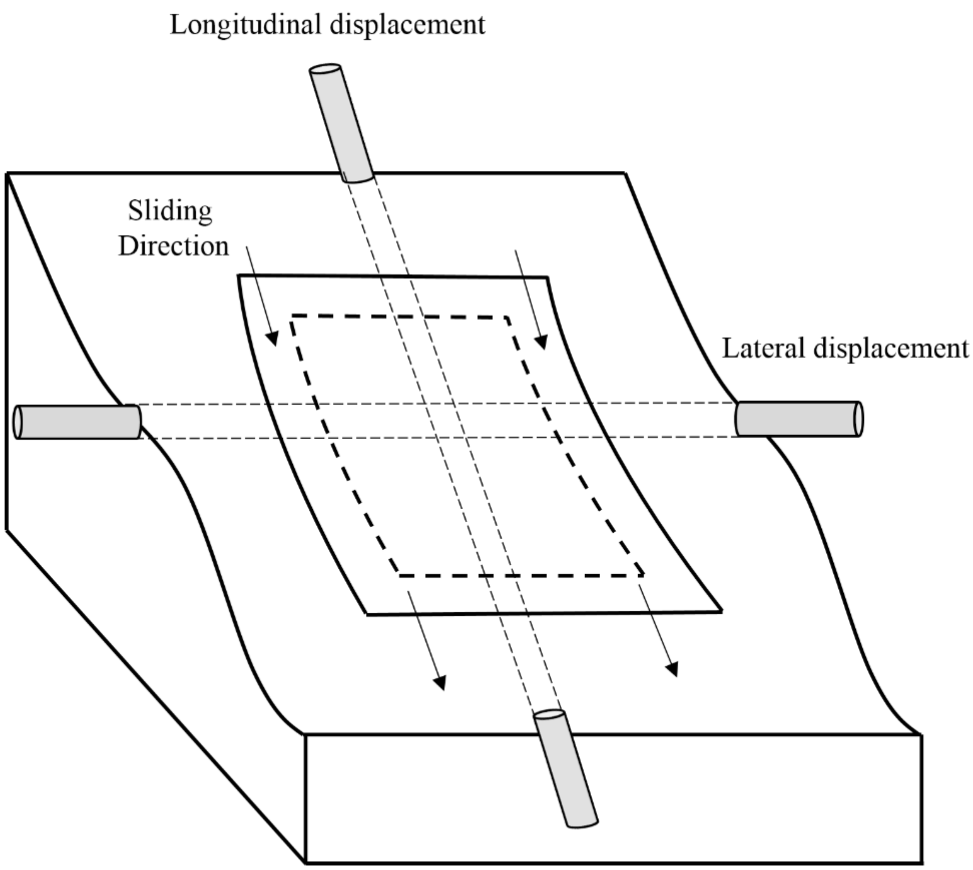

Figure 1-1 Soil load on pipeline passing throw an area subject to land-sliding

Since the early 1960s, researchers have studied soil-pipe interaction using experimental, theoretical, and numerical methods (e.g. Trautmann and O'Rourke, 1983; Honegger and Nyman, 2004; Wijewickreme et al., 2009; Daiyan et al., 2011; Ono et al., 2018). The current equations used to calculate the soil resistance for pipes buried in granular soil subjected to axial or lateral ground movement are the recommendations of guidelines such as ASCE (1984) or ALA (2001). These equations are developed based on simplified assumptions. However, using these equations for all different types of pipes and soils may lead to uncertainty in the calculated response. Karimian (2006) and Weerasekara (2007) showed that the soil axial forces acting on pipes buried in dense sand are much higher than the calculated values using commonly used guidelines equations.

The Finite Element Method (FEM) is powerful in soil-pipe interaction analysis under extreme loading; however, understanding soil-pipe interaction at the particle scale level is a challenging task for FEM. On the other hand, the discrete element method (DEM) has proven as an efficient tool for modeling soil-structure interaction including granular particles and large deformations (Cui and O'Sullivan, 2006; Lobo-Guerrero and Vallejo, 2006). However, there are some limitations in modeling structural elements using DEM. Thus, coupling the finite and discrete element methods is a promising approach to study soil-pipe interaction problems that involve large soil deformation and allowing for the response to be evaluated at the microscale level.

1.2 Research Motivation

Karimian (2006) and Weerasekara (2007) reported that the current recommendations in guidelines for calculating soil load on buried pipes in dense sand under axial ground movement have some limitations and they may underestimate the soil resistance. In addition, these equations are generally developed for rigid pipes (ALA, 2001), and the available equations for flexible pipe systems are very limited. This uncertainty is more significant for pipes under lateral soil movement as different equations are used to calculate the lateral forces on these pipes (Audibert and Nymann, 1977; Rowe and Davis, 1982; Trautmann and O'Rourke, 1983; Hsu, 1994; PRCI, 2004). Thus, more studies are mandatory to expand the knowledge in this area.

Furthermore, most of the coupling of FEM and DEM were initially performed to solve dynamic problems (Han et al., 2002; Dhia and Rateau, 2005; Bhuvaraghan et al., 2010) and their application in solving geotechnical engineering problems are limited. Fakhimi (2009) developed a coupled framework to simulate triaxial test. Villard et al. (2009) used coupled FE-DE analysis to study geosynthetic-reinforced earth structures, however, the analysis was not validated using experimental data. A new coupled framework was developed at McGill University by Dang and Meguid (2013) for quasi-static nonlinear soil-structure interaction problems. Tran et al. (2013) extended the application of the framework to study the performance of geogrid-soil interaction under pullout loading condition. Ahmed et al. (2015) conducted a research on the role of geogrid reinforcement in reducing earth pressure on buried pipes using the same coupled framework.

The aim of this study is to extend the application of the coupled FE-DE framework to investigate soil-pipe interaction to better understand the three-dimensional (3D) interaction of dense granular soil and buried pipelines under permanent ground deformation.

1.3 Objective and Scope

The proposed research is aimed at two major objectives. The first objective is extending the application of the coupled framework by performing a detailed calibration and validation procedures. The second objective is understanding the three-dimensional (3D) interaction of soil and buried pipelines under different permanent ground deformations. The specific objectives of the current study are:

1. Developing a coupled Finite-Discrete element model that is suitable for investigating soil-pipe interaction considering large deformation and establishing a calibration procedure using triaxial and direct shear test results.

2. Validating the coupled FE-DE model by comparing the analysis results with experimental data.

3. Using the discrete element method to understand the load transfer mechanism and the interaction of a steel pipe buried in granular sand subjected to axial ground movement.

4. Reviewing the different factors affecting soil-pipe interaction and evaluating the validity of the existing methods used to design buried pipes under permanent ground movement and developing a new equation to calculate the axial soil load on rigid pipes buried in dense sand.

5. Performing a series of 3D analysis using the proposed Finite-Discrete element method to simulate flexible pipe buried in dense sand under axial soil movement and comparing the behavior with rigid pipes.

6. Analysing the response of flexible pipes buried in dense sand and subjected to lateral soil movement using the coupled Finite-Discrete element framework.

1.4 Contribution of Authors

Papers J1, J2, J3, J4, C1, C2 and C3 given in the publication list are included in the thesis. All papers are the candidate's original work.

The coupled Finite-Discrete element framework employed in the thesis is a continuation of the original work of Dang and Meguid (2010, 2013) and Tran et al. (2013, 2014). Dang developed the framework and used it to analyse tunneling process. Tran updated the framework by moving the original finite element engines into a new version of the open source discrete element code *YADE* (Smilauer, V. et al. 2010) and performed a numerical pullout test on biaxial geogrid embedded in granular material. The author extended the application of the developed framework by performing lateral and axial pullout tests on rigid and flexible pipes buried in dense sand. Some parts of the original codes were modified by the author in order to make them compatible with the new model. Bugs detected from the original framework have been fixed. The model is precisely calibrated using two different laboratory tests and the results of the simulations are validated with experimental data. The author has evaluated the outcome of the simulations with the current guidelines and a new equation has been developed by the author to calculate axial soil load on rigid pipes under axial ground movement.

All the formulation, program coding, and the preparation of the manuscripts were completed by the candidate, under the supervision of Prof. Mohamed Meguid and Prof. Luc Chouinard, his thesis supervisors.

1.5 Thesis Organization

This thesis consists of eight chapters and three appendices. The chapters essentially reflect the order in which the research was carried out and presented below:

Chapter 1: Is the introduction chapter, which provides an overview on the thesis.

Chapter 2: In this chapter, a literature review on the soil-pipe interaction problems are presented with emphasis on buried pipes subject to axial and lateral ground movement. The chapter includes findings from previous studies in terms of both experiment and numerical modeling. Furthermore, a literature review on modeling soil-structure interaction problems including granular material and large deformation with a focus on coupling the finite and discrete element methods are presented in this section.

Chapter 3: This chapter is a modified version of the first journal paper (J1). The performance of a rigid steel pipe buried in dense granular sand subjected to soil axial movement was evaluated using a discrete element method. The input parameters of the model are obtained using a calibration procedure by modeling triaxial and direct shear tests and comparing the results with laboratory tests data. The model is validated by comparing the value of normal soil pressure acting on the pipe with analytical solutions. The pipe pullout force and the pipe the axial soil resistance acting on the pipe was compared with the available methods.

Chapter 4: Considering the outcome of the previous chapter, a parametric study was conducted to develop a new equation to calculate the maximum soil axial force on rigid pipes buried in dense sand. The main influential parameters were identified, and numbers of simulations were performed to evaluate the effect of each parameter. The accuracy of the proposed equation has been evaluated by comparing the calculated values with experimental results and other numerical solutions. The chapter presents the work carried out in paper J2 given in the publication list.

Chapter 5: In this chapter, the focus has been made on flexible pipe. The coupled FE-DE framework was employed to develop a model of an MDPE pipe buried in dense sand. The axial pullout force then applied to the pipe. The results of the numerical simulation were validated by comparing with experimental data. The deformations, strains and stresses in the pipe were captured during the pullout process and the results are compared with available guidelines. In addition, displacements, contact force network and orientations within the soil domain are also analyzed. It is found that the assumptions have been made in the guidelines are not valid for flexible pipes and more investigations are needed in this area. The chapter is a version of paper J3 in the publication list.

Chapter 6: The response of flexible pipe buried in dense sand under lateral soil movement was evaluated in this chapter. The developed coupled framework was used for the numerical simulation. The pipe under lateral ground movement is molded by applying the lateral pullout force on both ends of the pipes. The results of the simulation are compared with experimental data. It was found that the sections of the pipe located around the middle zone of the unstable soil are carrying the soil load by pure bending moment. This outcome was obtained by capturing the axial displacement and strain within the pipe length. The displacement field and contact force network within the soil domain supported the results for the pipe response. The chapter is presenting paper J4 in the publication list.

Chapter 7: This chapter includes a summary and conclusion of this research. Some recommendations are presented in this section followed by suggestions for future studies in this area.

Appendices: Three conference papers published by the author using the developed framework are presented in the appendices and they are briefly explained below:

Appendix A: In this paper, an analysis of interface shear damage to HDPE geomembrane in contact with gravel drainage layer are conducted using the coupled FE-DE framework. The geomembrane sheet is placed between a sand layer as a foundation and a gravel drainage layer. Then the geomembrane is pulled out and the displacements, strains and stresses within the geomembrane are captured. Results show that shear displacement developing between the drainage layer and the geomembrane should be considered in the design of landfill barrier system. A version of this study was published in the 7th International Conference on Discrete Element Methods in Dalian, China.

Appendix B: This paper was presented at the GeoVancouver 2017 conference. In this paper, a new procedure to calibrate a discrete element model of an HDPE geomembrane using spherical particles is presented. A constitutive model that considers particle normal and shear cohesion is used. Standard index tests used to measure the properties of HDPE geomembrane including tensile and puncture tests are applied to validate the model developed.

Appendix C: A study on analyzing HDPE geomembrane wrinkle overlying sand subgrade using a finite-discrete element framework is presented in this section. The geomembrane is modeled using finite elements (FE) whereas the drainage layer and the foundation soil are modeled using discrete elements (DE). The effects of the subgrade properties and overburden pressure on the wrinkle deformation are investigated. Results show that the presence of wrinkle increases the local strains in the geomembrane right next to the deformed wrinkle. A version of this research is presented in the GeoOttawa2018 conference.

Chapter 2. **Literature Review**

A comprehensive literature review has been conducted and summarized in this chapter. First, previous studies on pipelines subjected to permanent ground movement are presented covering the analytical, experimental and numerical methods. Furthermore, current guidelines recommendations to calculate the maximum axial and lateral soil force on buried pipes are presented. At the end, literature related to numerical methods for modeling soil-structure problems using finite element and discrete element methods in addition to the techniques used for coupling these two methods are summarized.

2.1 Response of Buried Pipes Subject to Ground Movement

Since the early 1960s, researchers have studied soil-pipe interaction to understand the behavior of buried pipelines subject to permanent ground movements. These studies consist of field or laboratory tests which include full-scale pipe pullout or centrifuge tests. In addition to experimental results, several numerical and analytical studies have been done to determine the response of buried pipes subjected to lateral or axial ground movements. Although soil-pipe interaction mechanisms have been investigated now for about half a century, these studies involved several simplifying assumptions and limitations. Some of the assumptions and limitations are listed in Table 2-1. A comprehensive literature review was performed relative to soil-pipe interaction and a summary of these studies are presented in Table 2-2.

Table 2-1 Prevalent assumptions and limitation in studies of soil-pipe interaction

Type of study	Simplifying assumptions and limitations
Analytical solutions	Simplified stress-strain behavior of soil (linear- spring elements). Assuming a constant pipe curvature near the area where abrupt ground displacements develop. Limitation of bending theory (beams on elastic foundations) to model the pipe deformation under lateral force.

Experimental investigations	Limitation of pipe length: pipe has to be long enough to allow for the development of axial strains in scale model. Boundary conditions: rigid boundaries have to be located far enough from the monitored section to minimize effects on measurements.
Numerical analysis	Assuming 2D or plain stress condition to simplify the problem. The challenge associated with modeling large soil movements using FEM. Modeling structural elements using particles in DEM method.

Table 2-2 Selected soil-pipe interactions studies

Author and year	Type of study	Application	Notes
Honegger and Nyman (2004)	Guideline	Guideline for seismic design of pipelines	Proposing lateral interaction factor
ASCE (1984)	Guideline	Guidelines for the Seismic Design of Oil and Gas Pipeline systems	-
American Lifelines Alliance. (2001)	Guideline	Buried steel pipe	-
Newmark and Hall (1975)	Analytical	Pipeline seismic design	Considering the effect of fault displacement
O'Rourke and Nordberg (1992)	Analytical	Buried pipelines	Pipe subjected to longitudinal soil movements
Rajani et al. (1996)	Analytical	Pipeline	-
Chan and Wong (2004)	Analytical	Buried steel pipe in slope	Validating the result with a case study
Cocchetti et al. (2009)	Analytical	Buried pipe in slopes	Three-dimensional approach
Audibert and Nyman (1977)	Experimental	Buried steel pipe	Loose and dense sand, Lateral displacement of soil
Trautmann and O'Rourke (1983)	Experimental	Buried steel pipe	Pullout test, Lateral and uplift loading

Hsu (1994)	Experimental	Pipeline	Loading rate effect, Lateral loading
Paulin et al. (1998)	Centrifuge test (C-CORE)	Buried steel pipe	Pullout test on large diameter pipes
Konuk et al. (1999)	Centrifuge test (C-CORE)	Buried pipe	Dense sand, Lateral loading
Turner (2004)	Experimental	Buried pipe	Lateral displacement
Almahakeri and Moore (2013)	Experimental	Buried steel pipe	Flexural behavior of the pipe with respect to lateral earth loading
Hsu et al. (2001)	Experimental	Buried pipe	Dense sand, oblique movement of soil
Phillips et al. (2004)	Centrifuge test (C-CORE)	Buried pipe	Clay, Lateral-axial soil movement
Karimian (2006)	Experimental	Buried steel pipe	Sand, Lateral and axial displacement
Weerasekara and Wijewickreme (2010)	Experimental	Buried plastic pipeline	Lateral and axial soil loading
Daiyan and Kenny (2011)	Centrifuge test	Buried pipe	Dense sand, Axial-lateral relative movement
Rizkalla et al. (1991)	Field test	Buried steel pipe	Longitudinal restraint test
Cappelletto et al. (1998)	Field test	Buried steel pipe	Longitudinal restraint test
Bilgin et al. (2007)	Field test	Buried cast iron pipe	Dense and loose sand, Pullout test
Yimsiri et al. (2004)	FEM	Buried pipe	Sand, Lateral and upward soil resistances
Guo and Stolle (2005)	FEM (ABAQUS)	Buried pipe	Lateral soil resistance
Karimian (2006)	FLAC2D	Buried steel pipe	2D modeling, lateral displacement
Daiyan and kenny (2011)	FEM (ABAQUS)	Buried pipe	Dense sand, Lateral-axial soil-pipe interaction
Kunert et al. (2012)	FEM	Buried pipe	Axial soil movements

2.1.1 Analytical methods

Early analytical studies to calculate axial and lateral soil loads on buried pipes were developed as an extension of studies on vertical anchors and retaining walls. One of the first analytical solutions was developed by Hansen (1961) for buried vertical anchors. Straight failure surfaces that extended to the ground surface were assumed. Ovesen (1964) performed several pullout tests on vertical anchors at intermediate burial depths. An analytical solution for vertical anchor plates was derived by assuming upward movement of the anchor plate. The difference between these studies is that Hansen (1961) restrained the vertical movement of the anchor whereas Ovesen (1964) considered the anchor to be free to move vertically.

The current approach to determine axial loads on pipes buried in cohesionless soils is presented in Eq. 2-1. This equation is developed by calculating average effective normal stress acting along the interface between the pipe and soil (Figure 2-1).

$$F_A = \gamma' \times H \times \left(\frac{1 + K_0}{2}\right) \times \tan(\delta) \times (\pi\, D\, L) \qquad 2-1$$

where F_A is the ultimate axial soil load, γ' is unit weight of soil, H is the pipe burial depth, D is pipe diameter, K_0 is the lateral earth pressure coefficient at rest and δ is the interface friction angle between the pipe and the soil. Value of the interface friction angle (δ) is a function of the pipe material and soil type. Research such as Kullhawy et al. (1983), Trautmann and O'Rourke (1983) and Leach and Row (1991) proposed tables for δ value for a variety of materails.

The assumptions in this equation are as follows:

1. The soil around the pipe remains at rest even after shear displacements occur at the soil-pipe interface.

2. The distribution of normal stresses on the pipe assumes that the pipe is rigid.

3. The axial soil resistance per-unit length of the pipe is constant along its length.

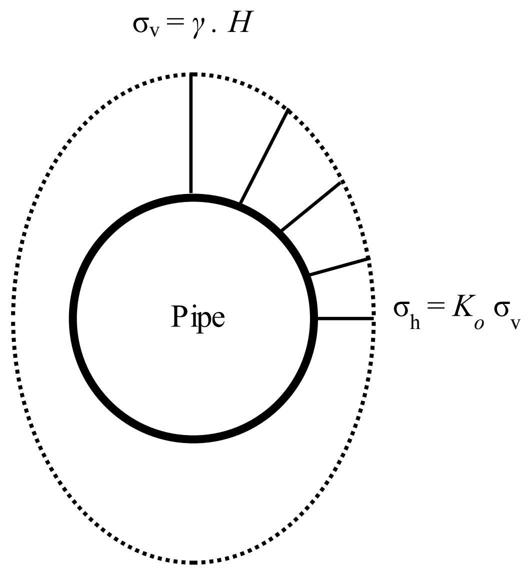

Figure 2-1 Assumption of normal stress distribution pattern around the pipe

Eq.2-1 has been recommended by the American Society of Civil Engineering (ASCE, 1984) "Guidelines for the Seismic Design of Oil and Gas Pipeline Systems", Honegger and Nyman (2004) "Guidelines for the Seismic Design and Assessment of Natural Gas and Liquid Hydrocarbons Pipelines (PRCI, 2004)" and American Lifeline Alliance (ALA, 2001) "Guidelines for the Design of Buried Steel Pipe" for the computation of ultimate soil resistance per unit length of the rigid pipe buried in sand under longitudinal ground movement. There are other equations which have been proposed in guidelines and handbooks such as Danish Submarine Pipeline Guidelines (1985) and McAllister (2001) to calculate the maximum axial soil loads on pipes. Weerasekara and Wijewickremre (2008) proposed a new closed-form solution to calculate the soil force on polyethylene gas pipelines subject to relative axial displacements. Their solution can estimate the pipe response (strain and stress) and the mobilized frictional length along the pipe.

Another group of analytical solutions focusses on pipes laid on slopes. Chan and Wong (2004) presented modified solutions for the design of pipelines subjected to a two-dimensional shallow, deep-seated, planar or nonplanar slip. Their solution allows one to assess if the pipeline yields at the critical locations of the slip. Proposed equations are validated using a case study. Also, Cocchetti et al. (2009) conducted a theoretical study to investigate pipe-soil interaction along unstable slopes.

The initial analytical models that were developed to estimate the lateral soil loads on pipe buried in granular soil are based on studies and experiments conducted on vertical anchor plates by Hansen (1961) and Ovesen (1964). The common equation used to calculate the ultimate lateral soil load on a buried pipe in granular soil can be expressed as follows:

$$P_u = \gamma \times H \times N_{qh} \times D \qquad 2-2$$

where P_u is the peak soil lateral resistance; H is pipe burial depth; D is diameter of pipe and N_{qh} is a dimensionless force factor. It is noted that N_{qh} is a function of *H/D* ratio and soil friction angle. There are different charts proposed by researchers to obtain this value. Audibert and Nyman (1977) performed experiments on steel pipes buried in both loose and dense sand. They concluded that lateral soil resistances obtained from pullout tests are in good agreement with the analytical solution proposed by Hansen (1961) and proposed the N_{qh} values presented in Figure 2-2. Trautmann and O'Rourke (1985) conducted a series of lateral pullout tests on steel pipes with different diameters and *H/D* ratios. They observed that lateral soil resistances were in good agreement with Ovesen (1964) results and developed a chart to estimate the N_{qh} values as presented in Figure 2-3.

The equation used to determine the ultimate soil load on laterally loaded pipe in granular soil is the one presented in Eq. 2-2. The chart for N_{qh} in ASCE (1984) guideline is based on the study of Trautmann and O'Rourke (1985), however, The American Lifeline Alliance (ALA, 2001) recommended the chart of Hansen (1961) to estimate N_{qh} value. The main assumption made in early analytical methods for analyzing pipes under lateral loading is that the pipe carries the entire soil load by bending. This assumption might be valid for pipes with relatively small deformation. However, studies such as Karamitros et al. (2006) and Weerasekara and Wijewickreme (2010) showed that pipes with higher allowable strain capacity resist soil load by combination of tension (axial capacity) and bending.

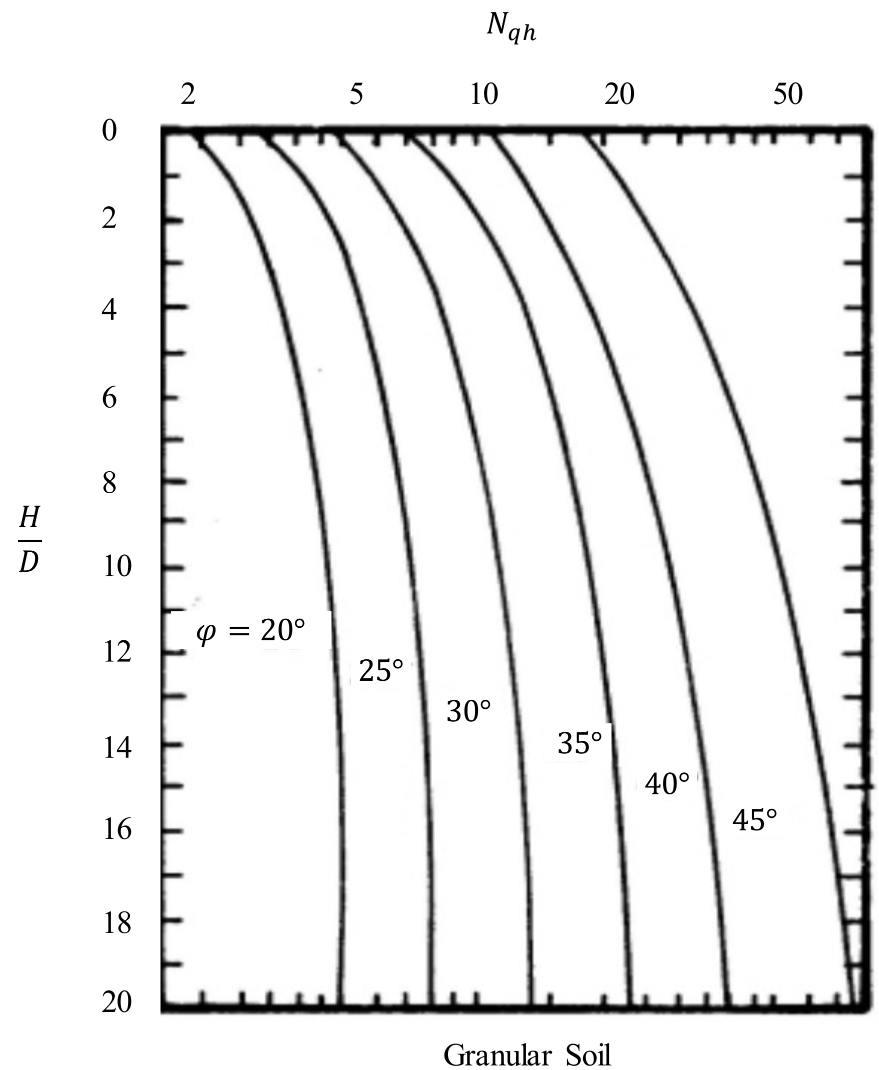

Figure 2-2 Value of N_{qh} reported by Audibert and Nyman (1977) based on Hansen (1961)

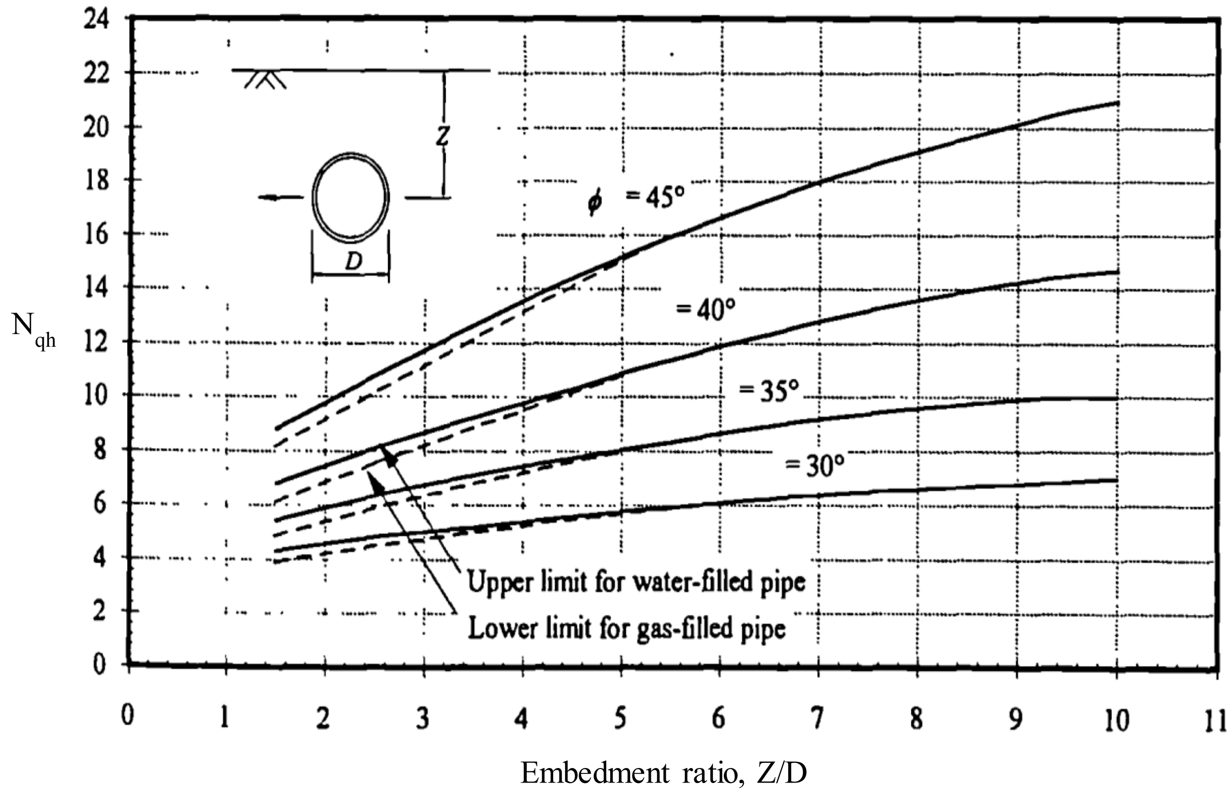

Figure 2-3 Value of N_{qh} reported by Trautmann and O'Rourke (1985) based on Ovesen (1964)

2.1.2 Experimental investigations

As mentioned in the previous section, the early approaches to determine the soil resistance were mainly based on studies and experiments conducted on vertical anchor plates (Hansen, 1961 and Ovesen, 1964). Audibert and Nyman (1977) and Trautmann and O'Rourke (1985) performed series of experiments and developed charts for N_{qh} value. Several laboratory-scale pullout tests have been conducted, for example, Hsu (1993) investigated the effect of rate of loading on lateral soil resistance. Several other studies were conducted at the Centre for Cold Ocean Resources Engineering (C-CORE). Paulin et al. (1998) conducted 24 large-scale tests on steel pipes including different types of soil movement (upward, lateral, downward and axial). The results of two large-scale tests to assess the bending behavior of buried pipes in dense sand during lateral loading were reported by Konuk et al. (1999).

Cappelletto (1998) performed a series of field tests on steel pipes buried in cohesive soil with different diameters. It was indicated that for pipes under low rate of axial ground movement, using an effective stress model to predict axial soil loads on pipes gives more reasonable results in comparison to the one suggested for cohesive soil.

Hsu et al. (2001) presented an experimental study involving pipe movement in dense sand. Pipes with different diameters were pulled out from a large box from an axial to a lateral direction. It was observed that for pipes under oblique movement, the axial soil restraint decreases, whereas the lateral soil restraint increases with increasing oblique angle. Furthermore, the components of the soil restraint can be calculated by multiplying the corresponding cosine and sine values of the movement angle with the associated axial and lateral soil restraints respectively.

Turner (2004) conducted lateral pullout tests on pipes buried in moist sand and concluded that moisture content has only a small effect on lateral soil resistance. However, a correction has been made to N_{qh} curves and presented by Trautmann and O'Rourke (1985) for sandy soil with moisture content of 10%.

Full-scale experiments have been conducted at the University of British Columbia (UBC) on pipes buried in granular soil. Karimian (2006) performed large scale axial pullout tests on a relatively large-diameter rigid steel pipe embedded in loose or dense sands. It was observed that axial soil restraint for pipes buried in loose sand is in agreement with the ASCE (1984) and ALA (2001) estimations, however, soil restraint for pipes buried in dense sand is significantly higher. Weerasekara and Wijewickreme (2010) conducted a series of experimental tests to study the response of plastic pipes buried in sand to lateral and axial soil loading. An analytical method was developed to estimate pipe performance during different types of ground movement.

Daiyan et al. (2011) performed a set of centrifuge tests on rigid pipes buried in dense sand to determine the axial, lateral and oblique interaction of the pipe-soil systems. The experimental results were used to calibrate a three-dimensional finite element model. Two different failure mechanisms were observed for axial-lateral soil-pipe interaction, which supports the failure criterion suggested by Phillips et al. (2004).

Almahakery et al. (2013a) conducted a series of full-scale bending experiments on a pipe made of glass fiber-reinforced polymers (GFRP) at different depth to diameter ratio. The deflection of the pipe, failure modes and the effect of laminate structure of the pipe were investigated. It was found that the deflection of the GFRP pipe at the peak load is 4-7 times larger than those of the equivalent steel pipes. Furthermore, Almahakery et al. (2013b) performed a series of pipe bending experiments on long steel pipes buried in dense sand at three different burial depth-to-diameter ratios. Strains and deflections along the pipes at various burial depths were measured and the shapes of deflected pipes were captured.

Jung et al. (2016) performed a large-scale test to evaluate the soil reaction to pipe lateral and upward movement in dry and partially saturated sand. The results of the experiment were used to validate a finite-element model. The numerical model was then employed to capture the force-displacement curve of the pipe under lateral, vertical upward, vertical downward and oblique orientations and the results were compared with conventional equations.

Recently, Ono et al. (2018) performed lateral loading experiments on a model pipe buried in saturated sand at different effective stresses. It was observed that the captured force-displacement patterns are in good agreement with hyperbolic curves and the bearing capacity factors (N_{qh}) obtained from the peak lateral force were in good agreement with the theoretical results (Trautmann and O'Rourke, 1985).

2.1.3 Numerical studies

Early numerical studies on soil-pipe interaction started in the 1980's. Rowe and Davis (1982) conducted a finite-element analysis on the behaviour of anchor plates buried in granular soil. A parametric study was performed and the effects of different parameters such as burial depth, dilation angle and the plate surface roughness on the anchor's capacity were evaluated. A series of charts were also presented to estimate the capacity of vertical anchors for different burial depths as presented in Figure 2-4. These charts could be used to determine the ultimate soil pressure on laterally loaded pipes.

Yimsiri et al. (2004) performed finite element analyses to study soil-pipe interaction under lateral and upward soil movements at deep burial conditions. A series of chart were proposed to predict the horizontal bearing capacity of the soil to buried pipes in deep embedment. Guo and Stolle (2005) conducted a numerical analysis using ABAQUS to explain the significantly different values obtained for lateral soil resistance by different researchers. They investigated the effects of burial depth, overburden ratio, soil dilatancy, strain hardening and scale effect in their research. It was concluded that soil loads on pipe are not only function of soil and pipe properties, but test procedure affects these values.

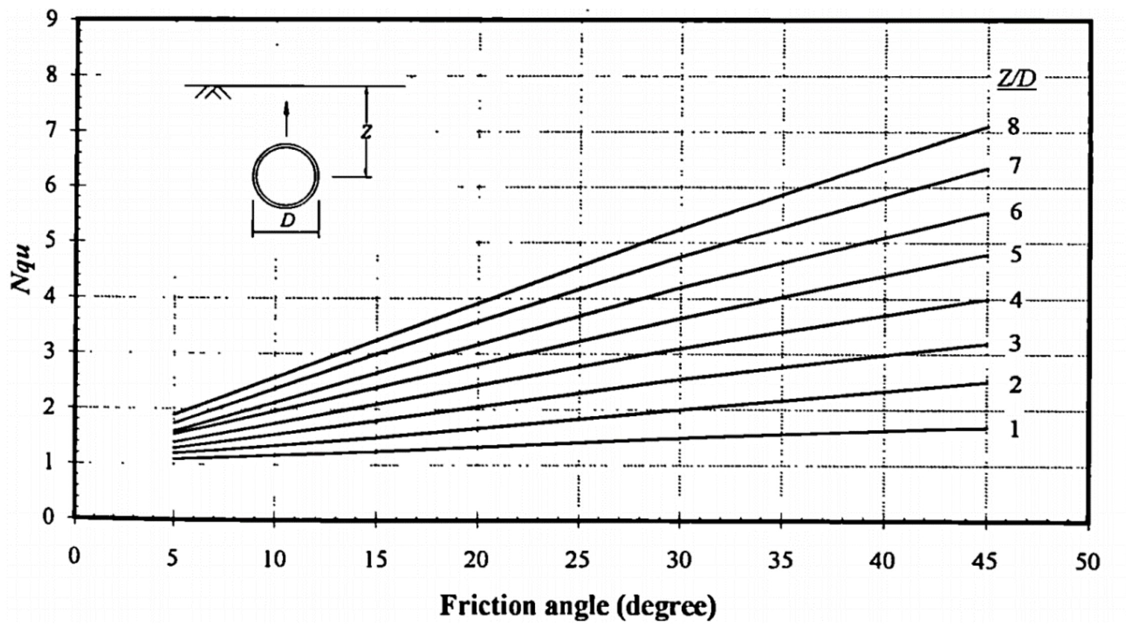

Figure 2-4 Value of N_{qh} factor reported by Rowe and Davis (1982)

Karimian (2006) conducted 2D numerical modeling using FLAC2D (Itasca 2002) to investigate the axial and lateral pullout behavior of a pipe buried in sand and the results supported the conclusions made by Guo and Stolle (2005). It was observed that the value of peak axial pullout force for pipe buried in dense sand is much higher than the recommended value which can be attributed to the dilative behavior of the dense sand during interface shear deformations.

Daiyan et al. (2011) developed an interaction curve for axial-lateral soil-pipe interaction in dense sand using finite element analysis. The interaction curve can be used to define the spring properties for use in conventional finite element procedure. Kunert et al. (2012) proposed a nonlinear finite element technique to assess the behavior of pipelines buried in rainforest regions, which are prone to failures by axial stresses from land movement. Roy et al. (2016) conducted a series of finite element analysis on pipelines buried in dense sand subjected to lateral soil movement. The simulation was performed under plain strain condition and the modified Mohr-Coulomb (MMC) model was used considering several important soil parameters such as friction and dilation angles within the developed range of plastic shear strain. It was found that mobilized friction and dilation angle are not constant along the failure surface which is developing progressively with lateral displacement of the pipe.

Almahakeri et al. (2016) conducted series of 3D finite-element simulations to examine the longitudinal bending in buried glass fiber reinforced polymers (GFRP) pipes subjected to lateral earth movements. Numerical models were validated using measured data and the performance of the GFRP pipe was compared to a steel pipe.

Zhang et al. (2016) investigated the mechanical behavior of buried steel pipeline crossing landslide area by finite element method. Effects of soil parameters, pipeline parameters and landslide scale on the pipe behavior were discussed. Naeini et al. (2016) developed a finite element model to investigate the response of buried HDPE pipeline to fault movements. The numerical results were validated with experimental data and compared with ASCE estimations. In addition, parametric study has been conducted to evaluate the influence of pipe diameter, buried depth and the surrounding soil friction angle and density on the ultimate bending strain and stress along the pipe length. It was found that the calculated maximum bending strains from the ASCE Guidelines are larger than those obtained using numerical simulation.

2.2 Soil-Structure Interaction Modeling Using the Discrete Element Method

Numerical methods such as finite element (FE), finite difference (FD) and discrete element (DE) are effective tools to study soil-structure interaction in different geotechnical engineering problems. In this section, a literature review has been made to summarize studies that employed discrete element method.

Finite element method has been widely used to simulate soil-pipe interaction problems (Section 2.1.3). One of the reported challenges in numerical simulation using conventional continuum approaches is related to modeling the soil-pipe interaction under large deformation and tracking particle movements in the close vicinity of the pipe (Guo and Stolle, 2005). Although soil-structure interaction with large deformation can be modeled using multiscale approach (Hughes, 1995) or adaptive remeshing (Zienkiewicz and Huang, 1990), considering particle discontinuity, capturing their response at the microscale level and tracking particle movement around the pipe did not receive much research attention in the literature.

As an alternative to continuum approaches, the discrete element method (DEM) has been used to model granular material under large deformation. The method was first proposed by Cundall and Strack (1979) and has been used to analyze geotechnical engineering problems.

Laboratory tests have been modeled using DEM to investigate the microscopic behavior of soil samples. Cui and O'Sullivan (2006) used DEM to evaluate the behavior of granular soil sample in a direct shear test at both the macroscopic and microscopic levels. Triaxial tests on granular sand have been modeled using DEM by Cui et al. (2007) and Belheine et al. (2009). Kozicki et al. (2014) conducted three-dimensional simulations of a triaxial test on sand and the effect of initial void ratio, particles shape, mean grain size and the stiffness of the boundaries were evaluated. Asadzade and Soroush (2017) investigated the macro and micro mechanical properties of a soil sample under cyclic simple shear test using 3D-DEM. Discussion has been made on the cyclic behavior, principle stress rotation and fabric anisotropy inside the sample. Validating the results of the above studies with experimental data showed the capability of the DEM method in modeling laboratory tests.

Soil-structure interaction problems have been also studies using DEM. Villard and Chareyre (2004) employed 2D discrete element method to simulate geosynthetic sheets anchored in trenches. The geosynthetics were modeled using "dynamic spar elements" while the surrounding soil was modeled by using disk elements. The new contact laws between geosynthetic elements and soil particles were suggested to model their interaction. Pullout force in different anchorage configuration as well as deformation and failure mechanism of the system were evaluated.

Lobo-Guerrero and Vallejo (2005) conducted 2D DEM simulation on the penetration resistance of driven piles in crushable sand. Breakable DE particles were employed to simulate particle crushing around the pile. Gabrieli et al. (2009) used DEM method to reproduce a physical model of a foundation on a sandy slope. Simplified spherical particles of the same porosity and particle size distribution were used to generate the DEM model. The model was calibrated based on the results of standard compression tests. The results showed acceptable performance of the DEM simulation in generating experiment results. Furthermore, parametric studies have been made to investigate the influence of soil properties and loading direction on the results.

Tran and Meguid (2014) conducted a 3D discrete element analysis and experimental investigation of the earth pressure distribution on cylindrical shafts. A new DEM sample generation method was proposed, and the soil sample was calibrated using the results of simulated direct shear tests. The results of the DE analysis were found to be in good agreement with experimental data and showed the efficiency of DEM in simulating soil-structure problems including granular soil with large displacement.

Macaro et al. (2015) used DEM method to analyze pipe-soil interaction for offshore pipelines on sand. Spherical particles were used to model the sand material. The pipe was modeled by using circular cylinder with the same contact law was considered for sphere-sphere and sphere-cylinder interaction. The numerical model was validated using experimental data, and the effect of the relative soil density and pipe roughness were investigated.

Wang et al. (2016) performed a 2D discrete element simulation on geogrid-soil interaction under pullout load. Granular soil was modeled using unbonded particles while the geogrid was modeled using bonded particles. The numerical direct shear and tensile tests were conducted to determine the micro input parameters of soil and geogrid in the DEM model. The validation has been made by comparing the analysis results with corresponding experimental data. Recently, Jing et al. (2018) investigated the macro and micro shear behavior of soil-structure interface using three-dimensional discrete element program.

2.3 Discrete Element Analysis

The discrete element method generally considers the interaction between particles in a dynamic process. Following contact detection between two particles, the contact forces are calculated, and the rotational and transitional accelerations are obtained using Newton’s second law of motion. The accelerations are integrated numerically over a defined time step and particle velocities and new positions are determined. This process is continued until static equilibrium condition is reached. Energy dissipation during particle collision and interaction is considered using damping coefficients for both forces and moments.

2.3.1 Contact law

The discrete element analysis in this study is performed using the open source code YADE (Kozichi and Donze, 2008, Smilauer et al., 2010). The contact law between particles is selected such that it includes the traditional Cundall's linear elastic-plastic law plus transmission of moments between particles. The contact law is briefly described below:

The microscopic parameters in this contact law involve elastic (E_{micro},K_T/K_N, β_r) as well as rupture parameters (φ_{micro} and η_r). Where, E_{micro} is the particle modulus; K_N and K_T are the normal and tangential stiffnesses at the contact point; β_r is the rolling resistance coefficient; φ_{micro} is the microscopic friction angle between particles, and η_r is a dimensionless coefficient to define a threshold for the resistant moment. It should be noted that the modulus (E_{micro}) and friction angle (φ_{micro}) are particle microscale parameters, which differ from the Young's modulus and friction angle of the soil domain.

Following the collision of two particles A and B with radii r_A and r_B, contact penetration depth is defined as:

$$\Delta = r_A + r_B - d_0 \qquad 2-3$$

where, d_0 is the distance between the centers of particles A and B.

Particle interaction is represented by the force vector F. This vector can be decomposed into normal and tangential forces:

$$F_N = K_N \,.\, \Delta_N \,, \quad \delta F_T = -K_T \,.\, \delta \Delta_T \qquad 2-4$$

where, F_N is the normal force; δF_T is the incremental tangential force; K_N and K_T are the normal and tangential stiffnesses at the contact point; Δ_N is the normal penetration between the particles and $\delta \Delta_T$ is the incremental tangential displacement between the two particles (Figure 2-5).

The normal stiffness between particles A and B at the contact point is defined by

$$K_N = \frac{K_N^A \,.\, K_N^B}{K_N^A + K_N^B} \qquad 2-5$$

where, K_N^A and K_N^B are the particles normal stiffnessess calculated using particle radius r and material modulus E as follows:

$$K_N^A = 2E_A r_A \qquad and \qquad K_N^B = 2E_B r_B \qquad 2-6$$

Therefore, the normal stiffness at the contact point can be written as:

$$K_N = \frac{2E_A r_A \,.\, 2E_B r_B}{2E_A r_A + 2E_B r_B} \qquad 2-7$$

The interaction tangential stiffness K_T is defined as a ratio of the computed K_N such that $K_T = \alpha\, K_N$.

The tangential force is limited by a threshold value expressed as:

$$F_T = \frac{F_T}{\|F_T\|}\ \|F_N\|.\tan(\varphi_{micro}) \quad if \quad F_T \geq \|F_N\|.\tan(\varphi_{micro}) \qquad 2-8$$

where, φ_{micro} is the microscopic friction angle between particles.

The rolling resistance is determined using a rolling angular vector θ_r obtained by summing the components of the incremental rolling (Smilauer et al., 2010)

$$\theta_r = \sum d\,\theta_r \qquad 2-9$$

A resistant moment M_r is calculated by:

$$M_r = K_r \,.\, \theta_r \qquad 2-10$$

where K_r is the rolling stiffness of the interaction defined as:

$$K_r = \beta_r \,.\, (\frac{r_A + r_B}{2})^2 .\, K_T \qquad 2-11$$

The resistant moment is limited by a threshold value such that:

$$M_r = \frac{\theta_r}{\|\theta_r\|} \,.\, \eta_r \,.\, \|F_N\|.\left(\frac{r_A + r_B}{2}\right) \; if \;\; K_r \,.\, \theta_r \geq \eta_r \,.\, \|F_N\| \,.\, \left(\frac{r_A + r_B}{2}\right) \qquad 2-12$$

where, η_r is a dimensionless coefficient and β_r is the rolling resistance coefficient.

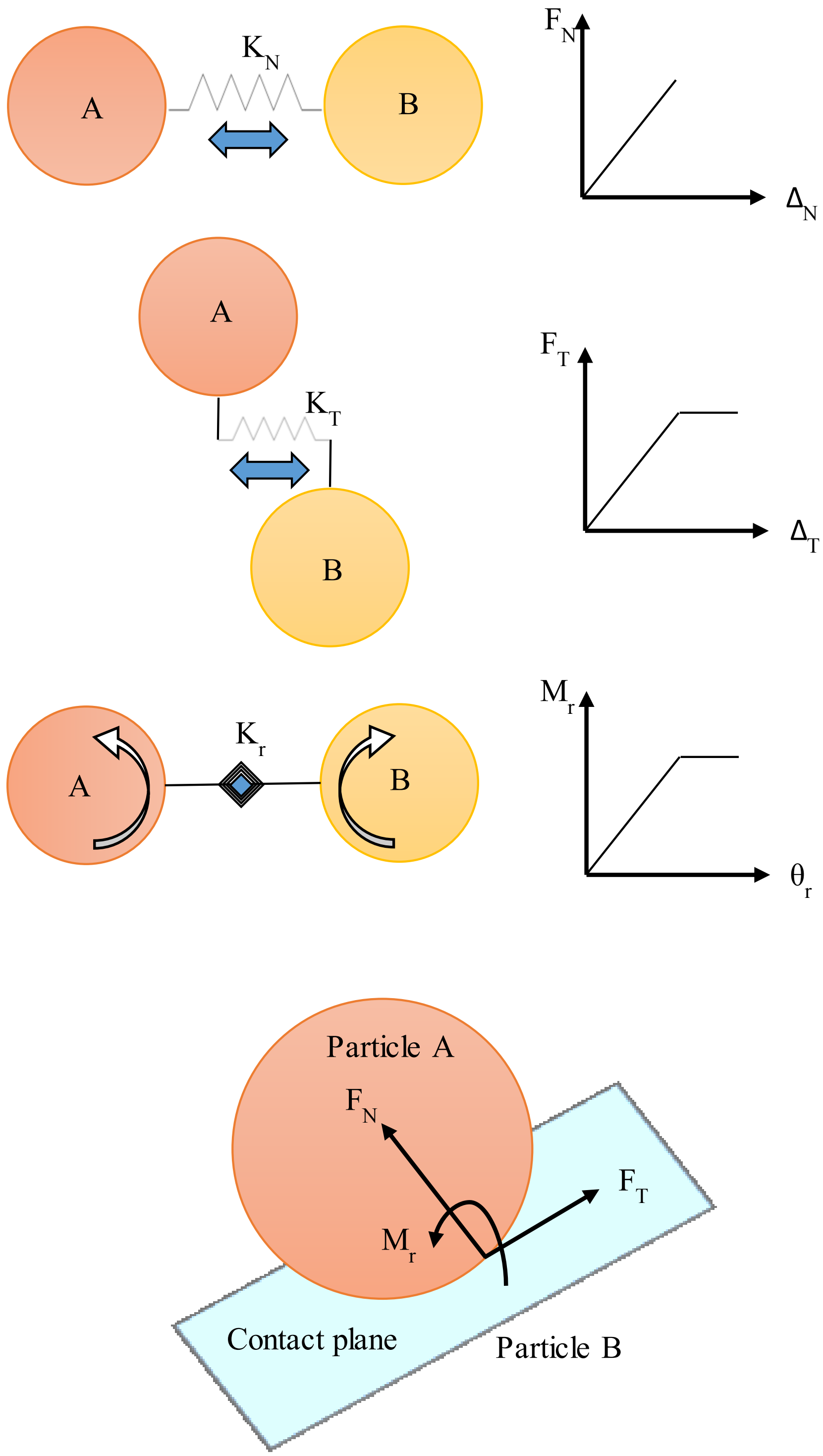

Figure 2-5 Description of the contact model

To ensure the stability of the DEM model, the critical time-step Δt_{cr} is defined as:

$$\Delta t_{cr} = \underset{i}{\text{minimum}} \sqrt{2} . \sqrt{\frac{m_i}{K_i}} \qquad 2-13$$

where m_i is the mass of particle *i,* and K_i is the per-particle stiffness of the contacts in which particle i participates.

2.3.2 Effects of particle scale factor on discrete element results

Accurate modeling of geotechnical problems requires the use of millions of particles. As accounting all discrete particles contained in the system is challenging, therefore ''scaled-up'' elements with larger sizes have to be used to reduce the size of the model to a reasonable level that is suitable for the available computer resources. In this section, the effects of particle upscaling and the resolution of the model (i.e., median particle size to sample size ratio) on the macroscopic response are briefly discussed.

In discrete element analysis, finding the microscopic input parameters and the model size are important aspects of the model preparation. Since the microscopic parameters cannot be derived directly using standard laboratory test results, calibration is performed by reproducing the macroscopic parameters obtained from experiments. This calibration process has been studied by several researchers and different procedures were suggested (Huang 1999; Potyondy and Cundall 2004; Yang et al. 2006; Cho et al. 2007; Koyama and Jing 2007; Plassiard 2009; Zhang and Wong 2012). Results showed that the scale factor and model dimensions have noticeable effects on the DEM simulation outcomes; however, there is no universal agreement on a standard method to choose the appropriate scaling ratio for all applications.

A summary of some of the relevant 2D and 3D studies in this area is given in Table 2-3 for various model configurations. The model dimensions are represented by the smallest length, *L*, which represents the cylindrical sample diameter or the width of a rectangular model. To facilitate the comparison of the used scale factors in each study, the *L/d* is calculated and included in the table where d, is the median of the simulated diameters. It can be seen that *L/d* ratio varies significantly for different models with increasing particle diameters as the model size increases.

Yang et al. (2006) examined the key factors controlling the strength and deformability of 2D models and concluded that the macroscopic properties of the model such as Young's modulus and Poisson's ratio are sensitive to *L/d* ratio, however, these properties tend to stabilize for *L/d* ratio of more than 32. Schopfer et al. (2007) conducted a series of 2D analysis to evaluate the effects of boundary conditions and model size on the response of the system at the macroscale level. A series of models was performed with the same micro-properties for different sample sizes. Results showed that the response of the system is related to both the scale and resolution of the model, however the elastic parameters (Young's modulus and Poisson's ratio) are independent of the sample size for samples with *L/d* more than 20. Ding et al. (2014) created 3D models with *L/d* rations ranging from 10 to 50 for four different particle size distributions (samples 1 to 4) as depicted in Figure 2-6. Results indicated that the model scale (represented by *L/d* ratio) influences both Young's modulus (Figure 2-6a) and Poisson's ratio (Figure 2-6b). Young's modulus rapidly decreased with the increase in *L/d* ratio from 10 to 20 with very little change beyond *L/d* of about 25. Similarly, Poisson's ratio continued to decrease up to *L/d* ration of about 30. Considering these results, it is concluded that a minimum *L/d* ratio of 30 should be considered in the 3D analysis as it strikes the balance between particle upscaling and the response of the system.

Table 2-3 Summary of studies on model scale factor effect on DEM simulation results

References	Simulation type	Model size (mm)	Median particle diameter, d_{50} (mm)	L/d
Huang (1999)	2D	150×150 – 50×500	1.25 – 3.5	28 - 200
Potyondy and Cundall (2004)	2D	63.4×31.7	0.36 – 2.87	11 – 88
Potyondy and Cundall (2004)	3D	63.4×31.7×31.7	1.53 – 5.97	5.5 – 20.7
Yang et al. (2006)	2D	20×10	0.4	5 – 64
Koyama and Jing (2007)	2D	10×10 - 100×100	0.875 – 1.4	10 - 95
Schopfer et al. (2007)	2D	2000×1000 100000× 50000	93.75	11.7 - 53
Yoon (2007)	2D	100×50	0.64 – 1.28	39 - 78
Schopfer et al. (2009)	3D	-	-	5 - 50
Zhang and Wong (2012)	2D	152×76	0.56	135
Ding et al. (2014)	3D	70×35 - 350×175	3.5	10 - 50

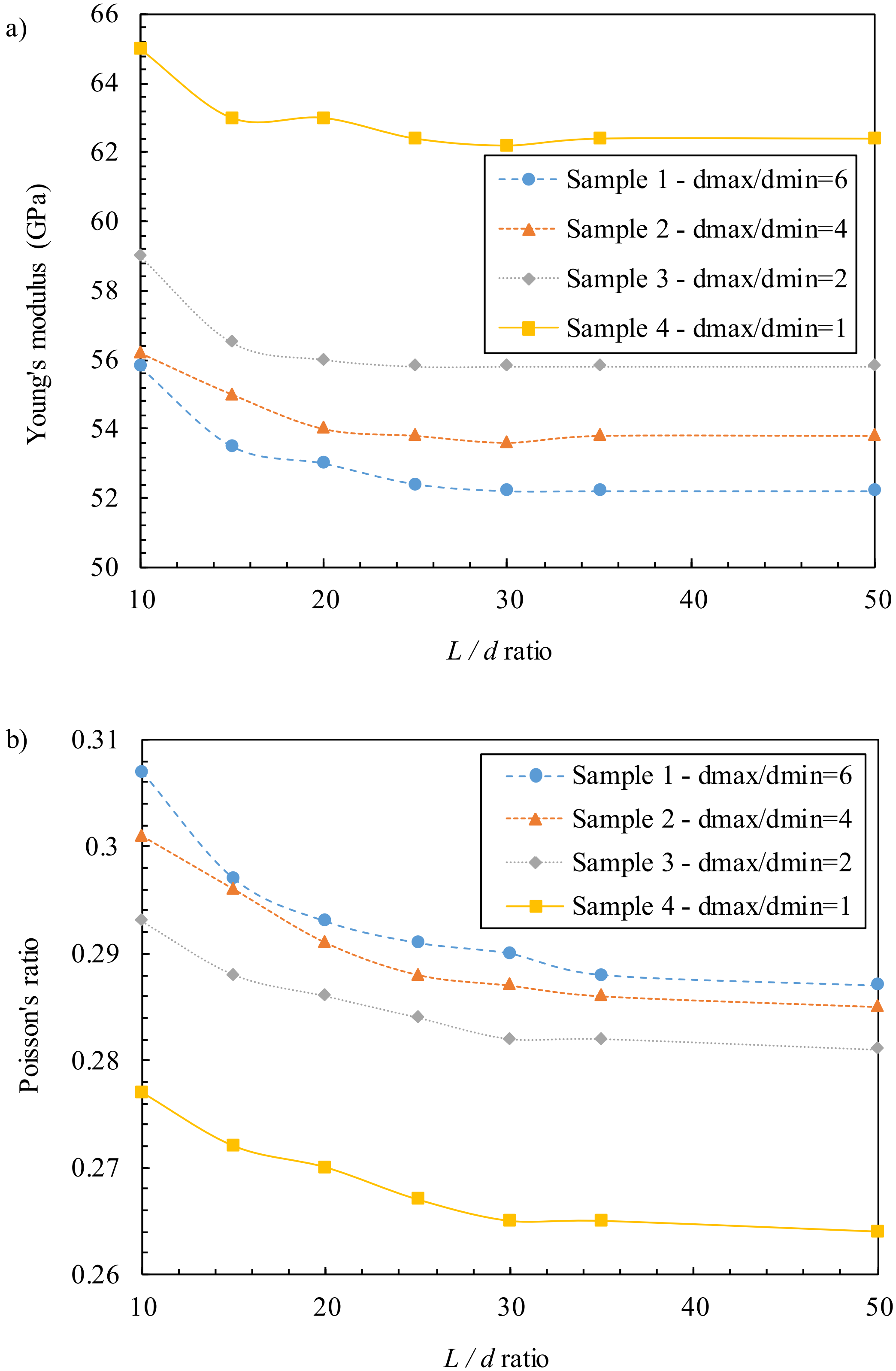

Figure 2-6 Model scale effect on a) Young's modulus and b) Poisson's ratio

2.3.3 Calibration of the Discrete Element Model

Discrete element modeling of triaxial tests (Figure 2-7) consists of particle-particle interaction. This interaction is modeled using a contact model[1] that uses six degrees of freedom. This law considers traction, compression, bending and twisting with cohesion and friction based on Mohr-Coulomb plasticity surface and failure criterion. This contact law includes several parameters to define the various stiffnesses and strengths. Working with these parameters simultaneously to calibrate the model is not possible. Plassiard (2009) proposed a calibration procedure for this contact law. The selected microscopic parameters are: elastic parameters involve elastic (E_{micro},K_T/K_N, β_r) as well as rupture parameters (φ_{micro} and η_r). These values are changed to reproduce, not only the correct shape of the stress-strain curve (Figure 2-8), but also the correct macroscopic values for the initial Young's modulus E_i, Poisson's ratio υ, the dilation angle ψ and the friction angle φ.

The calibration procedure can be summarized in the following steps:

E_{micro} is set first to calibrate the macroscopic elastic behavior. Duncan and Chang (1970) proposed Eq. 2-14 to find E_i from triaxial test results. It is done by plotting the axial strain over deviatory stress as a function of axial strain.

$$\frac{\varepsilon}{\sigma_1 - \sigma_3} = \frac{1}{E_i} + \frac{\varepsilon}{(\sigma_1 - \sigma_3)_{ult}} \qquad 2-14$$

Determining the K_T/K_N ratio is the next step. The macroscopic Poisson's ratio is determined by the K_T/K_N ratio. Eq. 2-15 is a relation between axial strain and volumetric strain in a triaxail test. This equation is applicable for the elastic part of behavior.

$$(1 - 2\vartheta) \times \varepsilon_1 = \varepsilon_V \qquad 2-15$$

---

[1] The contact formulation used is Law2-ScGeom6D-CohFrictPhys-CohesionMoment

The microfriction angle (φ_{micro}) influences both dilatancy angle and peak stress. In this case, it is chosen to control the dilatancy angle. Bolton (1986) proposed Eq. 2-16 as a relation between dilatancy angle and strain in a triaxial test. Both $\mathcal{E}_1$ and $\mathcal{E}_3$ are for the peak stress value.

$$Sin\left(\psi_{max}\right) = \frac{-\left(\frac{d\varepsilon_1}{d\varepsilon_3}\right) + 1}{\left(\frac{d\varepsilon_1}{d\varepsilon_3}\right) - 1} \qquad 2-16$$

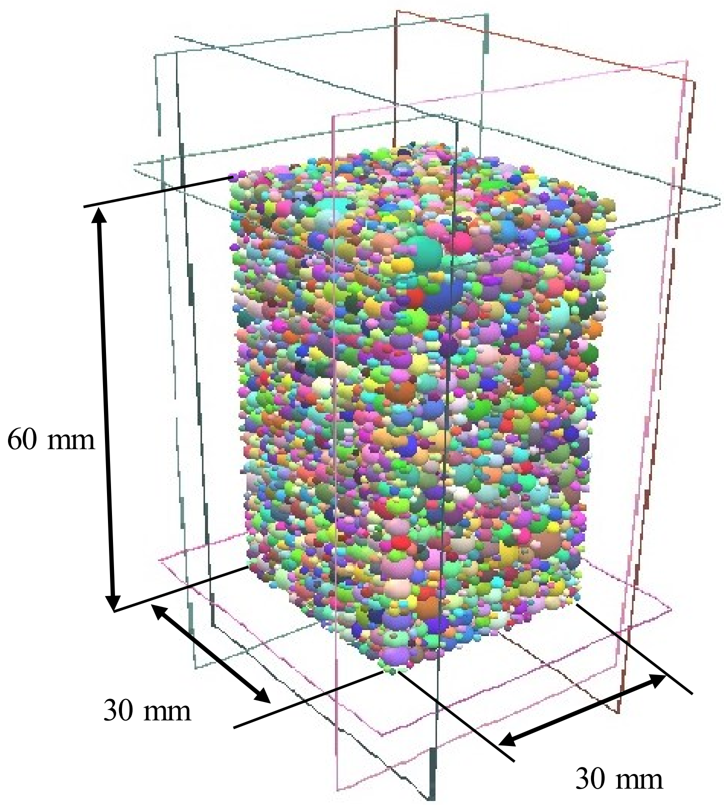

Figure 2-7 Triaxial test simulation using DEM

β_r is selected to match the residual stress of the test. Increasing β_r will increase the residual peak value.

η_r is the final parameter in the calibration procedure and greatly affects the peak stress. The macro friction angle is obtained from the peak stress value by using Eq. 2-17 (Bardet, 1997).

$$if\ c' = 0\ and\ p = \left(\frac{\sigma_1 + \sigma_3}{2}\right) and\ q = \left(\frac{\sigma_1 - \sigma_3}{2}\right) \qquad \sin(\varphi') = \frac{q}{p} = \frac{\left(\frac{\sigma_1}{\sigma_3}\right) - 1}{\left(\frac{\sigma_1}{\sigma_3}\right) + 1} \qquad 2-17$$

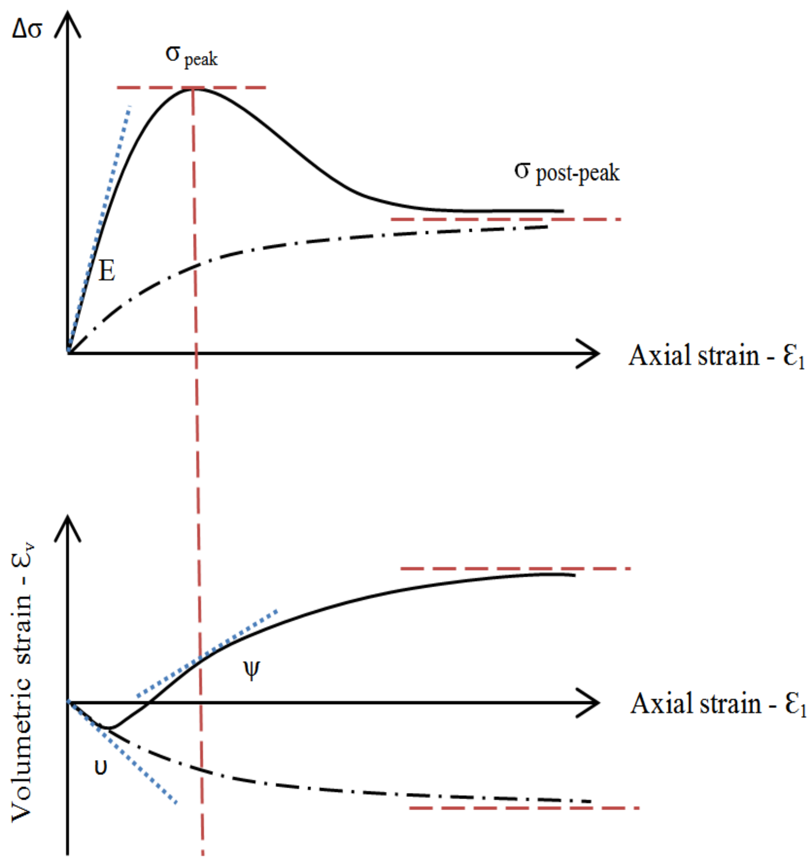

Figure 2-8 Typical responses obtained from triaxial tests for dense (solid lines) and loose (dashed lines) sands

2.4 Coupling the Finite and Discrete Element Methods

It was mentioned in section 2.2 that the structural elements in DEM simulation were either modeled using dynamic spar elements (Villard and Chareyre, 2004) or bonded particles which cannot model the continuous nature of the structure. Moreover, because of the rigidity of the bonded particles and dynamic spar elements, the real deformations as well as strains and stresses within the structure cannot be accurately captured.

To take advantage of both the finite and discrete element methods, coupling the two approaches has provided researchers with the flexibility of solving a wide range of geotechnical engineering problems involving buried structures. Structural elements are usually modeled using finite elements whereas the surrounding soil particles are modeled using discrete elements. Several algorithms have been developed to facilitate the load transfer between the two domains. A procedure for combining finite and discrete elements is to simulate the shot peening process was proposed by Han et al. (2002).

Fakhimi (2009) developed an algorithm for coupling the finite and discrete element methods and used the coupled model to simulate the deformable membrane and the encased soil samples in laboratory triaxial tests. The membrane was modeled using finite elements (FE) while the soil was modeled using discrete elements (DE).

Villard et al. (2009) proposed a coupled FE-DE approach to model earth structures reinforced by geosynthetic material. The framework was used to model the interaction between a geosynthetic sheet and the surrounding soil. Dang and Meguid (2013) proposed a coupled FE-DE approach to model soil-structure interaction problems involving large deformations. Interface elements were introduced at the boundary between the two domains to transmit the interaction forces between the finite and discrete elements. Tran et al. (2013) proposed a similar finite–discrete element framework for the 3D modeling of geogrid–soil interaction under pullout loading condition.

The coupled 3D Finite-Discrete element algorithm used for this study was originally developed by Dang and Meguid (2010, 2013) and Tran et al. (2013) to model the interaction between the finite and discrete element domains. The developed approach was implemented into *YADE*, an open source code for DE analysis (Kozichi and Donze, 2008; Smilauer et al., 2010) and is briefly discussed in the following sections.

2.4.1 The finite elements

The dynamic relaxation method is used in developing the coupled framework including both the finite and discrete element domains. The general equation of the FE approach is

$$\boldsymbol{K}x + c\boldsymbol{M}\dot{x} + \boldsymbol{M}\ddot{x} = \boldsymbol{P} \qquad 2-18$$

Where P the external force is vector; x is the displacement vector; M is the mass matrix; c is the damping coefficient and K represents the stiffness matrix.

The maximum time step $[\Delta_{FE}]$ that meets the convergence condition of the system is determined based on the maximum eigenvalue (λ_m) which is calculated using the element consistent tangent stiffness:

$$[\Delta_{FE}] = \frac{2}{\sqrt{\lambda_m}} \qquad 2-1$$

$$\lambda_m \leq \max_i \sum_{j=1}^{n} \frac{|K_{ij}|}{M_{ij}} \qquad 2-20$$

where M_{ij} is an element in the diagonal mass matrix; and K_{ij} is an element in the global tangent stiffness matrix.

2.4.2 The discrete elements

The details of the contact law employed in the DEM simulation have been presented in section 2.3.1.

2.4.3 Interface elements

Interface elements are employed in the coupled framework to transfer the contact forces between the FE and DE domains. These elements are generated such that they follow the finite element nodes. Since hexahedral elements are used for the FE domain, the contact surface between the two domains is divided into four interface elements by adding a temporary node at the center of each finite element as expressed below.

$$X^{(O)} = \frac{1}{4} \sum_{i=1}^{4} X^{(i)} \qquad 2-21$$

where $X^{(i)}$ is the coordinate of node i of the quadrilateral element. Figure 2-9 shows a schematic of the interaction between discrete particles, interface and finite elements. The contact law between the interface and discrete elements is the same as that used for particle-particle interaction. Following the contact between a DE particle and an interface element, the normal and tangential interaction forces are calculated using the normal overlap and incremental tangential displacement of the contact. The total contact force is determined by summing the normal and tangential force vectors ($\vec{F_N} + \vec{F_T}$). Eq. 2-22 is used to compute the transmitted forces to the FE nodes using the interaction forces.

$$\vec{F_i} = \vec{F}_{contact} \, . N_i = \left(\vec{F_N} + \vec{F_T}\right) . N_i \qquad 2-22$$

where N_i is the shape function calculated using the natural coordinates of the contact point. A typical FE-DE computational cycle was discussed and reported by Dang and Meguid (2010; 2013).

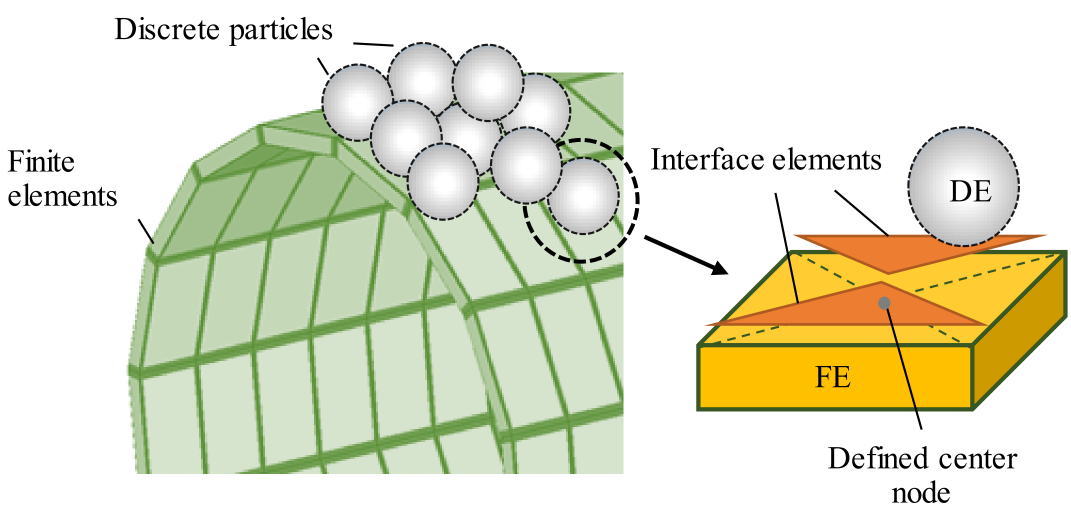

Figure 2-9 Schematic of the coupled FE-DE model showing the interface elements

2.5 Conclusion of the literature review

Review of studies on soil and buried pipe interaction showed that although numerous amount of analytical, numerical and experimental research has been performed, there are still some limitations in the current understanding of the buried pipes response subject to ground movement. A promising coupled numerical approach was suggested in this research to perform more studies on this subject. However, based on the literature review on coupled modeling, the number of studies in this area is limited especially on validating discrete element simulation and coupled finite-discrete element models. Therefore, a systematic numerical research was proposed in this thesis and the performance of the buried steel pipe under axial soil movement and buried flexible pipe under axial and lateral soil movement were presented in detail. The numerical models were calibrated precisely, and the validation has been done by comparing the results with experimental data. In addition to enrichment the conceptual understanding of the soil-buried pipe interaction, a new equation was proposed to estimate the soil axial load on steel pips buried.

Preface to Chapter 3

As discussed in Chapter 2 (Literature Review) that previous experimental studies reported that the maximum axial soil resistance for steel pipes buried in dense sand differs from that obtained using current guidelines. In this chapter, the interaction between a steel pipe buried in dense sand is investigated using a three-dimensional discrete element model. The discrete element model is calibrated and validated using experimental data and the detailed behavior of the pipe and soil as well as their interaction at the particle scale level is presented.

Chapter 3.

Evaluation of Soil-Pipe Interaction under Relative Axial Ground Movement*

Abstract

The expansion of urban communities around the world resulted in the installation of utility pipes near existing natural or man-made slopes. These pipes can experience significant increase in axial earth pressure as a result of possible slope movement in the pipeline direction. This research aims at utilizing discrete element method to investigate the response of a buried pipeline in granular material subjected to axial soil movement. To determine the input parameters needed for the discrete element analysis, calibration is performed using triaxial test results and the microscopic parameters are determined by matching the numerical results with experimental data. In addition, direct shear tests are numerically simulated to confirm the parameters obtained from the triaxial test. The soil-pipe system is then modeled and the detailed behavior of the buried pipe and the surrounding soil as well as their interaction at the particle scale level are presented. Conclusions are made regarding the suitability of the empirical approach used in practice to estimate the axial soil resistance in different soil conditions.

Keywords: Soil-structure interaction, DEM simulation, buried pipes, axial movement

---

* A version of this chapter has been published in *ASCE Journal of Pipeline Systems Engineering and Practice*, 2017, 8(4), 1-10.

3.1 Introduction

Buried pipes are among the most economical and safe methods of transporting natural resources (e.g., oil, natural gas, and water distribution networks). Permanent ground deformation resulting from earthquakes or movement of nearby slopes can impose additional loads on the pipe leading to unacceptable deformation and pipe separation from the surrounding soil. A report of the European Gas Pipeline Incident Data Group (2005) has indicated that ground movement represents the fourth major cause of gas pipeline failure with close to half of the reported cases resulting in pipe rupture.

The response of buried pipes to slope movements depends on the orientation of the pipeline with respect to the moving slope. If the pipe axis is parallel to the direction of the sliding soil, the pipe would be subjected to longitudinal (axial) strains and the pipe experiences either tensile or compressive stresses. The second condition occurs when the axis of the pipe is normal to the soil movement direction and, in this case, the relative soil movement imposes lateral deformation to the pipe resulting in strains and stresses on the pipe wall due to the development of bending moments and shear forces. ASCE (1984) recommended a closed-form solution to determine the axial loads on buried pipes in cohesionless soils using the following expression:

$$F_A = \gamma' \times H \times (\pi\, D\, L) \times \left(\frac{1 + K_0}{2}\right) \times \tan(\delta) \qquad 3-1$$

Where, F_A is the axial soil resistance, γ' is the soil effective unit weight, H is the depth of pipe from ground surface to the pipe springline, D is the pipe outer diameter, L is the pipe length, K_0 is the coefficient of lateral earth pressure at rest and δ is the friction angle between the soil and pipe.

Over the past few decades, researchers have studied soil-pipe interaction using experimental, theoretical, and numerical methods (e.g., Newmark and Hall 1975; Trautmann and O'Rourke 1983; O'Rourke and Nordberg 1992; Honegger and Nyman 2002; Chan and Wong 2004; Karimian et al. 2006; Wijewickreme et al. 2009; Daiyan et al. 2011; Rahman and Taniyama 2015; Liu et al. 2015; Almahakeri et al. 2016; Zhang et al. 2016). Most of the numerical analyses were performed using the finite-element (FE) method. Yimsiri et al. (2004) used FE analysis to study soil-pipe interaction under lateral and upward soil movements in a deep burial condition.

Guo and Stolle (2005) investigated the lateral earth pressure on buried pipes and concluded that capturing large soil movement interacting with a buried conduit is challenging using continuum approaches. Almahakeri et al. (2016) conducted a series of three-dimensional (3D) FE simulations to examine the longitudinal bending in buried glass fiber-reinforced polymer (GFRP) pipes subjected to lateral earth movements and compared the results with measured data. Most recently, Zhang et al. (2016) studied the mechanical behavior of a buried steel pipeline crossing a landslide area using finite-element analysis and highlighted the role of soil and pipeline parameters on the behavior of the system. Although soil-structure interaction with large deformation can be modeled using a multiscale approach (Hughes 1995) or adaptive remeshing (Zienkiewicz and Huang 1990), modeling particle movement and unpredictable discontinuities near existing pipes is very scarce in the literature.

The discrete element method (DEM) has proven to be suitable for modeling granular material and large deformation. The method was first proposed by Cundall and Strack (1979) and has been used to analyze various geotechnical engineering problems. Laboratory tests have been modeled using DEM to investigate the microscopic behavior of soil samples. Cui and O'Sullivan (2006) used discrete elements to study the macroscopic and microscopic behavior of granular soil under direct shear test conditions. Tran et al. (2013) proposed a finite-discrete element framework for the 3D modeling of geogrid-soil interaction under pullout loading condition. Also, Tran and Meguid (2014) conducted three-dimensional discrete element of the earth pressure distribution on cylindrical shafts. The analysis allowed for the soil arching and radial pressure distribution on the shaft wall to be visualized. Furthermore, Ahmed et al. (2015) conducted laboratory experiments and finite-discrete element analysis to study the role of geogrid reinforcement in reducing earth pressure on buried pipes. It has been shown in these studies that discrete-element or coupled finite-discrete element approaches are effective in capturing the response of structural elements such as pipe and geogrid and their interaction with the surrounding soils.

This study presents the results of a three-dimensional discrete-element investigation that has been conducted to examine the response of a steel pipe buried in dense granular material and subject to axial loading. A suitable discrete-element packing method is first utilized to prepare a soil sample with predefined properties. Material calibration is then performed using standard triaxial and direct shear tests to determine the input parameters needed for the discrete-element simulation. The calculated response of the pipe is compared with the reported experimental results. The validated model is used to determine the distribution of radial earth pressure on the pipe wall and understand the changes in in situ pressure around the pipe during and after the pullout process. The applicability of the available closed-form solution is also evaluated.

3.2 Description of the Numerical Model

The experimental results used to validate the numerical model are based on those reported by Wijewickreme et al. (2009). The response of a buried steel pipe subjected to axial soil movement was investigated in a test chamber (3.8 m long, 2.5 m wide and 1.82 m high) as depicted in Figure 3-1. Graded Fraser River sand with in situ density of 16 kN/m^3 was used as a backfill soil. The mechanical characteristics of the sand have been also reported based on triaxial and direct shear tests conducted under confining pressures that range from 15 to 50 kPa. A summary of the mechanical characteristics of the backfill soil is given in Table 3-1. The steel pipe used in the experiments has an outside diameter of 46 mm and a wall thickness of 13 mm. The interface friction angle (δ) between the backfill material and the steel pipe was reported to be 36°. The pipe is placed over 0.7 m of bedding layer up to the springlines and covered with 1.15 m of the backfill material. This corresponds to a height-to-diameter ratio ($H=D$) of 2.5.

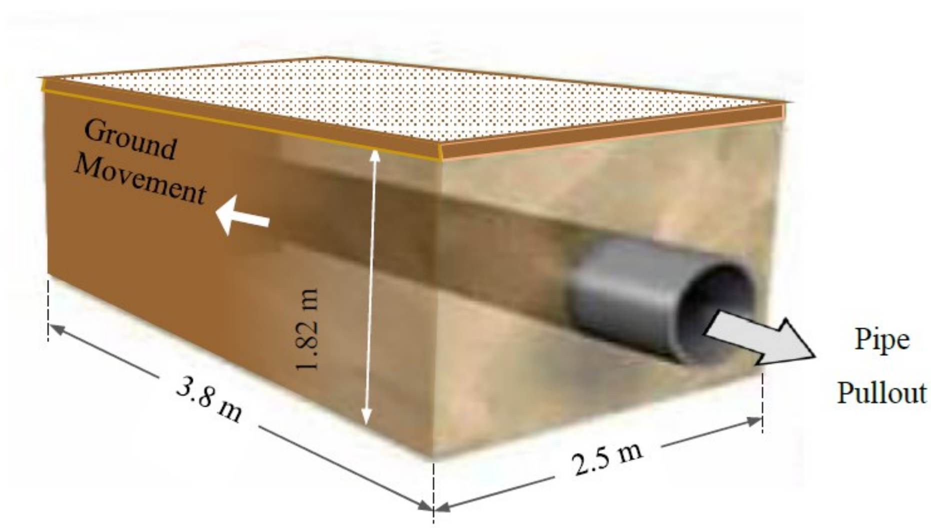

Figure 3-1 Configuration of the modeled experiments

The numerical model has been developed in this study such that it replicates the geometry and test procedure used in the experiments. All components are generated inside the *YADE* package. Various packing algorithms can be used to generate DEM samples for both standard soil tests and large-scale pullout simulations. Techniques such as the compression method (Cundall and Strack 1979), gravitational method (Ladd 1978), triangulation-based approach (Labra and Onate 2009), and radius expansion method (*PFC 2D*) are widely used for this purpose.

Table 3-1 Mechanical characteristics of Fraser River sand

Parameter	Value
Particle density (kg/m^3)	2720
φ_{peak} (degrees)	45
φ_{cv} (degrees)	33
ψ (degrees)	15
Cohesion (kN/m^2)	0
E_i (MPa)	36
υ – Poisson's ratio	0.3
γ (kg/m^3) - D_r=75% (dense sand)	1600

3.3 Generating the Discrete-element Particles

The soil sample is generated in this study using the radius expansion method following a grain size distribution similar to that of the backfill material. Given the size of the physical model, it is numerically impractical to simulate millions of particles with their actual size. Therefore, particle upscaling with two different scale factors has been adopted to gradually reduce the number of particles and maintain the time step size at a reasonable value. In this process, a balance between the computational costs and the scaling effects on the global response needs to be considered.

The soil in the test chamber is divided into four zones as illustrated in Figure 3-2. A particle scale factor of 90 is used in Zone 1, which represents the area immediately around the pipe, and increases to 140 in the remaining zones. A small-scale factor is applied to particles in the close vicinity of the pipe to improve the contact between the soils and pipe. The selected scale factors are also supported by the findings of previous researchers. Potyondy and Cundall (2004) noted that when the number of particles used in a discrete-element simulation is large enough (more than 265,000 particles in this study using the mentioned scale factors), the macroscopic response becomes independent of the particle size. Also, Tran et al. (2014) evaluated the effect of different scale factors in analyzing soil-structure interaction and confirmed that when the number of particles is greater than 245,000, the scale factor has an insignificant effect on the overall response of the system. Furthermore, Ahmed et al. (2015) suggested that creating a DEM sample with the number of soil particles around 300,000 makes the global response of the system insensitive to the change in particle size. The grain size distributions of the backfill material and the particles in the different zones are shown in Figure 3-3.

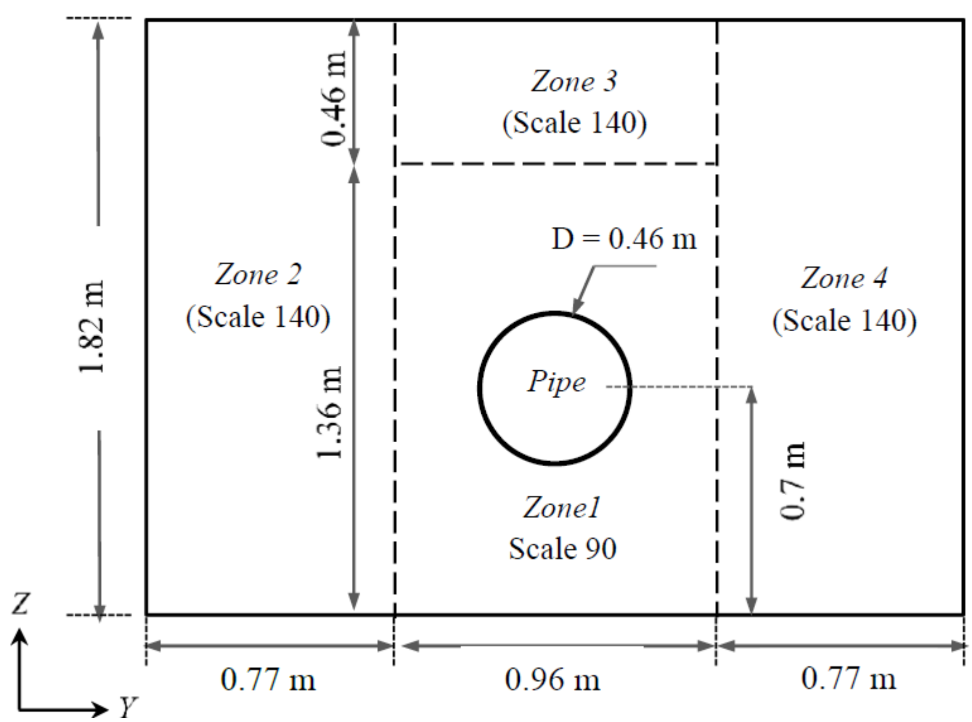

Figure 3-2 A schematic showing the different particle packing zones around the pipe

A cloud of non-contacting particles is first generated inside the box for each zone following a predetermined particle size distribution and scale factor. Particles located within the pipeline area are then removed. The radius expansion method is applied to each zone to achieve a target porosity of 0.41, which corresponds to that of the experiment. The radius expansion method is known to generate a specimen with an isotropic stress state (O'Sullivan 2011). To dissipate this effect, each zone was subjected to gravity forces and allowed to reach equilibrium. The entire packing, including the four different zones, is then assembled under gravity and the homogeneous distribution of the contact forces is checked using the fabric tensor. The total number of particles used in the final packing is approximately 265,000. It has been found that the fabric tensor components are nearly identical with *xx* and *yy* of approximately 0.33 and *zz* of approximately 0.34, where *z* is the gravitational direction. A partial view of the packing including the pipeline and its surrounding spherical particles is shown in Figure 3-4. To further illustrate the distribution of particle sizes near the pipe, a close view of the pipe and the nearby zones is also provided in Figure 3-5 (a).

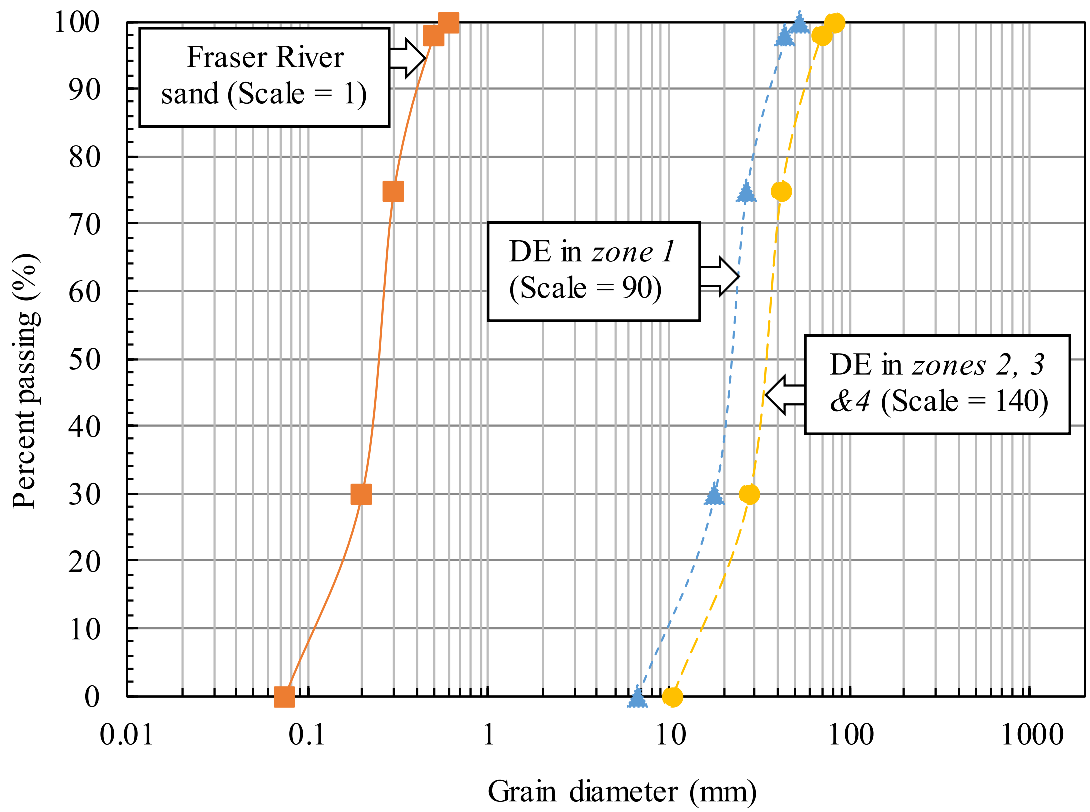

Figure 3-3 Grain size distribution with particle upscaling

The pipe is modeled in this study using triangular facet elements (flat discrete elements) with material modulus comparable to that of the steel pipe. The interface friction angle between the facet elements and the soil particles is known to play an important role in the analysis and needs to be properly chosen, as explained in the next sections. The pipe wall is modeled using a total of 1,216 facet elements arranged in a hexadecagonal shape. The length of the pipe is chosen such that it extends slightly outside the back of the chamber to ensure continuous contact with the soil during the pullout process. A 3D view of the simulated pipe is presented in Figure 3-5 (b).

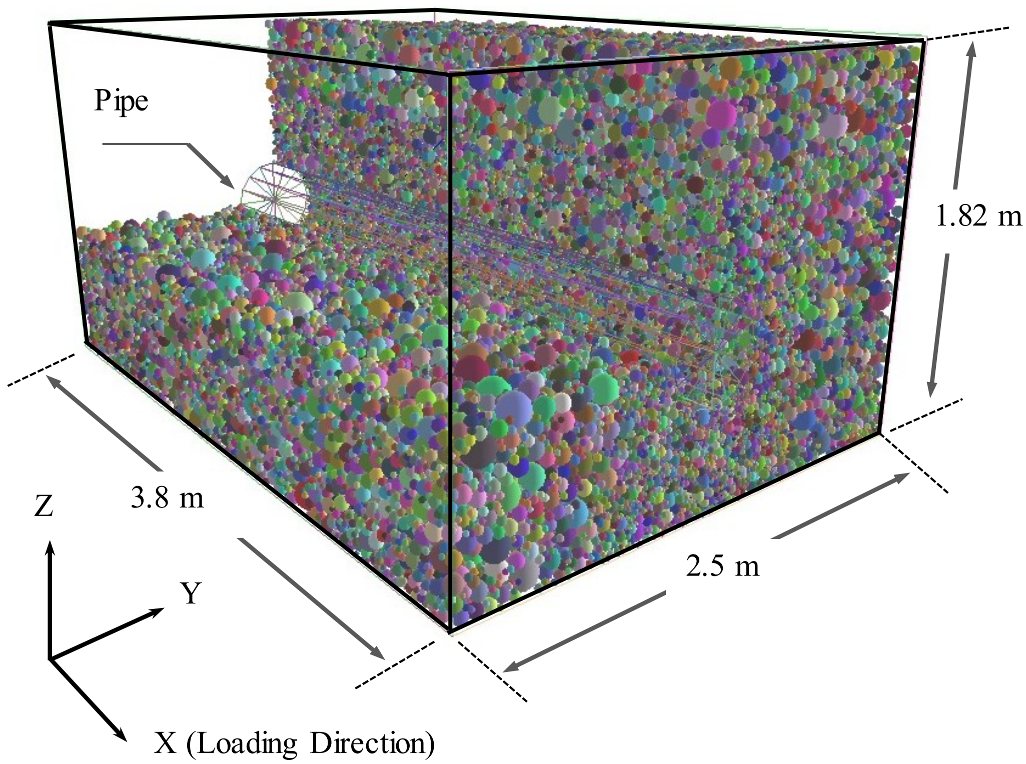

Figure 3-4 Partial view of the model showing the pipe and surrounding soil

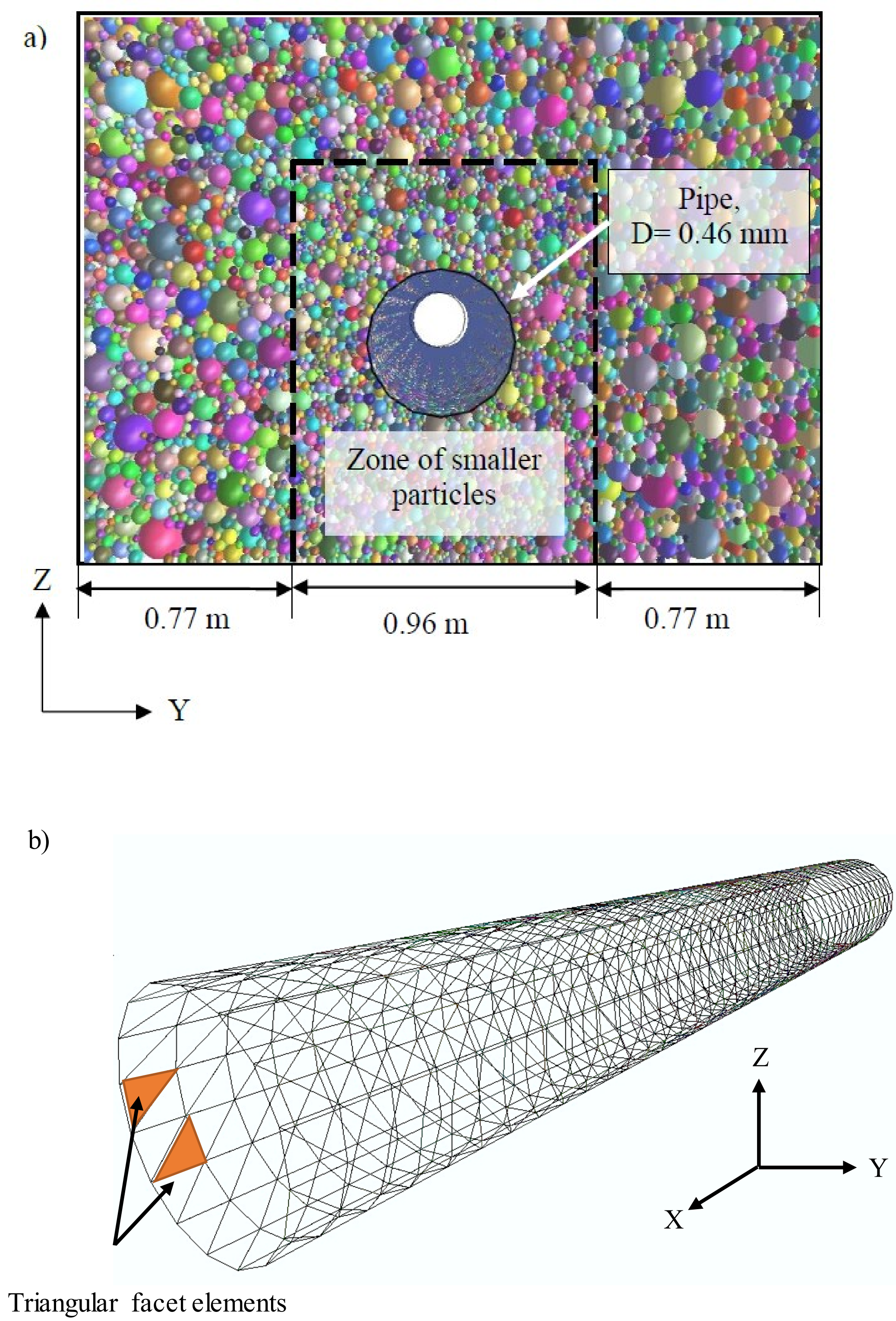

Figure 3-5 Numerical model: a) particle distribution in the close vicinity of the pipe; b) simulated pipeline using facet elements

3.4 Material Calibration

Input parameters used in the discrete-element simulation include two major groups: (1) physical parameters (friction angle, cohesion, and Young's modulus), and (2) dimensionless coefficients (e.g., rolling and shear stiffness coefficients, maximum resistant moment factor). A calibration procedure is required to determine these input parameters for a given soil condition before it is adopted in the DEM. The model used in this study is calibrated by simulating triaxial tests conducted on Fraser River sand (Karimian 2006) and comparing the calculated response with the measured values. In addition, direct shear tests are also modeled to confirm the input parameters to be used in the pullout simulation. A flowchart that summarizes the calibration process and the different micro parameters needed for the DEM simulation is given in Figure 3-6.

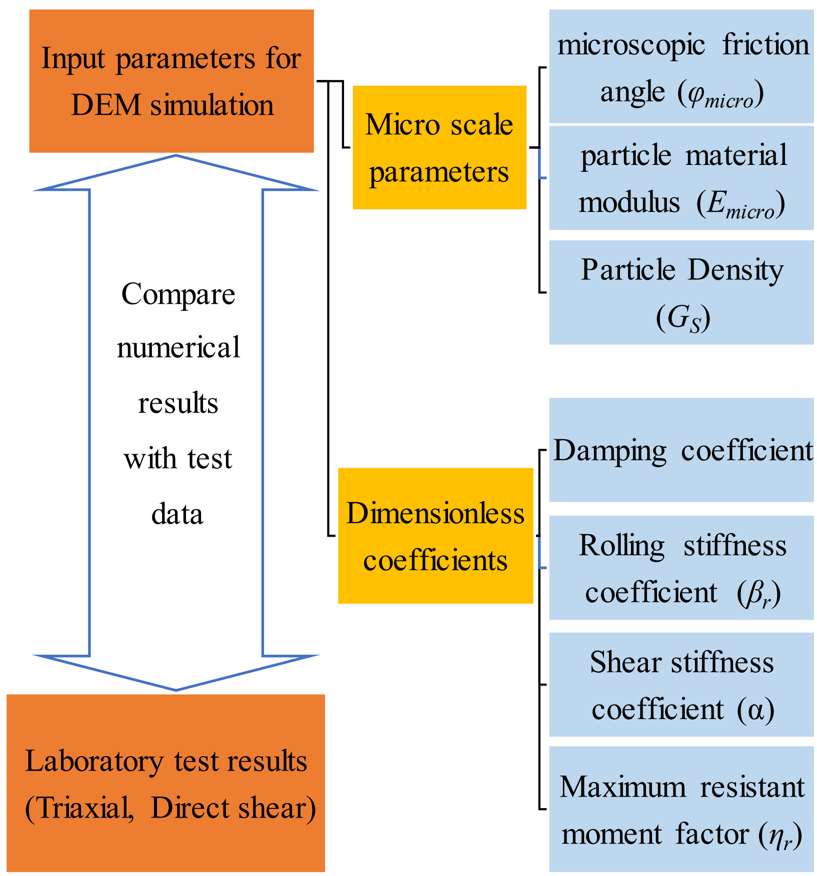

Figure 3-6 Input parameters required for the material calibration and the large-scale discrete-element analysis

3.4.1 Triaxial test

The numerically simulated triaxial test Figure 3-7 (a) consists of a rectangular prism with an aspect ratio of 2 (76 mm long, 76 mm wide, and 152 mm high) to approximate the geometry of the tested samples. The particle assembly is created using the radius expansion method described in the previous section. The final pack contains more than 23,000 spherical particles with a porosity of 0.41 (dense sand) and grain size distribution similar to that of the real sand material. The numerical simulation includes two stages: (1) the sample is compressed up to a target confining stress of 25, 35, or 50 kPa; and (2) the top wall can move downward at a constant strain rate to impose the deviatoric load while the stresses at the side walls are kept constant.

The interaction between particles is simulated using a contact model that considers traction, compression, bending, and twisting with cohesion and friction based on Mohr-Coulomb failure criterion. Plassiard et al. (2009) proposed a calibration procedure that involves elastic parameters ($E_{micro}, K_T/K_N$, β_r) as well as rupture parameters (φ_{micro} and η_r). These parameters are determined to satisfy the correct shape of the stress-strain curve and match the initial Young's modulus E_i, Poisson's ratio υ dilation angle ψ and the friction angle φ of the material. The calibration is performed for a confining pressure of 25 kPa and the obtained parameters are confirmed by repeating the analysis for confining pressures of 35 and 50 kPa. Figure 3-7 (b) presents the results of the discrete-element analysis along with the experimental data for all ranges of confining pressures. The soil properties obtained from the triaxial test simulation for confining pressure of 25 kPa are summarized in Table 3-2.

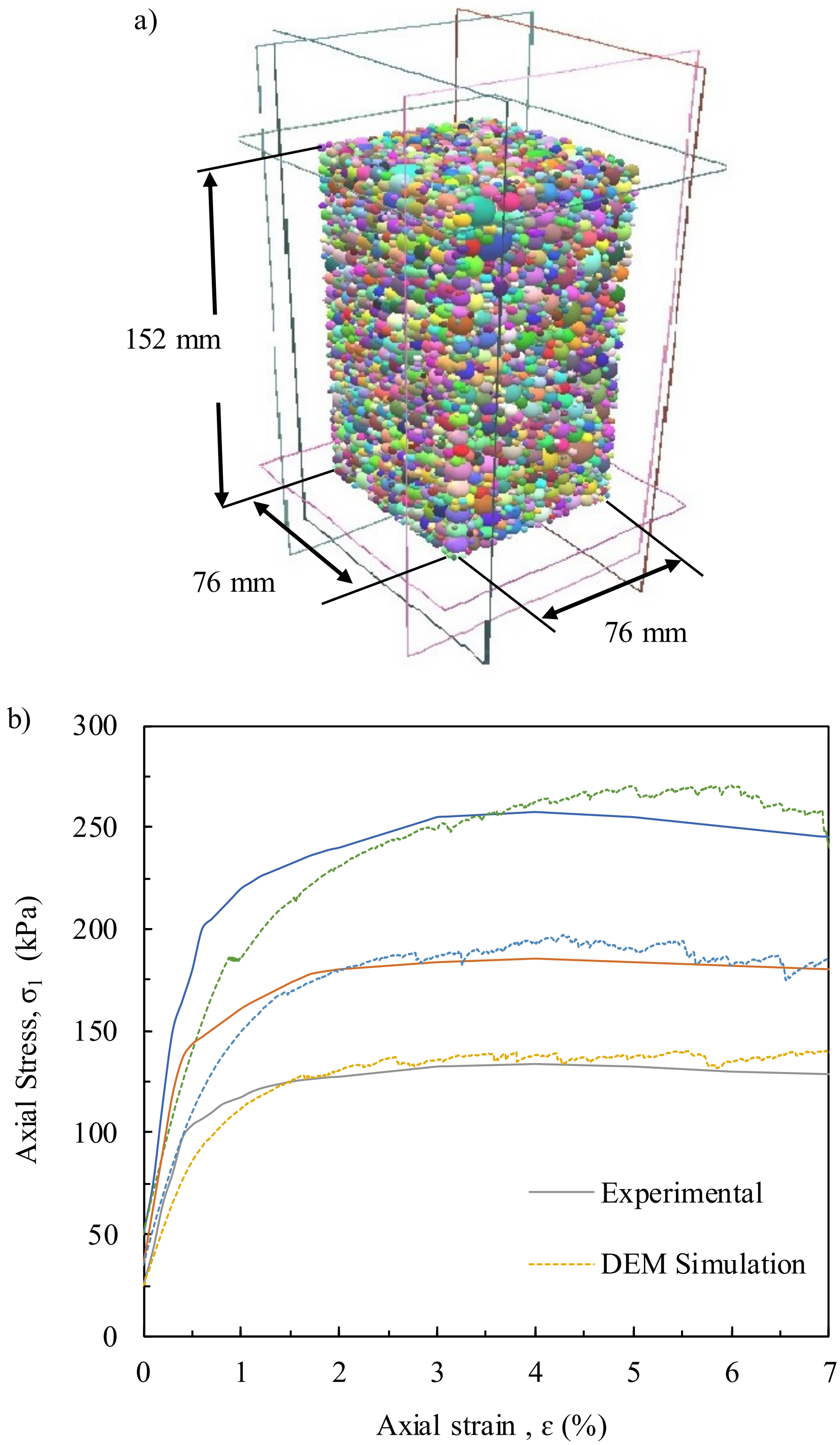

Figure 3-7 Triaxial test used for the material calibration: a) tested sample; b) results

Table 3-2 Soil properties based on triaxial tests with 25 kPa confining stress

Parameter	Value
φ_{peak} (degrees)	45
ψ (degrees)	15
E_i (MPa)	34
υ	0.28

3.4.2 Direct shear test

Modeling the direct shear test is used to confirm the macroscopic and microscopic parameters (Table 3-2 and Table 3-3) to be used in the simulation. The direct shear test (60 × 60 × 25 mm) was based on that reported by Karimian (2006) for Fraser River sand under three different normal stresses (20, 35, and 53 kPa). The discrete-element packing used in the direct shear test was created such that it has similar characteristics as that described in the triaxial test including porosity, coordination number (N_c), and fabric tensor (Φ_{ij}). The sample porosity and coordination numbers at the initial state were found to be 0.41 and 5.5, respectively. As shown in Figure 3-8 (a), specimen is created using the radius expansion method with a total of 24,688 spheres and using a scale factor 5. The input parameters given in Table 3-3 are then assigned to the particles. The results of the direct shear test for different normal stresses is shown in Figure 3-8 (b). The overall trend and the maximum shear stress values are found to be consistent with the laboratory results. A slightly softer response is observed for shear displacements of less than 0.5 mm. This may be attributed to the difference in particle shapes as compared to the spherical particles used in the discrete-element analysis. Similar observation was made by Yan (2008).

3.5 Modeling the Pullout procedure

Following the material calibration, a final specimen is created, and the properties are assigned to the discrete particles. No friction is used for the interaction between the particles and the walls of the box, which is similar to the condition of the experiments to eliminate the boundary effects. A parametric study is conducted to examine the effect of friction angle of the facets (used to model the pipe) on the pullout response. Results indicated that the soil-pipe system is sensitive to the interface friction and a friction angle of 30° was found to correspond to a maximum pullout force that matches the experimental data.

The pullout procedure is numerically simulated under displacement control with a movement rate of 5 mm/s applied to the facets to be consistent with the experiment. The pipe was incrementally pulled until a maximum displacement of 200 mm was reached. The corresponding pullout force is captured during the simulation by summing the forces on the facets in the pulling direction.

Table 3-3 Selected properties used in discrete element analysis

Parameter	Value
Particle density (kg/m^3)	2720
Particle material modulus, E_{micro} (MPa)	150
K_T/K_N ratio	0.7
β_r	0.15
φ_{micro} (degrees)	45
η_r	1
Damping ratio	0.2

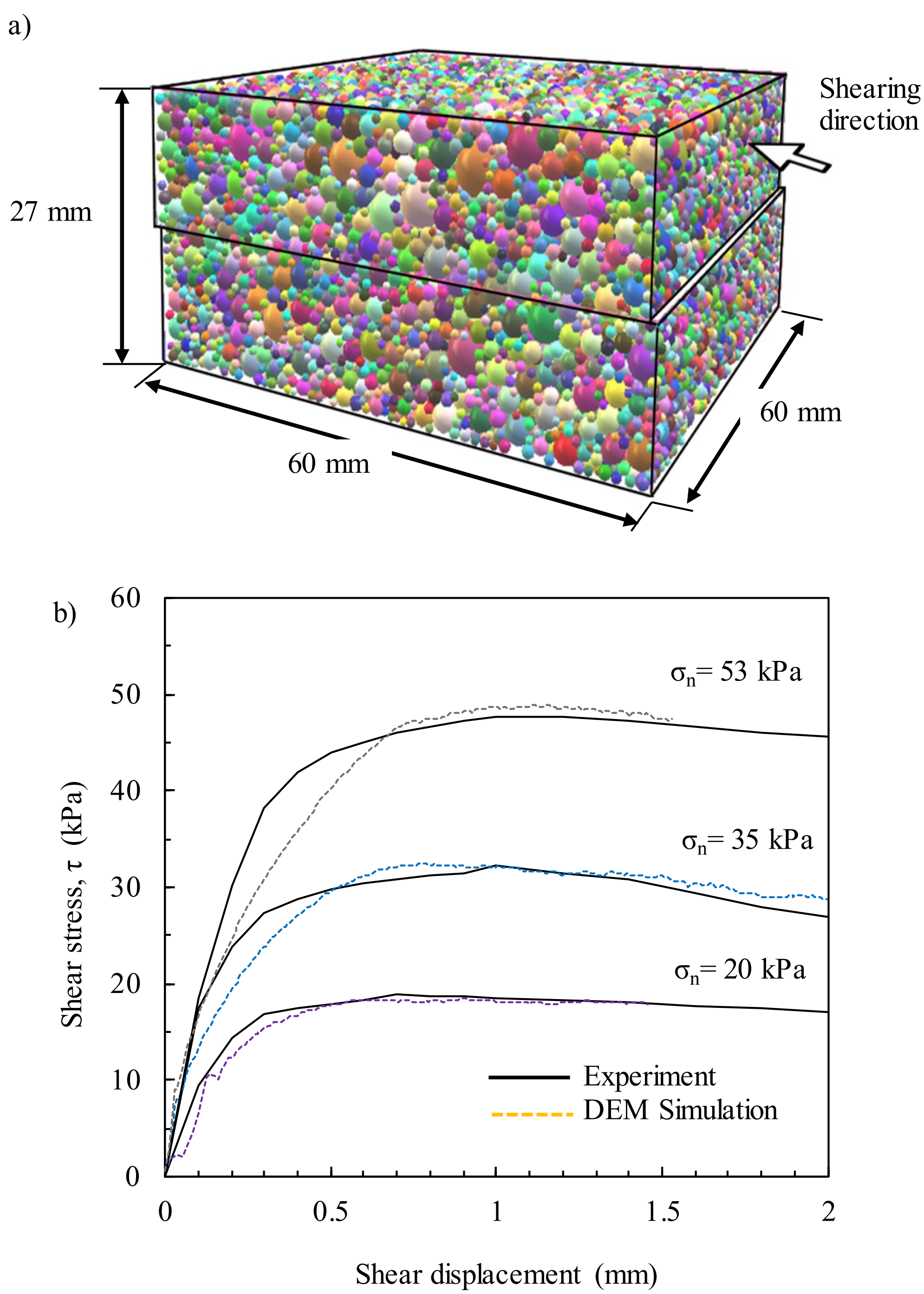

Figure 3-8 Direct shear test used to confirm the input parameters: a) tested sample; b) results

3.6 Radial Earth Pressure Distribution

After the final particle assembly in the chamber and the assignment of input parameters, the pipe and the surrounding particles were allowed to freely move under gravity. The initial stress distribution acting on the pipe is examined and compared with the analytical solution. The equation proposed by Hoeg (1968) allows for the radial pressure (σ_r) on buried pipes to be determined as follows:

$$\sigma_r = \frac{1}{2} P\left\{(1+k)\left[1-a_1\left(\frac{D}{2r}\right)^2\right]-(1-k)\left[1-3a_2\left(\frac{D}{2r}\right)^4-4a_3\left(\frac{D}{2r}\right)^2\right]\cos 2\theta\right\} \qquad 3-2$$

Where D is the pipe diameter, r is the distance from the pipe center to the soil element under analysis, k is the lateral earth pressure coefficient at rest, P is the soil vertical stress, θ is the angle of inclination from the springline and a_1, a_2 and a_3 are constants.

A comparison of the initial radial pressures calculated using DEM and that of Hoeg's solution at selected locations is shown in Figure 3-9. The pressure values are presented on opposite sides of the polar chart. The contact pressure ranged from 15 kPa at the crown (angle 0°) to approximately 20 kPa at the invert (angle 180°), which is consistent with the expected distribution for rigid pipes.

Vertical stress distribution in soil is also examined and compared with the expected values. To record macroscopic stress components, a measurement box of volume V is used and the average stress within the box is calculated as:

$$\sigma_{ij} = \frac{1}{V}\sum_{c=1}^{N_c} x^{c,i} f^{c,j} \qquad 3-3$$

Where , N_c is the number of contacts within the measurement box; $f^{c,j}$ is the contact force vector at contact c; $x^{c,i}$ is the branch vector connecting two contact particles A and B; and indexes i and j are the Cartesian coordinates.

The soil chamber is divided into three regions (Figure 3-10a) and the vertical stresses are calculated in each region using Eq. 3-3. Region 1 is selected near the wall to evaluate the effect of the rigid boundaries on the results. Regions 2 and 3 are chosen at the same distance in the opposite side of the pipe to assess the homogeneity of the generated particle packing. Vertical stresses are obtained using measurement boxes with dimensions of 0.25 × 0.25 × 0.25 m and the results are presented in Figure 3-10b. Vertical stress distribution in region 1 near the boundary is consistent with the expected values ($\gamma' z$). This signifies that the effect of the walls on the calculated vertical soil pressures is negligible. In addition, by comparing the vertical stress distribution in Regions 2 and 3, it is evident that the particle packing used in the simulation is homogenous.

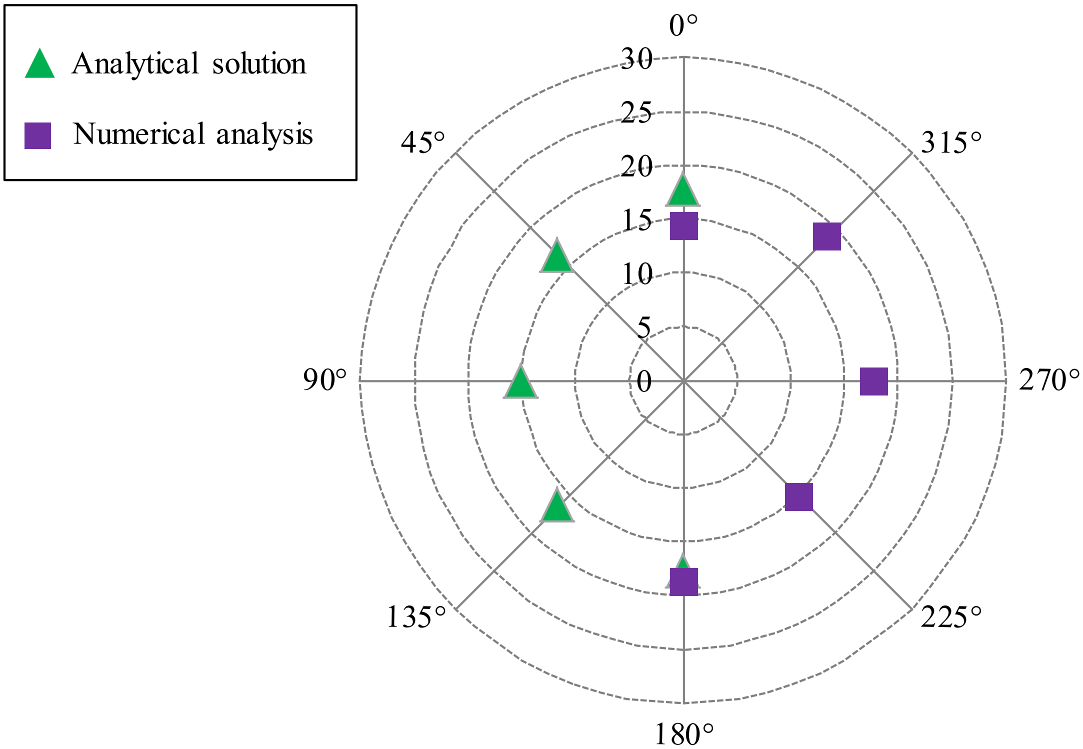

Figure 3-9 Initial earth pressure distribution on the pipe (kPa)

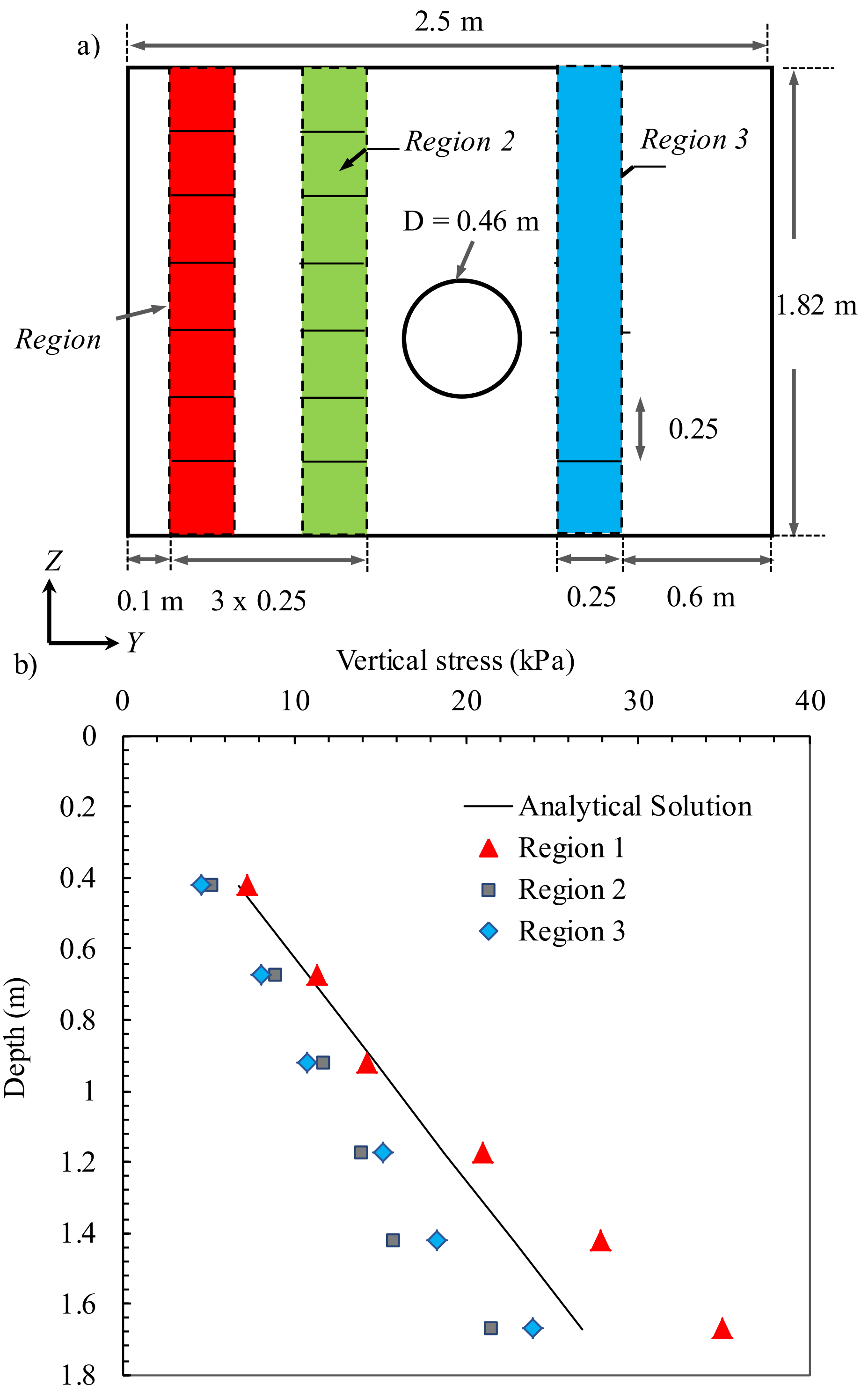

Figure 3-10 comparing in situ stresses with analytical solution: a) selected soil; b) vertical stress distribution

3.7 Evaluating the Applicability of the Closed-Form Solution

The relationship between the pullout force and corresponding pipe displacement is shown in Figure 3-11. To facilitate comparison between the numerical and experimental results, the axial resistance F_A is normalized with respect to soil density (γ'), pipe length (L), depth (H) and diameter (D) as represented by Eq. 3-4.

$$F'_A = \frac{F_A}{\gamma' \times H \times \pi \times D \times L} \qquad 3-4$$

The calculated pullout response (Figure 3-11) shows a peak normalized axial force F'_A of approximately 1.0 at pipe displacement of approximately 9–12 mm with post peak value of 0.89 after reaching axial displacement of approximately 115 mm. The overall response of the soil–pipe system is found to be reasonably captured by the model and the calculated peak value of the pullout force is similar to the measured value with 20% overestimation in post peak resistance. Because the maximum axial soil resistance (pullout force) is of prime importance in this case, and given the simplified nature of the DEM model, the calculated response is considered to be acceptable.

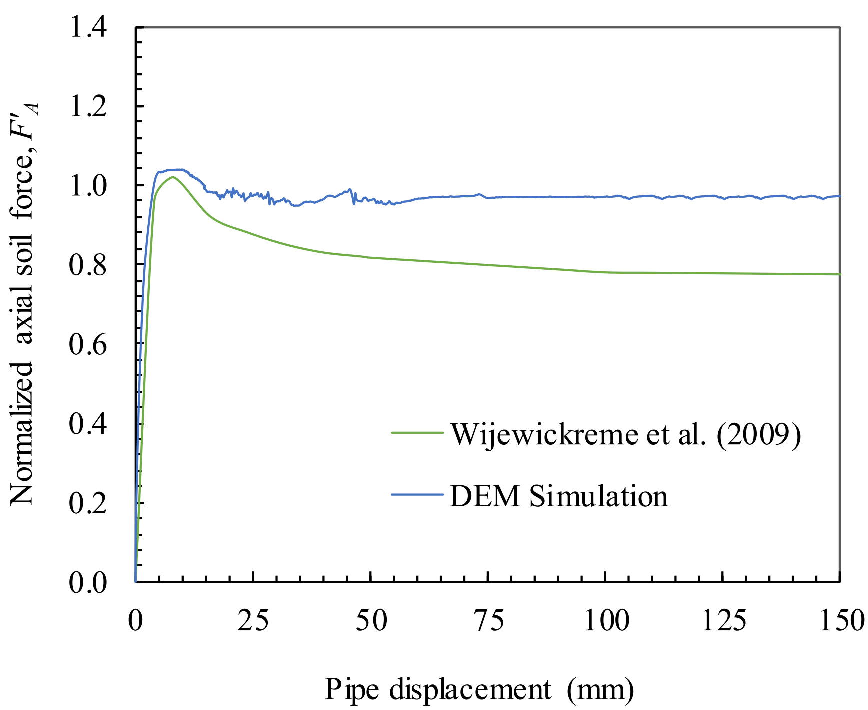

Figure 3-11 Comparison between calculated and measured pullout response of the pipe

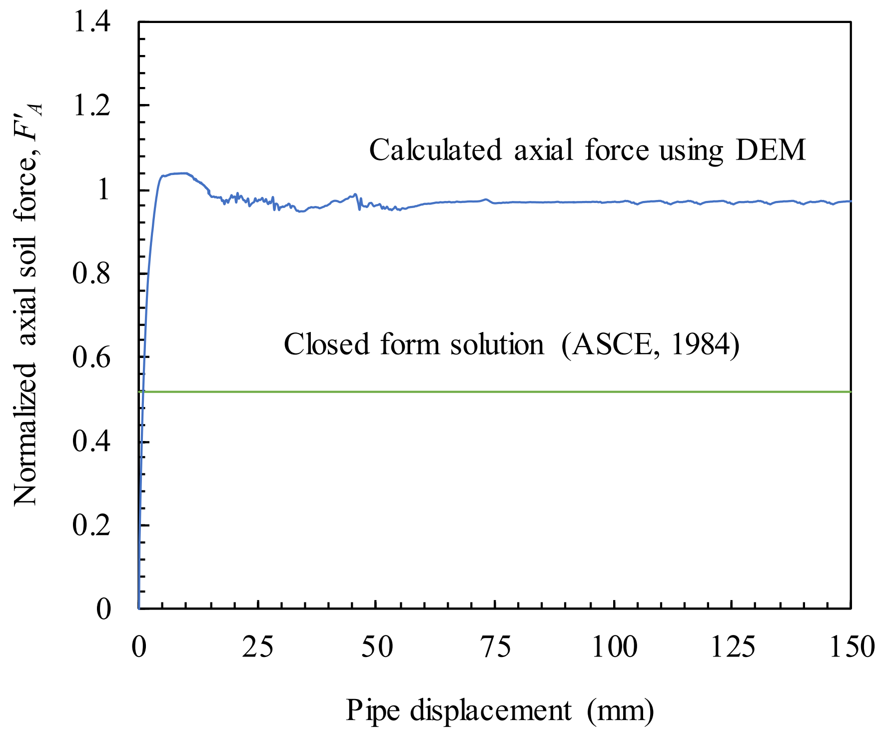

Figure 3-12 Normalized soil load (F'_A) in the axial direction versus pipe displacement

The normalized pullout load (F'_A) is compared with the maximum axial load recommended by ASCE (1984). Eq. 3-1 is used to determine the peak pullout load, F_A , where K_0 value ($K_0 = 1 - \sin\ \varphi'$) is calculated using φ' of 44° and the interface friction angle (δ) is assumed to be 36°. This corresponds to the reported peak friction angle of Fraser River sand. Figure 3-12 shows the normalized axial pullout load (F'_A) obtained using DEM and peak axial soil resistance calculated based on the ASCE recommendation. It can be seen that for the material investigated in this study, the ASCE formula resulted in a significantly lower pullout load as compared to that calculated using DEM. Among the parameters in Eq. 3-1, the use of K_0 value under these loading conditions seems to be unrealistic. The discrepancy between the analytical and numerical solutions arises mainly from the underestimated normal stresses. To investigate the role of normal stresses on the pullout load, the calculated pressure acting on the pipe before (at rest) and during the pullout test (at peak pullout load) are plotted in Figure 3-13. For comparison purpose, the distributions of pressure on pipe before and after pullout are presented on opposite sides of the polar chart. It is clear that normal stresses on the pipe during pullout are higher as compared to the "at rest" condition. It is, therefore, possible to back-calculate the value of K using the average normal stresses acting on the pipe. For the given soil density (dense sand) and pipe depth (γ' of 16 kN/m^3 and H of 1.12 m) the average normal stress on the pipe at the end of the pullout procedure is found to be about 23 kN and the corresponding K value is about 1.6.

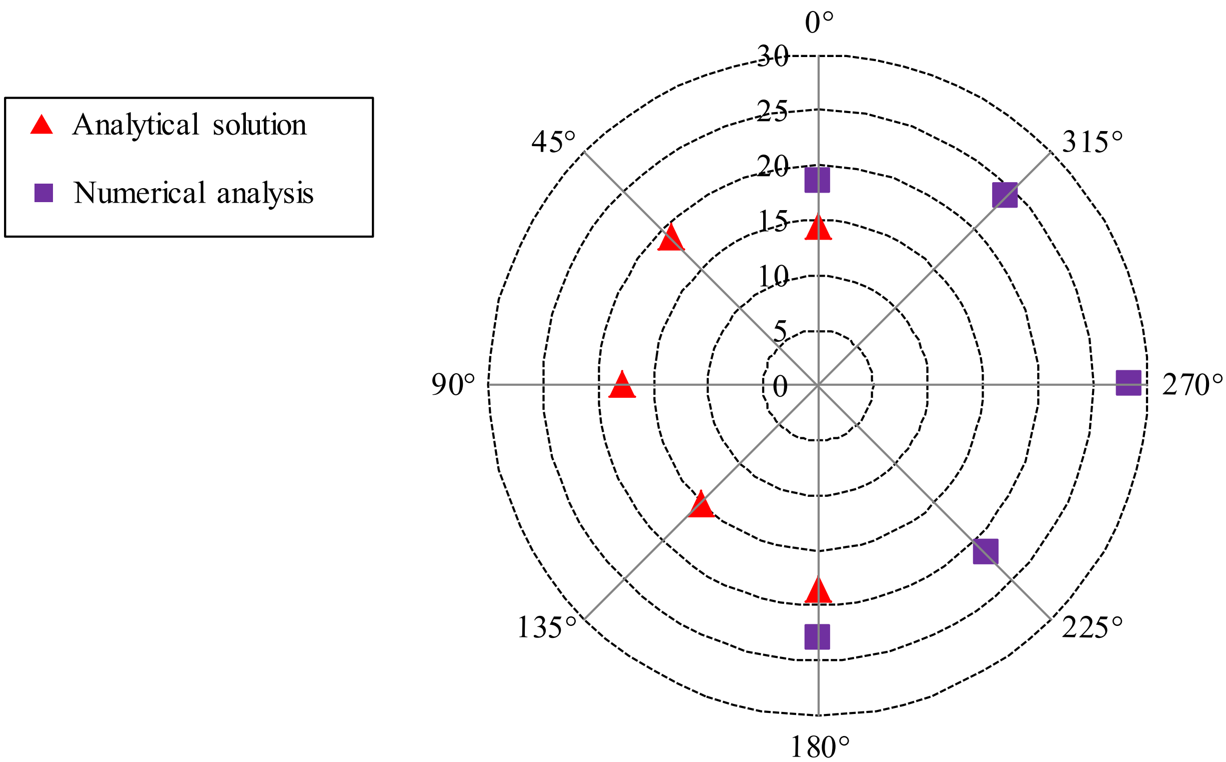

Figure 3-13 Normal stress distribution on the pipe before and after the pullout test (kPa)

Figure 3-14 presents the normalized axial force (F'_A) for different values of K calculated at a constant friction angle between the pipe and the backfill material (δ = 36°). A lateral earth pressure coefficient K of 1.8 was found to correspond to a reasonable agreement between the DEM results and that calculated using Eq. 3-1. The back-calculated value of K based on the average normal stress on the pipe during pullout is found to be equal to 1.6.

It is evident from Figure 3-14 that the using K_o to represent the pressure on the pipe under pullout condition is not suitable, particularly for dense sand. The suggested value by ASCE (1984) for predicting the maximum axial soil resistance may be more suitable for loose to medium backfill material. This can be attributed to the dilation of dense sand that develops in the close vicinity of the pipe under large displacement resulting in a stress state that exceeds the at-rest condition.

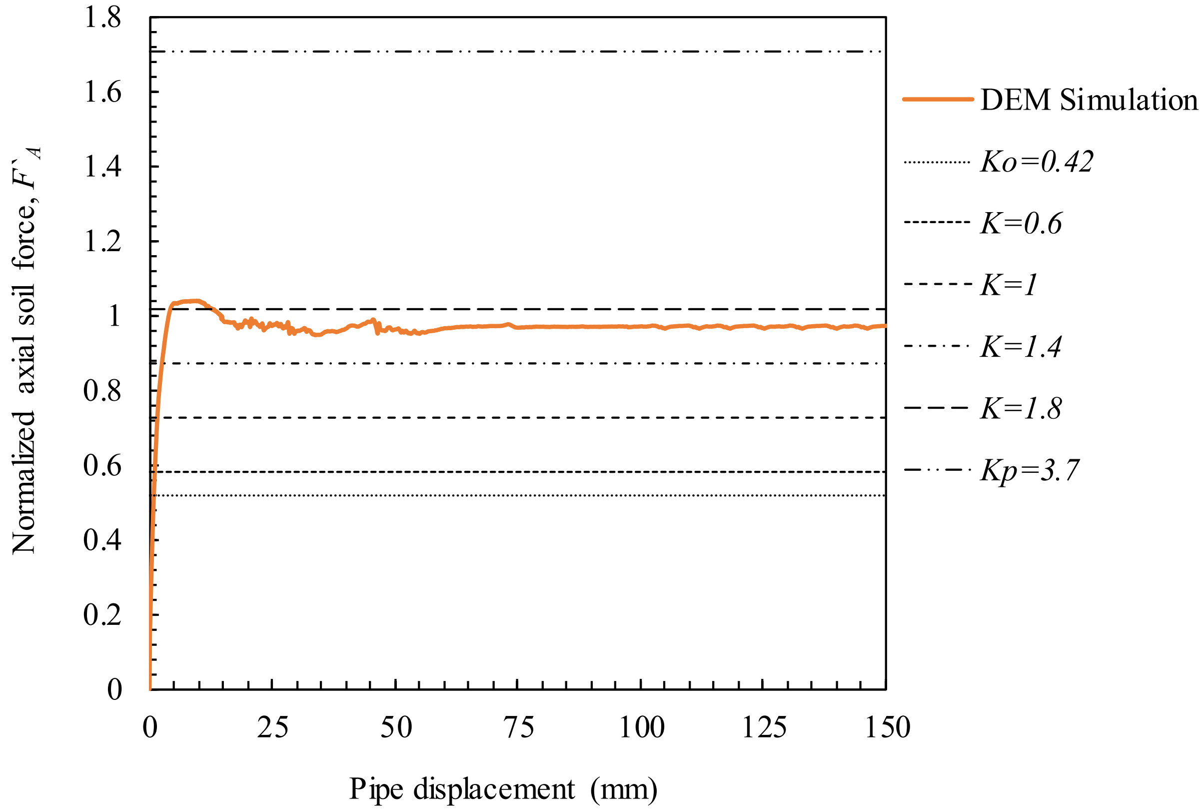

Figure 3-14 Normalized axial soil resistance using ASCE (1984) equation for different K values

3.8 Soil Response to Pipe movement

To illustrate the changes that develop in the backfill material around the pipe as a result of the relative movement, the contact force network before and after the pullout test in both the transverse and longitudinal directions are shown in Figure 3-15 and Figure 3-16, respectively. Each contact force is illustrated by a line connecting the centers of two contacting elements, while the width of the line is proportional to the magnitude of the normal contact force. Figure 3-15a shows that the density of the contact forces is homogeneous around the pipe before applying the pullout load. As the pipe is pulled (Figure 3-15b), soil particles start to move, resulting in volume change and an increase in normal stresses acting on the pipe. This behavior is manifested in the large contact forces observed in the vicinity of the pipe.

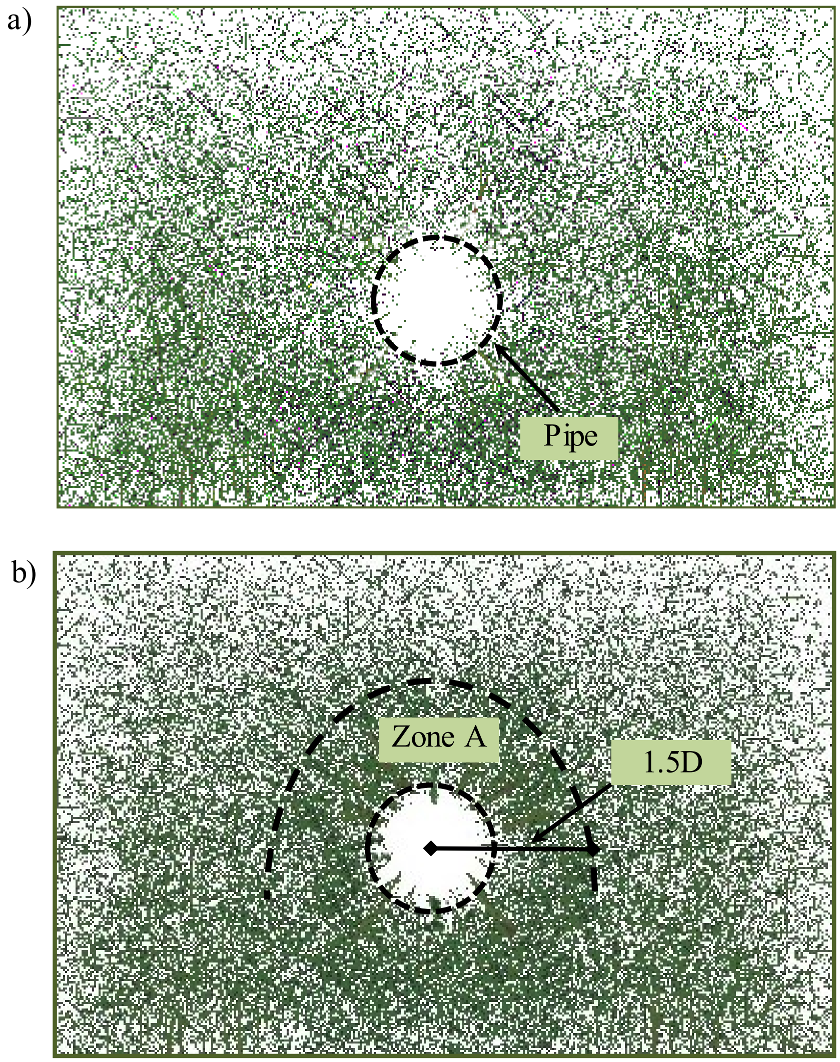

Figure 3-15 Contact force network: a) before pullout; b) after pullout

The pullout effect can be further examined by inspecting the contact force distribution within the soil zones that are most affected by the pullout process. Zone A in Figure 3-15b represents the extent of the disturbed area around the pipe selected by comparing the density of the contact forces around the pipe before and after the pullout process. The shape of this zone resembles a circle with radius of approximately 1.5 times the pipe diameter (1.5*D*). Contact forces are found to be denser and oriented radially within this zone.

Figure 3-16 presents the variation in contact forces in the longitudinal direction looking downward at the soil surface. The results are presented for the initial condition (Figure 3-16a) and after pullout (Figure 3-16b). As the pipe is pulled out, the density of contact forces increased along the pipe (Zone B) with further increase in density near the front face of the box (Zone A), which is consistent with the progressive particle movement in the pullout direction.

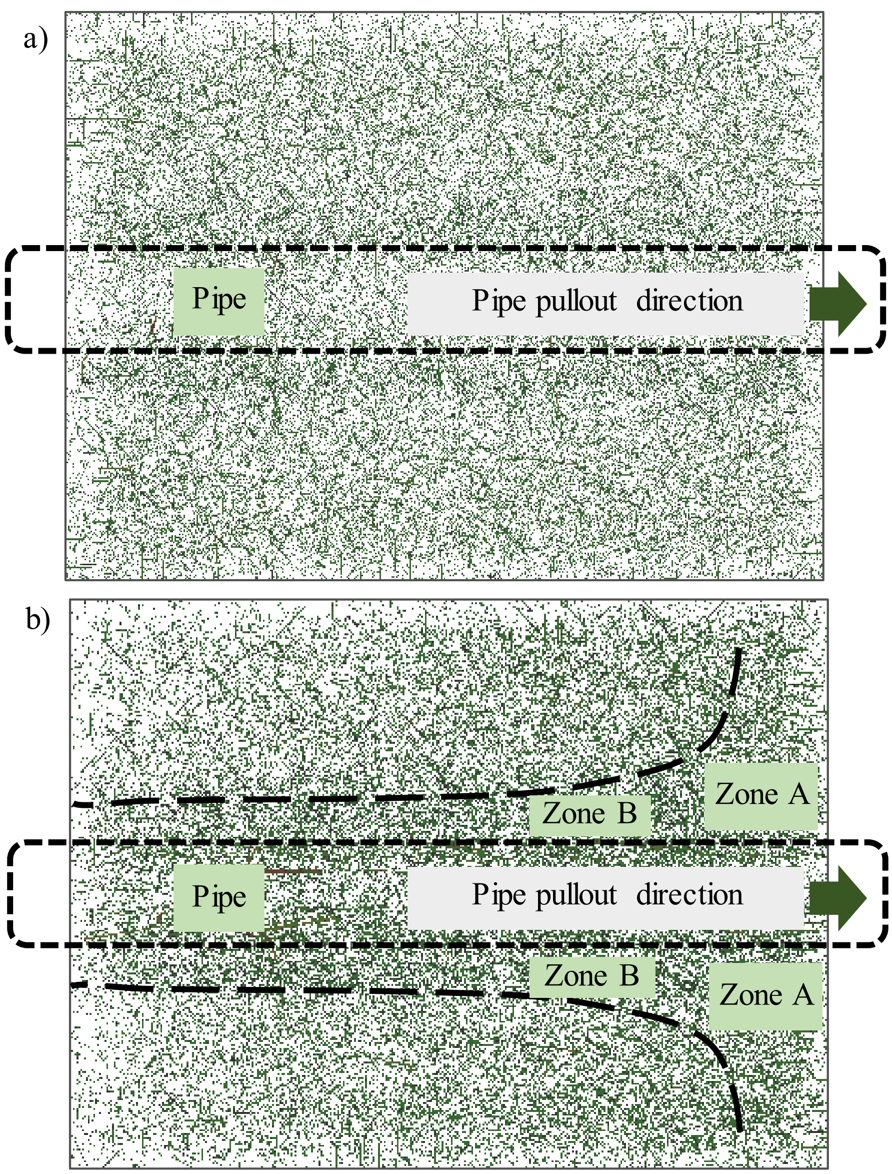

Figure 3-16 Top view of the contact force network: a) before pullout; b) after pullout

Displacement fields across the soil domain in X (pullout) direction are shown in Figure 3-17. Three different displacement fields are plotted at three elevations from the base of the chamber with z = 1.13 m the closest to the pipe crown. The displacement results at the three investigated sections (Figure 3-17a-c) demonstrate that the pullout effect resulted in not only pipe movement but propagated into the surrounding soil as well. It has been found that most of the soil movement occurred in the close vicinity of the pipe and progressed incrementally in the pullout direction.

3.9 Summary and Conclusion

In this paper, a 3D numerical study was conducted to investigate the behavior of a steel pipe buried in dense sand material and subjected to axial soil movements. A discrete-element model was developed and used to simulate the pipe pullout process. Particles were generated to match the particle size distribution of the Fraser River sand and capture some of the important mechanical properties of the material. Calibration was performed to determine the input parameters needed for the discrete-element analysis using triaxial and direct shear test results. The vertical stress distribution within the soil domain as well as the initial radial pressure on the pipe were calculated. Pipe pullout was numerically simulated, and the results compared with the available experimental data and closed-form solutions. The axial soil resistance and normal stress distribution on the pipe were analyzed.

The results of the discrete-element analysis of the pullout test are found to agree with the experimental data. The maximum soil resistance in the axial direction is higher than that predicted using the recommended closed-form solution reported in ASCE (1984).

The measured soil stresses acting on the pipe under the pulled loading condition in dense sand material are significantly higher compared to the initial radial stresses before the pullout. This increase in radial stresses on the pipe can be explained by the dilation of the dense sand during shear deformation. Hence, the soil condition surrounding the pipe is not considered at rest and a new lateral pressure coefficient K (as opposed to K_o) needs to be determined for the calculation of peak axial resistance of the soil. It can be concluded that the equation recommended in ASCE (1984) needs to be used with caution to calculate axial soil resistance on a buried pipe placed in a relatively dense sand material. A stifle lateral earth pressure coefficient (K) should be considered as a function of the soil and pipe properties. The results of this investigation suggest that a range of values between K_o and 2 is considered to be reasonable for pipelines under similar conditions. The numerical modeling approach proposed in this study has proven to be efficient in modeling pipelines subjected to relative soil movement and could be adapted for similar applications.

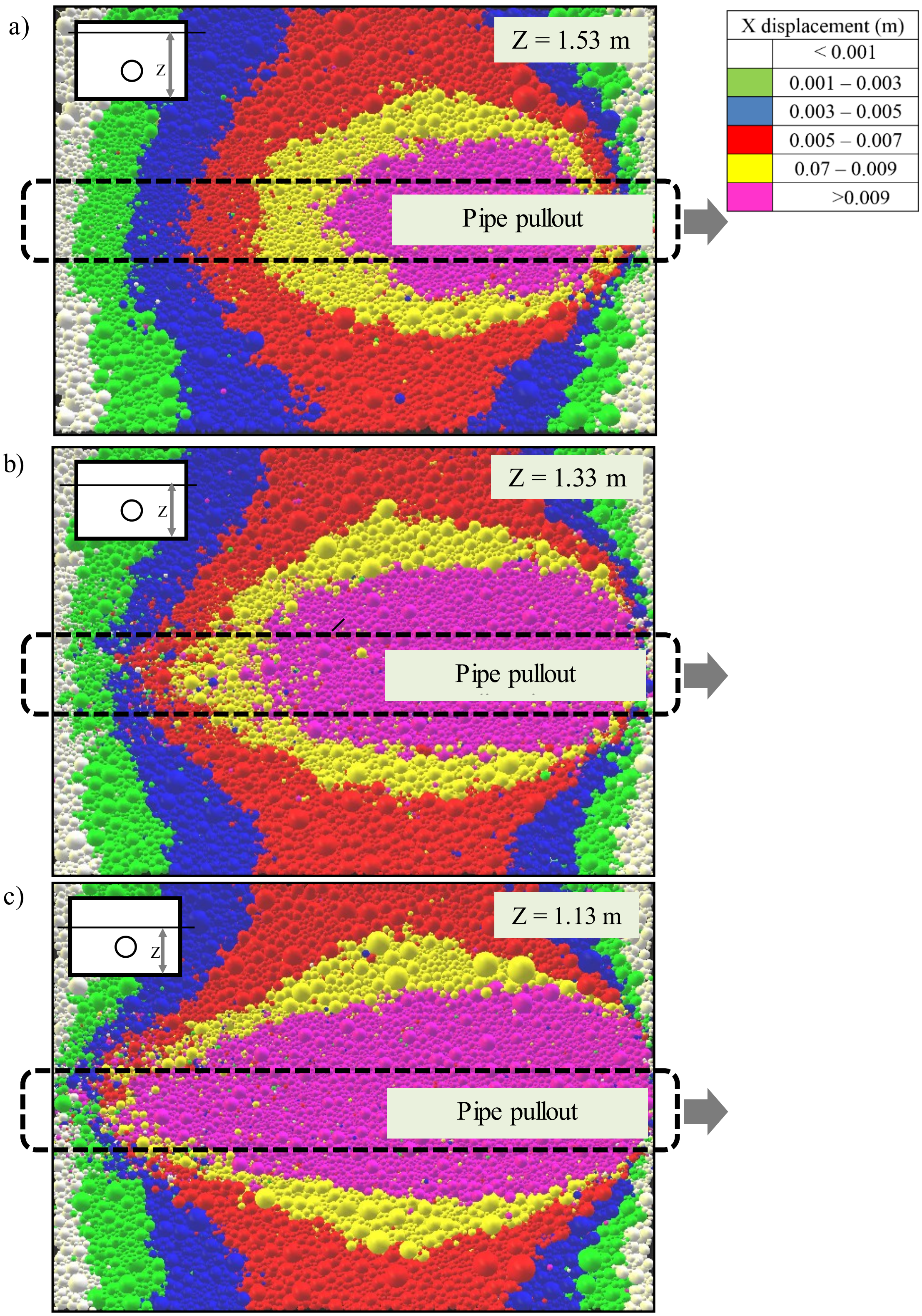

Figure 3-17 Plan view showing the soil particle displacement in the horizontal direction at different elevations: a) z=1.53 m; b) z=1.33 m; c) z= 1.13 m

Preface to Chapter 4

The results presented in the previous chapter demonstrate the efficiency of the discrete element method in studying soil-pipe interaction problems for pipes buried in granular material. It was observed that the maximum soil resistance in the axial direction is higher than that predicted using the current guidelines. This can be attributed to the change in soil stresses acting on the pipe under pullout loading. Hence, a suitable lateral earth pressure coefficient should be determined. In this chapter, a parametric study was conducted using the validated model in the previous chapter to find the controlling factors that affect on the earth pressure coefficient during the pipe pullout. The results were used to develop an expression to estimate the maximum axial soil resistance acting on the pipe structure.

Chapter 4.

Estimating Earth Loads on Buried Pipes under Axial Loading Condition: Insight from 3D Discrete Element Analysis*

Abstract

The response of a buried pipe subjected to relative axial ground movement is investigated in this study using three-dimensional discrete element analysis. A discrete element model that is able to simulate the particulate nature of the granular material and the continuous nature of the pipe was developed. The Micro-parameters of the model were calibrated using triaxial tests. The developed pipe-soil model was validated using experimental data and then used to calculate the pipe response to axial loading under varying soil conditions. A comparison was also made between the calculated response and the available closed-form solutions. Results indicated that, for pipes installed in dense sand, existing solutions may not properly account for the dilative behavior of the soil and hence underestimate the axial soil resistance. A parametric study was performed using the validated model to evaluate the factors controlling the axial soil resistance under these loading conditions. The contributing parameters are found to be the pipe diameter, burial depth, and soil properties. Results of the parametric study were used to develop an expression to estimate the earth pressure coefficient that reflects the dilative nature of the soil. An example is provided to illustrate the use of the proposed expression in estimating the maximum soil resistance to pullout loading.

Keywords: Soil-pipe interaction, pullout capacity, steel pipelines, axial soil resistance, discrete element analysis

---

* A version of this chapter has been published in *International Journal of Geo-Engineering, 9(1), 1-20*.

4.1 Introduction

Buried pipelines are considered to be among the safest, most efficient and economical ways of transporting and delivering natural resources. According to the Canadian Energy Pipeline Association (CEPA), pipelines network transport more than 90 percent of onshore oil and gas from producing fields to markets throughout North America. Therefore, they are considered strategic infrastructure and often referred to as “lifeline” systems. Failures of these systems can have a significant impact on the environment, and the economy as well as public safety.

Damage to buried pipelines may occur due to corrosion, external loading, construction defects and ground movement. Permanent ground deformations (PGD) resulting from seismic activities may lead to lateral spreading, liquefaction, slope movement, and landslides. Although the risk of PGD is usually limited to small regions of the pipeline network, the damage potential could be very high as a result of the induced differential movements (O’Rourke, 1992). A report of the European Gas Pipeline Incident Data Group (2015) has indicated that ground movement represents the fourth major cause of gas pipeline failure with close to half of the reported PGD cases resulting in pipe rupture.

Ground movement induced by slope instability can be classified as shallow or deep-seated depending on the geometry and geotechnical conditions of the slope (Chan and Wong, 2004). The interaction between a buried pipe and a moving slope is a function of the pipe orientation with respect to the slope. When the pipe axis is normal to the direction of soil movement, the pipe is subjected to lateral forces resulting in bending stresses and shear forces in the pipe wall. When the pipe is parallel to the slope, tensile or compressive stresses are induced in the pipe due to the slope movement. This study focuses on estimating the axial load on a pipe subjected to relative axial soil movement.

The interaction between a buried pipe and the surrounding soil is conceptually similar to the shaft resistance of displacement piles. The ultimate axial soil resistance of a buried pipe in granular material is obtained by considering the interaction at the interface between the pipe and the surrounding soil. A commonly used approach to determine the axial soil load F_A for pipes buried in cohesionless sand is that suggested by the American Society of Civil Engineering (ASCE, 1984):

$$F_A = 0.5 \times \gamma' \times H \times (\pi\ D\ L) \times (1 + K_0) \times \tan(\delta) \qquad 4-1$$

where, γ' is the soil effective unit weight, H is the depth to pipe centerline, D is the pipe outer diameter, L is the pipe length, K_0 is the coefficient of earth pressure at-rest and δ is the interface friction angle between the soil and the pipe. Eq. 4-1 has been also recommended by the American Lifeline Alliance (ALA, 2001) and Honegger and Nyman (2004) to calculate axial soil loads on buried pipe in granular material. The term $0.5\pi D\gamma' H(1 + K_0)$ in Eq. 4-1 represents the average effective normal stress acting on the outer perimeter of the pipe, which corresponds to the "at-rest" condition. When lateral strains develop in the soil due to the relative movement between the soil and the pipe, normal stresses on the pipe increase compared to the at-rest condition and consequently Eq. 4-1 would underestimate the axial soil resistance. Several researchers (e.g. Paulin et al., 1998, Karimian, 2006, Weerasekara, 2008, Meidani et al. 2017) reported significant discrepancies between the predicted values calculated using Eq. 4-1 and the experimentally measured axial soil resistance. It was also found that the peak axial pullout force for pipelines in dry dense sand is several times higher than those obtained using the closed-form solutions. The increase in axial pullout force is attributed to the increase in normal stresses due to the dilatant behaviour of the sand under interface shear deformations. A parameter K was proposed instead of K_0 in Eq. 4-1based on experimental data to account for the increase in the radial soil stresses acting on the pipe.

In this study, three-dimensional (3D) discrete element models are developed and used to simulate large-scale pullout experiments on pipes in granular material. The model is first calibrated using experimental data and then used to carry out a parametric study to evaluate the effect of soil and pipe parameters on the soil resistance and the associated pullout forces. The results from these numerical simulations are then used to derive an expression that could be used to estimate an appropriate earth pressure coefficient that predicts the maximum axial soil resistance in these conditions.

4.2 Modeling buried structures subjected to soil movements

The response of buried pipes to different modes of ground movements has been extensively investigated in the last few decades (e.g. Newmark and Hall, 1975, Trautmann and O'Rourke, 1983, O'Rourke and Nordberg, 1992, Honegger and Nyman, 2002, Chan and Wong, 2004, Karimian, 2006, Weerasekara et al., 2008, Wijewickreme et al., 2009, Daiyan et al., 2011, Almahakeri et al., 2016). Roy et al. (2015) used finite element (FE) analysis to model soil-pipe interaction in dense sand subjected to lateral ground displacements. Different soil models were evaluated, and a parametric study was performed to examine the effect of both the pipe and soil properties on the response of the soil-pipe system. Zhang et al. (2016) performed FE simulation to study the mechanical behavior of buried pipes crossing landslide zones. Despite the effectiveness of the FE analysis in studying this class of problems, modelling granular material and capturing particle movements during the pullout process is challenging using conventional continuum approaches (Guo and Stolle, 2005).

As an alternative to continuum approaches, the discrete element method (DEM) has been used by researchers to model granular material under large deformation. The method was first proposed by Cundall and Strack (1979) and was proven to be efficient in capturing the behavior of granular material. Tran et al. (2013) developed a finite-discrete element framework for the 3D modeling of geogrid-soil interaction under pullout loading condition. The results demonstrated the capability of the coupled model to analyse this class of soil-structure interaction problems. In addition, Tran et al. (2014) conducted discrete element analysis and experimental studies to determine the earth pressure distribution acting on cylindrical shafts experiencing large soil movement. Results confirmed the capability of the DEM in solving geotechnical engineering problems involving structural elements in moving granular materials. Ahmed et al. (2015) investigated the distribution of earth pressures on buried pipes overlain by geogrid layer using finite-discrete element analysis. The results allowed for the evaluation of the effect of soil reinforcement on the radial earth pressure acting on the pipe. Rahman and Taniyama (2015) conducted 3D discrete element analysis to calculate the response of a buried pipeline subjected to fault movement. Meidani et al. (2017) evaluated the response of a buried steel pipe in granular soil to large ground movement using 3D discrete element analysis. Results confirmed the suitability of this numerical approach in solving soil-structure interaction problems under large deformation.

The above studies provided an insight into the response of buried structures to large soil movement using both finite and discrete element analysis. However, further investigations are needed to develop a better understanding of the role of different parameters on the response of rigid pipes to axial soil movement and propose an expression that could be used by practitioners to estimate the resistance of dense backfill material to pullout loading.

4.3 Description of the numerical model

The results of the pullout experiments performed on a buried steel pipe in Fraser River Sand reported by Karimian (2006) are used in this study to develop and calibrate the discrete element model. The dimensions of the soil container are 1.8 m in height, 2.5 m in width and 3.8 m in length. Graded Fraser River sand with a unit weight of 16 kN/m^3 (D_r = 70%) and d_{50} = 0.22 mm was used as a backfill soil. The solid line in Figure 4-1 represents the particle size distribution of this soil. The mechanical characteristics of the backfill material have been reported based on triaxial tests conducted under confining stress levels that vary from 15 to 50 kPa. Table 4-1 summarizes the sand properties used in the experiments. The steel pipe has an outside diameter of 46 cm and a wall thickness of 13 mm which represents a ring stiffness (EI / r^3) of 4.2E6 (kN/m). This stiffness level prevents the generation of significant axial straining in the steel pipe during the pullout. The interface friction angle (δ) between the pipe surface and the backfill material was reported to be 36 degrees. The pipe was embedded in a 0.7 m layer up to the springline and covered with 1.15 m of backfill (H/D =2.5). The pipe was pulled out at a fixed rate of 5 mm/s and the pullout force was continuously measured.

4.3.1 DEM specimen generation

The discrete element model is created to reproduce the geometry and test procedure of the experiment. Up-scaled spherical particles are used to model the sand to reduce the number of particles and the required computation time. Based on the results of the scale-effect discussed before and considering a minimum L/d ratio of 30, particle scaling factors of 90 and 140 are chosen for the analysis and the generated samples follow the grain size distribution curves shown in Figure 4-1. The DEM model used to simulate the experiment is divided into four zones (see Figure 4-2). *Zone 1* represents the area immediately around the pipe and contains smaller particles that have scale factor of 90. This is important to improve the contact between the soil and the pipe. The outer *Zones 2*, 3 and 4 located away from the pipe contain larger size particles (scale factor of 140) as the stress gradients are expected to be much lower. Using these scale factors, a total number of 265,000 spheres are generated to create the soil specimen. The fabric tensor of the sample was investigated following the approach proposed by Dang and Meguid (2010). It was found that the fabric tensor components are almost identical in all directions, which confirms that the discrete element sample is homogeneous.

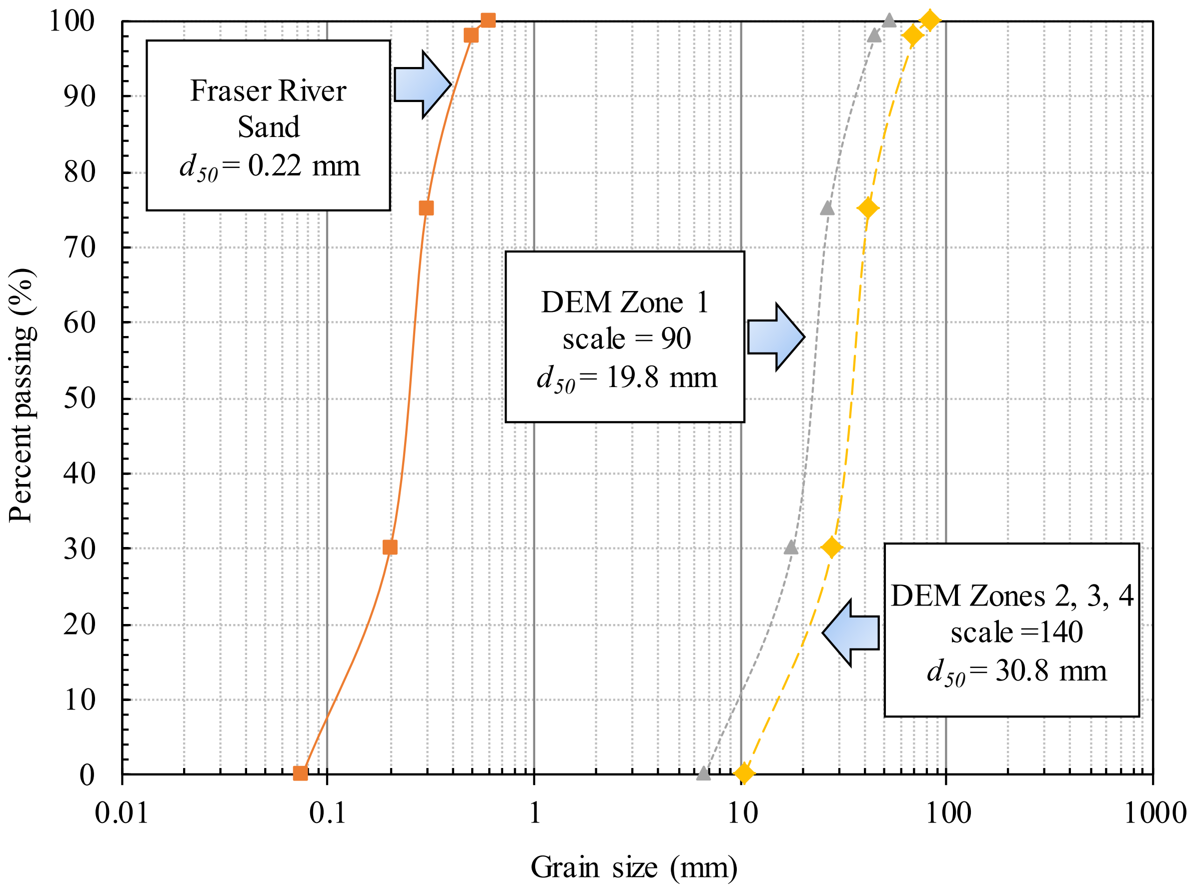

Figure 4-1 Grain size distributions

Table 4-1 Soil properties of backfill material

Parameter	Value
Specific gravity	2.72
Young's modulus, E_i (MPa)	40
Unit weight (kN/m^3)	16
Internal friction angle, φ (Degree)	45
Cohesion (kN/m^2)	0
Poisson ratio, υ	0.3
Porosity, n	0.41

The radius expansion packing method (Itasca, 2004) is employed in this study to generate the discrete element particles. First, a box of non-contacting spheres is created in each zone following the particle size distribution given in Figure 4-1. Particle radii are increased to match the porosity (0.41) of the backfill material. According to O'Sullivan (2011), radius expansion method tends to generate specimens with isotropic stress state. To eliminate this effect, each zone is allowed to reach equilibrium independently. All four zones are then assembled together under gravity until equilibrium is re-established. A cut-out perspective of the created 3D model is presented in Figure 4-3. The pipeline is modeled using 1216 facet discrete elements arranged in a hexdecagonal shape. Facets are triangular flat discrete particles that follow the same contact laws used of spherical particles. This means that facet-sphere collision is treated similar to sphere-sphere collision (Šmilauer et al. 2010). The length of the pipe is created that it is longer than the length of the chamber to allow for constant and continuous interactions between the pipe and soil during the pullout process. A close view of the pipeline and facet elements is presented in Figure 4-3.

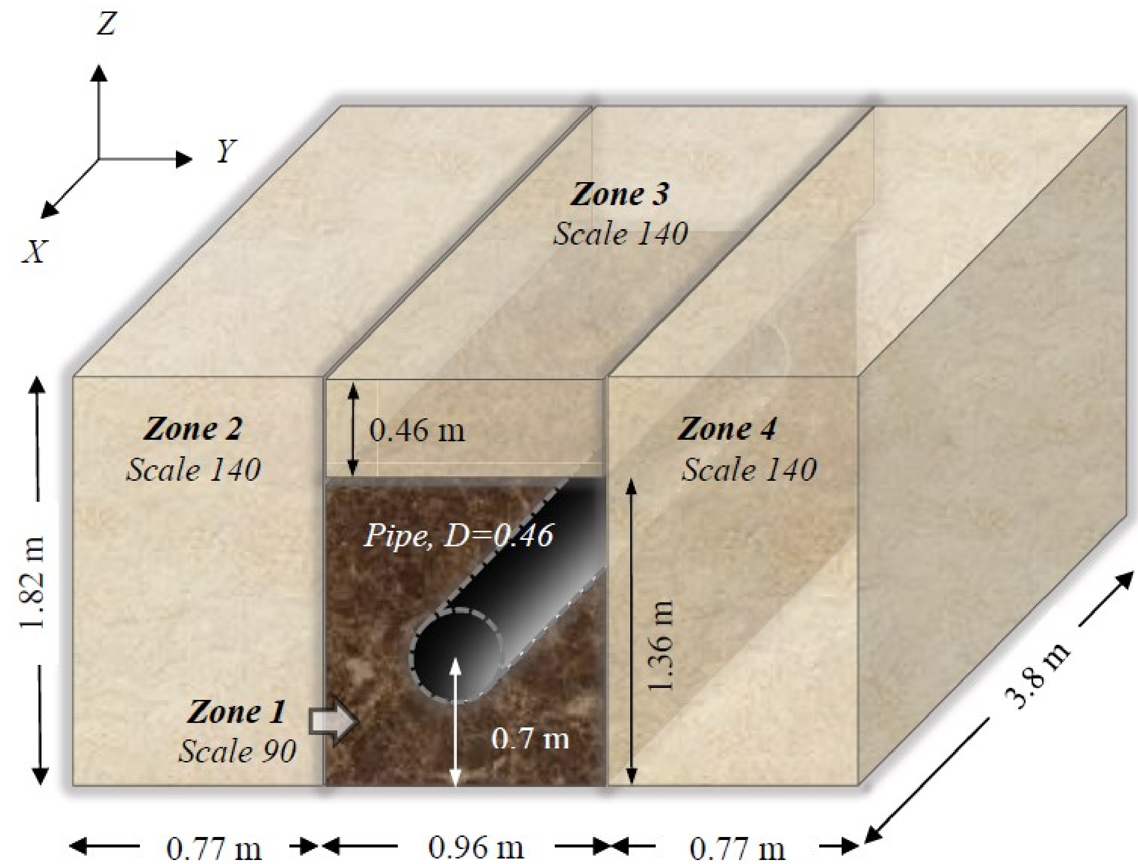

Figure 4-2 Different particle size zones used to generate the discrete element model

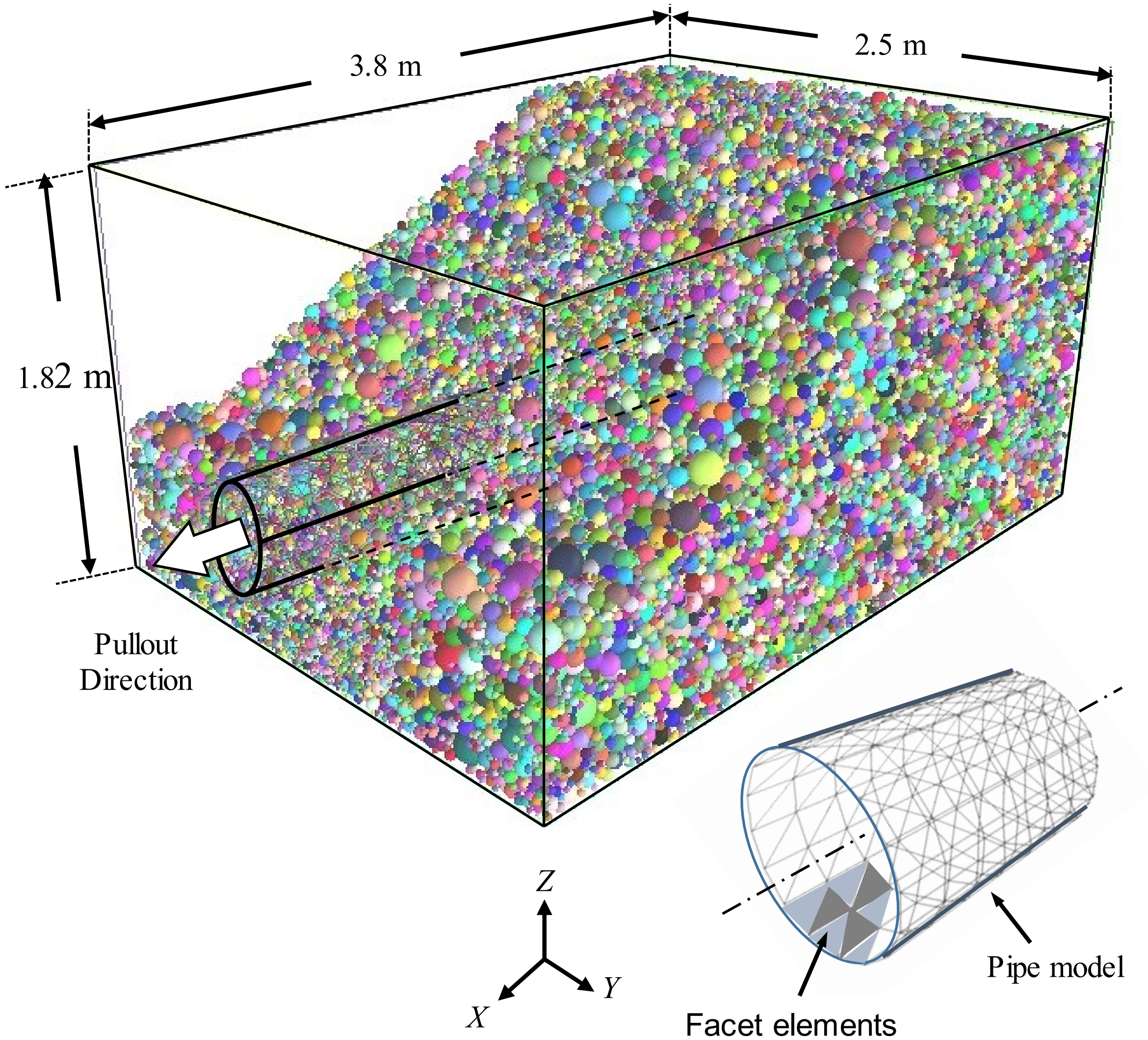

Figure 4-3 Cut-out view of the model showing the pipeline and the surrounding soil

4.3.2 Model calibration

The input parameters for the discrete element analysis are determined by modeling triaxial tests and matching the results with the reported experimental data (Karimian, 2006). The detailed procedure of the calibration has been described in section 3.4 (Material Calibration). A summary of the soil input parameters is presented in Table 4-2.

Table 4-2 Input parameters used in the numerical analysis

Parameter	Value
Density (kg/m^3)	2720
Particle modulus, E (MPa)	150
K_T/K_N ratio, α	0.7
Micro friction angle, φ_{micro} (Degree)	35
Rolling resistance coefficient (β_r)	0.15
η_r	1
Damping ratio	0.2

4.3.3 Modeling the pullout experiment

Following the generation of the discrete particles in the predefined zones (see Figure 4-2), the pipe is allowed to freely move under gravity before applying the pullout load. The accuracy of the created model is evaluated by calculating the radial earth pressure acting on the pipe and comparing the results with existing analytical solution (Hoeg, 1968). The radial earth pressure on the pipe is calculated at five different locations (Invert, lower haunch, springline, upper haunch and crown) and then compared with the values obtained using the numerical model. Table 4-3 summarizes the radial earth pressure values at these five locations. Although earth pressure was slightly overestimated near the springline, the overall distribution was consistent with the analytical solution. This demonstrates the effectiveness of the discrete element model in representing the interaction of the backfill material with the buried pipe. The difference in pressures at the springline and haunches is attributed to sensitivity of the contact pressures at these locations to the level of soil compaction around the pipe. Similar observations were made by Karimian, (2006) and Ahmed et al., 2015.

The pullout test is simulated using a displacement control scheme with no friction between the box walls and the discrete particles, which is consistent with the boundary conditions used in the experiments. The pipe is pulled out in the analysis following the same displacement rate used in the experiment (5 mm/s). Karimian (2006) found that when the pullout rate ranges from 2 mm/s to 50 mm/s, the difference in peak axial force is negligible. Given the rate used in the analysis (5 mm/s), the effect on the calculated pullout load is expected to be insignificant. The effect of the friction angle of the facet elements on the pullout force was evaluated using a parametric study (Meidani et al., 2017). Results indicated that the friction coefficient of the facet elements can affect the overall response of the model. Therefore, the friction angle needs to be determined accurately using experimental results. A friction angle of 30^{o} is found to bring the numerical results as close as possible to the experimental data. Figure 4-4 compares the measured and calculated axial soil resistance (F_A) for a wide range of pipe displacements. The model seems to be able to accurately predict the axial resistance up to the peak value. Post peak, however, the model over-predicts the response by about 20%. Since the focus of this study is on predicting the maximum axial soil resistance (pullout force), the performance of this simplified numerical model is judged to be adequate.

Table 4-3 Comparison of calculated pressures with analytical solutions

Initial earth pressure (kPa)		
Location	Hoeg's analytical solution	Discrete element analysis
Crown	17	15
Upper haunch	16	18
Springline	14	17
Lower haunch	16	15
Invert	17	17

4.3.4 Evaluating the effect of different parameters on the pullout force

The axial soil resistance calculated using the closed-form solution (Eq. 4-1) is plotted in Figure 4-4. It is clear that Eq.4-1 significantly underestimates the pullout force. This difference is attributed to the increase in normal stresses acting on the pipe during the loading process, which is not accounted for in Eq. 4-1. The increase in normal stresses is generally explained by the dilatant behavior of the dense sand mobilized by the relative displacement between the sand material and the moving pipe (Meidani et al., 2017). Since K_0 parameter in Eq. 4-1 controls the average normal stresses on the pipe, a parametric study is performed using DEM to investigate the effect of different soil and pipe parameters on the pullout resistance and to propose a suitable expression for K_0 (K^* hereafter). The value of the modified earth pressure coefficient K^* is bounded by K_0 and K_p (the passive earth pressure coefficient).

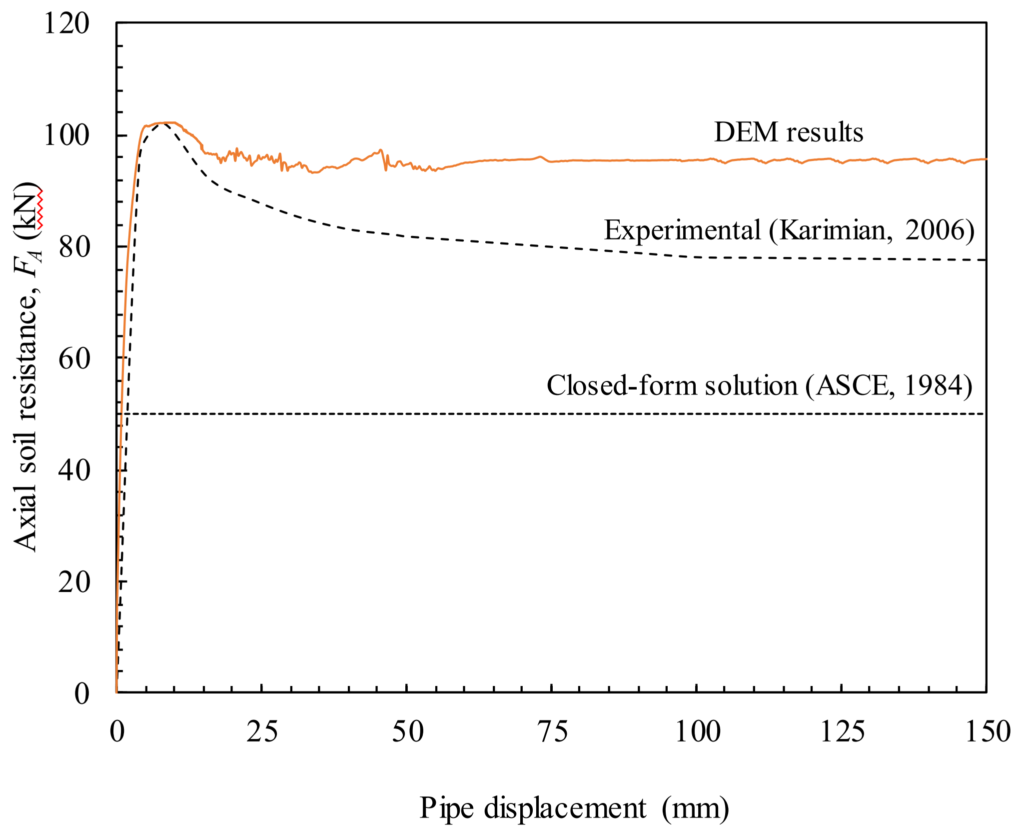

Figure 4-4 Relationship between axial soil resistance and pipe displacement using different methods

The investigated parameters include: 1) The burial depth (H); 2) The soil friction angle (φ); 3) The soil Young's modulus (E_i); 4) The pipe diameter (D); and 5) The friction angle between the pipe and the soil (δ). The parametric study is performed by varying each parameter independently using the range of values given in Table 4-4. It should be noted that the soil modulus and friction angle in Table 4-4 are macro parameters. Simulations of triaxial tests were performed to determine the DEM micro parameters that correspond to the parameters listed in the table. The steps taken in developing the expression are listed below:

1- Substituting the numerically calculated pullout resistance for each case in Eq. 4-1 a value of K^* is back-calculated.

2- A general relationship between K^* and each of the examined parameters is established.

3- Combining all results and knowing the interaction of each parameter with K^*, a final expression is extracted using a multivariate regression analysis.

Table 4-4 Different soil and pipe parameters used in the parametric study

Parameter	Examined range of values
Burial depth, H (m)	1.1, 1.35, 1.6, 1.85, 2.1, 2.35, 2.6, 2.85
Soil Young's modulus, E (MPa)	40, 45, 50, 55
Soil friction angle, φ (Degree)	41, 43, 45, 47
Interface friction angle, δ (Degree)	22.5, 27, 31.5, 36, 41, 45

4.4 Results and discussions

4.4.1 Effects of pipe burial depth (H)

Burial depths are varied from 1.1 m to 2.85 m which corresponds to overburden pressures that range from 17 kPa to 46 kPa at the springline. The soil and pipe properties summarized in Table 4-2 are used in the analysis keeping the pipe diameter constant at 46 cm. As illustrated in Figure 4-5 Effect of burial depth on: a) pullout force; b) modified earth pressure coefficient, the pullout load (F_A) increases almost linearly with the increase in burial depth, which is consistent with the expected increase in radial pressure acting on the pipe.

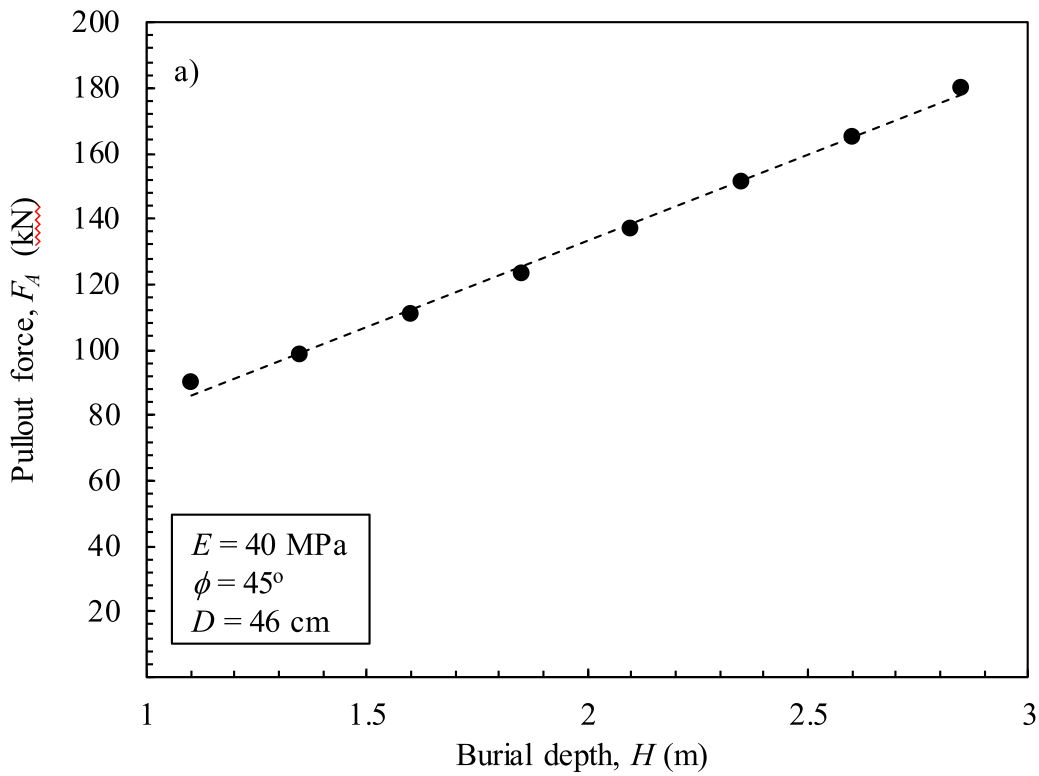

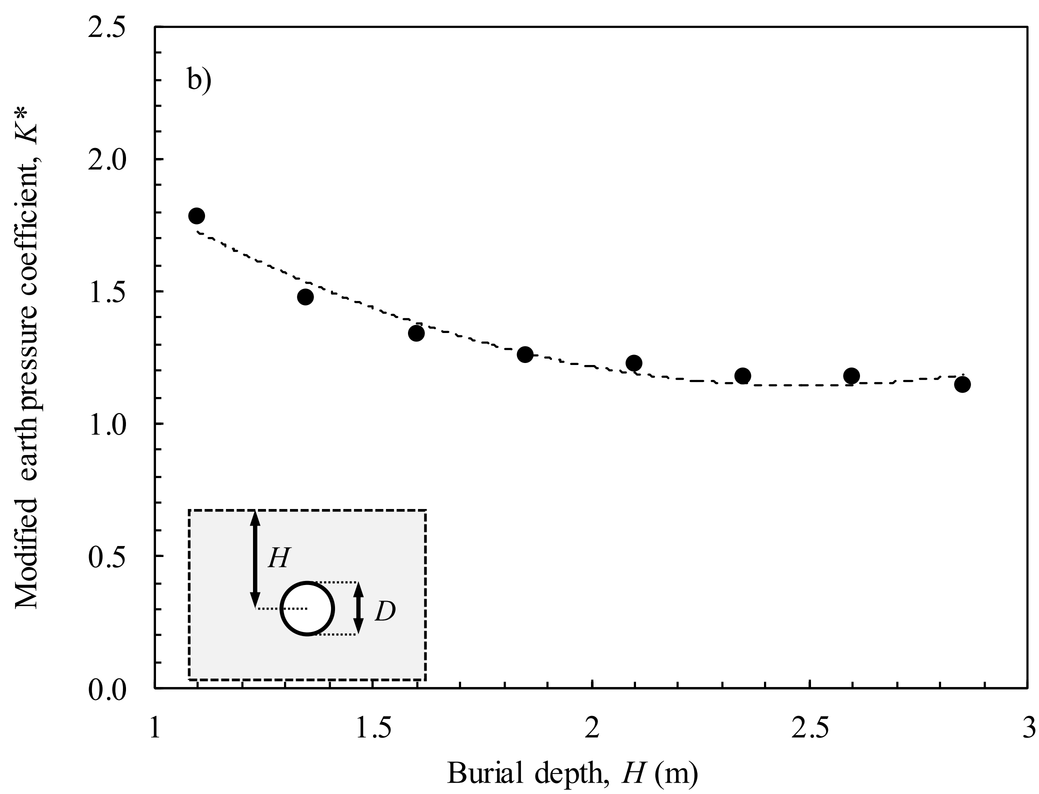

Figure 4-5 Effect of burial depth on: a) pullout force; b) modified earth pressure coefficient

Given the properties of both the soil and the pipe, the corresponding K^* value is calculated using Eq. 4-1 and the results are presented in Figure 4-5b. For the investigated properties, K^* was found to decrease from 1.8 to 1.2 as the burial depth increased from 1.1 m to 2.85 m, respectively. No significant change in K^* was found with further increase in burial depth. This is in agreement with the previously published results such as those reported by Karimian (2006) and summarized in Table 4-5.

Table 4-5 Variation of K with burial depth (Karimian, 2006)

	Dilation level (Expansion at pipe surface) in mm		
	1	1.5	2
Burial depth (m)	Calculated K values		
0.93	2.3	2.6	2.8
1.86	2.2	2.4	2.6
2.8	2.1	2.3	2.4

4.4.2 Effects of soil modulus (E_i)

Four different E_i values were examined, namely, 40, 45, 50 and 55 MPa, which represent a range of values that are suitable for dense Fraser River sand material (Karimian, 2006) under effective stress range between 15 and 50 kPa. Each of these values is used in the analysis along with three different burial depths, 1.6 m, 2.1 m and 2.85 m. Figure 4-6a shows the relationship between the pullout force (F_A) and the soil modulus for the examined burial depths. Pullout force generally increased with the increase of burial depth. For a given value of H, the increase in Young's modulus resulted in a slight increase in the pullout force. Given the pipe diameter and backfill properties, K^* is calculated for various soil moduli and the results are presented in Figure 4-6b. The modified earth pressure coefficient, K^* was found to decrease with the increase in burial depth. It was also found that the stiffer the soil (increasing elastic modulus), the higher the calculated K^* coefficient.

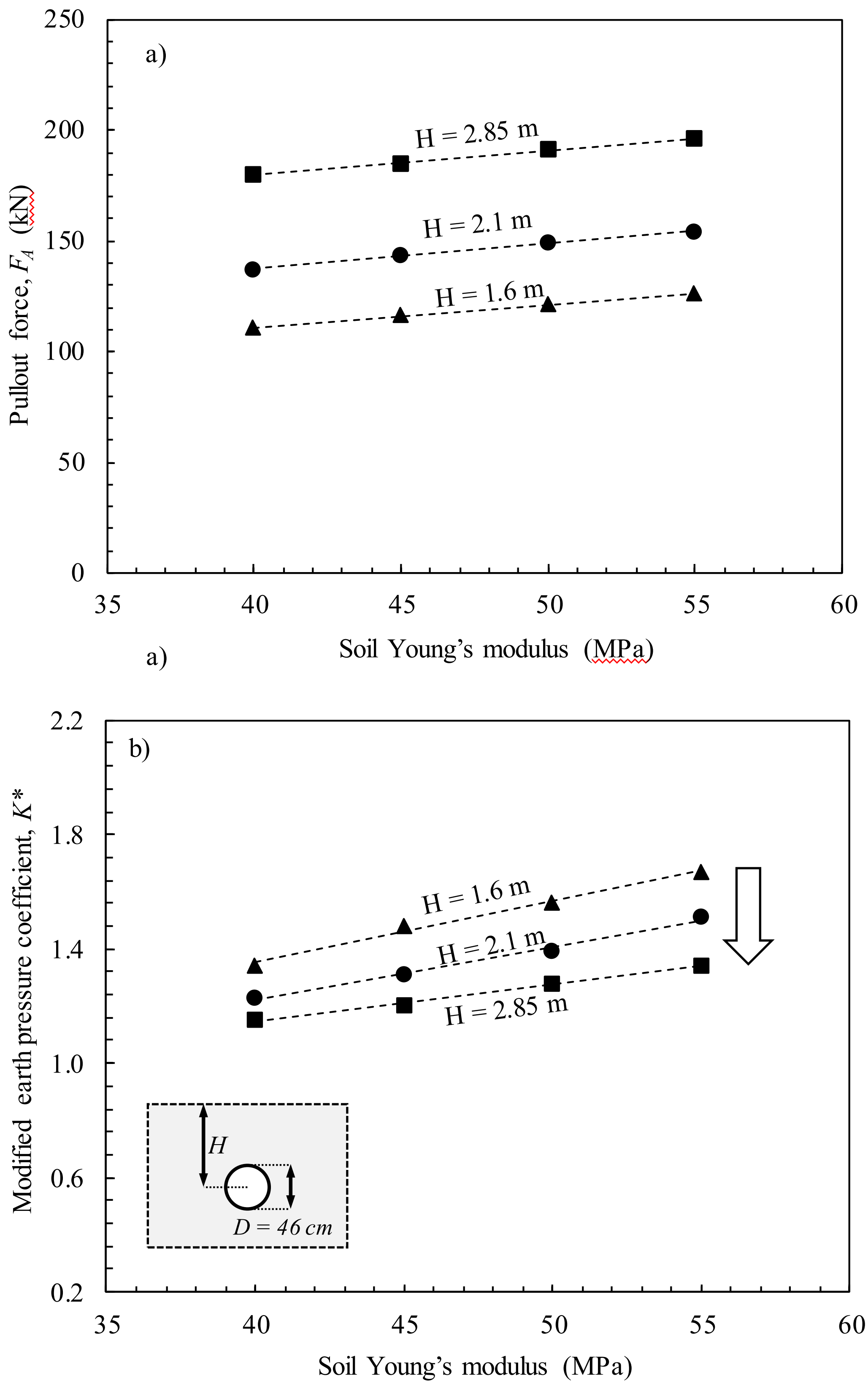

Figure 4-6 Effect of soil modulus on: a) pullout force; b) modified earth pressure coefficient

The above results indicate that the soil surrounding the pipe became stiffer as the radial pressure increased during the pullout process. This is consistent with the cylindrical cavity solution of Gibson and Anderson (1961):

$$\Delta\sigma_n = \frac{4\ G}{D} \times \Delta t \qquad 4-2$$

where G is the soil shear modulus, D is the pipe diameter and Δt is the thickness of the shearing zone. This equation shows that the increase in normal stresses acting on the pipe due to soil dilation ($\Delta\sigma_n$) is proportional to the shear stiffness of the soil (G). Consequently, increasing the soil stiffness generally results in more pressure on the pipe

4.4.3 Effect of soil friction angle (φ)

In this part of the analysis, the Fraser River sand friction angle is increased in four increments (41, 43, 45 and 47 degrees) and its effect is evaluated for the investigated soil depths (1.6 m, 2.1 m and 2.85 m). Soil modulus and pipe diameter are kept constant at assigned values of 40 MPa and 0.46 m, respectively. The interface friction angle (δ) is adjusted to maintain the pipe roughness at a value of 0.8 of the soil friction angle throughout the analysis. As depicted in Figure 4-7a, the pullout load slightly increased with the increase in soil friction angle for the three investigated burial depths. When the friction angle increased about 6^o, the soil resistance (represented by F_A value) increased about 17%. Since the soil friction angle is directly related to the coefficient of earth pressure at rest (K_0), the modified earth pressure coefficient K^* is normalized in Figure 4-7b with respect to K_o. It is also found that for a given soil height, K^*/K_o ratio increased with the increase in friction angle. In addition, increasing the burial depth resulted in a slight decrease in the earth pressure coefficient ratio as illustrated in Figure 4-7b.

4.4.4 Effect of interface friction angle (δ)

Six different interface friction angles (22.5, 27, 31.5, 36, 41, 45 degrees) are examined. These values represent δ/φ ratios that range from 0.5 to 1 which are typical for sand-steel contacts (ASCE, 1984). To allow for the role of interface friction angle to be investigated, the rest of the variables including the pipe diameter, burial depth, particles friction angle and soil Young's modulus were kept constant. The results showed that the pullout force significantly increased as the interface friction angle increased as illustrated in Figure 4-8a. It was also found that changing the interface had little effect on K^* which remained constant for the investigated cases (Figure 4-8b). This is in agreement with the observations made by Karimian (2006) based on a sensitivity analysis of K value with respect to the soil parameters (e.g. interface friction).

4.4.5 Effect of pipe diameter (D)

The effect of pipe diameter on the modified earth pressure coefficient K^* is evaluated using the results reported by Karimian (2006) for the same experiments investigated in this study. In addition to the pipe diameter used in the experiments (46 cm), two other diameters are examined, namely, 23 cm and 92 cm. Burial depth was kept at 1.1 m with internal friction angle of 45^{o} and Young's modulus of 40 MPa. It should be noted that the wall thicknesses of the pipe were chosen to keep the rigidity of the pipe consistent in all investigated cases. The results presented in Figure 4-9 showed that K^* is inversely proportional to the pipe diameter. Since the normal pressure acting on the pipe due to soil dilation ($\Delta\sigma_n$) is a function of K^* (Eq. 4-2), it can be concluded that $\Delta\sigma_n$ is also inversely proportional to the pipe diameter.

4.4.6 Development of an expression for *K**

An expression for the maximum axial soil resistance against the movement of a steel pipe buried in dense sand is developed in this section based on the previous results. The proposed expression is a modification of Eq. 4-1 with K^* replacing K_o. The modified earth pressure coefficient K^* is a function of the burial depth (H), soil modulus (E_i), soil friction angle (ϕ) and pipe diameter (D). The modified expression can be written as follows:

$$F_A = 0.5 \times \gamma' \times H \times (\pi\, D\, L) \times (1 + K^*) \times \tan(\delta) \qquad 4-3$$

K^* is expressed by

$$K^* = C \times K_o \times \left({}^{E}/_{\gamma\, H}\right)^{\alpha} \times \left({}^{\varphi}/_{45}\right)^{\beta} \times \left({}^{\Delta t}/_{D}\right)^{\theta} \qquad 4-4$$

where K^* is the modified coefficient of earth pressure, C is constant, K_o is the coefficient of earth pressure at rest, E is the soil Young's modulus, γ is the soil unit weight, H is the pipe burial depth, φ is the soil friction angle, Δt is the shear zone thickness and D is the pipe diameter.

Previous research related to shear zones developing in granular materials (e.g. Roscoe 1970, Bridgewater 1980) revealed that the thickness of the active shear zone (Δt) can be estimated as $10d_{50}$ where d_{50} is the median grain size of the soil. Karimian (2006) observed that the thickness of the active shear zone surrounding the pipe is in the order of 1.2 mm to 2.8 mm. This is in agreement with $10d_{50}$ for Fraser River sand (d_{50} = 0.22 mm) and consequently the thickness of the shear zone is set here to 2.2 mm in Eq. 4-4.

Using the data obtained from "Effects of pipe burial depth (H)" through "Effect of interface friction angle (δ)" sections and utilizing multivariate regression analysis, the exponent α is calculated as 0.38. This parameter accounts for the interaction between the soil stiffness and the vertical stresses at the springline of the pipe. The two other exponents, β and θ, are determined as 1.39 and 0.42, respectively, and the constant C is found to be 2.75. The final expression can then be written as:

$$K^* = 2.75 \times K_o \times \left({}^{E}/_{\gamma H}\right)^{0.38} \times \left({}^{\varphi}/_{45}\right)^{1.39} \times \left({}^{\Delta t}/_{D}\right)^{0.42} \qquad 4-5$$

4.4.7 Validation of the proposed expression

The validation was performed in two steps: (1) The changes in pullout force with the modified earth pressure coefficient were calculated numerically as well as using the proposed expressions; (2) a case study is presented where the pipe response measured during centrifuge experiments is compared with the pullout force calculated using the proposed method. This allows for the validity of the expression to be verified for different soil and pipe conditions. Finally, a numerical example is provided to illustrate the use of the proposed approach.

Figure 4-10 compares the estimated values using Eq. 4-3 and Eq. 4-5 with the 3D numerical analysis. The results show a consistent agreement between the estimated and calculated values with a maximum difference of 6%. Wijewickremre et al. (2009) suggested that when using Eq.4-10 to find the axial resistance in compacted sand, K value should be considered within a range between K_0 and 2.5. The predicted K^* values in this study (Figure 4-10) are found to be within that range which shows the prediction is also consistent with recommended practice.

A case study (Daiyan et al., 2011) that involves centrifuge tests and numerical analysis performed on a rigid pipe buried in dense sand and subjected to relative axial movement is used to further validate the proposed expression. The geometry and soil properties used in the experiments are provided in Figure 4-11a. It was concluded that the ultimate axial soil resistance measured in the centrifuge tests was found to be higher than that predicted using Eq. 4-1.

Figure 4-11b compares the experimental results with the closed-form solution (Eq. 4-1) as well as the proposed expression. The vertical axis represents the axial interaction factor (N_t) defined as:

$$N_t = {}^{F_A}\!/_{\gamma\ H\ D} \qquad 4-6$$

where F_A is the ultimate axial force per unit length.

The value of the normalized N_t factor is determined based on the centrifuge test results for a steel pipe 504 mm in diameter buried to a depth of 1 m in sandy soil (density = 16 kN/m^3, D_r = 0.82, friction angle of 43^o) and is found to be about 2.1. The closed-form solution (Eq. 4-1) calculated N_t value of about 0.38 whereas the proposed expression predicted N_t value of 1.95 as shown in Figure 4-11b.

Example: To illustrate the use of the proposed expression (Eq. 4-1) to estimate the pullout resistance of a typical steel pipe, a numerical example is given below.

Consider a steel pipe that has a diameter (D) of 0.5 m buried at a depth (H) of 1.5 m in dense sand with friction angle (φ) of 38 degrees, d_{50} = 0.2 mm, Young's modulus (E) of 45 MPa, unit weight of 17 kN/m^3 and interface friction angle (δ) of 30^o. Based on the classical ASCE equation, the maximum axial soil resistance (F_A) obtained using Eq. 4-1 is about 16 kN/m.

Using the proposed expression, the corrected K^* value can be estimated as follows:

$$\left({}^{E}\!/_{\gamma\ H}\right)^{0.38} = \left({}^{4.5\text{ e4 kPa}}\!/_{(17\ kN/m^3\ \times 1.5\ m)}\right)^{0.38} = 17.13$$

$$\left({}^{\varphi}\!/_{45}\right)^{1.39} = \left({}^{38°}\!/_{45°}\right)^{1.39} = 0.791$$

$$\left({}^{\Delta t}\!/_{D}\right)^{0.42} = \left({}^{(10\ \times\ 0.0002\ )\ m}\!/_{0.5\ m}\right)^{0.42} = 0.0984$$

$$K^* = 2.75\ \times\ (1-\sin(38))\ \times\ 17.13\ \times\ 0.791\ \times\ 0.0984 = 1.41$$

Knowing K^* and using Eq. 4-3, the maximum axial soil resistance (F_A) is estimated as 28 kN/m.

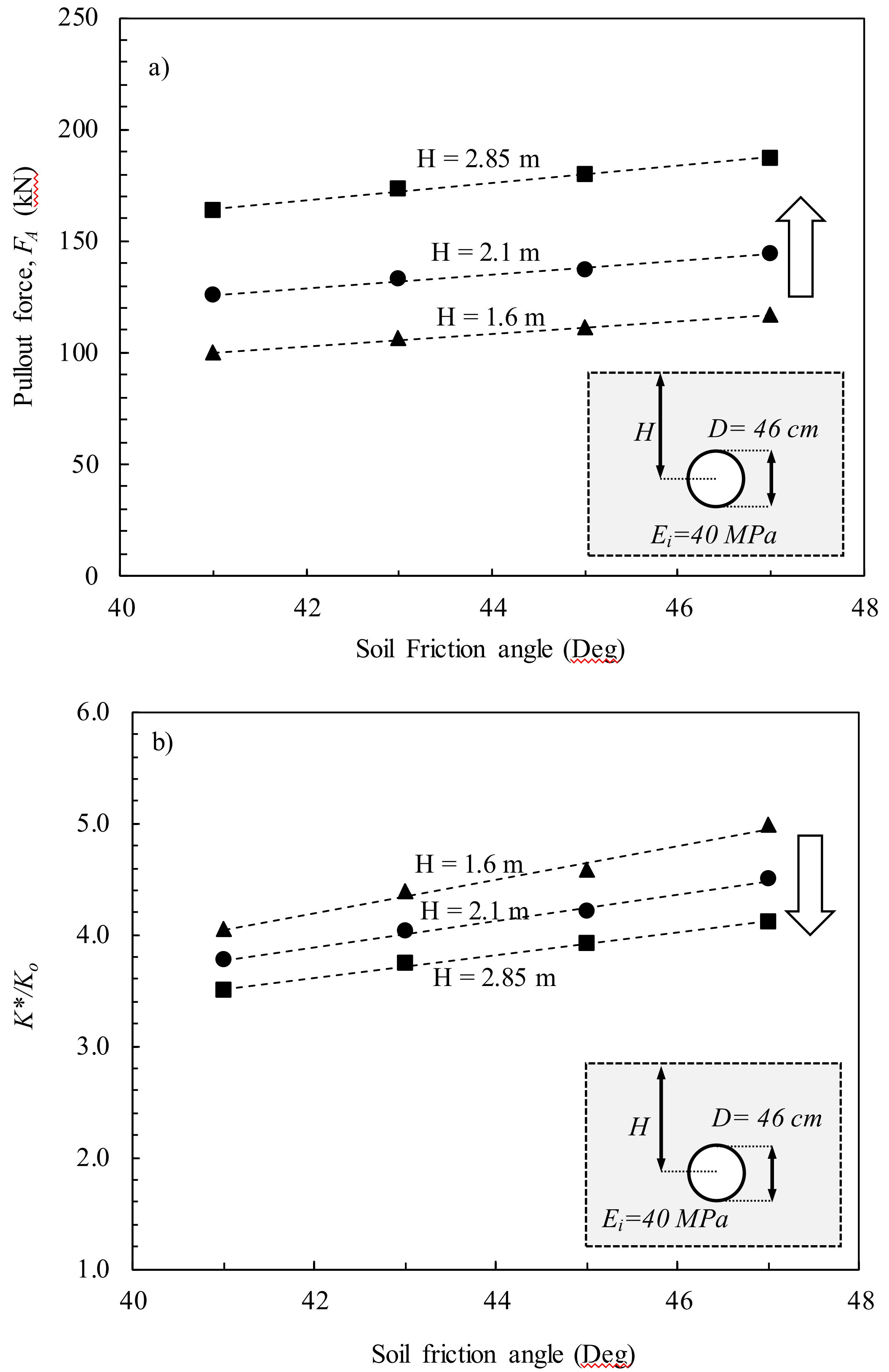

Figure 4-7 Effect of friction angle a) pullout force; b) modified earth pressure coefficient

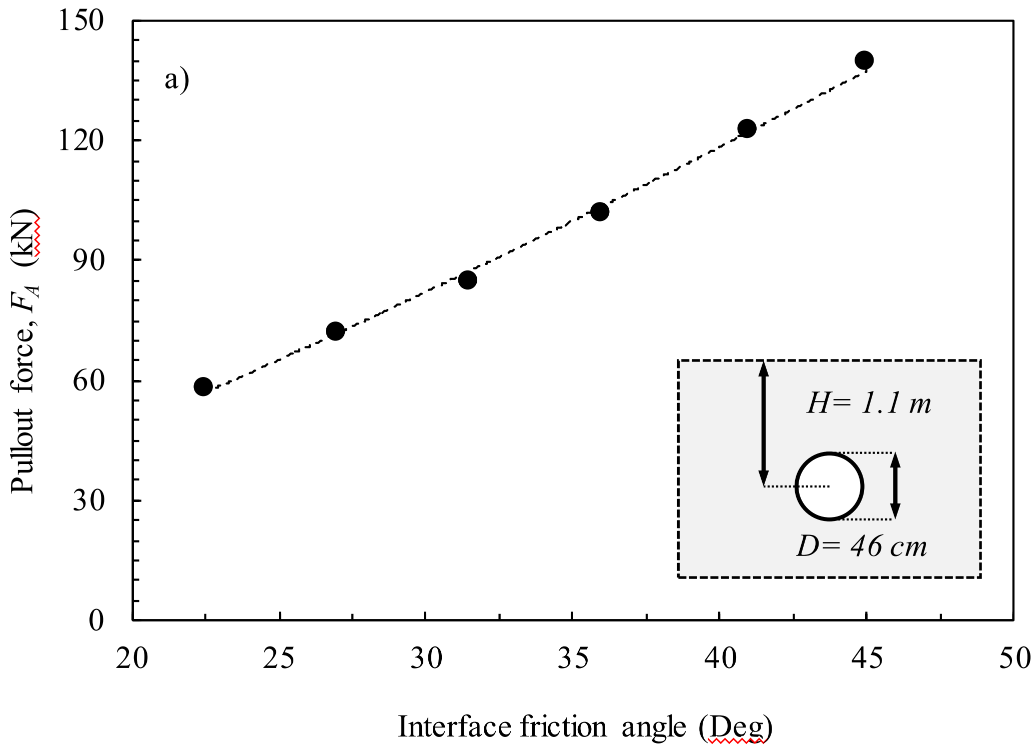

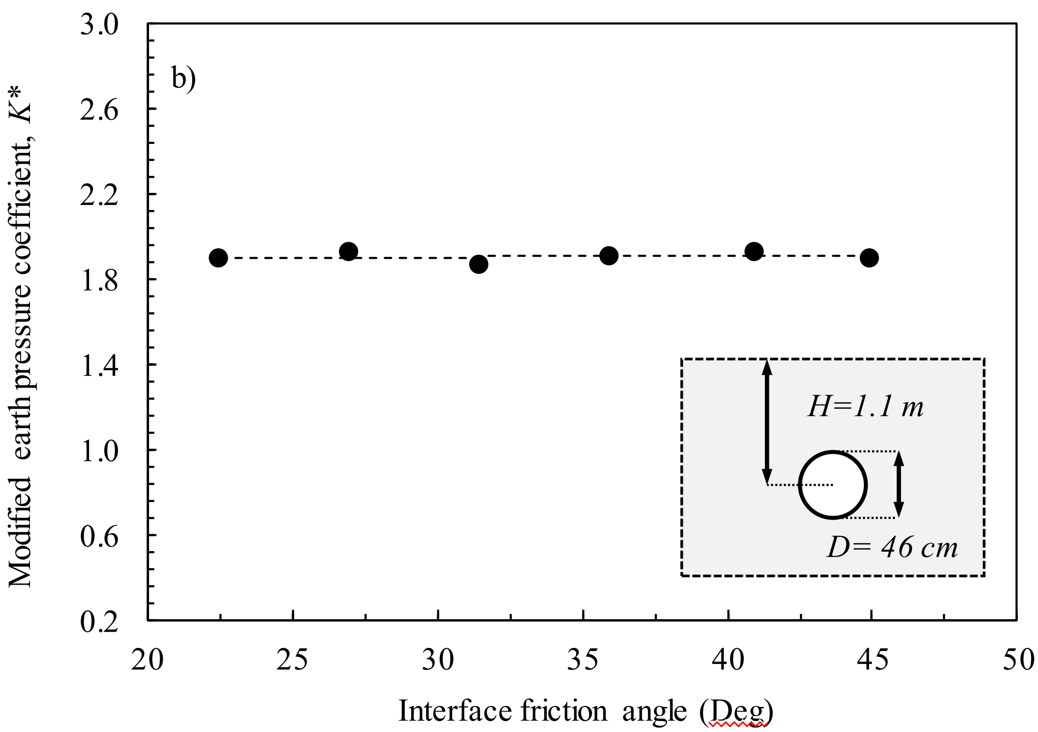

Figure 4-8 Effect of interface friction angle a) pullout force; b) modified earth pressure coefficient

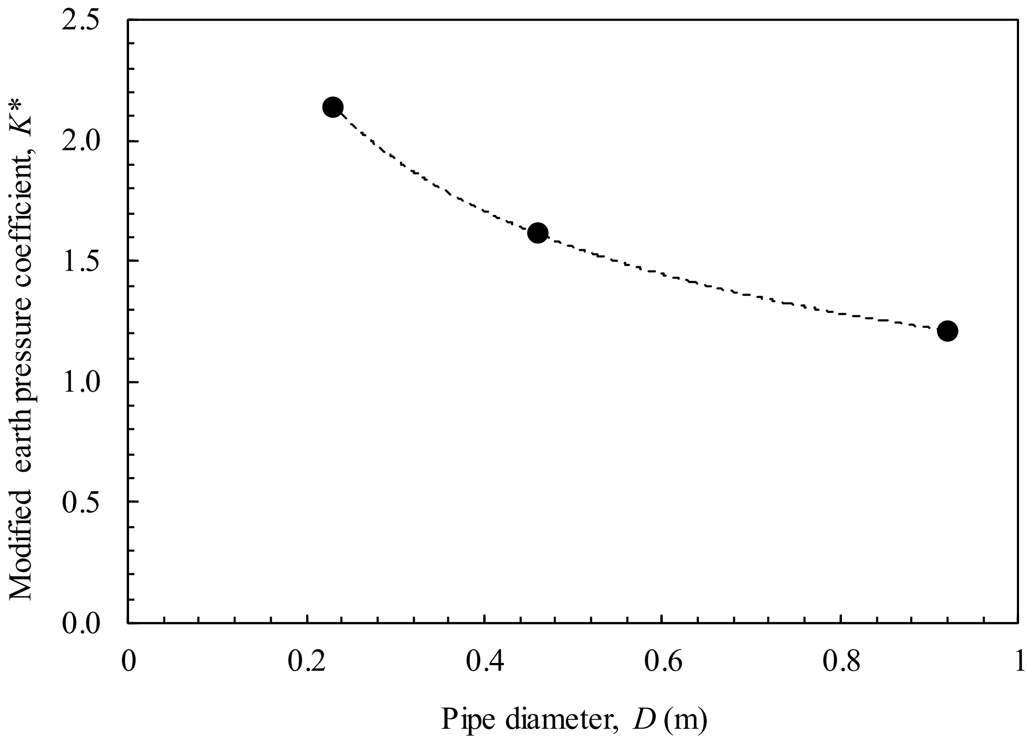

Figure 4-9 Effect of pipe diameter on K^*

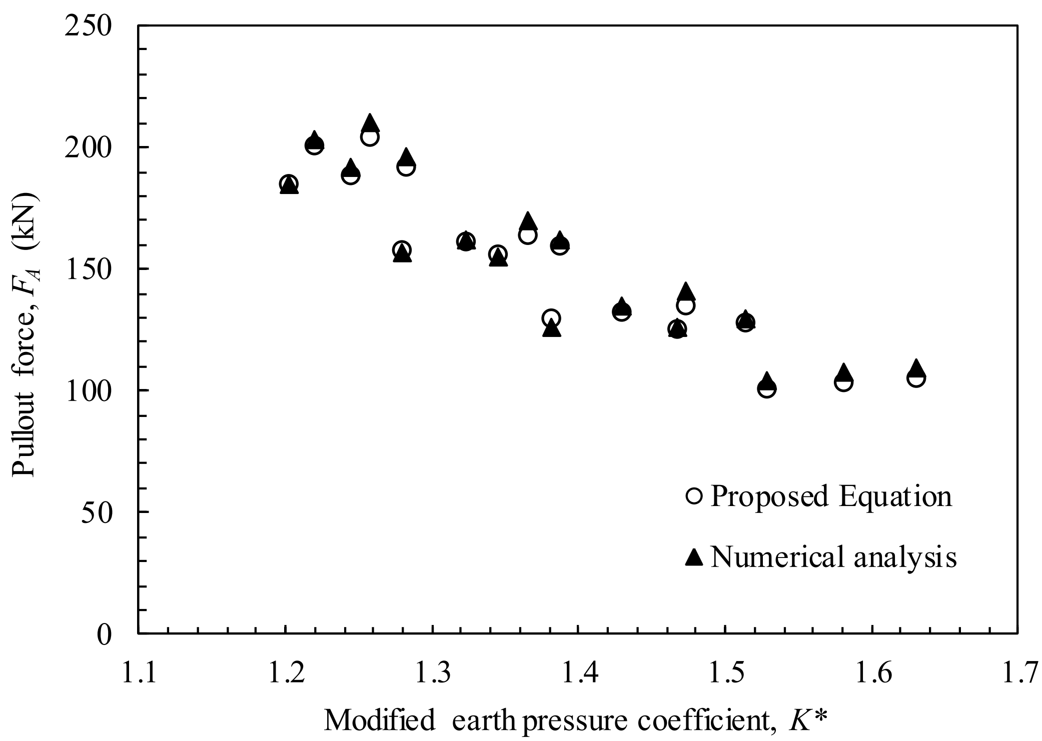

Figure 4-10 Calculated pullout force using the proposed expression

a)

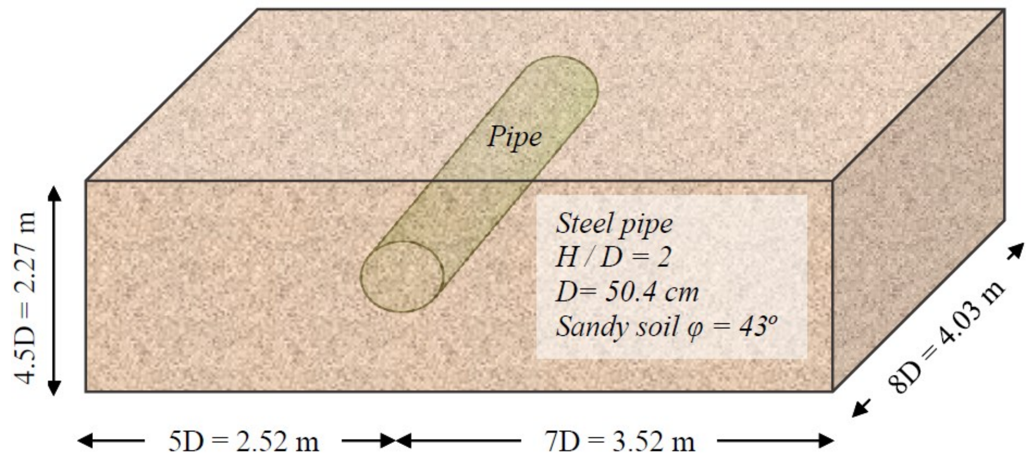

b)

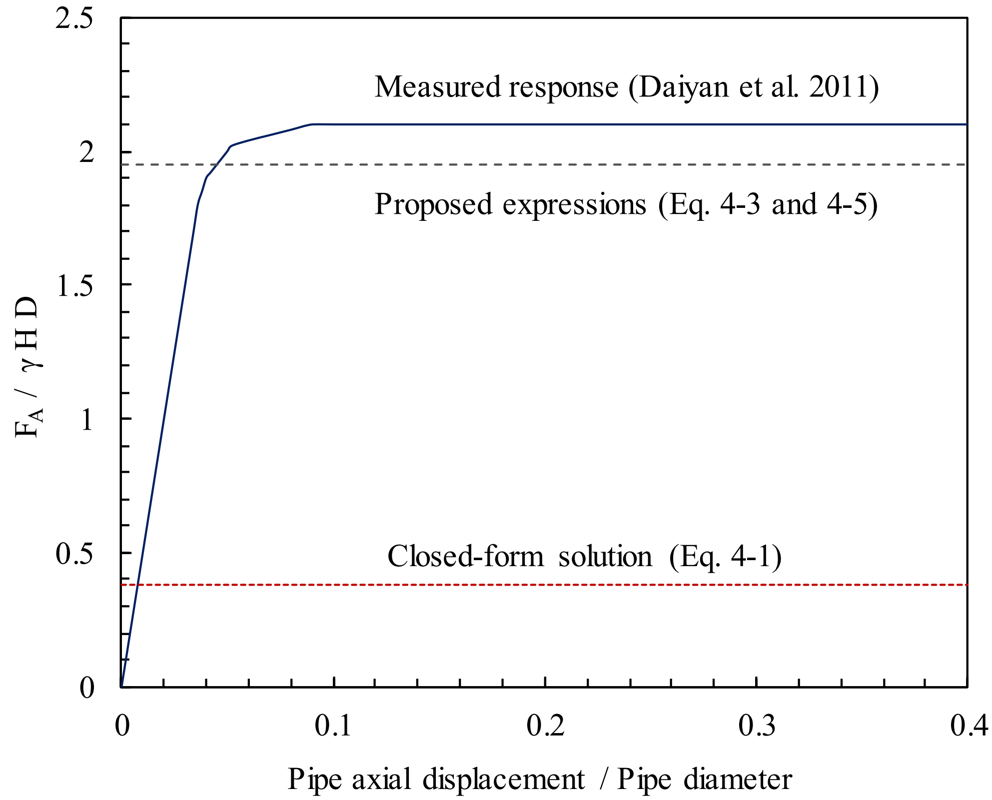

Figure 4-11 Case study a) Problem geometry, b) Comparison between calculated and measured axial interaction factor

4.5 Limitations

Despite the ability of the proposed expression to reasonably estimate the earth pressure coefficient for steel pipes subjected to axial soil movement, further research is needed to develop a more comprehensive relationship that is applicable to other buried pipes and backfill material. The focus of this study was directed towards steel pipes buried in dense sand under static pullout loading condition. Changing the sand type may affect the thickness of the shear zone around the pipe and, therefore, the results may deviate from the proposed expression and the reported experimental data. In addition, the proposed approach may not be applicable for flexible pipes (e.g. thin-walled polyethylene) as they are relatively extensible and may experience changes in cross-sectional dimension under axial loading condition.

Although using simplified spherical elements in this study was justified by the problem size and the associated computational cost, using non-spherical elements (clumps) may improve the numerical predictions. However, this was not considered in the present study.

4.6 Summary and conclusions

To evaluate the effect of ground movement on existing pipelines, it is sometimes necessary to estimate the maximum soil resistance to axial loading. Although the available closed-form solution (ASCE, 1984) can provide a reasonable estimate of the axial soil resistance for loose backfill, it significantly underestimates the resistance for dense sand material. In this study, a series of 3D discrete element analyses is performed to investigate the response of a steel pipe buried in dense sand subjected to axial soil movement. Model validation is performed by comparing the calculated pullout resistance with experimental data. Pullout forces developing in dense sand material are found to be significantly higher as compared to the values obtained using closed-form solution. Based on the results of this study, a modified expression is proposed to estimate a modified earth pressure coefficient that is appropriate for dense sand condition.

The proposed expression for the modified earth pressure coefficient (K^*) is found to be function of the soil and pipe properties, including pipe diameter and burial depth, soil modulus, and particle friction angle. For a given soil and pipe parameters, the pullout response predicted using the proposed expression is found to be in agreement with that measured in the experiments and calculated using numerical analysis.

This paper suggests that for a steel pipe buried in dilative soils, using the available closed-form solution may significantly underestimates the axial soil resistance. It is noted that the proposed expression is suitable only for steel pipes buried in dense sand material. More experimental studies are needed to confirm the applicability of the expression to other types of dilative soils.

Preface to Chapter 5

In two previous chapters (Chapter 3 and Chapter 4), the focus was made on rigid steel pipes. As discussed in Chapter 2 (Literature Review) the current guidelines used to calculate the maximum axial soil resistance for pipes subject to axial ground movement are generally developed for rigid pipe and the research done on flexible pipes is generally limited. Since it is challenging to simultaneously model both the 3D discontinuous nature of the soil and the flexible nature of the pipe structure using traditional discrete or finite element methods, the coupling of the finite and discrete element methods allows for the simulation of this interaction. In this chapter, a coupled Finite-Discrete framework is described and used to investigate the behavior of an MDPE pipe embedded in dense sand material subjected to axial pullout loading.

Chapter 5.

A Finite-Discrete Element Approach for Modeling Polyethylene Pipes Subjected To Axial Ground Movement*

Abstract

The response of medium-density polyethylene (MDPE) pipes subjected to ground movement is often investigated using soil-pipe interaction models that were originally developed for steel pipes. In this study, the behavior of MDPE pipes buried in dense sand under pullout force is investigated using a coupled finite-discrete element framework. The pipe is modeled using finite elements whereas the granular soil is modeled using discrete elements. The model is validated using experimental data and then used to investigate the response of the pipe and the surrounding soil. The response of the MDPE pipe-soil system to axial loading is found to differ significantly from that of steel pipes due to the elongation and distortion that develop in the MDPE pipes, which affect the mobilized friction forces along the pipe. This study demonstrates that caution must be exercised when using current methods in the analysis of MDPE pipes. The coupled approach proposed in this study has proven to be efficient in capturing the relative movement between the pipe and the surrounding soil and in calculating the pipe response under axial loading conditions.

Keywords: Soil-pipe interaction, Finite-discrete element, polyethylene pipes, axial ground movement

---

* A version of this chapter has been published in *International Journal of Geotechnical Engineering*, 2018, 1-13.

5.1 Introduction

Buried pipelines are used worldwide to transport natural resources such as water, oil, and gas. These critical infrastructures are considered to be lifelines for modern cities and failure of these pipes can have significant impact on the economy and the environment. Some of the common causes of failure are generally related to the deterioration of the pipe material or the surrounding backfill soil. However, natural hazards such as permanent ground deformation (PGD) caused by earthquakes can have damaging effects on pipelines. The ninth report of the European Gas Pipeline Incident Date Group (EGIG, 2015) presented a distribution of failure incidents that happened from 2004 to 2013. It was concluded that about 16% of pipeline incidents happened due to ground movement which rank third among major causes of incidents.

Since the early 1960s, researchers have studied soil-pipe interaction to understand the behavior of buried pipelines subject to permanent ground movements. These studies include field tests, full scale laboratory experiments, and centrifuge models (e.g. Trautmann and O'Rourke, 1983; Rizkalla et al., 1991; Konuk et al., 1999; Phillips et al., 2004; Weerasekara and Wijewickreme, 2008; Daiyan and Kenny, 2011; Mohamedzein et la. 2016; Joshaghani et al., 2016; Robert et al. 2016; Ono et al. 2018). For example, Daiyan and Kenny (2011) performed a set of centrifuge tests on rigid pipes buried in dense sand to determine the axial-lateral interaction of the soil-pipe system; Bilgin et al. (2007) conducted two field pullout tests on cast iron pipes buried in dense and loose sands to determine the impact of thermal variation on the pipe response to different loading conditions. In addition to the experimental studies, numerical and analytical investigations have been performed to determine the response of buried pipes subjected to either lateral or axial ground movements (e.g. Cocchetti et al. 2009; Weerasekara and Wijewickreme 2010; Rahman and Taniyama 2015; Roy et al. 2016; Almahakeri et al. 2016; Zhang et al. 2016; Meidani et al. 2017). Most of these studies used the finite element method (FEM) to model both the pipelines and the surrounding soil. Guo and Stolle (2005) carried out a numerical investigation using ABAQUS software to explain the range of lateral soil resistance obtained by different researchers. The effects of burial depth, overburden ratio, soil dilatancy and strain hardening were investigated. Kunert et al. (2012) proposed a nonlinear finite element technique to assess the behavior of pipelines buried in rainforest regions, which are prone to failures by axial stresses from land movement. Recently, Naeini et al. (2016) developed a finite element model to investigate the response of buried HDPE pipeline to fault movements. The numerical results agreed with experimental data and, therefore, it was concluded that the FEM method is suitable for analyzing this class of problems. One of the reported challenges was related to modeling the soil-pipe interaction under large deformation and understanding particle movements in the close vicinity of the pipe.

An alternative approach to analyze this class of problems and capture the soil behavior around the pipe is using the discrete element method (DEM). This approach has been used by researchers to investigate different soil-structure interaction problems (e.g. Cui and O'Sullivan 2006; Chen et al. 2012; Tran and Meguid 2014; Ahmed et al. 2015). Meidani et al. (2017) conducted 3D discrete element analysis of a steel pipe buried in granular material to investigate the response of the pipe under relative ground movement. Using the DEM, particle movements around the pipe and the changes in radial stresses were evaluated with a reasonable accuracy. The rigid steel pipe was modeled using facet discrete elements that do not allow for the development of axial or radial deformation in the pipe structure. Although this is suitable for rigid pipes, flexible polyethylene pipes (PE) may undergo both axial and radial deformation under axial loading and therefore, the pipe response and the associated interaction with the surrounding soil may not be accurately modeled using discrete elements.

To take advantage of both the finite and discrete element methods, coupling the two approaches has provided researchers with the flexibility of solving a wide range of geotechnical engineering problems involving buried structures. Structural elements are usually modeled using finite elements whereas the surrounding soil particles are modeled using discrete elements. Several algorithms have been developed to facilitate the load transfer between the two domains. A procedure for combining finite and discrete elements is to simulate the shot peening process was proposed by Han et al. (2002). Fakhimi (2009) developed an algorithm for coupling the finite and discrete element methods and used the coupled model to simulate the deformable membrane and the encased soil samples in laboratory triaxial tests. The membrane was modeled using finite elements (FE) while the soil was modeled using discrete elements (DE). Villard et al. (2009) proposed a coupled FE-DE approach to model earth structures reinforced by geosynthetic material. The framework was used to model the interaction between a geosynthetic sheet and the surrounding soil. Dang and Meguid (2013) proposed a coupled FE-DE approach to model soil-structure interaction problems involving large deformations. Interface elements were introduced at the boundary between the two domains to transmit the interaction forces between the finite and discrete elements. Tran et al. (2013) proposed a similar finite–discrete element framework for the 3D modeling of geogrid–soil interaction under pullout loading condition.

In this study, a coupled FE-DE approach is developed and used to investigate the response of MDPE pipe buried in dense sand and subjected to axial soil movements. A numerical model that is able to capture the response of both the pipe and backfill material is created. Microstructure parameters needed for the discrete element analysis are determined using triaxial test data and the overall model performance is validated using analytical solutions. The validated model is then used to determine the response of the pipe and the backfill material. The numerical results are also compared with experimental data. Using the developed approach, the detailed behavior of the soil surrounding the pipeline is investigated and the stresses developing in the pipe structure are evaluated. Finally, current guidelines for estimating soil loads on flexible pipes subjected to relative axial displacement are reviewed on the basis of the numerical results

5.2 Coupled finite-discrete element framework

The coupled 3D Finite-Discrete element algorithm used for this study was originally developed by Dang and Meguid (2010, 2013) and Tran et al. (2013) to model the interaction between the finite and discrete element domains. The developed approach was implemented into *YADE*, an open source code for DEM analysis (Kozichi and Donze, 2008; Smilauer et al., 2010). The detailed description of the framework and the DEM contact law were explained in Chapter 2 (section 2.3.1 "Contact law" and section 2.4 "Coupling the Finite and Discrete Element Methods").

5.3 Modeling pipe-soil interaction

Previous studies on pipeline resistance to axial soil movements have been mainly focusing on steel pipes and only a few studies addressed PE pipes (e.g. Anderson, 2004; Weerasekara, 2007). Design guidelines (e.g. ASCE, 1984 and ALA, 2001) are based on results obtained using steel pipes and their application to PE pipes may not be appropriate given the viscoelastic nature and the relatively low stiffness of the PE material. In addition, Karimian (2006) and Meidani et al.

(2017) reported that the available guidelines may underestimate the axial soil pressure acting on pipes installed in cohesionless soil, particularly for dense soil.

5.3.1 Model generation

The FE-DE model used in this study is created based on the experimental work reported by Weerasekara (2007). The experiments comprised an MDPE pipe with outside diameter of 114 mm buried in a soil chamber 3.8 m in length, 2.5 m in width and 1.3 m in height. The pipe was installed at a depth of 0.6 m below the surface. Dense Fraser River sand with relative density of 75% was used in the experiment. The grain size distribution of the sand material is shown in Figure 5-1 and the relevant properties are summarized in Table 5-1. The rigid box hosting the soil and the pipe was reinforced with steel frames to prevent lateral deformation and the inner surface was designed to ensure minimum friction between the soil and the walls of the chamber. The pipe was pulled out incrementally from the backfill following a displacement-controlled loading condition and the reaction force was continuously measured.

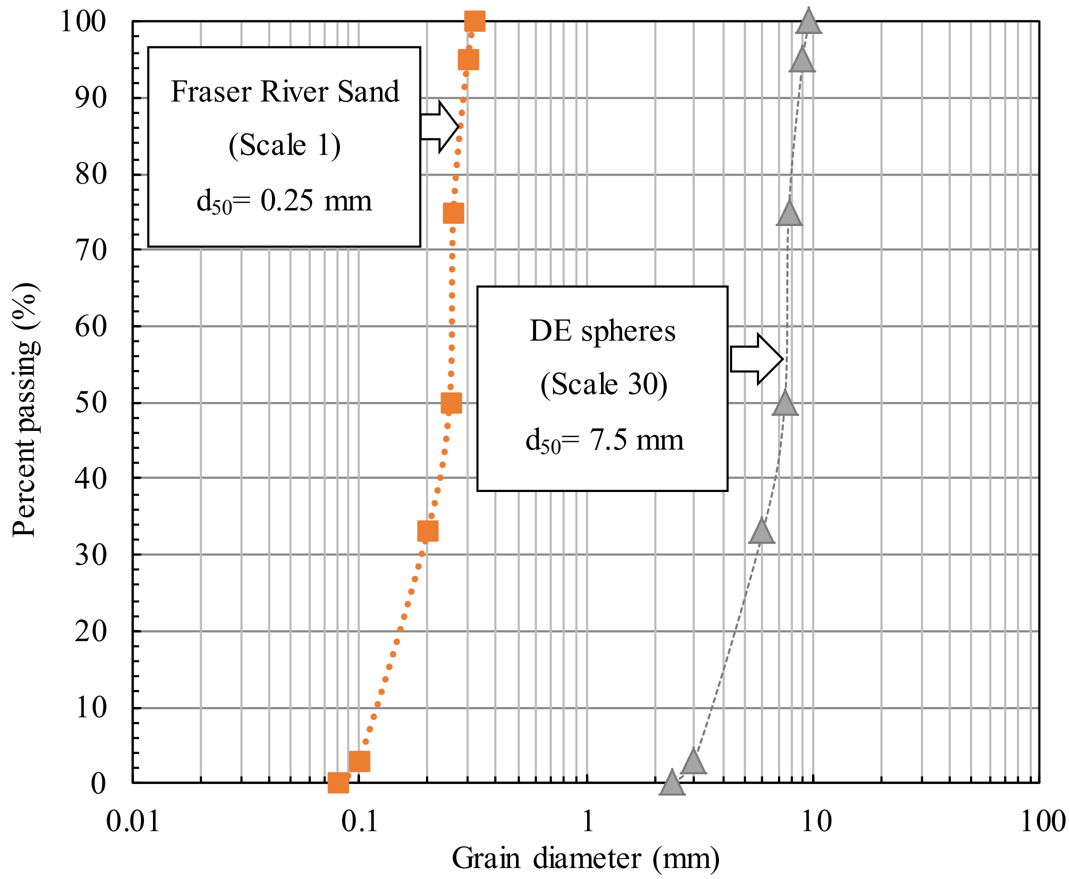

Figure 5-1 Particle size distribution of Fraser River Sand and up-scaled DE particles

Table 5-1 Soil properties of backfill material (Fraser River Sand)

Parameter	Value
Specific gravity	2.72
Young's modulus, E_i (MPa)	40
Unit weight (kN/m^3) – (75% relative density)	16
Internal friction angle φ (Degree)	45
Cohesion (kN/m^2)	0
Poisson ratio, υ	0.3
Porosity, n	0.41

The numerical analysis is conducted using a modified version of the open source code *YADE* (Kozicki and Donzé 2008; Šmilauer et al. 2010). The soil particles are modeled using discrete elements while the pipeline is modeled using finite elements. Interface elements are employed to model the interaction between these two domains. The MDPE pipeline is modeled using 8-noded hexahedral elements. The modelled pipe has 114.3 mm outside diameter and 10.3 mm wall thickness. The results of the laboratory experiments performed on the MDPE pipe based on uniaxial compression (Anderson, 2004) and pullout (tensile) test data (Weerasekara, 2007) are presented in Figure 5-2a. The response is characterized by slight nonlinear response up to 3% strain. Konder (1963) proposed a hyperbolic stress-strain relationship for PE pipes as follows:

$$\sigma = E_i \left(\frac{\varepsilon}{1 + \eta\,\varepsilon}\right) \qquad 5-1$$

where ε is the strain, Ei is the initial Young's modulus, σ is the stress and η is a constant. The hyperbolic relationship for the investigated PE pipe is superimposed on the experimental data in Figure 5-2a. The relationship was found to represent the pipe response and agree well with the experimental data. Given the small strain level expected in the pullout experiments, the hyperbolic model was used to determine an approximate linear elastic model that represents the pipe response as shown in Figure 5-2b. At strain level of up to 5%, the modulus of elasticity E_i was found to be approximately 550 MPa.

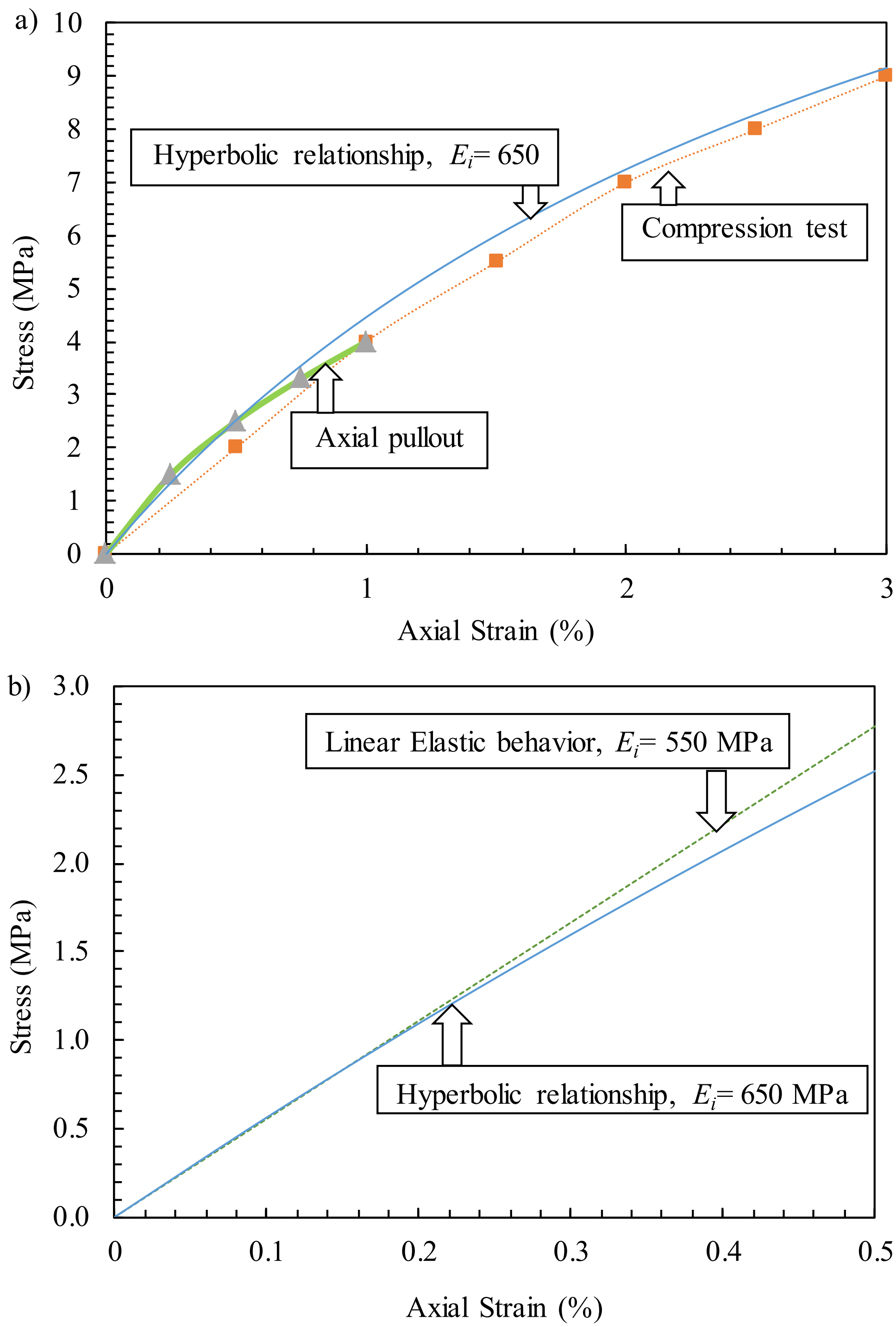

Figure 5-2 a) Stress-strain response of the MDPE pipe from compression test, axial pullout test and the hyperbolic model, b) comparison between linear elastic and the hyperbolic model

The 3.85 m long MDPE pipe was modelled using 1232 solid elements that measure 5 cm × 2.25 cm each overlain by 4928 interface elements. Details of the different components of the finite element model used to represent the pipe are shown in Figure 5-3.

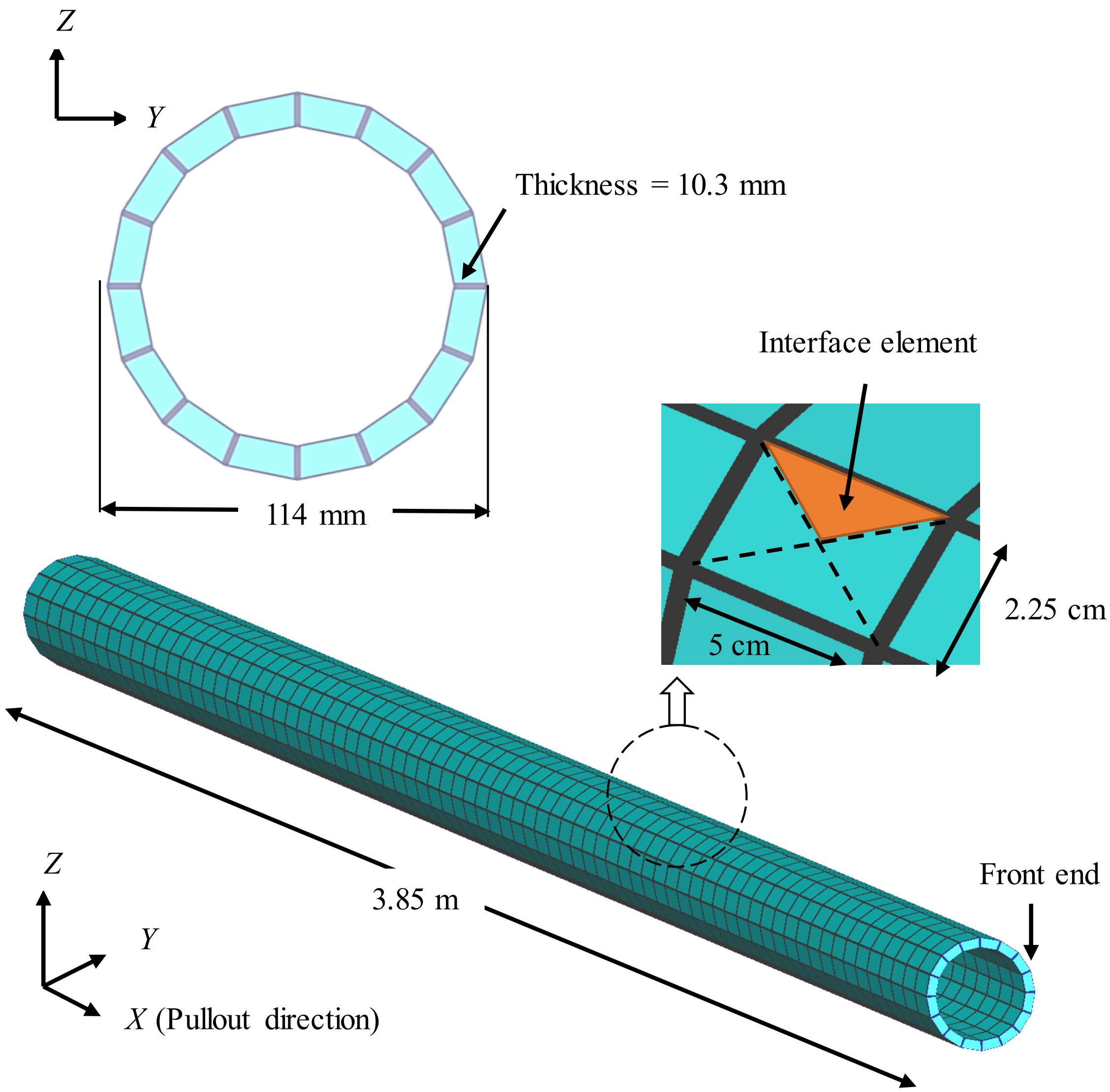

Figure 5-3 Geometry, finite element mesh and interface elements used to model the MDPE pipe

Particle upscaling is used to keep the number of particles within a feasible range for the DEM. Ding et al. (2014) conducted a 3D numerical study on the effect of particle upscaling on the macroscopic response of discrete element samples. It was found that the ratio between the smallest sample lengths *(L)* to the median of the particle diameters (*d*) should be kept below 30 to minimize the effects of particle upscaling. Given the size of the test chamber and the pipe diameter in this study, d_{50} of 7.5 mm is selected for the discrete elements, which results in 4,9000,000 particles. The corresponding scaled particles size distribution is shown in Figure 5-1.

To keep the problem size manageable and further reduce the number of particles, a parametric study was performed to determine the minimum width (*Y*) and the height (*Z*) of the model that does not affect the pipe response, while preserving the full length (*X*) of the pipe (see Figure 5-4Figure 5-3a). The results of the parametric study are presented in Figure 5-4b and Figure 5-4c for the model width and height, respectively. Figure 5-4b shows the change in the pullout force as the model width increases from 0.3 m to 2.75 m for applied displacement of 15 mm. The pullout force was found to rapidly decrease as the model width (*Y*) increased and reached a plateau at a model width of about 0.5 m. This means that increasing the model width beyond 0.5 m does not have a significant impact on the pullout response of the pipe. Similarly, Figure 5-4c shows that the pipe response reached a plateau at *Z/2* of 0.25 m which corresponds to a model height 0.5 m. These model dimensions were, therefore, adopted in the numerical analysis presented in this study. The overlying backfill material above 0.5 m was replaced using equivalent surcharge pressure that is uniformly distributed at the model surface.

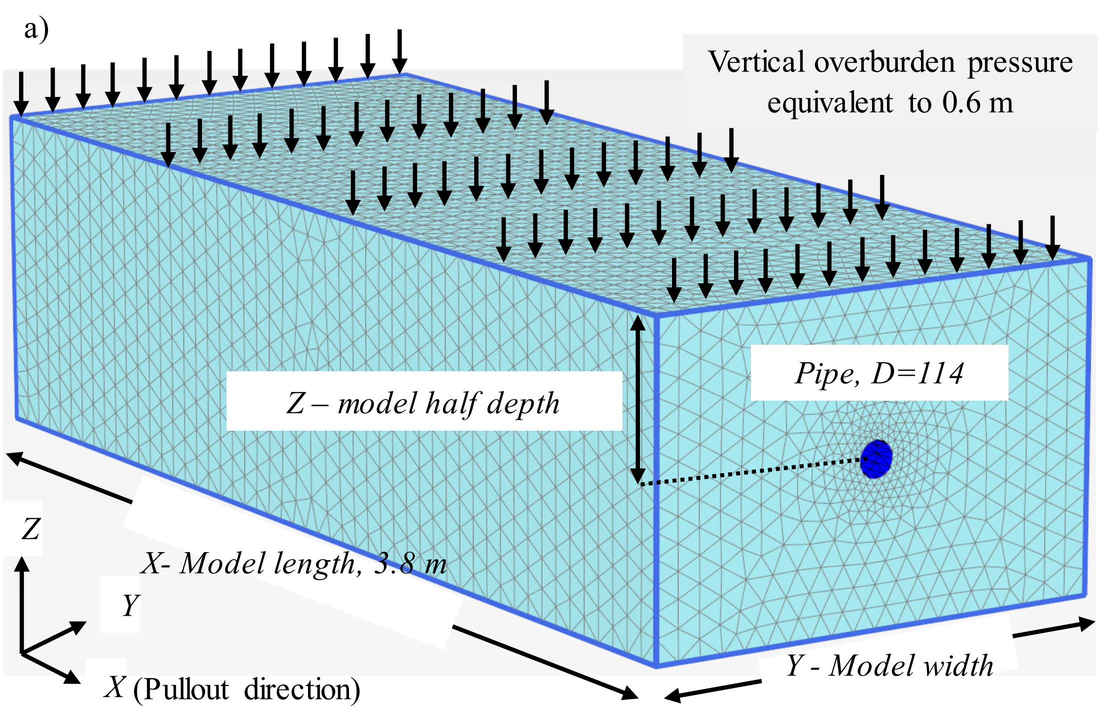

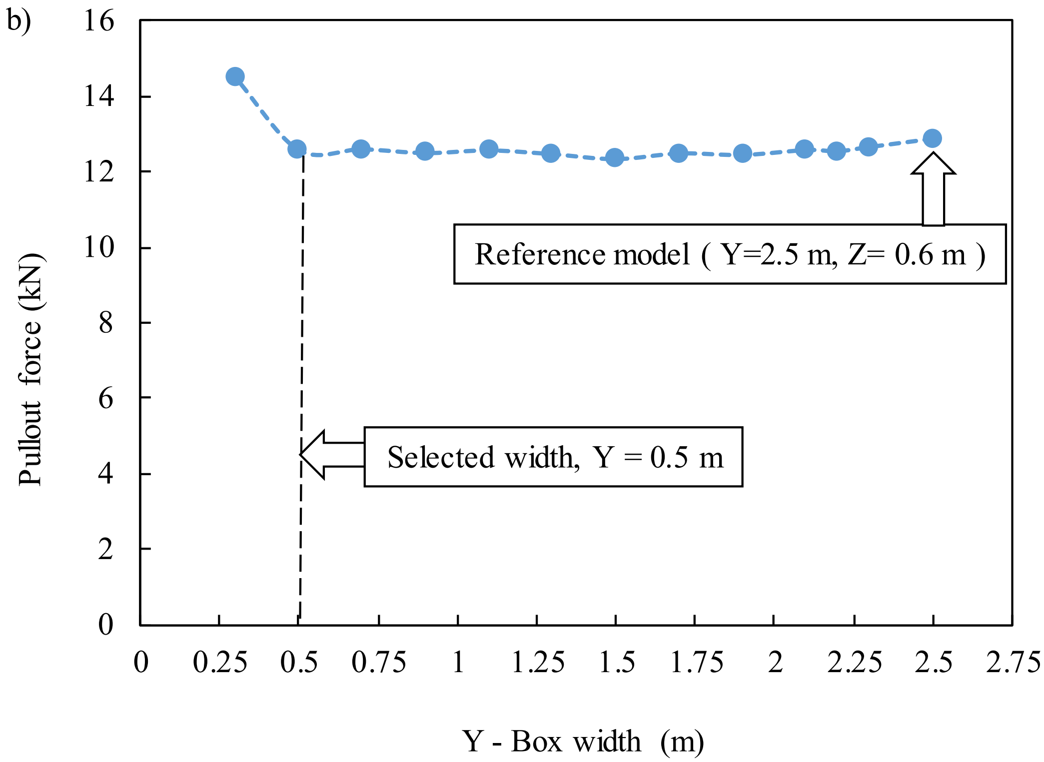

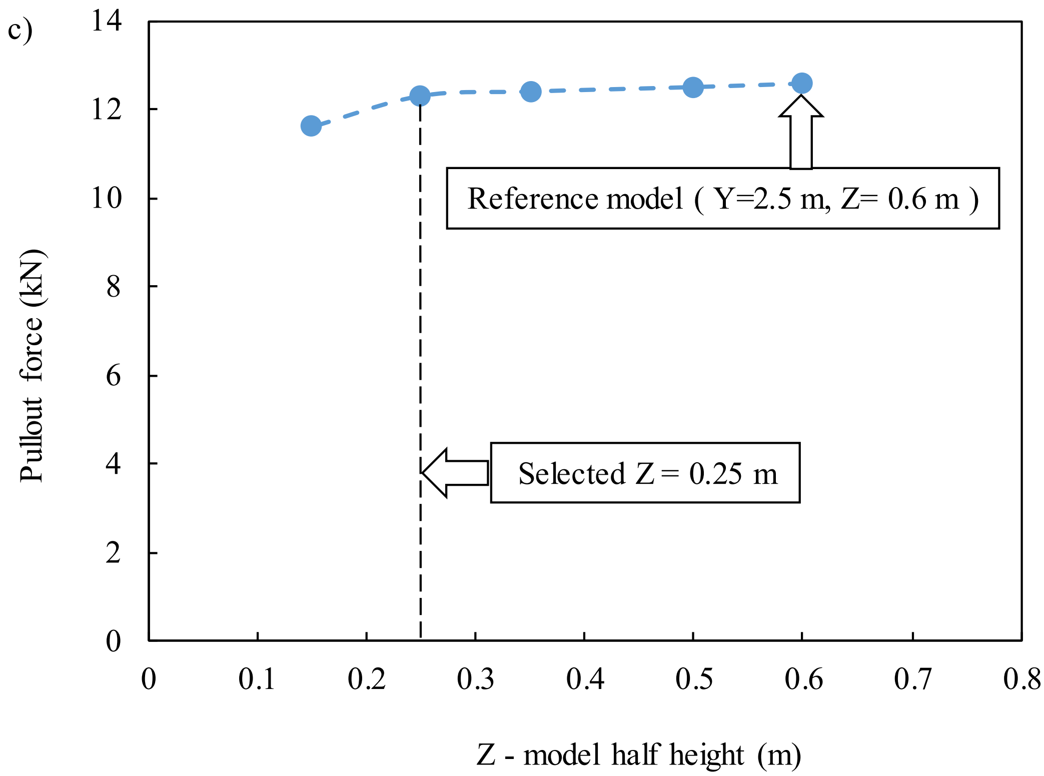

Figure 5-4 a) Finite element model used to examine the effect of model dimensions, b) the effect of model width on pullout force, c) the effect of model height on pullout force

To generate the discrete element particles, the radius expansion method is used in combination with the particle size distribution shown in Figure 5-1. A cloud of non-contacting particles is first created, then the particles located within the pipe circumference are removed and the radius of the spheres are increased to achieve the target porosity of 0.41, which corresponds to that used in the experiment. The set of particles is allowed to move under gravity and the assembly is then cycled until equilibrium condition is reached. The final three-dimensional model includes a total of 345,000 spherical particles as depicted in Figure 5-5a. To illustrate the particle distribution in the close vicinity of the pipe, a front view of the model (in the *Y-Z* plane) is shown in Figure 5-5b.

5.3.2 Model calibration

Input parameters used in the discrete element analysis include two major groups: (i) physical parameters (friction angle, cohesion and Young's modulus), and (ii) dimensionless coefficients (rolling and shear stiffness coefficients, maximum resistant moment factor, etc.). A calibration procedure is needed to determine these parameters for a given soil condition. The model used in this study was calibrated by simulating triaxial tests conducted on Fraser River sand (Karimian, 2006) and comparing the calculated response with the measured values. Table 5-1 presents the mechanical properties of the Fraser River Sand based on triaxial tests performed at 25 kPa confining pressure. Model calibration details have been reported in Chapter 3 (3.4) and only a summary of the obtained parameters that are needed for the discrete element analysis is provided in Table 5-2 Input parameters used in the coupled FE-DE analysis.

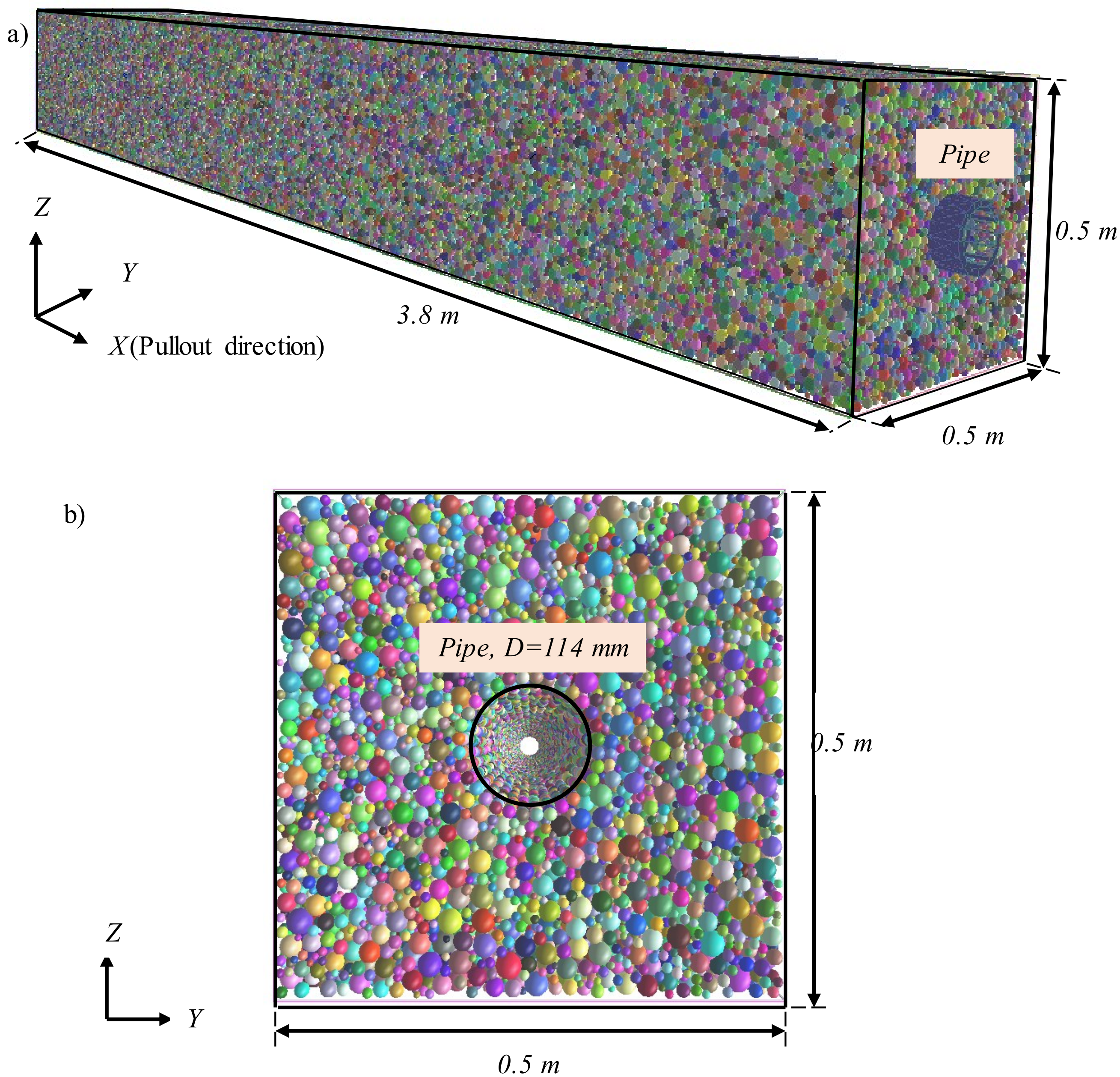

Figure 5-5 a) 3D view of the model showing the pipe and surrounding soil, b) front view of the model (only particles)

Table 5-2 Input parameters used in the coupled FE-DE analysis

Type of element	Parameter	Value
Discrete particle	Density (kg/m^3)	2720
	Particle modulus, E (MPa)	150
	Ratio K_T / K_N , α	0.7
	Micro friction angle, φ_{micro} (Degree)	45
	Rolling resistance coefficient (β_r)	0.15
	η_r	1
	Damping ratio	0.2
Finite element	Young's modulus, E (MPa)	550
	Poisson's ratio,	0.46
Interface element	Material modulus, E (MPa)	150
	Ratio K_T/K_N , α	0.7
	Micro friction angle, φ_{micro} (Degree)	40

5.3.3 Validation of the numerical model

After creating both the discrete element assembly and the finite element model of the pipe, the coupled model is allowed to freely settle under gravity using the input parameters presented in Table 5-2. No friction was considered between the rigid walls and the contained particles to properly simulate the test conditions. A vertical pressure equal to 5.6 kPa was then applied over the coupled model to represent the removed soil layer (γ = 16 kN/m^3). The contact pressure distribution acting on the pipe is first calculated at selected locations along the pipe circumference using the developed model and the results are compared with Hoeg's analytical solution (Hoeg, 1986). The numerical calculation was performed at several zones along the pipe to ensure that the model provides consistent results everywhere in the model. The investigated zones (shown in Figure 5-6) include: (1) from X = 0.5 m to 1 m; (2) from X = 1.75 m to 2.25 m; (3) from X = 3 m to 3.5 m. The average soil pressure acting on the pipe using the analytical solution and the numerical model are compared for each zone (Figure 5-6a and Table 5-3). The calculated pressure at the crown of the pipe for the three examined zones (1, 2 and 3 in Fig. 7b) was found to be 6.22, 6.01 and 5.98 kPa, respectively. These values are consistent with the analytical solution that predicted a pressure of 5.24 kPa at the same location. Based on the results presented in Table 5-3, the maximum difference between the average pressure calculated at the three zones and the 2D analytical solution was found to be ±15%. This level of accuracy is considered acceptable given the 3D nature of the problem and the approximations made in developing the numerical model.

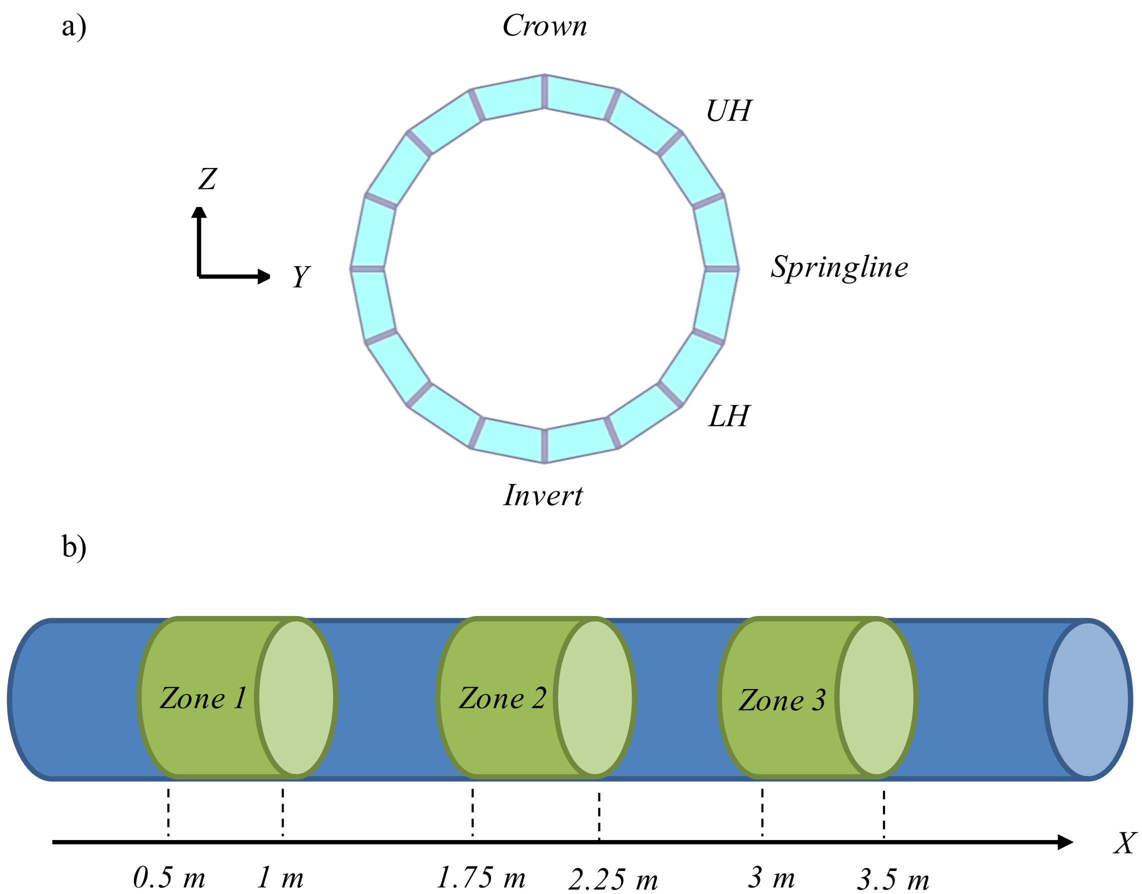

Figure 5-6 a) Pipe section and investigated locations, b) different zones used for initial stress calculation

After the initial conditions are verified, the pullout test is performed using a displacement control approach. The vertical pressure acting on the model is kept constant throughout the analysis at σ_v = 5.6 kPa using the method developed by Tran et al. (2013). The stiffness of the interface is set equal to that of the discrete particles and the interface friction angle is determined by matching the experimental results. This approach is consistent with that reported by Tran et al. (2013) and Villard et al. (2009). The pullout force is incrementally applied to the pipe and the corresponding displacements at the leading end are presented in Figure 5-7 Comparison between the pullout response of the pipe in numerical simulation and experimental test. The pullout force increased nonlinearly with the initial increase in displacement. The maximum pullout force reached about 6.4 kN at applied displacement of 14 mm. The measured response is superimposed on the numerically calculated results as shown in Figure 5-7. Close agreement was found between the experimental and numerical responses with a maximum difference in pullout force of about 9% with a maximum measured value of 6.8 kN.

Table 5-3 Comparison between the numerical results and the analytical solution of initial pressure distribution (kPa) around the pipe

Location	Hoeg (1986)	Zone 1	Zone 2	Zone 3
Crown	5.24	6.22	6.01	5.98
UH	7.70	8.95	7.94	8.29
Springline	10.16	11.34	11.82	10.78
LH	7.70	6.89	6.63	7.24
Invert	5.24	4.87	4.45	4.51

In addition to the model validation using the mobilized soil resistance to pullout loading, the changes in axial strains (ε_x) developing at the leading end of the pipe are also calculated for different pullout forces and the results are compared with the measured values as shown in Figure 5-8. The relationship is almost linear for the range of strains experienced by the pipe during the pullout process. The axial strain calculated at the maximum pullout force is found to be 3740 $\mu\varepsilon$. This is consistent with the experimental results reported by Weerasekara (2007) where the maximum measured strain was found to be 3800 $\mu\varepsilon$. The corresponding displacements at the leading end are also examined in Figure 5-9. The maximum displacement obtained using the numerical model is about 14 mm whereas the measured value is about 12 mm. However, the overall relationship is properly captured using the developed model experimental results are respectively 14 mm and 12 mm (Figure 5-9). These results validate the adequacy of the developed model in representing the soil-pipe interaction under axial loading conditions.

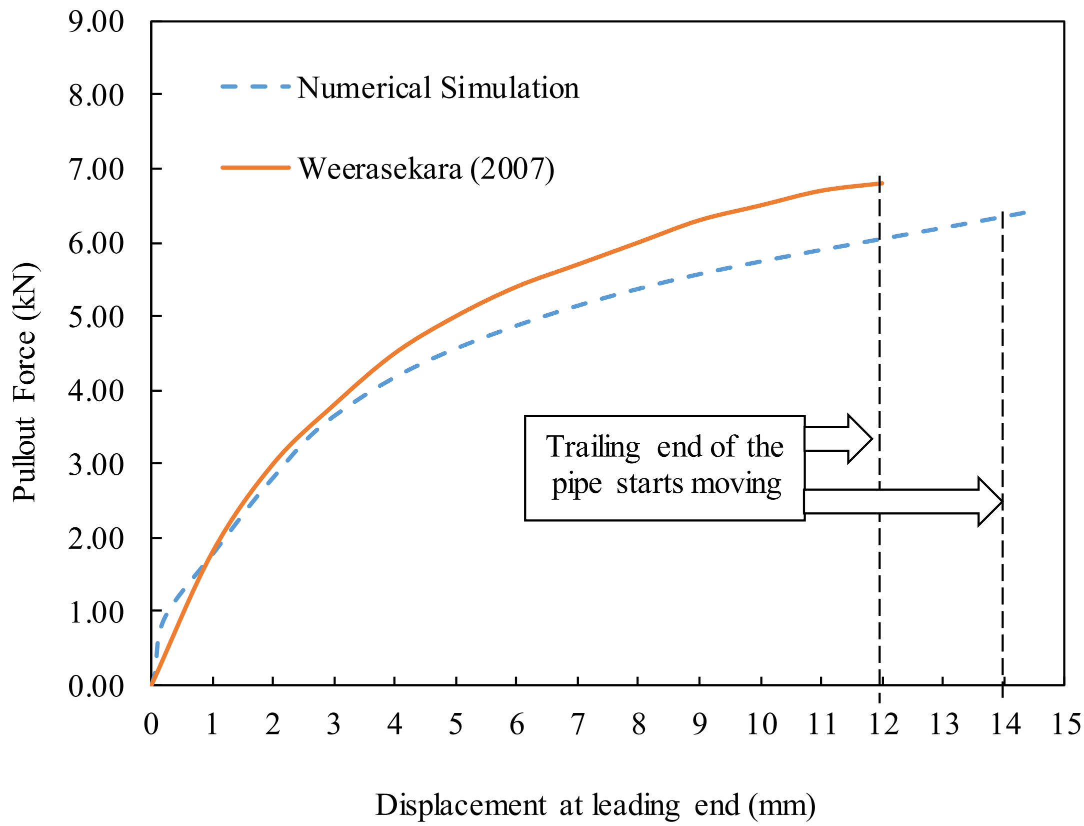

Figure 5-7 Comparison between the pullout response of the pipe in numerical simulation and experimental test

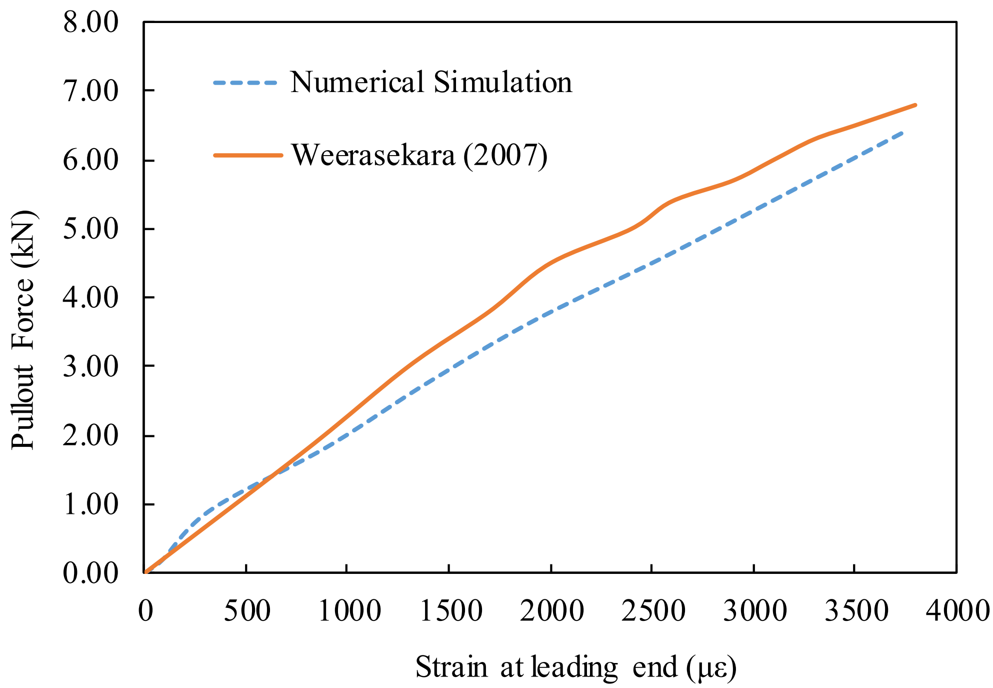

Figure 5-8 Relationship between the pullout force and strain at leading end in numerical and experimental test

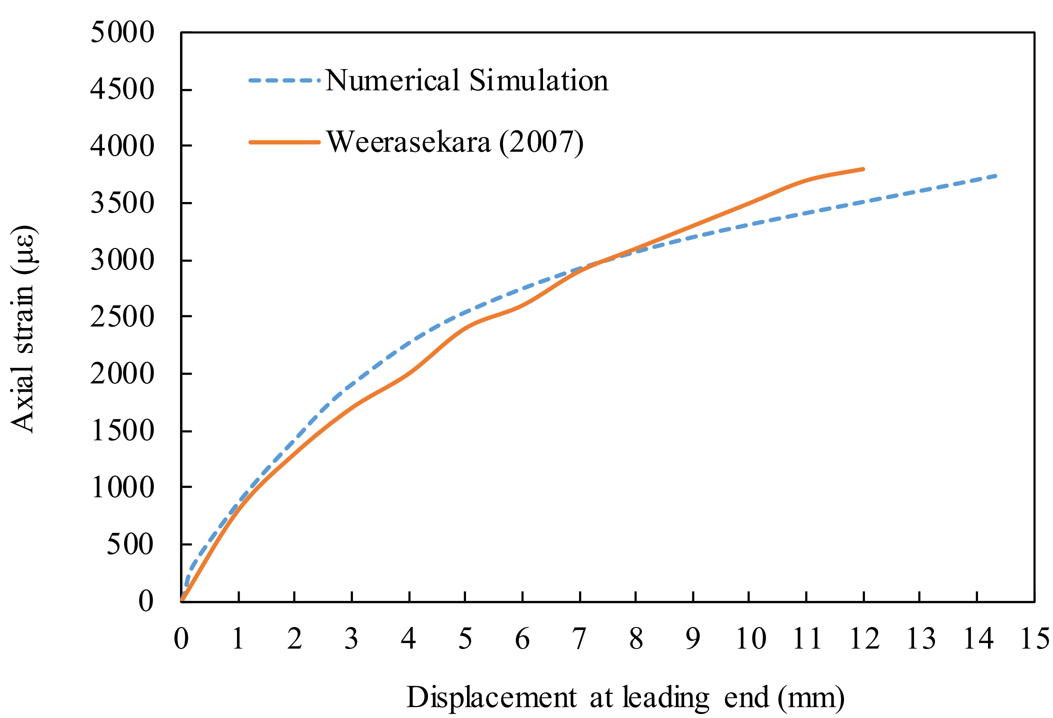

Figure 5-9 Relationship between the strain and displacement at leading end in numerical and experimental test

5.4 Results and discussions

The detailed response of the pipe and the surrounding soil are investigated in this section. This includes the strains and displacements developing along the pipe in the longitudinal and transverse directions. The accuracy of the available closed-form solution in predicting the maximum pullout force is then evaluated. To take advantage of the coupled model, the changes in contact force distribution and the displacement field around the pipe is also examined.

5.4.1 Response of the pipe

The distributions of horizontal displacements developing along the pipe for different pullout displacements (U_x) are presented in Figure 5-10a. The pipe displacements are found to be generally non-uniform with most of the movements occur near the leading end of the pipe (length = 3.8 m). Small displacements were calculated within half of the pipe length located in the opposite side of the applied load. The contour of horizontal displacement in the pipe structure at applied displacement of 14 mm is illustrated in Figure 5-10b. The figure shows the concentration of displacements developing in the pipe.

To understand the displacement pattern presented in Figure 5-10 the investigated PE pipes, it is worthwhile comparing the response with that reported for rigid pipes. Pullout experiments performed on rigid steel pipes (Karimian, 2006) revealed that entire length of the pipe starts to move immediately after applying the axial force indicating that the friction between the soil particles and the pipe is mobilized over the entire length of the pipe. This is attributed to the difference in stiffness between the rigid pipe and the surrounding soil. Hence, the pullout test of a rigid pipe can be assumed as an "element" test, and the frictional resistance can be considered uniform along the entire length of the pipe. On the other hand, for MDPE pipe a small section of the pipe experiences slipping at the beginning of the test. With the increase in loading, the slipping section propagates along the pipe. Hence, the frictional resistance along the MDPE pipe is not uniform and the maximum pullout force is reached when the entire length of the pipe starts to move. It is also noted that MDPE pipes are more extensible than rigid steel pipes, and therefore both elongation and reduction in cross-section may develop during the pullout process. It can, therefore, be concluded that the axial soil resistance in this case is a function of the pipe length and the force-displacement results are valid as long as the pipe does not completely slip out of the soil.

The evolution of the axial strains (ε_x) along the length of the pipe is presented in Figure 5-11a for different leading-end displacements (U_x). The distribution of strains is found to be consistent with the displacement patterns presented in Figure 5-10 as well as the results reported by Weerasekara (2007). Figure 5-11b shows the contours of the axial strains at applied leading-end displacement of 14 mm. It can be seen that at this displacement level, the axial strain at front edge of the pipe is about 3300 $\mu\varepsilon$ whereas at the middle of the pipe the calculated strain is found to be about 1000 $\mu\varepsilon$ which is approximately 3 times smaller in magnitude compared to the strain found at front of the pipe. This confirms the non-uniform nature of the frictional resistance mobilized on the pipe surface resulting from the non-uniform elongation developing in the pipe.

To investigate the distortion that develops in the pipe cross-section during the pullout process, the displacements in the transverse (Y) direction are presented in Figure 5-12a at four selected locations on the pipe circumference. The maximum deformation in the Y direction was found to develop at the springline in the positive Y direction with no significant displacement calculated at the crown. This reveals that the circular shape of the pipe experiences slight distortion during the pullout process. This can be illustrated by the displacement contours presented in Figure 5-12b. The three-dimensional distribution of displacement along the pipe length at applied displacement of 14 mm indicates that the distortion of the pipe cross-section is more pronounced near the front side of the pipe.

a)

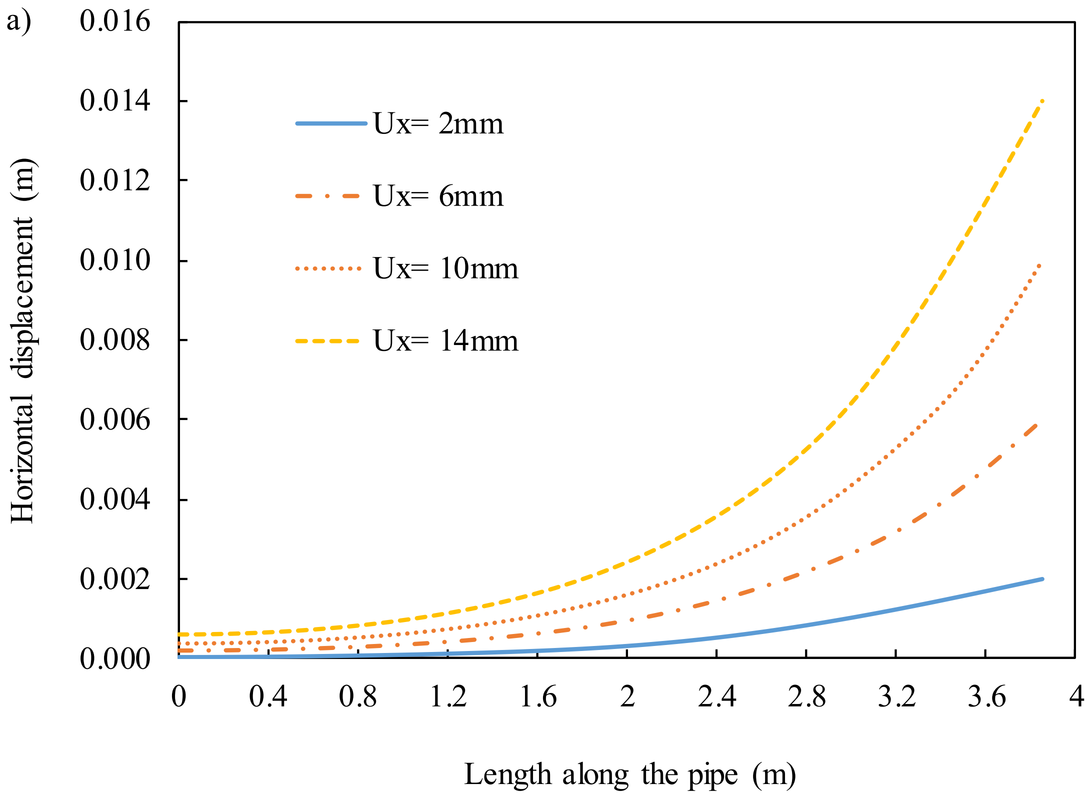

b)

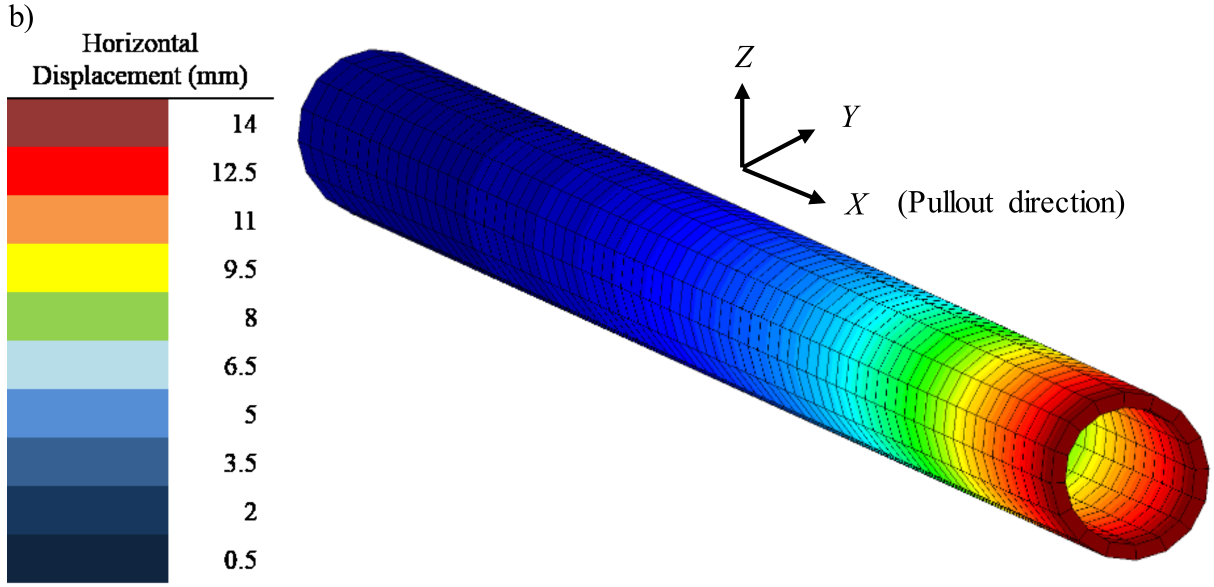

Figure 5-10 Horizontal displacement along the MDPE pipe at different leading end displacement (U_x), b) Pipe horizontal displacement at U_x = 14 mm

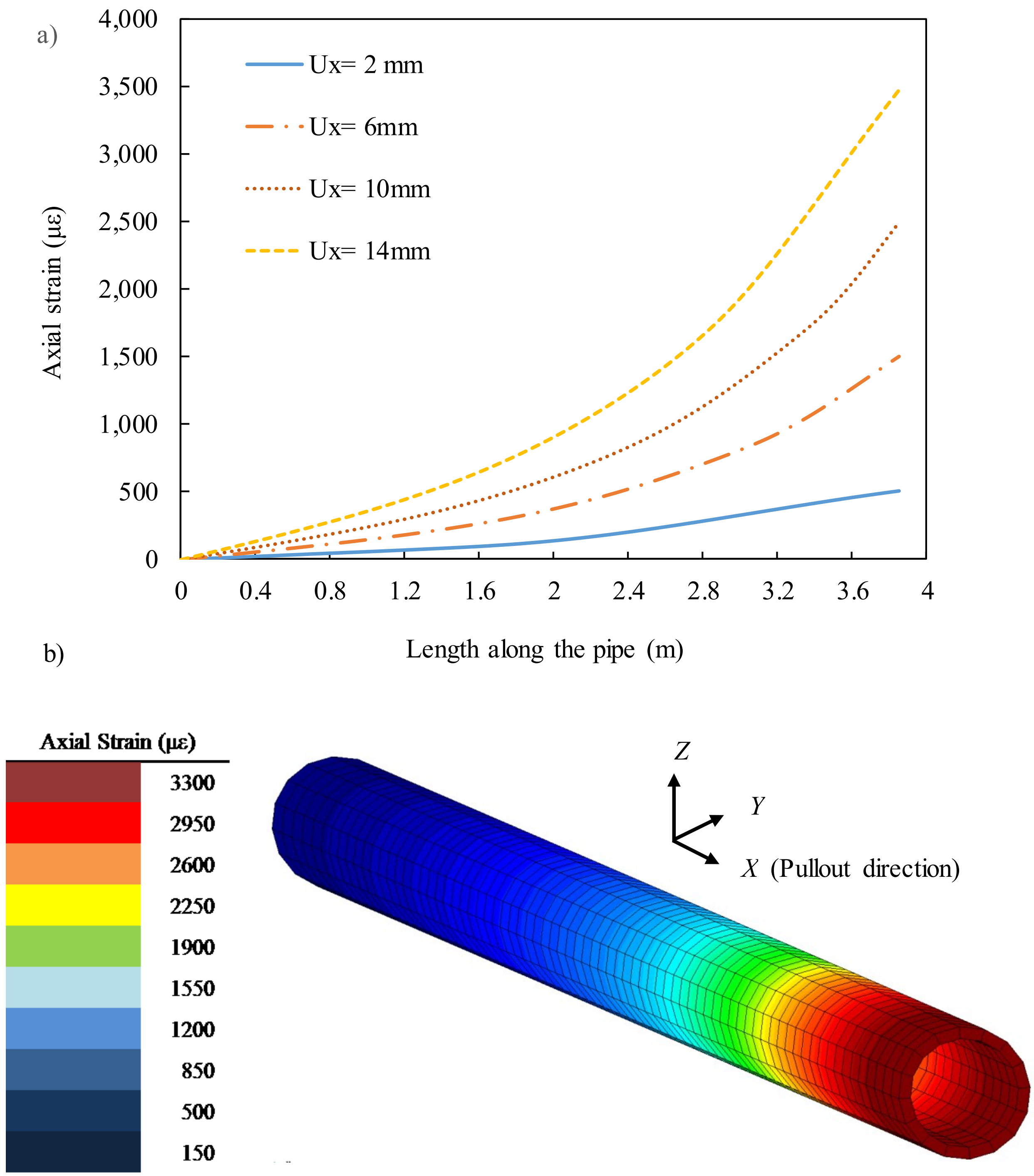

Figure 5-11 a) Axial strain (ε_x) distribution along the MDPE pipe at different leading end displacement (U_x), b) Pipe axial strain at U_x = 14 mm

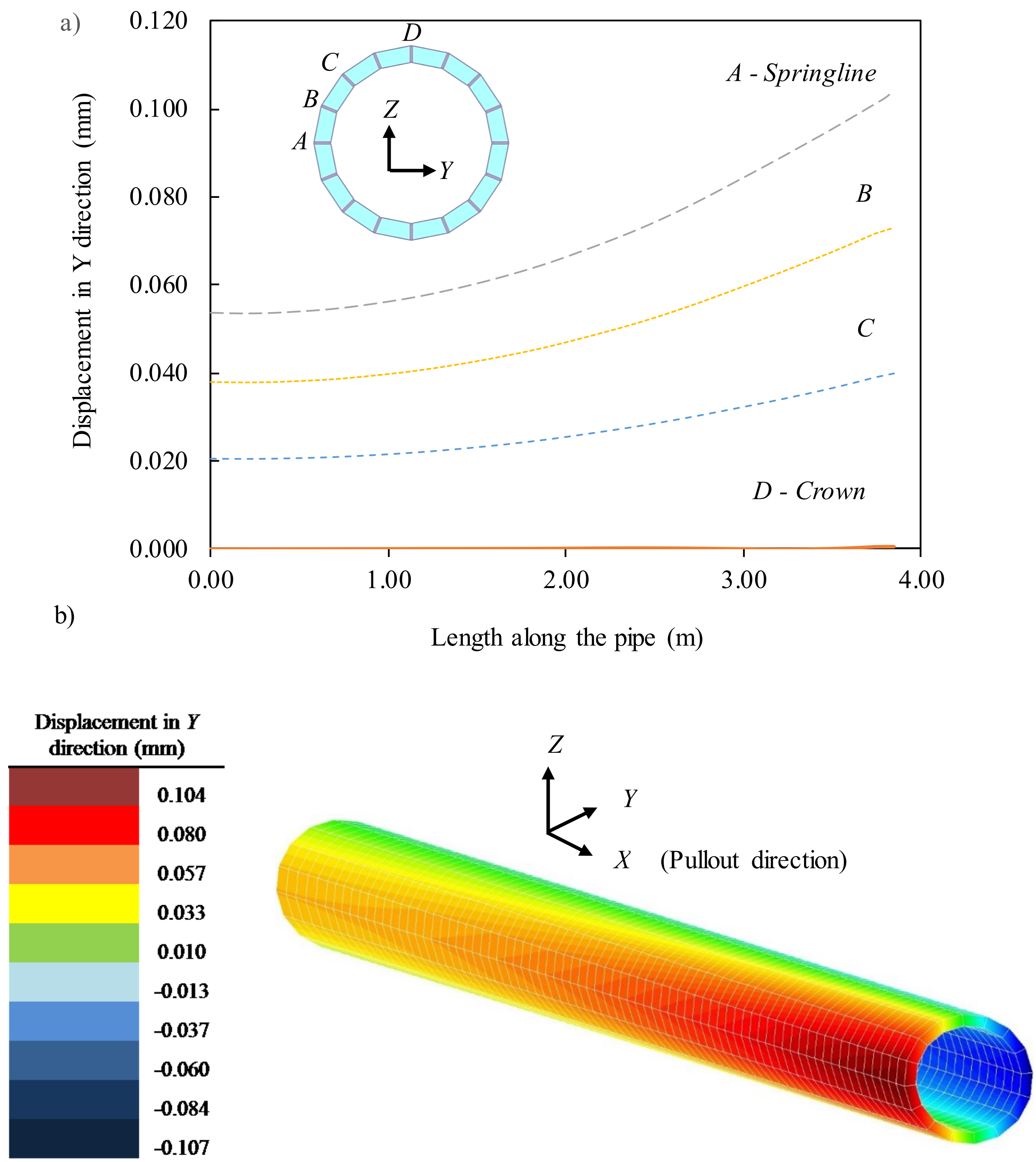

Figure 5-12 a) Displacement in *Y* direction along the MDPE pipe at four different points after 14 mm movement of the leading end (U_x =14 mm), b) distribution of pipe lateral deformation in *Y* direction at U_x =14 mm

5.4.2 Pullout resistance

The pullout force (F_A) per pipe unit length according to ASCE (1984) guidelines is expressed by,

$$F_A = \gamma' \times H \times (\pi D L) \times \left(\frac{1 + K_0}{2}\right) \times \tan(\delta) \qquad 5-2$$

Where γ is soil density; H is the burial depth; D is the pipe diameter; L is the pipe length; K_0 is the coefficient of lateral earth pressure and δ is the interface friction angle between pipe. For the test sample, the resulting pullout force is 1.13 kN/m.

The relationship between the pipe displacement (U_x) at the leading-end and the corresponding pullout force per unit length of the pipe is presented in Figure 5-13. The numerical analysis showed a maximum of pullout force of 1.68 kN/m. Compared with the closed-form solution, it can be seen that the current guideline underestimates the maximum unit pullout force for PE pipes. Another limitation of Eq.5-2 is the related to assumptions of the soil state around the pipe during axial ground movements. In deriving this expression, the soil was assumed to remain at-rest condition. However, Meidani et al. (2017) showed that this assumption may not be valid when the pipe is buried in dense granular soil as the earth pressure condition becomes somewhere between passive and at-rest modes which significantly changes the value of K_0 in Eq.5-2.

5.4.3 Soil response to pipe movement

Figure 5-14 shows the displacement field within the soil domain in the vicinity of the pipe when the leading end displacement reaches 14 mm. Most of the soil movement was found to occur near the front face of the box where the pipe experiences the most elongation. No significant particle movement was recorded near the end of the pipe. Particle movements were characterized by a horizontal pattern that gradually changed to point upward near the front side of the box. It was also found that particle displacements are more significant above the pipe where no wall or rigid boundary exists as compared to the lower boundary below the pipe. The particle movement pattern is in general agreement with the pipe elongation and shows the effect of pipe stiffness on the response of the surrounding soil.

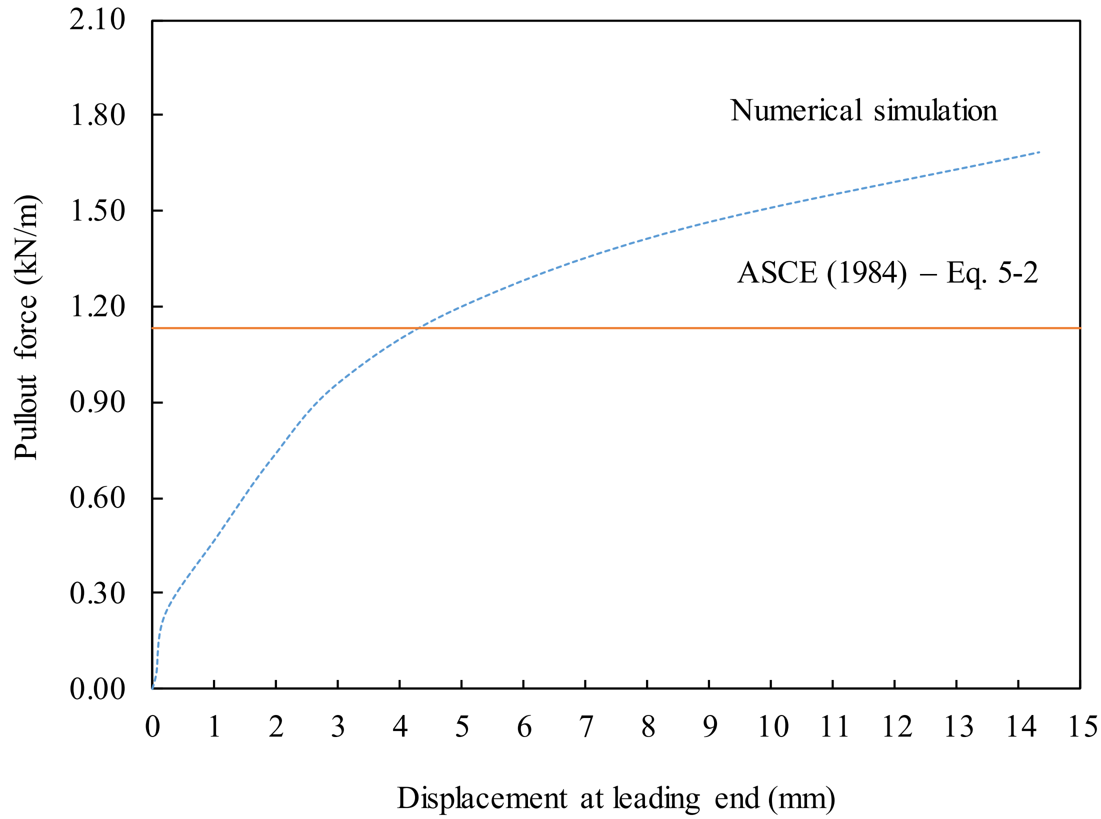

Figure 5-13 Comparison of soil axial resistances (pullout force) between numerical and closed form solution

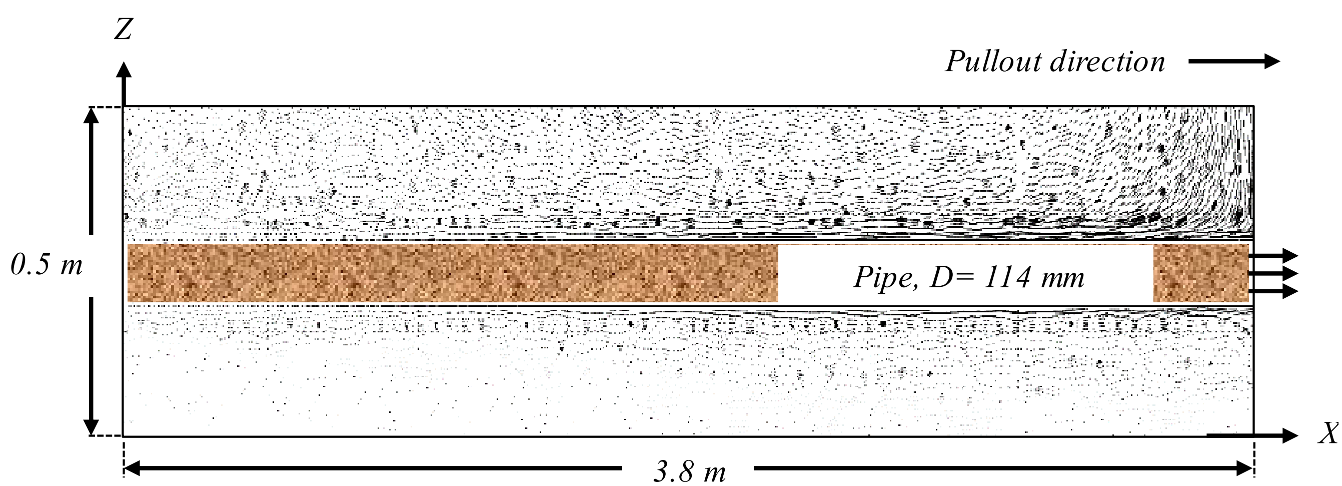

Figure 5-14 Displacement field of the soil domain at U_x= 14 mm

Figure 5-15 shows the contact force network developing within the soil domain for two different loading stages: a) initial condition; and b) at applied displacement of 14 mm. Each contact force is represented by a line such that the line width is proportional to the magnitude of the contact force. Before the pullout force is applied (Figure 5-15a), the contact forces are found to be relatively homogeneous around the pipe. As the pipe is pulled out, the particles near the front face start to move in the pullout direction resulting in dilative response in the close vicinity of the pipe. This has led to an increase in the magnitude of the contact forces in zone *A* as shown in Figure 5-15b. These results allowed for better understanding of the interaction between PE pipe and the surrounding soil material under axial loading conditions.

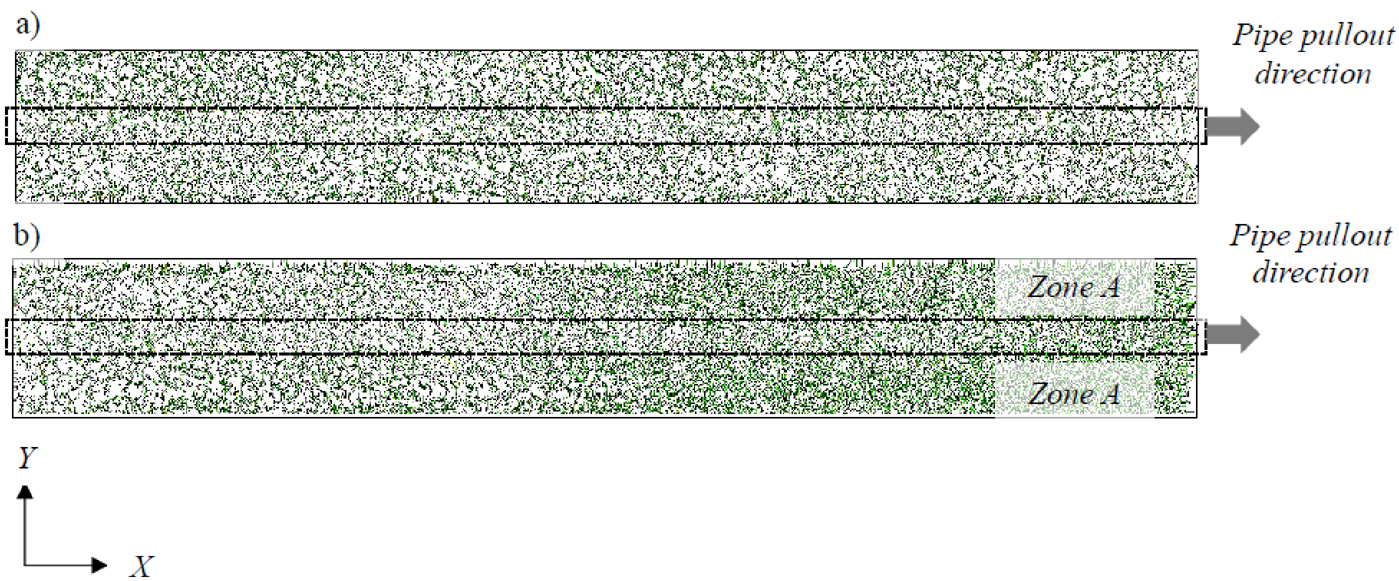

Figure 5-15 Contact force network within the soil domain around the pipe: a) initial condition (before pullout), b) after pullout at U_x=14mm

5.5 Summary and conclusions

In this study, a finite-discrete element framework is employed to investigate the behavior of a MDPE pipe buried in dense sand under axial loading condition. In this 3D analysis, soil particles are modeled using discrete elements whereas the pipe structure is modeled using finite elements. Interface elements are introduced to transfer the forces between the discrete and finites element domains. Particles are generated following the grain size distribution of the Fraser River Sand used in the experiments. Input parameters required for the discrete elements are determined by calibrating the generated assembly using triaxial test results. The pullout process is numerically simulated, and the results are compared with experimental data as well as the available closed-form solution. Deformations and strains developing in the pipe as well as the response of the backfill material are investigated.

Most of the pipe deformation and strains developed near the loaded side and progressively decreased with distance towards the trailing end. For the investigated conditions, the pipe experienced significant elongation combined with a slight distortion in the pipe cross-section. This finding is in contrast with the assumption used in closed-form solutions that considers the pipe as a rigid element with uniform frictional resistance mobilized along the entire length of the pipe. This assumption can result in overestimating the soil frictional resistance for flexible pipes. In addition, dilation of the dense sand material during pullout results in earth pressure that differs from the at-rest condition. This can be significant and may result in underestimating the axial soil resistance for flexible pipes buried in dense material.

Finally, the coupled FE-DE framework presented in this study has proven to be effective in studying the response of buried PE pipe subjected to axial ground movement. The pipe deformation and strain as well as the soil response can be captured using the proposed framework.

Preface to Chapter 6

The developed coupled Finite-Discrete element framework has demonstrated its efficiency in capturing the response of MDPE pipe under axial ground movement. To expand the knowledge on the response of MDPE pipe to ground movement, the coupled framework is now employed to analyze the behavior of MDPE pipe under lateral soil movement. A specific region of the pipe is selected for the simulation and the pipe and surrounding soil behavior are investigated. The capability of the framework to model the soil-pipe interaction at the microscopic scale is demonstrated.

Chapter 6.

A Finite-Discrete Element Approach for Modeling Polyethylene Pipes Subjected to Lateral Ground Movement*

Abstract

The current knowledge of the behavior of polyethylene pipes subjected to lateral soil movement is limited and commonly used design equations were originally developed for steel pipe. In this study, an attempt has been made to understand the soil-structure interaction using a three-dimensional coupled finite-discrete (FE-DE) element model of a medium density polyethylene (MDPE) pipe buried in dense sand and subjected to soil lateral movement. The soil particles are modeled using discrete element whereas the pipe is modeled using finite element and interface elements are introduced to transfer the forces between the two domains. Validation is performed using experimental data. This study shows that on both sides of the loaded section, the pipe will resist lateral forces by bending. The pattern of pipe lateral displacement and axial strain confirm this finding. Particle displacements and the contact force network within the soil show that passive wedges are created close to the pipe ends and the remaining sections of the pipe experienced negligible deformation. Furthermore, it is found that the current equations to estimate the ultimate lateral soil force on the buried pipe in granular soil which is generally developed for rigid steel pipes should be used with caution as they overestimate the load on MDPE pipe. Finally, the coupled framework used in this study has proven to be efficient in studying this class of soil-structure problem.

Keywords: Soil-pipe interaction, Finite-discrete element, polyethylene pipes, lateral ground movement

---

* *A version of this chapter submitted to International Journal of Geomechanics, July 2018.*

6.1 Introduction

Buried Pipes are widely used for transporting oil, gas and water. Natural Resources Canada (NRC) reported that there is more than 840,000 km of transmission and distribution pipelines in Canada. Considering the significant benefits of pipelines on the economy, these infrastructures are classified as lifelines. Only in 2014, Canada has spent \$1.5 billion on monitoring and maintenance to ensure the safety of pipelines; however, the Transportation Board of Canada reported over the past 10 years more than 1200 pipeline incidents occurred in Canada. Parts of the incidents (failures) are related to material corrosion, excavation damage or incorrect operation; however, permanent ground displacement (PGD) causes pipeline failure too. Permanent ground movements due to earthquakes, slope movements and landslides impose unequal displacements between the pipe and surrounding soil which induces excessive flexural and axial strains on pipe structure.

The level of strains and stresses induced by PGD on a pipe are a function of the relative displacement between the soil and the pipe, the spatial distribution of the PGD, the dimensions of the ground movement sector, and the direction of the ground movement relative to the axis of the pipe. For example, if the ground movement is parallel to the pipe (Longitudinal PDG), axial forces are imposed on the pipe and the pipe experiences only axial strains. On the other hand, if the direction of the pipeline is perpendicular to the ground movement (Lateral PGD), then both axial and flexural strains are generated in the pipe. In the past five decades, research has been conducted to study pipe-soil interaction using theoretical, experimental and numerical methods (e.g. Ovesen, 1964; Trautmann and O'Rourke, 1983; Konuk et al., 1999; Weerasekara and Wijewickreme, 2008; Daiyan and Kenny, 2011; Robert et al. 2016; Meidani et al. 2018a). While experimental studies are useful and allow insight on the load-displacement behavior of the buried pipe under soil movements numerical approaches are more suitable to investigate the response of both the pipe structure and the backfill soil.

Finite element methods (FEM) have been widely used to investigate soil-pipe interaction problems (e.g. Guo and Stolle 2005; Xie 2008; Roy et al. 2015; Zhang et al. 2016; Naeini et al. (2016). Roy et al. (2015) conducted a series of finite element analyses on pipelines buried in dense sand subjected to lateral soil movement. The simulation was performed under plain strain condition and the modified Mohr-Coulomb (MMC) model was used considering a number of important soil parameters such as friction and dilation angles within the developed range of plastic shear strain. While the FE method is capable of analyzing soil behavior at macroscopic scale, it is still challenging to consider particle discontinuity and capture their response at the microscale level. The discrete element method (DEM) is an alternative tool to study this class of problems. This method was introduced by Cundall and Strack (1979) and has been employed by several researchers such as Han et al. (2002) and Tran et al. (2014) to study different soil-structure problems. Meidani et al. (2017) performed a large-scale three-dimensional discrete element analysis on a rigid steel pipe buried in dense sand to evaluate the response of the pipe under relative axial ground movement. Although the discrete element method is a promising approach to capture the discontinuous nature of granular material (Lin et al., 2013), modeling structural components using bonded discrete particles (McDowell et al., 2006) may lead to inaccurate prediction of strains and stresses within the structural elements. This has been attributed to the inflexibility of the bonded particles particularly when modeling flexible pipes. Coupling the DE and FE methods is a possible solution that takes advantage of both methods. Several algorithms have been proposed for transferring the loads and displacements between the discrete and finite element models (e.g. Han et al, 2002; Fakhimi, 2009; Villard et al., 2009). Dang and Meguid (2013) proposed a coupled FE-DE approach to model soil-structure interaction problems involving large deformations. They introduced Interface elements between the two domains such that the forces are transferred between the discrete particles and the nearby finite element nodes. Tran et al. (2013) and Meidani et al. (2018b) employed this to study soil-structure interactions.

In this study, a coupled FE-DE approach is presented and employed to evaluate the response of an MDPE pipe buried in dense sand and subjected to lateral ground movements. The backfill material is modeled using discrete particles whereas the MDPE pipe is created using finite elements. A triaxial test is simulated using the adopted particles to determine the micro parameters needed for modeling discrete particles. The model is then used to investigate the response of the MDPE pipe to lateral soil movement and the results are then validated using experimental data. The detailed behavior of the pipe and the surrounding soil such as strains, stresses; contact force network and particle displacement pattern are investigated. Finally, the available design guidelines such as ALA (2001) used to calculate lateral loads on buried pipes is evaluated.

6.2 Soil-pipe interaction

Plastic polyethylene (PE) pipes are commonly used in natural gas distribution networks. Although extensive research has been previously conducted on buried pipes subjected to ground movement, it was mostly limited to steel pipelines. Hence, the developed equations for steel pipes are usually used in guidelines such as ALA (2001) to evaluate the response of the PE pipes. This may result in inaccurate estimates of forces due to the smaller stiffness of polyethylene pipes as compared to steel pipes.

The current approach to calculate the soil resistance to transverse pipe movement is based on a bilinear relationship (Figure 6-1) (Rajani et al. 1995).

$$F_L = K_L \times (U_P - \delta_P) \qquad 6-1$$

where F_L is the soil resistance; K_L is the soil modulus; U_P is the pipeline lateral displacement and δ_P is the soil lateral movement. The response is considered to be linear elastic before the relative displacement exceeds its limiting value (D_p); then the lateral soil resistance reaches its peak value. The common equation used to calculate the ultimate soil resistance on a buried pipe can be expressed as follows:

$$P_u = \gamma \times H \times N_q \times D \qquad 6-2$$

where P_u is the peak soil lateral resistance; H is pipe burial depth; D is diameter of pipe and N_q is a dimensionless force factor. It is noted that N_q is a function of H/D ratio and soil friction angle and there are different charts proposed by researchers and guidelines to obtain this value. For instance, the chart for N_q in ASCE (1984) guideline is based on a study of Trautmann and O'Rourke (1985); however, The American Lifeline Alliance (ALA, 2001) recommended the chart of Hansen (1961) to estimate N_q value.

A schematic diagram of the soil-pipe interaction under lateral ground movement is presented in Figure 6-2. It is noted that the soil force acting on the pipe is not constant, and it depends on soil-pipe relative displacement. For example, the soil resistance on the pipe in region 1 is less than the peak value as the relative displacement is less than D_p. However, in region 2 the pipe is subjected to maximum soil force although the soil is stable in this region. The soil force in region

3 is similar to that of region 2 but the soil displacement is not zero. Finally, region 4 is located close to the center of unstable soil zone and the soil resistance is less than peak value as the pipe and soil displacements are very similar.

The induced lateral force on the pipeline is resisted by two modes of response; bending strains and axial Strains. Early analytical studies on the response of the pipe subjected to lateral soil loading assumed that only pipe bending (bending strains) resists the entire soil force. However, this assumption is only valid for pipe sections under small relative displacements where the stresses remain in the elastic range. For large relative pipe displacements, the pipe sections deform mainly under axial loads where the axial strains carry the soil load. In this case, both axial and shear forces are imposed on the pipe. It has been reported (Chan and Wong, 2004) that pipe sections close to the boundary between stable and unstable soil (regions 2 and 3 in Figure 6-2) bear the soil load via a combination of bending and axial strains; whereas, the remaining section (region 4) carry soil forces entirely by bending. In this study, only sections of the pipeline that carry loads by bending (region 4) are investigated and the equations used to calculate the peak soil lateral forces are reviewed.

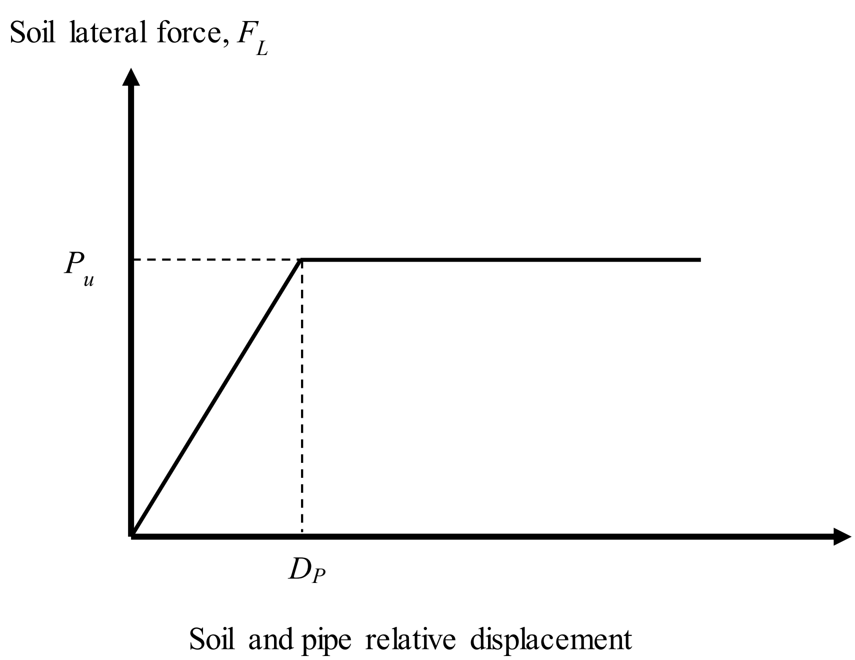

Figure 6-1 Relationship between soil resistance and relative displacement

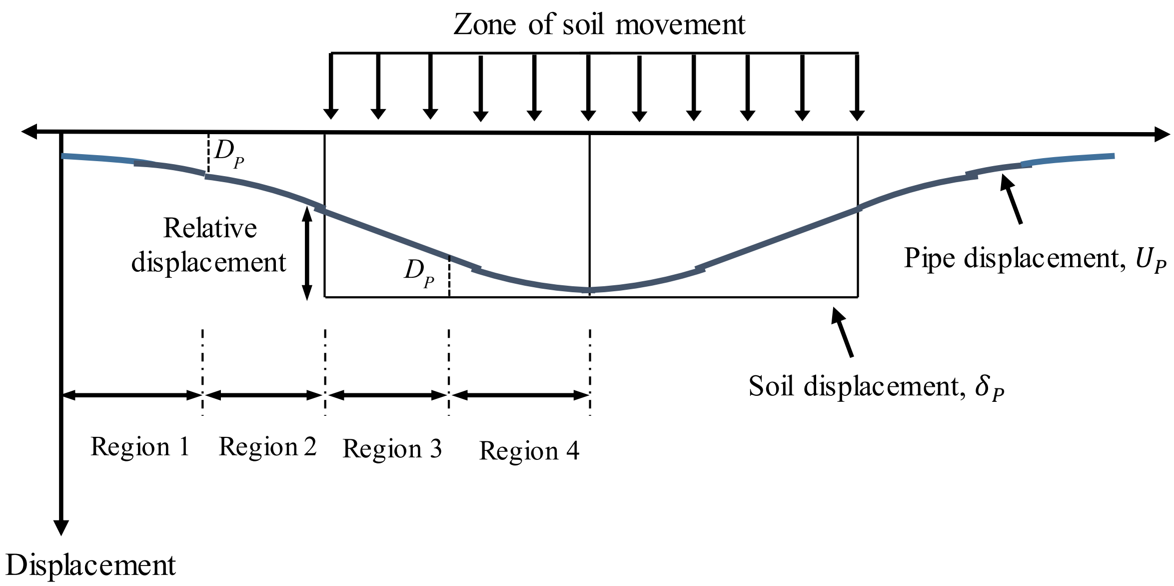

Figure 6-2 Displacement profiles of both the soil and the pipe under lateral soil movement

6.3 Coupled finite-discrete element framework

The code used in this research is based on that of Dang and Meguid (2010, 2013) who developed a coupled *3D FE-DE* framework by implementing an algorithm into an open source discrete element program (*YADE*; Kozichi and Donze, 2008; Smilauer et al., 2010). The general equations of the framework have been already discussed in section 2.4 "Coupling the Finite and Discrete Element Methods" and 2.3.1 "Contact law".

6.4 Model generation

The FE-DE numerical model of this study is created based on the experimental work reported by Weerasekara (2007). A polyethylene pipe 1.5m in length was buried under 0.6 m of Fraser river sand and pulled out laterally while recording pipe deformations and pullout forces. Table 6-1 shows the properties of the backfill material used in the experiment. The numerical model is created to represent the actual experiment. Details of the numerical model are presented below.

The Fraser River sand used in the experiment with relative density of 75% is modeled using spherical particles following the same particle size distribution of the actual soil. As it is numerically impossible to model the exact diameters of sand particles, upscaling is employed to maintain computational feasibility. Ding et al. (2014) reported that the ratio between the smallest sample length *(L)* to the median of the particle diameters (d_{50}) needs to be an above 30 to minimize the effects of particle upscaling on the response of the DEM model. Considering the diameter of the pipe (114 mm) and the soil chamber dimensions, particles with d_{50} of 7.5 mm are chosen for the discrete elements particles. Figure 6-3 presents the particles size distributions of both Fraser river sand and the discrete particles.

Table 6-1 Soil properties of backfill material (Fraser River Sand) based on laboratory and simulated triaxial test with 25-kPa confining stress

Parameter	Value from laboratory triaxial test, Karimian (2006)	Value from the simulated triaxial test
Specific gravity	2.72	-
Young's modulus, E_i (MPa)	40	36
Unit weight (kN/m^3) at $D_r = 75\%$	16	-
Internal friction angle φ (Degree)	45	45
Cohesion (kN/m^2)	0	0
Poisson ratio, υ	0.3	0.28
Porosity, n	0.41	0.41

To determine the optimum model dimensions, 3D finite-element study is first conducted on a box of a width Y ($L_1 + L_2 = Y$) and a pipe length of 1.5 m. The pipe is placed at a distance (Z) from the base (See Figure 6-4). The burial depth ($H = 0.6\ m$) is kept the same as that used in the experimental. Figure 6-5a to Figure 6-5c presents the results of analysis. It is found that, for a displacement of 30 mm, the pullout force is affected if L_1 is less than 0.3 m, L_2 is less than 1.2 m and Z is less than 0.25 m. Therefore, the optimum dimensions of the model are chosen as $1.5\ m \times 1.5\ m \times 0.85\ m$ (Figure 6-6a).

Radius expansion method (Itasca 2004) is employed to generate the discrete particles. It is reported by O'Sullivan (2011) that this approach leads to creating a specimen with isotropic stress state. A cloud of non-contacting spherical particles is created following the particle size distribution presented in Figure 6-3. Spheres located within the pipe circumferences are deleted and the radiuses of the spheres are increased to reach a porosity to 0.41 that represents that of the soil used in the experiment. Gravity is then applied to the model to reach static equilibrium. The final 3D soil specimen that consists of 345’000 spherical particles is presented in Figure 6-6a. A close view of the pipeline and the surrounding soil is shown in Figure 6-6b, confirms the adequacy of the particles sizes to model the soil-pipe interactions.

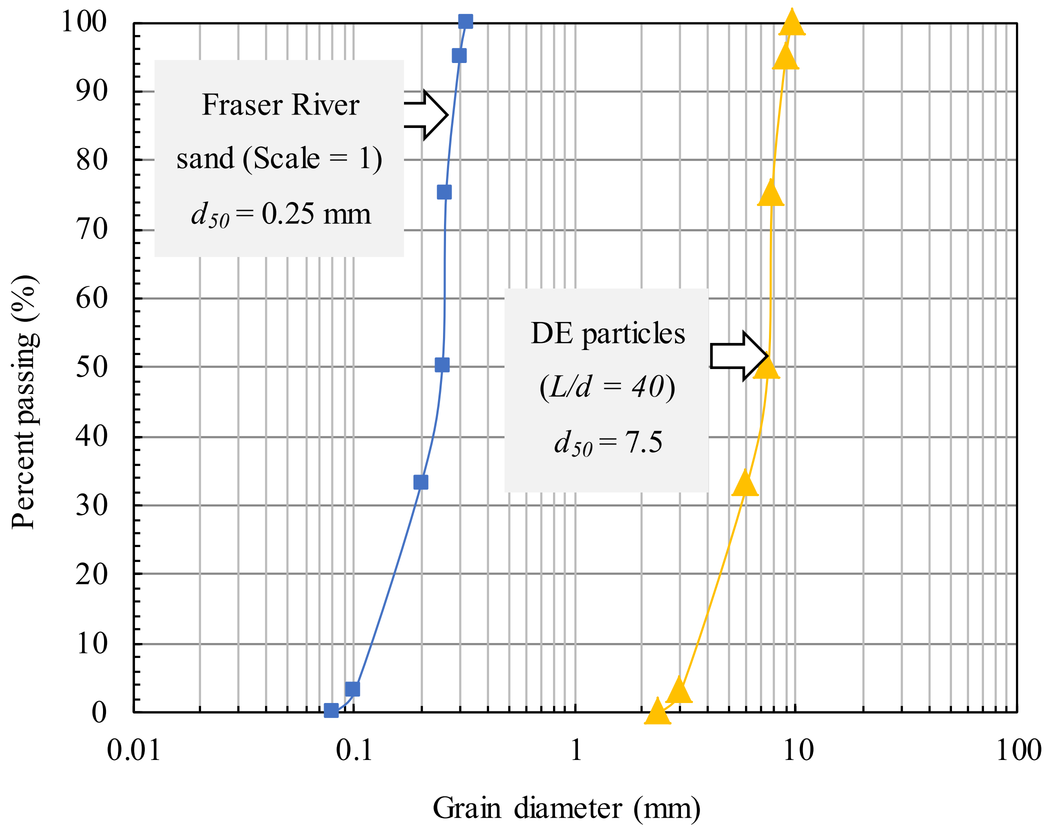

Figure 6-3 Particle size distribution of the Fraser River Sand and the up-scaled discrete element particles

The MDPE pipe (length 1.5 m, diameter 114 m and a wall thickness 10.5 mm) is modeled using 8-noded brick elements. Anderson (2004) and Weerasekara (2007) reported the stress-strain behavior of the used MDPE obtained using compression and axial pullout tests and the results are presented in Figure 6-7a. In addition, the non-linear hyperbolic model proposed by Konder (1963) is also shown in Figure 6-7a. The model is expressed by Eq.6-3 below:

$$\sigma = E_i \left(\frac{\varepsilon}{1 + \eta\, \varepsilon}\right) \qquad 6-3$$

where σ is the stress and ε is the strain. The initial Young's modulus (*Ei*) and η are functions of the strain rate and temperature. It is found that *Ei* of 645 MPa and η of 30 are required to match the experimental data reported by Anderson (2004) and Weerasekara (2007). Given the small level of non-linearity obtained using both experiment and analytical solutions at small strain level, a simplified linear–elastic response with a Young's modulus of 550 MPa is assumed for the MDPE pipe. This assumption is reasonable as the maximum amount of recorded strain is around 0.5%. Figure 6-7b confirms the agreement between the response of hyperbolic model and linear-elastic for the selected range of strains in the MDPE pipe. The pipe model, which comprises 1088 solid elements and 4352 interface elements, is presented in Figure 6-8.

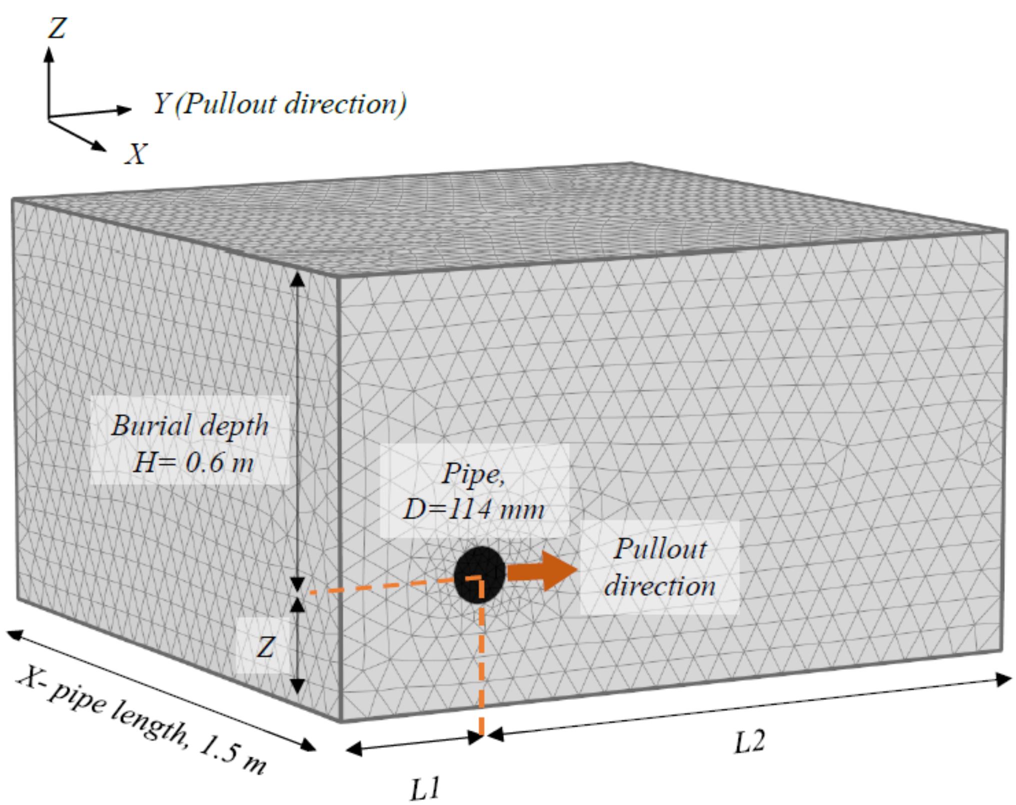

Figure 6-4 Three-dimensional finite element model used to investigate the effect of model dimensions

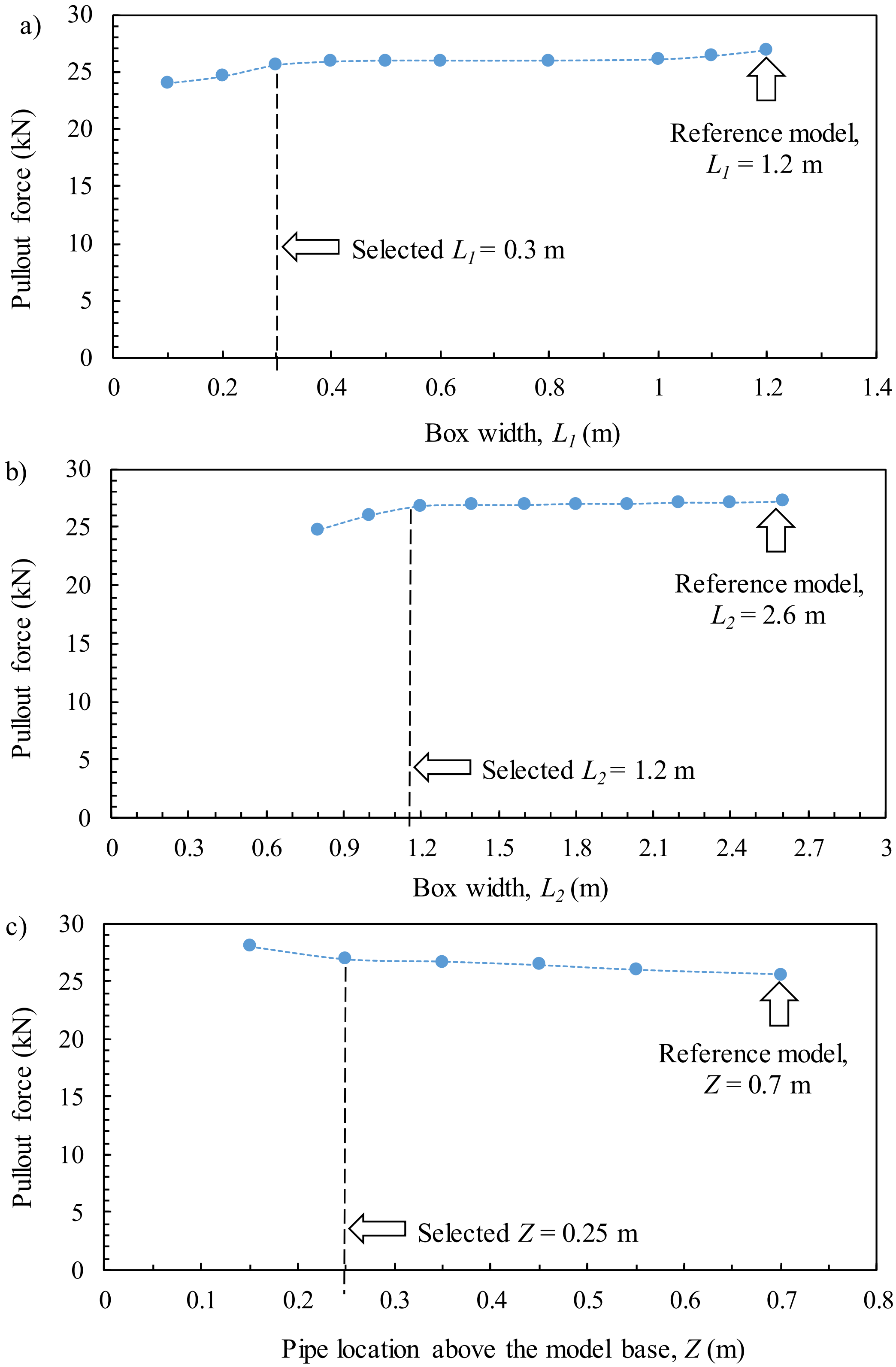

Figure 6-5 Effect of model dimensions on force: a) effect of L_1; b) effect of L_2; c) effect of Z

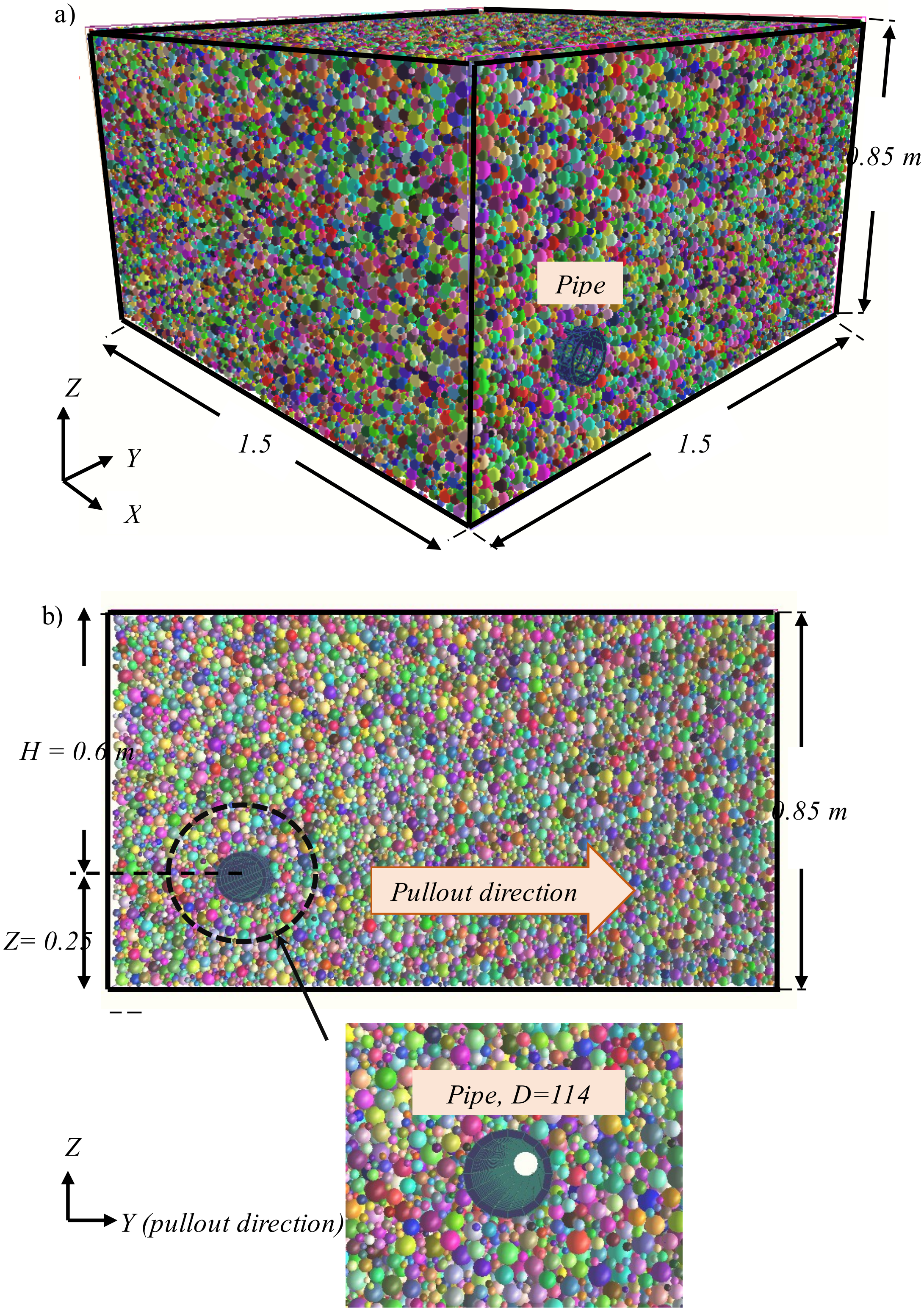

Figure 6-6 The DEM model, a) 3D view showing the pipe and the surrounding particles; b) A close view of the pipe

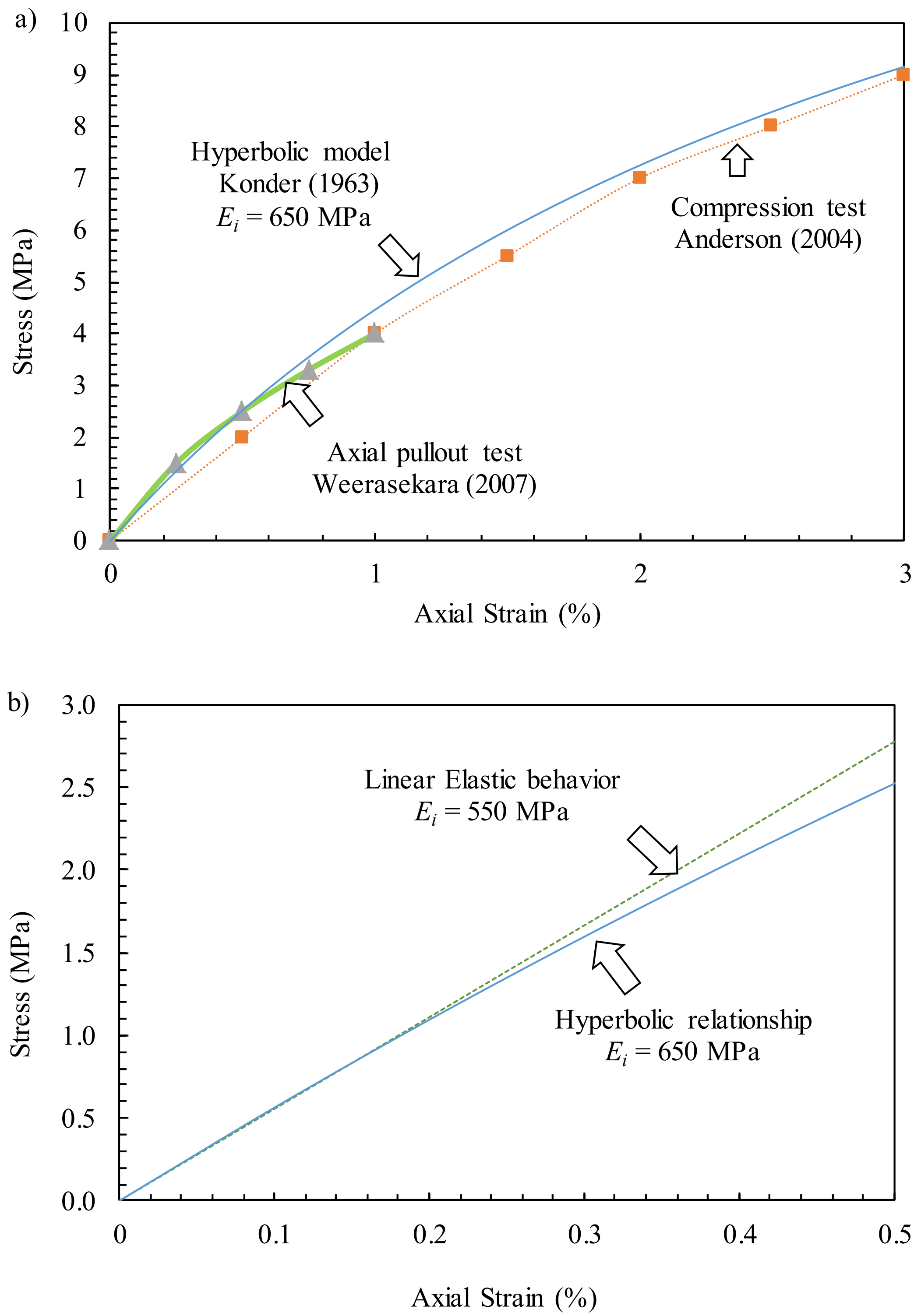

Figure 6-7 a) Experimental stress-strain response of the MDPE vs. the hyperbolic model, b) comparison between linear elastic and hyperbolic models at small strain

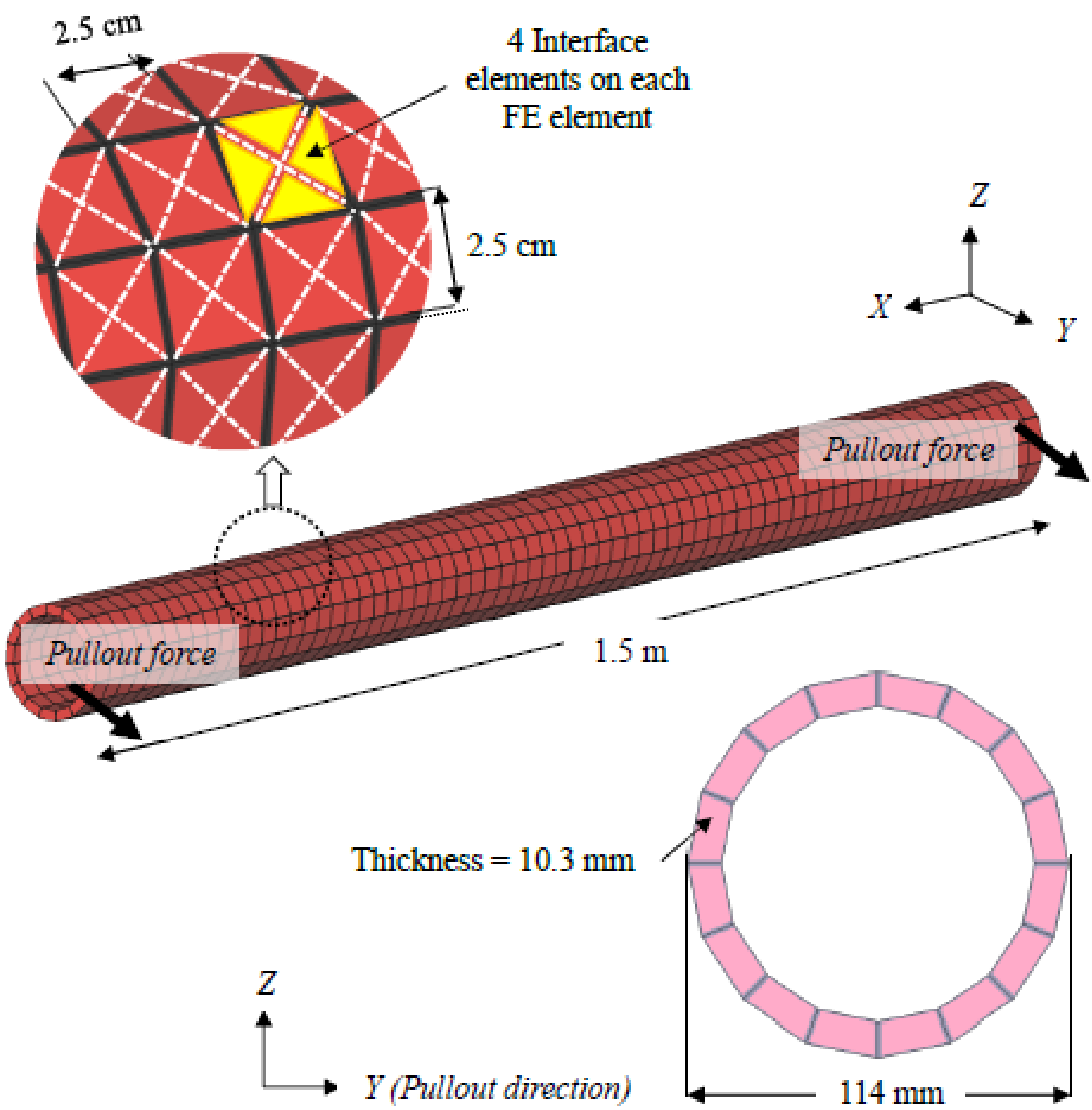

Figure 6-8 Geometry of the simulated MDPE pipe and interface elements

6.5 Pullout test simulation

Input parameters needed for the discrete element analysis are obtained by calibration of the modeled particles using triaxial test results. Karimian (2006) performed a number of triaxial tests on Fraser River sand under different confining stresses. The triaxial test specimen is created following the same particle size distribution used in the pipe test. The details of the calibration procedure were reported by Meidani et al. (2017). The mechanical properties of the Fraser River sand based on laboratory and simulated triaxial tests conducted at 25 kPa confining stress are presented in Table 6-1. Results show a good agreement between the calculated and measured values which confirms the suitability of the used particle assembly. A summary of the input parameters used in the analysis is given in Table 6-2.

The coupled model is created, and the input parameters presented in Table 6-2 are assigned to both the FE and DE. No friction was considered along the walls to follow the conditions in the experiment (Weerasekara, 2007). A parametric study is conducted to evaluate the effect of the properties of the interface elements (Stiffness and interface angle) on the pullout test results. It is found that the changes in interface friction angle have negligible effects on the pullout force. Hence, a friction angle similar to that of the particles (45 degrees) was adopted for the interface elements. It is also found that interface stiffness plays an important role in results of the analysis. Interface stiffness of 500 MPa is found to provide a good match between the calculated and measured responses. The properties of the interface elements are presented in Table 6-2.

Table 6-2 Input parameters used in the coupled FE-DE analysis

Type of element	Parameter	Value
Discrete particle	Density (kg/m^3)	2720
	Particle modulus, E (MPa)	150
	Ratio K_T/K_N , α	0.7
	Micro friction angle, φ_{micro} (Degree)	45
	Rolling resistance coefficient (β_r)	0.15
	η_r	1
	Damping ratio	0.2
Finite element	Young's modulus, E (MPa)	550
	Poisson's ratio,	0.46
Interface element	Material modulus, E (MPa)	500
	Ratio K_T/K_N , α	0.7
	Micro friction angle, φ_{micro} (Degree)	45

The MDPE pipe is pulled laterally following a displacement control approach. Lateral displacement was applied to the pipe ends to simulate the conditions in region 4 (Figure 6-2 Displacement profiles of both the soil and the pipe under lateral soil movement). The lateral pulling continued until a displacement of 65 mm is reached, where the pullout force converged to a constant value. The relationship between the pipe pullout force and the lateral displacement are presented in Figure 6-9. It should be noted that the pullout force reported in this figure is for one end of the pipe. The outcome of the analysis is found to be in agreement with the experimental results and the peak lateral force (P_u) is estimated at 7.9 kN. The maximum difference between simulation results and the experiment is 15% at a lateral displacement of 10 mm in the early stage of the test. Since the peak lateral force (soil lateral resistance) is of paramount importance in this study, and given the simplified nature of the analysis, the results of the coupled simulation are considered to be acceptable.

6.6 Results and discussions

6.6.1 Response of the pipe

The lateral deformation of the MDPE pipe in the *Y* direction as a function of end displacements (U_y) of 5, 20, 40 and 65 mm are plotted in Figure 6-10a. The largest displacement of the pipe occurs around the edges and decreased rapidly towards the pipe center. This can be attributed to the small Young's Modulus of the polyethylene and the high flexibility of the pipe. This is in contrast with rigid steel pipes where the entire length of the pipe moves as a rigid body within the soil domain under lateral force. In addition, it is concluded from Figure 6-10b that the pattern of the lateral displacement is uniform in all pipe sections with no significant changes found in the shape of the cross-section.

The horizontal displacement distribution within the pipe at U_y=65 mm is presented in Figure 6-11. Figure 6-11a shows the displacement at the springlines, A and B. The horizontal displacement patterns are found to be the same for both sides of the springline and no horizontal displacement calculated at the pipe center which means that no axial strains have developed in these areas. The displacement direction indicates, that the front side of the pipe is under compression whereas the back-side experiences tension. However, the maximum displacement in the backside (line A) is more than front side (Line B). The horizontal displacement distribution shown in Figure 6-11b illustrates the pipe elongation is not constant and decreases towards the bending neutral axis which confirms the lateral soil force is carried by pipe bending.

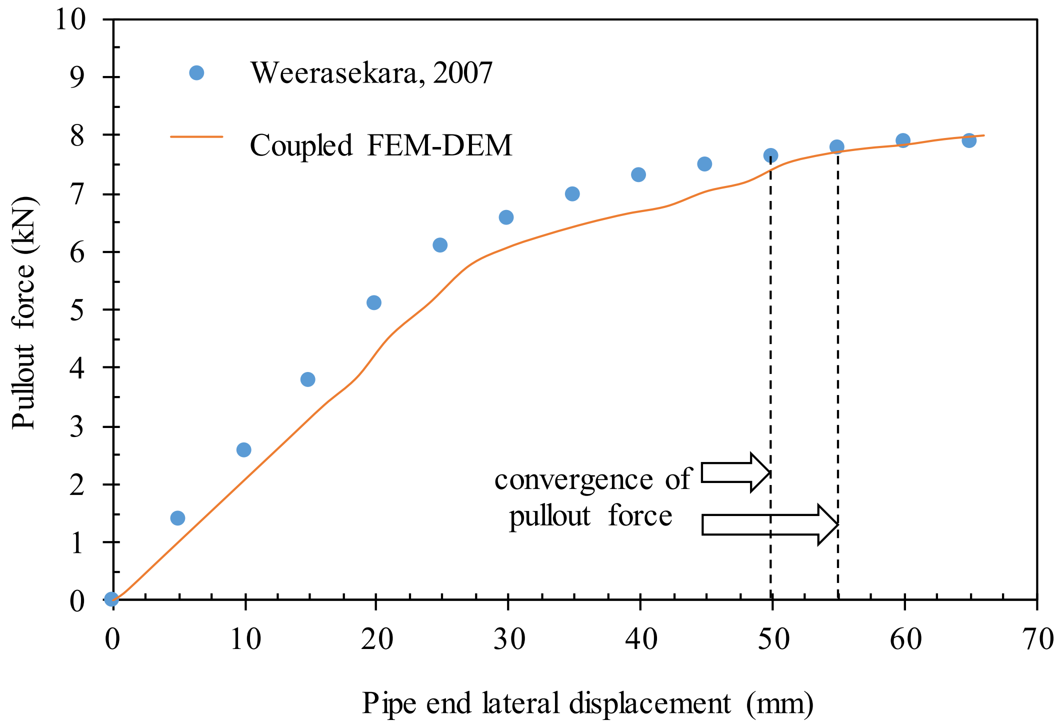

Figure 6-9 Comparison between the measured and calculated pullout responses of the pipe

Axial strains (ε_{XX}) along the pipe length are analyzed to understand the load carrying mode of the MDPE pipe under lateral movement. Figure 6-12 presents the axial strains along the pipe at applied displacement U_y of 65 mm. The strain on line A which represents the back side of the pipe is found to be positive which means that tensile strains and stresses developed on this face of the pipe. However, the front side of the pipe (Line B) is under compression. The values of strains at the diametrically opposite location of the pipe are opposite in direction but almost similar in magnitude which confirms the pipe section resists the soil force entirely by bending in comparison. This conclusion agrees with Chan and Wang (2004) that reported the bending stresses on the pipe under lateral soil movement develop in sections far from the abrupt differential ground movement (Region 4 in Figure 6-2).

The bending moment of the pipe can be calculated using the obtained axial strains utilizing a bending moment equation (Eq. 6-4). Since the strains are small enough and the neutral axis passes through the centroid of the section.

$$\sigma_X = E \times \varepsilon_X = \frac{M_Z \times C}{I_Z} \qquad 6-4$$

Figure 6-13 presents the calculated bending moments (M_z) at three different pipe lateral displacements. It was observed that the maximum bending moment occurs close to the pipe edges at the location of the maximum relative soil-pipe displacement and decreases rapidly toward the center of the pipe where the relative displacement is almost zero.

6.6.2 Pullout resistance

As mentioned in previous sections, Eq.6-2 is generally used to estimate the peak lateral soil load on pipes in granular soil. In this equation N_q is the capacity factor and researchers used different charts based on empirical results. Pipe burial depth, pipe diameter and soil friction angle are the main parameters used to determine N_q. However, despite the importance of pipe stiffness and soil relative density, these are not considered in the equation. This implies that, two pipes of different material (e.g. steel and MDPE) and the same diameter buried at the same depth, are expected to carry the same maximum lateral soil force. Therefore, predictions made by Eq. 6-2 for those cases are not reasonable. In this section, the results of the coupled analysis are compared with five different proposed solutions to calculate the peak force for laterally loaded pipes in sand. The selected studies are Audibert and Nyman (1977), Rowe and Davis (1982), ASCE (1984) which is based on O'Rouke (1988), Wilson-Fahmy, Koerner and, Sansone (1994) and ALA (2001) which is based on Hansen (1961). Table 6-3 compares the results of the numerical analysis with above selected methods. It can be seen that the above solutions generally overestimate the ultimate soil force by several folds. Rowe and Davis (1982) and ASCE (1984) solutions are the closest to the numerically calculated values. However, Audibert and Nyman (1977) and ALA (2001) recommendations show significant discrepancies. Karimian (2006) performed a lateral pullout test on a steel pipe located in sand and reported that the O'Rouke (1989)'s chart which is recommended by ASCE (1984) predicted similar ultimate soil force values. The ALA (2001) formulation on the other hand produced force values that are several times higher than those predicted by simulation.

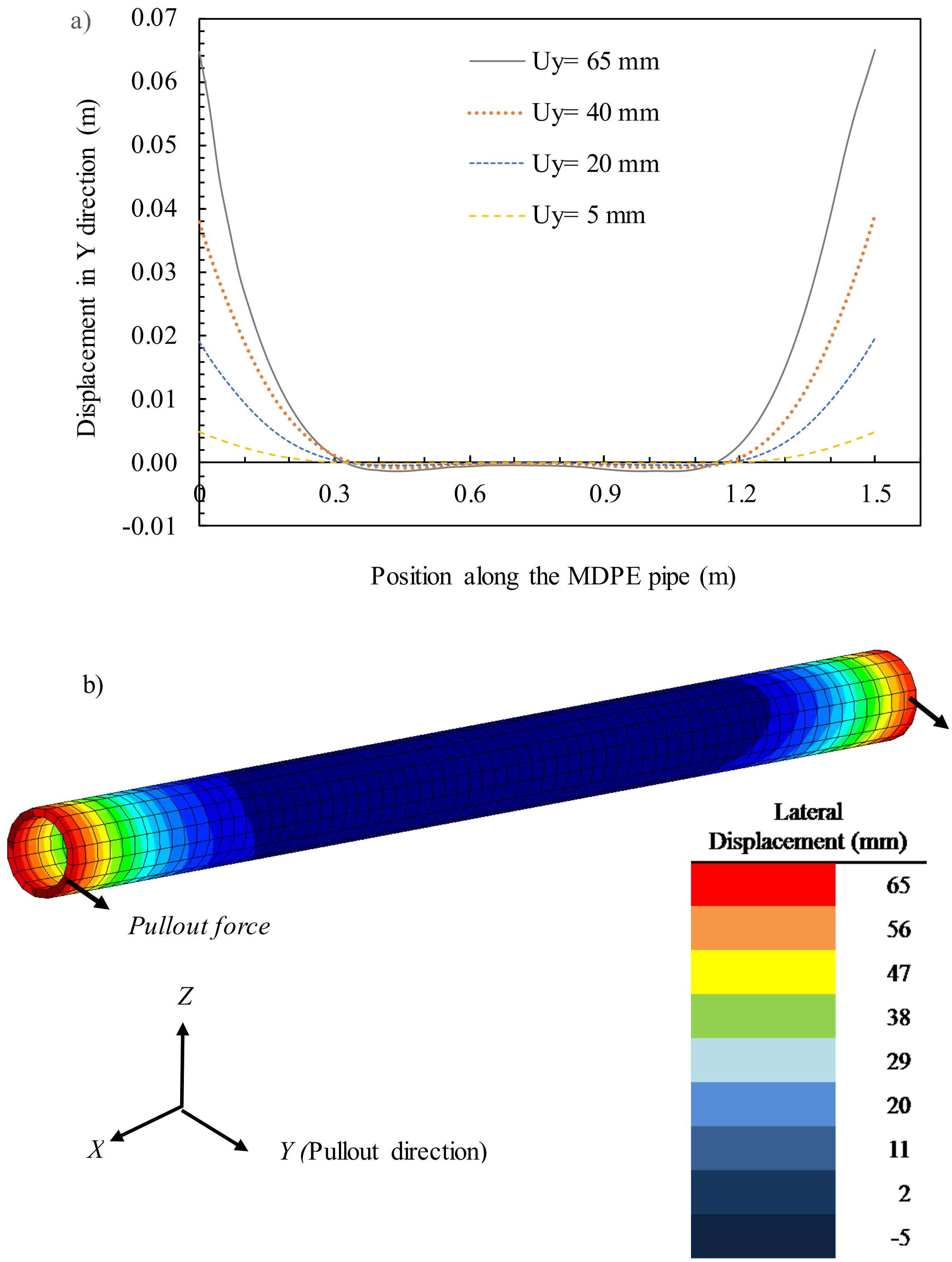

Figure 6-10 Lateral displacement along the pipe length, a) for different applied displacements; b) at maximum displacement of U_y = 65 mm

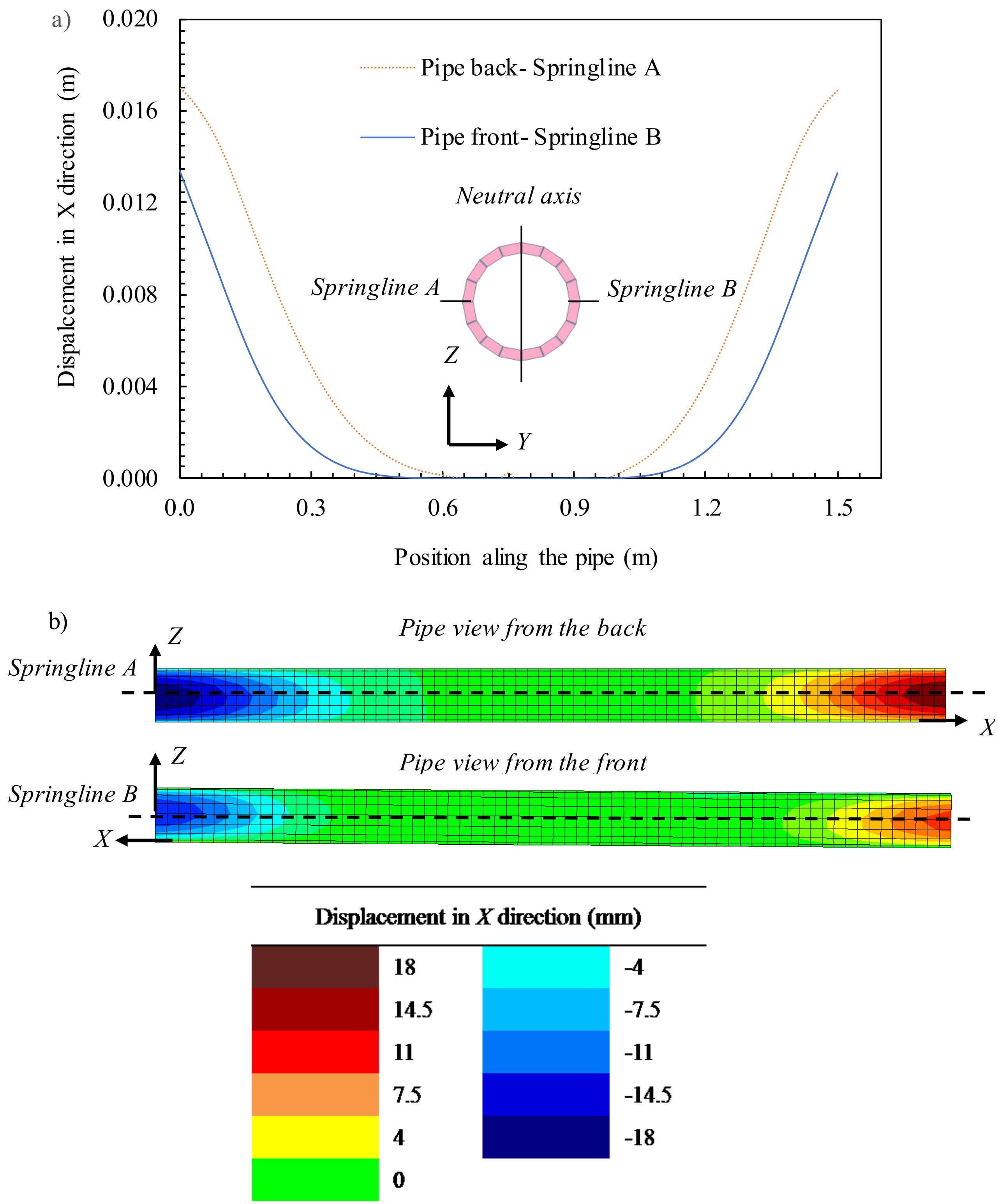

Figure 6-11 Axial displacement along the pipe at applied lateral displacement U_y of 65 mm

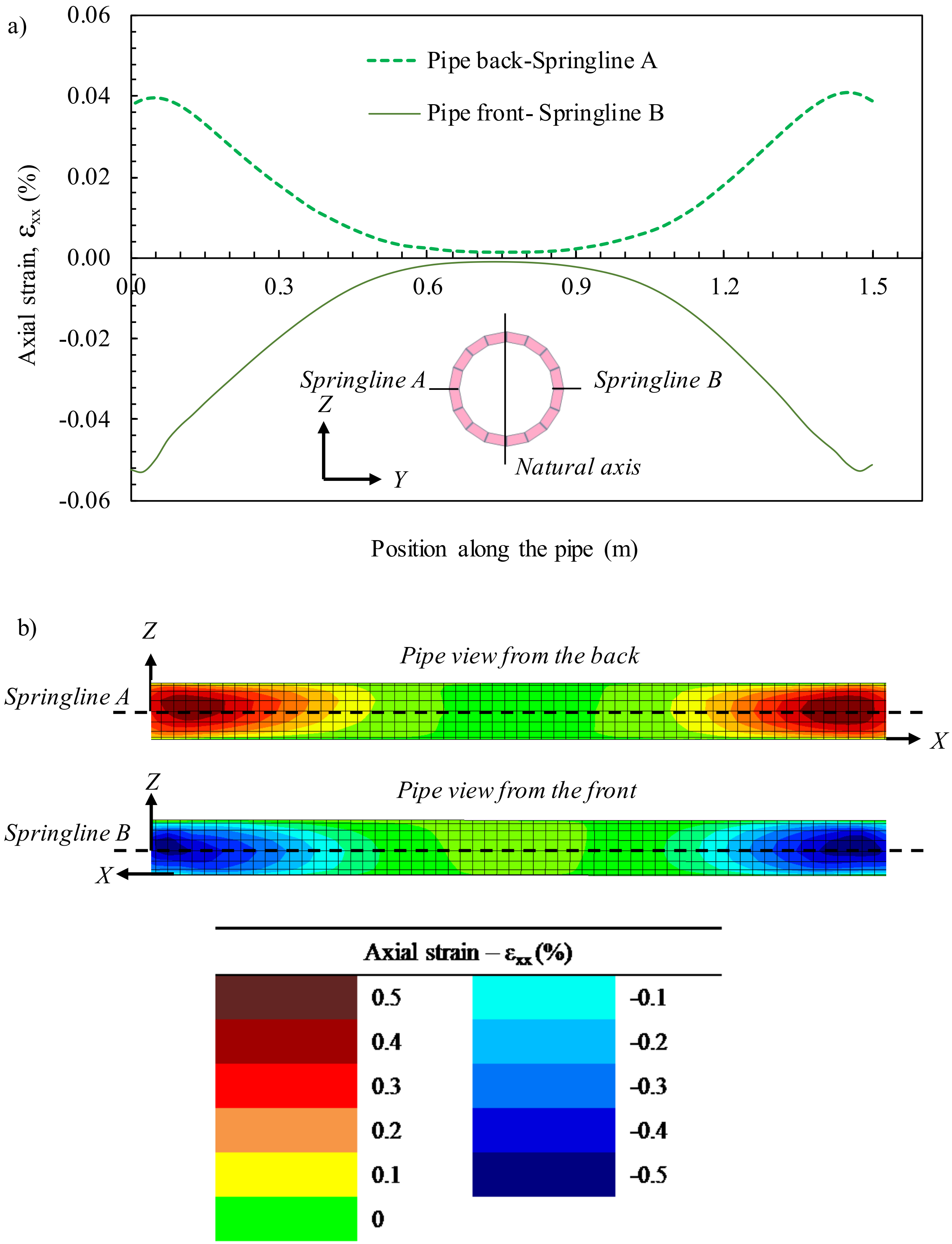

Figure 6-12 Axial strain along the pipe at U_y of 65 mm

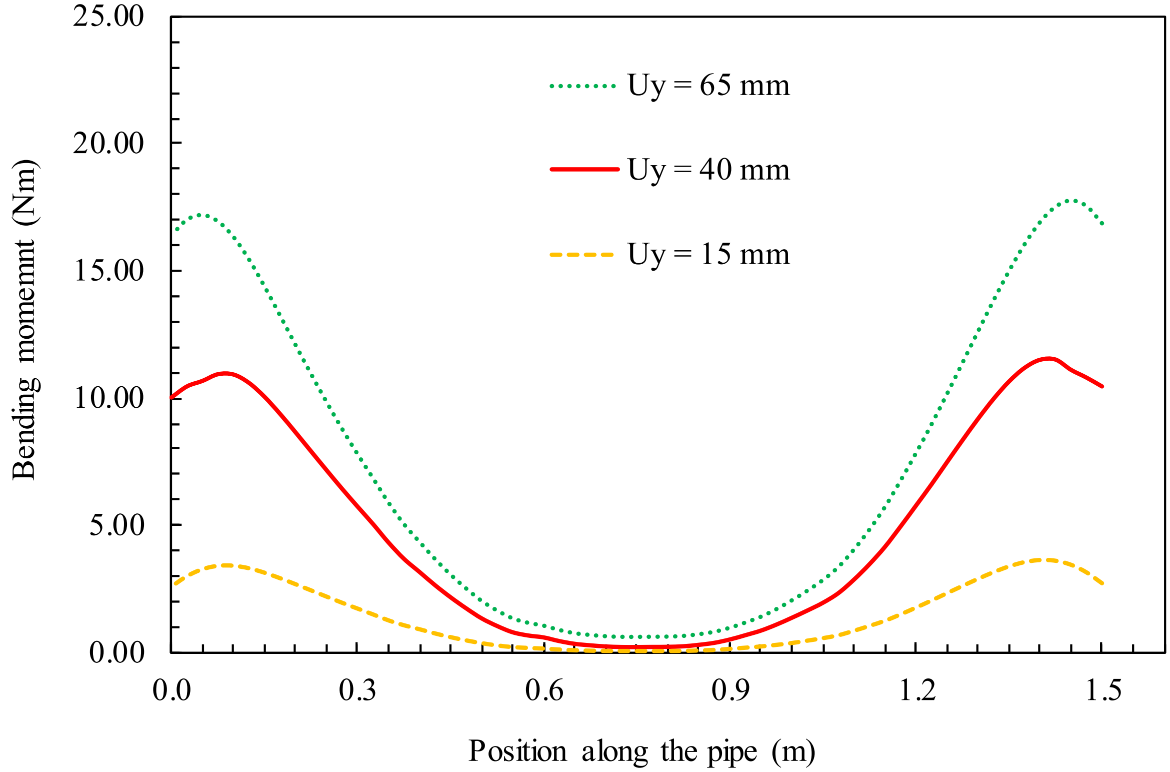

Figure 6-13 Bending moment (M_z) along the pipe for different applied displacements

Table 6-3 Comparison between the numerical results and the proposed formulation to determine the ultimate pressure for laterally loaded pipe in sand

Reference	Nq	P_u (kN)
Current study	-	15.8
Audibert and Nyman (1977)	37	65.8
Rowe and Davis (1982)	15	26.7
ASCE (1984) - Based on Trautmann and O'Rourke (1985)	16	28.5
Wilson-Fahmy, Koerner and Sansone (1994)	25	44.5
ALA (2001) Based on Hansen (1961)	40	71.1

6.6.3 Soil response to pipe movement

Particle displacements can be used to better understand the response of the soil domain. Figure 6-14 presents particle displacements within the test box at lateral displacement of 65 mm. It is observed from Figure 6-14a that most of the soil displacements occurred near the pipe ends resulting in soil densification in these areas (*Zone A*). Particle movements decreased gradually and became negligible near the middle of the pipe. In addition, particles behind the pipe and the near the walls experienced insignificant displacements. Particles in *zone A* moved toward the pipe center as the pipe starts bending. Figure 6-14b shows particle movements as seen from the side view. It is clear that particles close to the pipe move in the horizontal and upward direction which creates a passive soil zone in front of the pipe and a shear failure path within the soil domain. The creation of passive wedge within the soil is found to be non-uniform along the pipe length which is in contrast with observations by Karimian (2006) for a rigid steel pipe. It can be concluded that MDPE pipes do not behave as a rigid element due to their relatively low Young's modulus as compared to steel and only some segments of the pipe reach the ultimate lateral force.

The deformation of the soil surface is depicted in Figure 6-15. Figure 6-15a shows that upward movement occurs at the top of the pipeline due to the pipe lateral movement and the creation of a passive wedge. However, the soil deformation at the pipe ends are larger than the middle parts. The difference of soil movement along the pipe is illustrated in Figure 6-15b.

The soil-pipe interaction under the lateral pipe movement can be further investigated by plotting the contact force network within the particle domain (Figure 6-16). Each line represents the force between two contacting particles and the line thickness represents the relative magnitude of the normal contact force. As the lateral displacement is applied to the pipe at two ends, the pipe starts bending and the soil particles movement cause an increase in a contact force value around the pipe ends which is labeled *Zone A* in Figure 6-16. Contact force network closer to the middle part of the pipe are negligible as no significant pipe movements are calculated in these areas (*Zone B*). The contact force network of particles is found to be in agreement with the deformation of the pipe-soil system and confirms the development of passive wedges near the pipe ends.

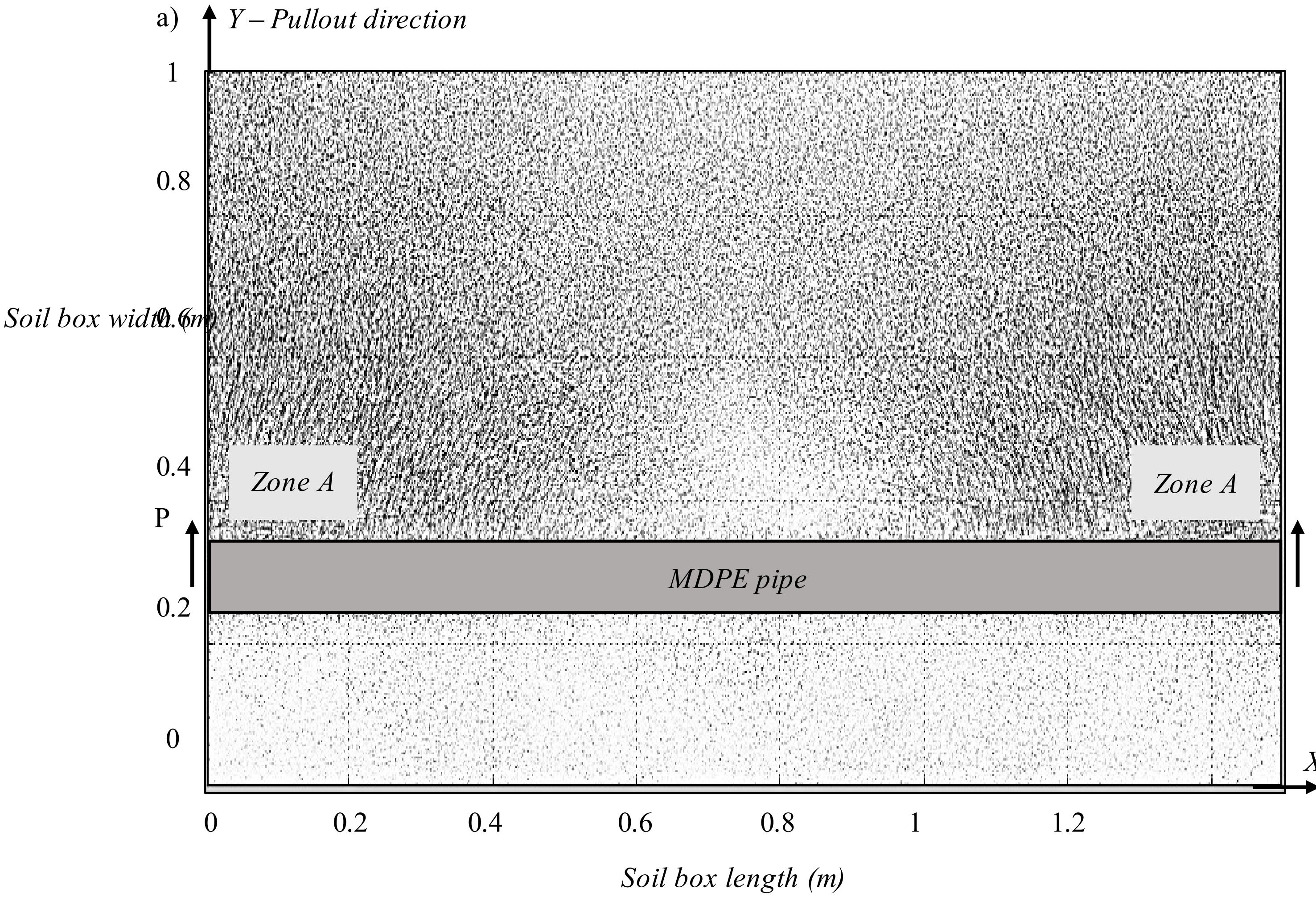
a)
Y – Pullout direction
1
0.8
Soil box width (m)
0.6
0.4
Zone A
Zone A
P
P
MDPE pipe
0.2
0
X
0
0.2
0.4
0.6
0.8
1
1.2
Soil box length (m)

b)

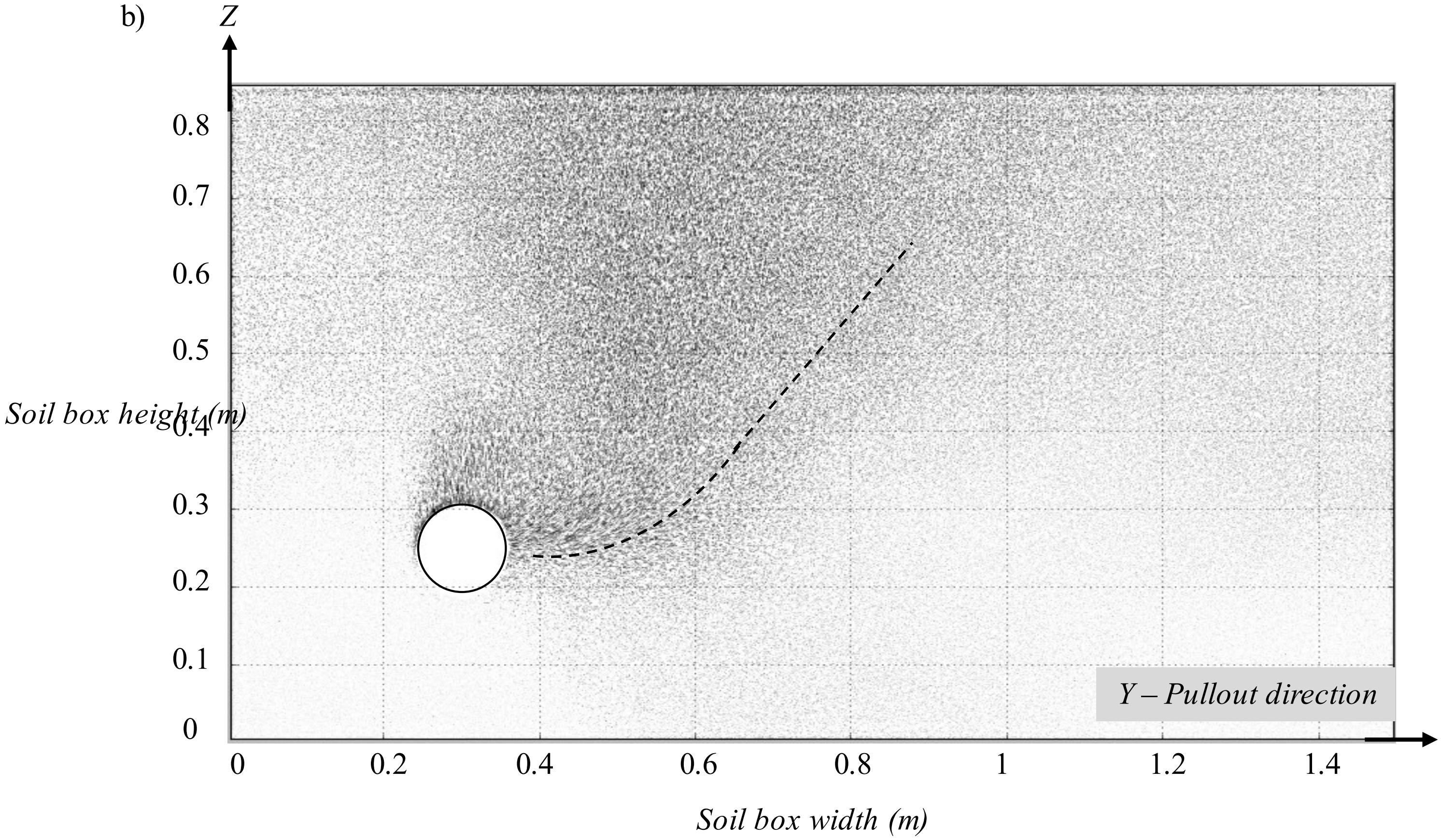

Figure 6-14 Displacement field within the soil domain at U_y of 65 mm, a) Partial plan view; b) Side view

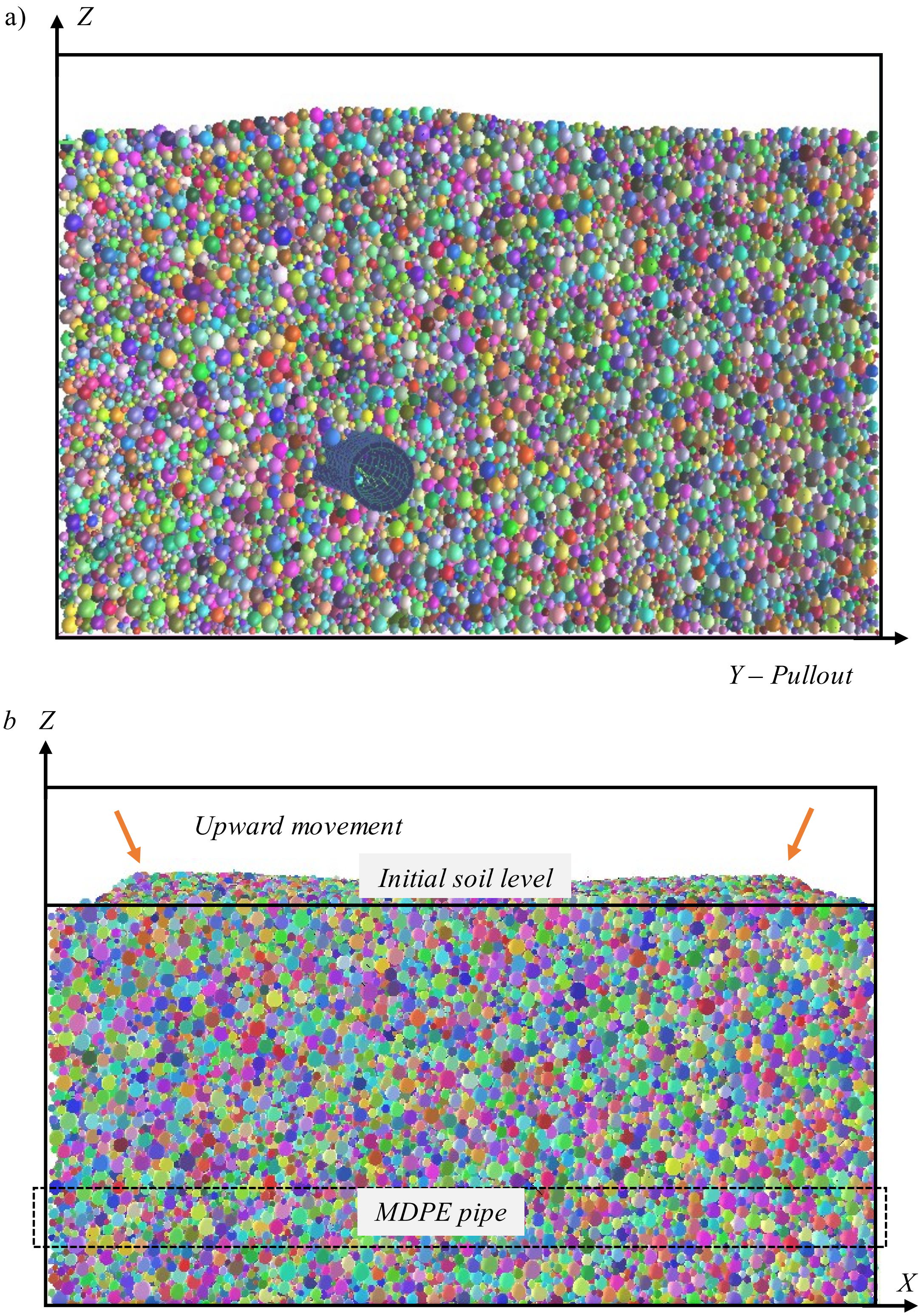

Figure 6-15 Snapshots of the particle displacements at applied displacement of Uy = 65 mm; a) Y-Z view, b) X-Z view

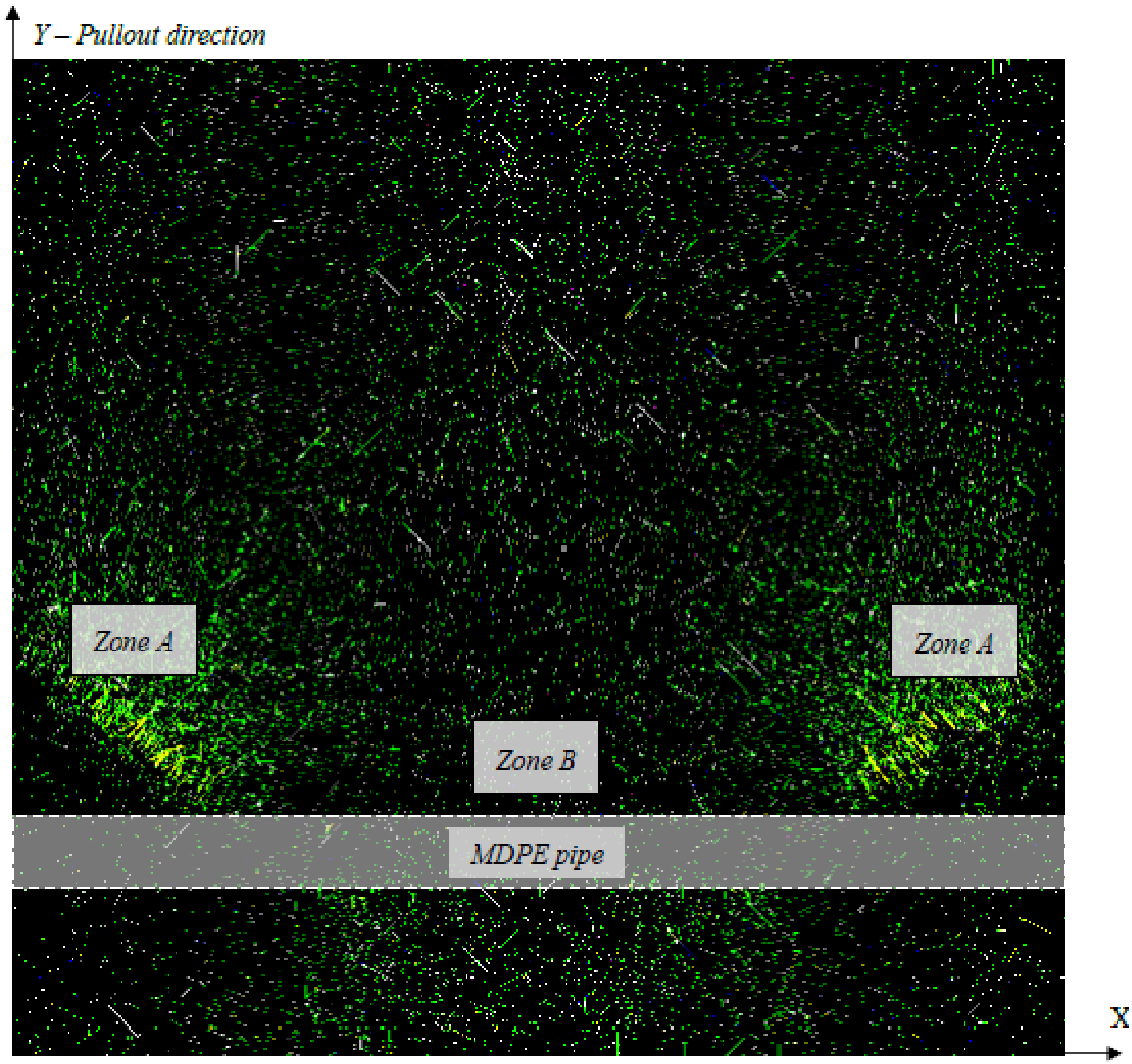

Figure 6-16 Top view of the contact-force network within the particle domain at Uy of 65 mm

6.7 Summary and conclusions

In this study, the interaction of dense granular soil and MDPE pipe under lateral soil movement is evaluated using a coupled finite-discreet element framework. In this framework, pipe structure is modeled using finite elements and the soil particles are modeled using discrete element method. The soil domain is generated following the particle size distribution and density of Fraser River sand used in experiments. A calibration procedure is followed to determine the micro scale parameters of the particles. The lateral pullout force is numerically applied to the pipe and the pipe response including displacements, strains and bending moments are calculated. The maximum value of the lateral force is compared with experimental result as well as five of the commonly used equations. In addition, the particle deformation and contact force network are examined. The conclusions of this study are presented below:

1- Buried MDPE pipes in dense sand subjected to lateral ground movement carry external load via a combination of bending and tensile strains. However, the pipe sections far from the abrupt displacement area carry the soil load totally by bending.
2- The deformation pattern of MDPE pipe to lateral load is in contrast with rigid steel pipes as the middle sections of the MDPE pipe experience no lateral deformation, which means there is no relative soil and pipe displacement.
3- The maximum strains and bending moments are calculated near the pipe ends where the maximum soil and pipe displacement occurs. These locations experience the maximum lateral soil force.
4- The ultimate lateral soil load on the MDPE pipe is significantly smaller than that found using the current guidelines particularly the ALA (2001) recommendations. These guidelines are generally developed for steel pipes and the relatively small Young's modulus of the polyethylene as compared to steel explains these discrepancies.
5- Surface movement is found to be larger within the areas experiencing higher relative soil and pipe displacement, which are located close the pipe ends. Surface movement decreased towards the middle of the pipe.
6- The coupled FE-DE framework employed in the research has proven to be effective in studying the response of the buried MDPE pipes subjected to lateral ground movement.

The pipe deformation, strains, and stresses as well as the response of the soil domain can be captured using the proposed framework.

Chapter 7.

Conclusions and Recommendations

7.1 Conclusions

In this thesis, the discrete element method has been used to evaluate the response of steel pipes buried in dense sand subject to axial soil movement. Results of the numerical simulation were validated using experimental data and compared with current available solutions. A comprehensive parametric study has been conducted to evaluate the effect of different parameters on the pipe response and a new expression has been proposed. The discrete element method has proven to be an efficient tool in modeling rigid pipes buried in granular material involving large deformation. Furthermore, a coupled finite-discrete element framework has been modified and employed to evaluate the response of flexible pipe interaction under relative axial and lateral ground movements. The results of the coupled finite-discrete element simulations were first validated using experimental data and then used to provide a new insight into the nature of the three-dimensional interaction between the flexible pipe and the surrounding soil. The following statements can be concluded from the thesis:

1) Using 3D discrete element analysis, it was found that the maximum soil axial resistance on the pipe is higher than that predicted using the commonly used solutions (e.g. ASCE (1984)). This increase in soil axial force can be attributed to the change in normal pressure acting on the pipe. This can be explained by the dilation of the dense sand during interface shear deformation. It means that the soil condition around the pipe is no longer in at-rest condition after the relative soil-pipe deformation and a new lateral pressure coefficient (K^*) needs to be defined. This study suggests that the commonly used equations to calculate axial soil resistance on pipe under axial ground movement should be used with caution. Also, the outcome of the simulations suggests that K^* value ranges between K_o and 2. Results obtained in this chapter provided the needed confidence in the discrete element framework in modeling soil-pipe interaction problems.

2) In chapter 4, a series of analysis was performed a new expression was proposed to obtain a modified earth pressure coefficient (K^*) that is appropriate for dense sand condition.

After conducting a comprehensive parametric study, it is found K^* value is a function of pipe diameter, burial depth, soil friction angle and soil modulus. It is found that the predicted maximum axial soil resistance using the proposed expression agrees with the measured value and the numerical results. It should be noted that the suggested equation for K^* is only valid for steel pipes buried in dense sand material.

3) In chapter 5, a coupled Finite-Discrete element framework was modified and employed to simulate flexible pipe-soil interaction. The framework allows for coupling finite and discrete element methods. The interaction between the finite and discrete element domains is controlled using interface elements. The developed model was used to investigate the three-dimensional response of an MDPE pipe buried in dense sand subject to axial soil movement. The pipe was modeled using finite elements while the surrounding soil was modeled using discrete elements. A good agreement between numerical results and experimental data was found. The peak axial soil resistance is more than that predicted using the available closed-form solution. Most of the pipe deformation occurred around the front end of the pipe and it decreases progressively with distance toward the tailing end. This is in contrast with the assumption used in the closed-form solution that considers the pipe as a rigid element with uniform frictional resistance. Furthermore, the dilation of the dense sand around the pipe surface can change the soil condition around the pipe due to interface shear displacement resulting in underestimating the axial soil resistance for flexible pipe buried in dense granular material. Also, particle movement pattern and the contact force network within the soil domain agreed with the experimental observations.

4) In chapter 6, the developed coupled Finite-Discrete element framework was used to evaluate the interaction of dense granular soil and MDPE pipe under lateral soil movement. Validation of the developed model was conducted by comparing the calculated and measured data. The maximum lateral force is compared with experimental results as well as five of the commonly used equations. It is found that pipe sections far from the abrupt ground movement carry soil load totally by bending. Lateral deformation of the MDPE pipe is in contrast with the pattern of rigid steel pipe and middle sections of the pipe experiences no lateral deformation meaning no relative soil and pipe

displacement.The maximum strains and bending moments occurred around the pipe ends where the maximum lateral force was applied. The maximum lateral soil load is significantly smaller than the predicted value using the current guidelines, particularly ALA (2001). These guidelines are generally developed for steel pipes and the relatively smaller Young's modulus of the polyethylene compared to steel material explain these discrepancies.

5) The coupled FE-DE framework employed in the research has proven to be effective in studying the response of buried pipes in granular soil subjected to axial and lateral ground movement.

7.2 Recommendations for future work

Various pipe-soil interaction problems can be studied using the developed coupled finite-discrete element framework including:

- The response of rigid and flexible pipes under oblique ground movement.
- The effect of backfill properties on the maximum soil load acting on the pipe under ground movement
- The effect of particle size distribution of the backfill material on the pipe response.
- The efficiency of geosynthetic materail elements such as expanded polystyrene (EPS) on reducing soil pressure on pipes subject to ground movement
- Investigating the response of the pipe wrapped in geotextile to the axial and lateral ground movement

Chapter 8.
References

Ahmed, M.R., Tran, V., and Meguid, M.A., 2015. On the role of geogrid reinforcement on reducing earth pressure on buried pipes: experimental and numerical investigations. Soils and Foundations, 55(3), 588-599.

American Lifelines Alliance (ALA), 2001. Guideline for the design of buried steel pipe. available from www.americanlifelinealliance.org/Product_new3.htm

Almahakeri, M., Fam, A. and Moore, I.D., 2013a. Longitudinal Bending and Failure of GFRP Pipes Buried in Dense Sand under Relative Ground Movement, Journal of Composites for Construction, ASCE , Vol. 17:702-710, September.

Almahakeri, M., Fam, A., & Moore, I. D., 2013b. Experimental investigation of longitudinal bending of buried steel pipes pulled through dense sand. Journal of Pipeline Systems Engineering and Practice, 5(2), 04013014.

Almahakeri, M., Moore, I. D., & Fam, A., 2016. Numerical Study of Longitudinal Bending in Buried GFRP Pipes Subjected to Lateral Earth Movements. Journal of Pipeline Systems Engineering and Practice, 04016012.

Anderson, C. 2004. Soil–pipeline interaction of polyethylene natural gas pipelines in sand. M.Sc. thesis, Department of Civil Engineering, University of British Columbia, Vancouver, B.C.

Asadzadeh, M., & Soroush, A., 2017. Macro-and micromechanical evaluation of cyclic simple shear test by discrete element method. Particuology, 31, 129-139.

ASCE. 1984. Guidelines for the seismic design of oil and gas pipeline systems. Committee on Gas and Liquid Fuel Lifelines, American Society for Civil Engineering (ASCE), New York.

Audibert, J. M. E., and Nyman, K. J., 1977. Soil restraint against horizontal motion of pipes. Journal of the Geotechnical Engineering Division, ASCE, 103(GT10), 1119- 1142.

Bardet, J.-P., 1997. Experimental soil mechanics, Prentice Hall Upper Saddle River, NJ.

Belheine, N, J-P Plassiard, F-V Donzé, F Darve, and A Seridi, 2009. Numerical simulation of drained triaxial test using 3D discrete element modeling. Computers and Geotechnics, Vol. 36, No. 1, pp 320-331.

Bhuvaraghan, Baskaran, Sivakumar M Srinivasan, Bob Maffeo, Robert D McCLain, Yogesh Potdar, and Om Prakash, 2010. Shot peening simulation using discrete and finite element methods. Advances in Engineering Software, Vol. 41, No. 12, pp 1266-1276.

Bilgin, O., Stewart, H. E., O'Rourke, T. D., 2007. Thermal and mechanical properties of polyethylene pipes, Journal of Materials in Civil Engineering, 19 (12): 1043-1052.

Bolton, M. D., 1986. The strength and dilatancy of sands, *Géotechnique*, p. 65-78.

Bridgewater, J. 1980. On the width of failure zones. Geotechnique, 30(4): 533–536.

Cappelletto, A., Tagliaferri, R., Giurlani, G., Andrei, G., Furlani, G. and Scarpelli, G., 1998. Field full scale tests on longitudinal pipeline-soil interaction, Proceedings of International Pipeline Conference, Calgary, Alberta, ASME, Vol. 2, pp.771-778.

CEPA: about pipelines. C2016. Canadian Energy Pipeline Association (CEPA). http://www.cepa.com/.

Chan, P. D. S., Wong, R. C. K., 2004. Performance evaluation of a buried steel pipe in a moving slope: a case study. Canadian Geotechnical Journal, 41, 5, 894-907.

Cho N, Martin C, Sego D., 2007. A clumped particle model for rock. Int J Rock Mech Min Sci 44(7):997–1010.

Cocchetti, G., di Prisco, C., Galli, A., and Nova, R., 2009. Soil–pipeline interaction along unstable slopes: a coupled three-dimensional approach. Part 1: Theoretical formulation. Canadian Geotechnical Journal, 46(11): 1289–1304.

Cui, L, O'Sullivan, C., 2006. Exploring the macro-and micro-scale response of an idealized granular material in the direct shear apparatus. Geotechnique. 56(7), 455-468.

Cui, L, C O'sullivan, and S O'neill, 2007. An analysis of the triaxial apparatus using a mixed boundary three-dimensional discrete element model. Geotechnique, Vol. 57, No. 10, pp 831-844.

Cundall, P. A, Strack, O. D., 1979. A discrete numerical model for granular assemblies, Geotechnique, Vol. 29, No. 1, pp 47-65.

Daiyan, N., Kenny, S., Phillips, R. and Popescu, R., 2011. Investigating pipeline–soil interaction under axial–lateral relative movements in the sand. Canadian Geotechnical Journal. 48(11), 1683-1695.

Dang, H.K. and Meguid, M.A., 2010. Evaluating the performance of an explicit dynamic relaxation technique in analyzing nonlinear geotechnical engineering problems. Computers and Geotechnics, 37(1), 125-131.

Dang, H. K, Meguid, M. A. 2013. An efficient finite-discrete element method for quasi-static nonlinear soil-structure interaction problems, International journal for numerical and analytical methods in geomechanics, Vol. 37, No. 2, pp 130-149.

Danish Hydraulic Institute (DHI) and Ramboll and Hannemann, 1985. Danish Submarine Guidelines. Danish Energy Agency.

Dhia, Hashmi Ben, and Guillaume Rateau, 2005. The Arlequin method as a flexible engineering design tool. International journal for numerical methods in engineering, Vol. 62, No. 11, pp 1442-1462.

Ding, X., Zhang, L., Zhu, H., & Zhang, Q., 2014. Effect of Model Scale and Particle Size Distribution on PFC3D Simulation Results. Rock Mechanics and Rock Engineering. 47, 2139-2156.

European Gas Pipeline Incident Data Group, 2018. Gas pipeline incidents. European Gas pipeline Incident Data Group (EGIG), Groningen, Netherlands. 10th EGIG Report 1970–2018, No. EGIG 05-R-0002.

Fakhimi, A., 2009. A hybrid discrete–finite element model for numerical simulation of geomaterials, Computers and Geotechnics, Vol. 36, No. 3, pp 386-395.

Gabrieli, F., Cola, S., & Calvetti, F., 2009. Use of an up-scaled DEM model for analysing the behaviour of a shallow foundation on a model slope. Geomechanics and Geoengineering: An International Journal, 4(2), 109-122.

Gibson, R.E., and W.F. Anderson, 1961. "In situ measurement of soil properties with the pressuremeter." Civil engineering and public works review, 56(658), 615-618.

Guo, P. J., Stolle, D. F. E., 2005. Lateral pipe-soil interaction in sand with reference to scale effect, Journal of Geotechnical and Geoenvironmental Engineering, ASCE, 131 (3): 338-349.

Han, K, DRJ Owen, and D Peric, 2002. Combined finite/discrete element and explicit/implicit simulations of peen forming process. Engineering Computations, Vol. 19, No. 1, pp 92-118.

Hansen, B.J., 1961. The ultimate resistance of rigid piles against transversal forces. Bulletin 12, Danish Geotechnical Institute, Copenhagen, Denmark.

Hoeg, K., 1968. Stresses against underground structural cylinders. Journal of Soil Mechanics and Foundations. ASCE 94(4), 833–858.

Honegger, D.G., Nyman, D.J., 2004. Guidelines for the seismic design and assessment of natural gas and liquid hydrocarbon pipelines. Pipeline Research Council International (PRCI), Inc., Arlington, VA. Catalogue No. L51927.

Hsu, T. W., 1994. Rate effect on lateral soil restraint of pipeline. Soils and Foundations, 33(4), 159-169.

Hsu, T. W., Chen, Y. J. and Wy, C. Y., 2001. Soil resistant to oblique movement of buried pipes in dense sand, Journal of Transportation Engineering, 127 (1): 82-87.

Huang, H., 1999. Discrete element modeling of tool-rock interaction. PhD thesis, University of Minnesota, Minneapolis, MN.

Hughes, Thomas JR, 1995. Multiscale phenomena: Green's functions, the Dirichlet-to-Neumann formulation, subgrid scale models, bubbles and the origins of stabilized methods, Computer methods in applied mechanics and engineering, Vol. 127, No. 1, pp 387-401.

Itasca 2002, FLAC-Fast Lagrangian Analysis of Continua; User’s Guide. Itasca Consulting Group.

Itasca, 2004. PFC 2D 3.10 particle flow code in two dimensions, theory and background volume, 3rd Ed., Minneapolis.

Jing, X. Y., Zhou, W. H., Zhu, H. X., Yin, Z. Y., & Li, Y., 2018. Analysis of soil-structural interface behavior using three-dimensional DEM simulations. International Journal for Numerical and Analytical Methods in Geomechanics.

Joshaghani, M.S., Raheem, A. M., Mousavi, M. R., 2016. Analytical Modeling of Large-Scale Testing of Axial Pipe-Soil Interaction in Ultra-Soft Soil. American Journal of Civil Engineering and Architecture, 4(3), 98-105.

Jung, J. K., O'Rourke, T. D., & Argyrou, C., 2016. Multi-directional force–displacement response of underground pipe in sand. Canadian Geotechnical Journal, 53(11), 1763-1781.

Karamitros, D. K., Bouckovalas, G. D., & Kouretzis, G. P., 2007. Stress analysis of buried steel pipelines at strike-slip fault crossings. Soil Dynamics and Earthquake Engineering, 27(3), 200-211.

Karimian, H., 2006. Response of buried steel pipelines subjected to longitudinal and transverse ground movement. Ph.D. thesis, Department of Civil Engineering, The University of British Columbia, Vancouver, B.C.

Karimian, H., Wijewickreme, D., and Honegger, D.G., 2006. Buried pipelines subjected to transverse ground movement: Comparison between full-scale testing and numerical modeling. In Proceedings of the 25th International Conference on Offshore Mechanics and Arctic engineering, Hamburg, Germany.

Konder, R.B. 1963. Hyperbolic Stress-Strain Response: Cohesive Soils. Journal of the Soil Mechanics and Foundations Division, ASCE, 89(SM1): 115-143.

Konuk, I., Hilips, R., Urley, S. and Paulin, M. J., 1999. Preliminary ovalization measurement of buried pipelines subject to lateral bending. Submitted to 18th offshore mechanics and arctic engineering conference, St. John's, NF.

Koyama T, Jing L., 2007. Effects of model scale and particle size on micro-mechanical properties and failure processes of rocks—a particle mechanics approach. Eng Anal Boundary Elem 31(5):458–472.

Kozicki, J., Tejchman, J., & Mühlhaus, H. B., 2014. Discrete simulations of a triaxial compression test for sand by DEM. International Journal for Numerical and Analytical Methods in Geomechanics, 38(18), 1923-1952.

Kulhawy, F. H., Trautmann, C. H., Beech, J. F., O'Rourke, T. D., and McGuire, W., 1983. Transmission line structure foundations for uplift-compression loading. Report No. EL-2870, Electric Power Research Institute.

Kunert, H. G., Otegui, J. L., Marquez, A. (2012). Nonlinear FEM strategies for modeling pipe–soil interaction. Engineering Failure Analysis, 24, 46-56.

Labra, C., and On˜ate, E., 2009. High density sphere packing for discrete element method simulations. Commun. Numer. Methods Eng., 25(7), 837–849.

Ladd, R. S., 1978. Preparing test specimens using under compaction. Geotech. Test. J., 1(1), 16–23.

Leach, G. & Row, S. A., 1991. Geotechnical Site Investigation on Alrewas-Audley Pipeline near Hildersione, Staffordshire, British Gas Engineering Research Station, internal report R.4258 (confidential and restricted to British Gas).

Lin, Y. L., Zhang, M. X., Javadi, A. A., Lu, Y., & Zhang, S. L. (2013). Experimental and DEM simulation of sandy soil reinforced with H–V inclusions in plane strain tests. Geosynthetics International, 20(3), 162-173.

Liu, R., Guo, S., and Yan, S., 2015. Study on the lateral soil resistance acting on the buried pipeline. J. Coastal Res., 73, 391–398

Lobo-Guerrero, S., & Vallejo, L. E., 2005. DEM analysis of crushing around driven piles in granular materials. Géotechnique, 55(8).

Lobo-Guerrero, S., & Vallejo, L. E., 2006. Discrete element method analysis of rail track ballast degradation during cyclic loading. Granular Matter, 8(3-4), 195.

Macaro, G., Utili, S., & Martin, C. M., 2015. DEM analyses of pipe-soil interaction for offshore pipelines on sand.

McAllister, E. W., 2001. Pipeline rules of Thumb handbook. Gulf Professional Publishing, 648 p.

Meidani, M., Meguid, M. A., & Chouinard, L. E., 2017. Evaluation of Soil‑Pipe Interaction under Relative Axial Ground Movement. Journal of Pipeline Systems Engineering and Practice, 4, 4017009.

Meidani, M., Meguid, M.A. and Chouinard, L.E., 2018a. Estimating earth loads on buried pipes under axial loading condition: insights from 3D discrete element analysis. International Journal of Geo-Engineering, 9(1), 1-20.

Meidani, M., Meguid, M.A. and Chouinard, L.E., 2018b. A finite-discrete element approach for modeling polyethylene pipes subjected to axial ground movement. International Journal of Geotechnical Engineering. DOI: 10.1080/19386362.2018.1483812.

Mohamedzein, Y. E., & Al-Aghbari, M. Y., 2016. Experimental study of the performance of plastic pipes buried in dune sand. International Journal of Geotechnical Engineering, 10(3), 236-245.

Naeini, S.A., Mahmoudi, E., Shojaedin, M.M. and Misaghian, M., 2016. Mechanical response of buried High-Density Polyethylene pipelines under normal fault motions. KSCE Journal of Civil Engineering, 20(6), pp. 2253-2261

Newmark, M., Hall, W.J., 1975. Pipeline design to resist large fault displacement. In Proceedings of the U.S. National Conference on Earthquake Engineering, Ann Arbor, Mich. Earthquake Engineering Research Institute, Oakland, Calif. Paper No. UILU-ENG-75. pp. 416–425.

Ng, T. T., (2004). Triaxial test simulations with discrete element method and hydrostatic boundaries, Journal of engineering mechanics, Vol. 130, No. 10, pp 1188-1194.

Ono, K., Yokota, Y., Sawada, Y., & Kawabata, T., 2018. Lateral force–displacement prediction for buried pipe under different effective stress condition. International Journal of Geotechnical Engineering, 12(4), 420-428.

O’Rourke, M. J., Nordberg, C., 1992. Longitudinal permanent ground deformation effects on buried continuous pipelines, Technical report NCEER-92-0014, National Center for Earthquake Engineering Research, Buffalo, N.Y.

O’Sullivan, C., 2011. Particulate discrete element modeling, a geomechanics perspective, Spon Press, New York.

Ovesen, N. K. (1964). Anchor slabs, calculation methods and model tests, Bulletin No. 16, The Danish Geotechnical Institute, Copenhagen, Denmark.

PFC 2D version 3 [Computer software]. Itasca Consulting Group, Minneapolis.

Paulin, M. J., Phillips, R., Clark, J. I., Trigg, A. and Konuk, I., 1998. A full-scale investigation into pipeline-soil interaction, Proceedings of International Pipeline Conference, ASME, Calgary, AB., pp. 779-788.

Phillips, R., Nobahar, A., and Zhou, J., 2004. Combined axial and lateral pipe–soil interaction relationships. In Proceedings of the International Pipeline Conference (IPC2004), Calgary.

Plassiard, J.-P., Belheine, N., & DonzâE, F.-V., 2009. A spherical discrete element model: calibration procedure and incremental response. Granular Matter. 11, 293-306.

Potyondy, D.O., Cundall, P.A., 2004. A bonded-particle model for rock. International Journal of Rock Mechanics and Mining Science. 41(8), 1329–1364.

Rahman, M. A., and Taniyama, H., 2015. Analysis of a buried pipeline subjected to fault displacement: A DEM and FEM study. Soil Dyn. Earthquake Eng., 71, 49–62.

Rajani, B., Zhan, C., Kuraoka, S., 1996. Pipe–soil interactions analysis of jointed water mains. Canadian Geotechnical Journal, 33, 3, 393-404.

Rizkalla, M., Simmonds, G. R. and Uptirove, J. T., 1991. Field longitudinal restraint tests, NPS 16 Nevis Lateral, Internal report, Nova Corporation of Alberta.

Robert, D.J., Soga, K., O'Rourke, T.D. and Sakanoue, T. 2016. Lateral load-displacement behavior of pipelines in unsaturated sands. Journal of Geotechnical and Geoenvironmental Engineering, 142(11), p.04016060.

Roscoe, K.H. 1970. 10th Rankine lecture: The influence of strains in soil mechanics. Geotechnique, 20(2): 129–170.

Rowe, R. K., and Davis, E.H., 1982. The behaviour of anchor plates in sand. Geotechnique, 32(1), 25-41.

Roy, K., Hawlader, B., Kenny, S., Moore, I. 2016. Finite element modeling of lateral pipeline–soil interactions in dense sand. Canadian Geotechnical Journal, 53, 3, 490-504.

Schöpfer, MPJ., Childs, C., Walsh, JJ., 2007. Two-dimensional distinct element modeling of the structure and growth of normal faults in multilayer sequences: 1. Model calibration,

Smilauer, V., et al., 2010. Yade documentation. The Yade project 2010, (http://yade-dem.org/doc/æ) (Oct. 28, 2013).

Tran, V.., Meguid, M.A., Chouinard, L.E., 2013. A Finite-Discrete Element Framework for the 3D Modeling of Geogrid–Soil Interaction under Pullout Loading Conditions. Geotextiles and Geomembranes, 37, 1-9.

Tran, V., Meguid, M.A., and Chouinard, L.E., 2014. Discrete element and experimental investigations of the earth pressure distribution on cylindrical shafts. ASCE International Journal of Geomechanics, 14(1) 80-91.

Turner, J. E., 2004. Lateral force displacement behaviour of pipes in partially saturated sand, M.A.Sc. Thesis, Cornell University, Ithaca, N.Y.

Trautmann, C.H., O'Rourke, T.D., 1983. Behavior of pipe with dry sand under lateral and uplift loading, Geotechnical Engineering Report 83-7, Cornell University, Ithaca, N.Y.

Villard, P. B., Chevalier, B., Hello, L, and Combe, G., 2009. Coupling between finite and discrete element methods for the modeling of earth structures reinforced by geosynthetic, Computers and Geotechnics, Vol. 36, No. 5, pp 709-717.

Villard, P., Chareyre, B., 2004. Design methods for geosynthetic anchor trenches on the basis of true scale experiments and discrete element modelling. Canadian Geotechnical Journal, Vol. 41, No. 6, pp 1193-1205.

Wang, Z., Jacobs, F., & Ziegler, M., 2016. Experimental and DEM investigation of geogrid–soil interaction under pullout loads. Geotextiles and Geomembranes, 44(3), 230-246.

Weerasekara, L. 2007. Response of buried natural gas pipelines subjected to ground movements. M.A.Sc. thesis, Department of Civil Engineering, University of British Columbia, Vancouver, B.C.

Weerasekara, L., and Wijewickreme, D., 2008. Mobilization of Soil Loads on Buried, Polyethylene Natural Gas Pipelines Subject to Relative Axial Displacements. Canadian Geotechnical Journal. 45: 1237-1249.

Weerasekara, L., & Wijewickreme, D., 2010. Response of Buried Plastic Pipelines Subject to Lateral Ground Movement. In 2010 8th International Pipeline Conference (pp. 179-186). American Society of Mechanical Engineers.

Wijewickreme, D., & Weerasekara, L., 2010. Full-scale testing of buried extensible pipes subject to axial soil loading. In 7th International Conference on Physical Modelling in Geotechnics (pp. 657-662).

Wilson-Fahmy, R. F., Koerner, R. M., & Sansone, L. J., 1994. Experimental behavior of polymeric geogrids in pullout. Journal of geotechnical engineering, 120(4), 661-677.

Xie, X. 2008. Numerical analysis and evaluation of buried pipeline response to earthquake-induced ground fault rupture. Ph.D. thesis, Rensselaer Polytechnic Institute, New York.

Wijewickreme, D., Karimian H, and Honegger D., 2009. Response of buried steel pipelines subjected to relative axial soil movement. Canadian Geotechnical Journal. 46 (7), 735-752.

Yang B, Jiao Y, Lei S., 2006. A study on the effects of microparameters on macroproperties for specimens created by bonded particles. Eng Comput 23(6):607–631.

Yan, W. M., 2008. Effects of particle shape and microstructure on strength and dilatancy during a numerical direct shear test. Proc., 12th Int. Association for Computer Methods and Advances in Geome- chanics, India, 1340–1345.

Yimsiri, S., Soga, K., Yoshizaki, K., Dasari, G. R. and O'Rourke, T. D., 2004. Lateral and upward soil-pipeline interactions in sand for deep embedment conditions, Journal of Geotechnical and Geoenvironmental Engineering, ASCE, 130 (8): 830-842.

Yoon, J., 2007. Application of experimental design and optimization to PFC model calibration in uniaxial compression simulation. Int J Rock Mech Min Sci 44:871–889.

Zhang, Jie, Zheng Liang, and Chuanjun Han. 2016. Mechanical Behavior Analysis of the Buried Steel Pipeline Crossing Landslide Area. Journal of Pressure Vessel Technology. 138, no. 5: 051702.

Zhang, X-P, Wong, L., 2012. Cracking processes in rock-like material containing a single flaw under uniaxial compression: a numerical study based on parallel bonded-particle model approach. Rock Mech Rock Eng 45(5):711–737.

Zienkiewicz, O. C., Huang, G. C. (1990) . A note on localization phenomena and adaptive finite-element analysis in forming processes, Commun. appl. numer. methods, Vol. 6, pp 71–76.

Chapter 9.

Appendixes

Three conference papers published by the author are presented in this section and they are briefly explained below:

Appendix 1:

Finite-Discrete Element Analysis of Interface Shear Damage to HDPE Geomembrane in Contact with Gravel Drainage Layer*

Abstract

High density polyethylene (HDPE) geomembrane (GM) is usually used as a hydraulic barrier in waste containment applications including municipal solid waste facilities. Stress concentration resulting from direct contact with stones, gravel and other drainage material may cause significant damage to the GM sheet. Protection layers are generally used to keep the GM safe against puncture and tear. However, GM sheets are sometimes placed directly under crushed stones drainage layer containing relatively large size particles protruding from the surface. Under these conditions, interface shear displacement may develop within the liner system causing damage to the GM material. In this study a coupled finite-discrete framework has been developed to investigate the behaviour of a gravel drainage layer located above HDPE geomembrane sheet and subject to moderate to high normal stress conditions. The geomembrane is modelled using finite elements (FE) whereas the drainage layer and the underlying foundation are modelled using discrete elements (DE). Numerical simulation is performed based existing experimental results for the same configuration and detailed behaviour of the GM sheet is then investigated. Results show that shear displacement developing between the drainage layer and the HDPE geomembrane should be considered in the design of landfill barrier system.

***Keywords*:** FE-DE; Interface shear displacement; GM; Drainage layer

---

* A version of this chapter has been published in the processing of the *7th International Conference on Discrete Element Methods*, August 1 to August 4, 2016. Dalian, China Paper Number: G010498 , April 14 2018.

Introduction

High-density polyethylene (HDPE) geomembrane (GM) is usually used as a hydraulic barrier in waste containment applications including municipal solid waste facilities. One of the greatest risks of damage to geomembrane arises from holes created during installation or stress concentration caused by contact with overlying coarse gravel particles over a period of time (Rowe et al., 2004). Soil-GM interface acts as a possible plane of instability under different load conditions. Interface shear displacement can occur between soil and geomembrane due to different reasons, including seismic loading, waste settlement and slope movements. Fox et al. (2014a and 2014b) conducted various experiments using large-scale direct shear test machine to investigate the interface shear damage to the HDPE geomembranes when placed under coarse (i.e., gravelly) soils and over gravelly compacted clay liners (CCLs). These studies showed that interface shear displacement can cause significant more damage to geomembranes than static pressure alone.

This paper presents a coupled finite-discrete element framework that is used to investigate the response of the HDPE geomembranes subjected to static pressure and shear displacement of the interface. The specimen configuration includes HDPE geomembrane placed between gravelly soil as a drainage layer and sand as a foundation. The three-dimensional geometry of the geomembrane is properly modelled using finite elements (FE), while the soil particles are modelled using discrete elements (DE). The numerical simulation is created based on an experimental study reported by Fox et al. (2014b). The main objective of this research is to examine the efficiency of the coupled FE-DE method in modelling soil-GM interaction under interface shear displacement. It should be noted that the created model is a simplification of the experimental test and the results are used to understand the behaviour of the soil-GM system.

Experimental Study

The experimental data was based on those reported by Fox and his group (Fox et al., 2014b). A large-scale direct shear apparatus was used to study HDPE GM-soil interaction. Figure 1a shows the specimen configuration and dimensions. Dimensions of the soil chamber are 1.064 m (length) × 0.152 m (width) × 0.13 m (height). The GM specimen has a thickness of 1.5 mm with blown-film texturing on both sides. The GM material properties are given in Table 1. The drainage layer consists of hard angular gravel with a particle size distribution from 25 to 38 mm.

The particle size distribution of the drainage layer and also the subgrade sand layer are presented in Figure 1b. The sand subgrade was compacted by tamping to a final thickness of 5 cm with a smooth top surface. Then the geomembrane was placed on top of the sand layer and a gravel drainage layer with 75 mm thickness was deposited on the geomembrane without compaction. A normal stress equal to 700 kPa and 1389 kPa was applied and the specimen was sheared to a final displacement of 200 mm at a constant displacement rate of 1.0 mm/min.

Table 1- Material properties of HDPE geomembrane

Properties	Thickness	Density	Tensile strength at yield	Tensile elongation at yield
Value	15 mm	0.949 g/cc	28.4 kN/m	18 %

Coupled finite-discrete element framework

The coupled FE-DE framework used in this study is a continuation of the original work of Dang and Meguid (2010a, 2010b, 2013). The developed algorithm is implemented into an open source discrete element code YADE (Kozicki and Donze, 2009; Smilauer et al., 2010).

Interface elements are added to the simulation to connect FE and DE domains. Triangular facets are used as interface elements generated using the finite elements coordinates. Since hexahedral elements are used for the FE domain, the contact interface between a DE particle and a FE element is divided into four triangular facets by creating a temporary center node. Figure 2 illustrates the interaction between a DE particle and interface elements created on the FE domain. The interaction between a DE particle and interface elements is similar to the particle-particle interaction. In each computational step, all particle-interface contacts are determined, and the normal penetration Δ_N and the incremental tangential displacement $\delta\Delta_T$ of each contact are calculated. Based on these values, normal and tangential forces are calculated. The contact force ($\vec{F}_{contact}$), which is determined by adding the normal and the tangential force vectors ($\vec{F}_N + \vec{F}_T$), result in the movement of DE particles and deformation of the FE domain. The FE domain deformations cause the movement of interface elements and the generation of new particle-interface interactions. A typical FE-DE computational cycle and its main steps were explained in detail by Dang and Meguid (2010a, 2010b, 2013).

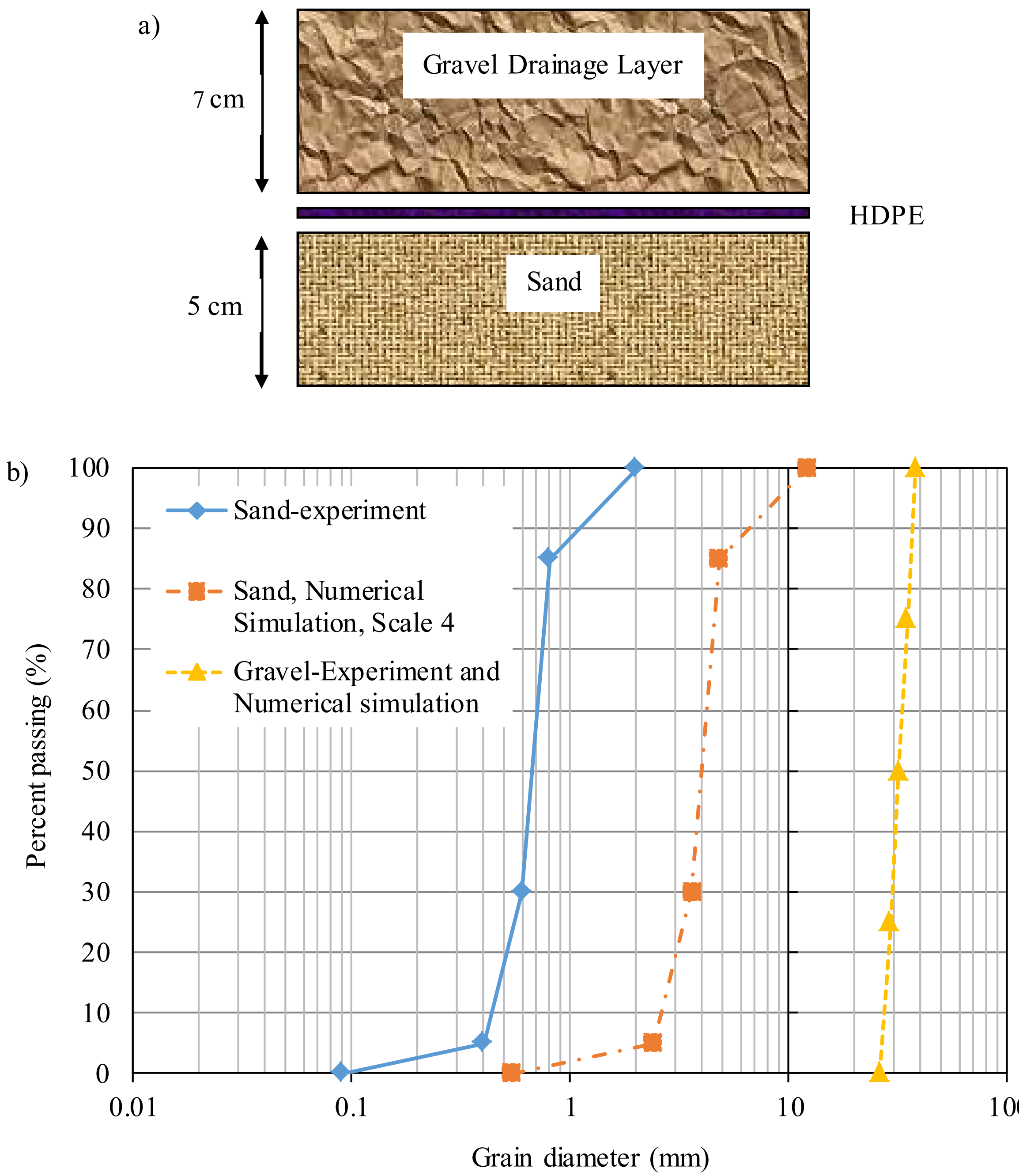

Figure 1 (a) specimen configuration (b) Particle size distribution of the drainage layer and sand subgrade in the experiment and numerical simulation

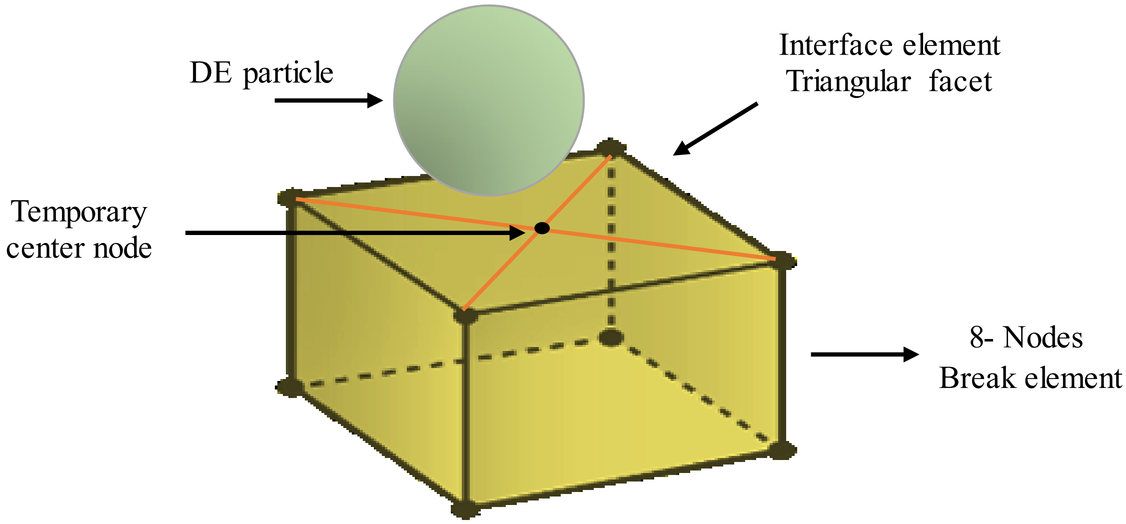

Figure 2 Coupling FE and DE using interface elements

Model generation

The numerical model is developed such that it follows the geometry and the test procedure used in the actual experiment. The geomembrane, including 8 transverse elements and 67 longitudinal elements, is modeled using 8-noded brick elements with 8 integration points (Figure 3). The length of the geomembrane is kept 20 cm longer than the soil chamber from the rear side to ensure a constant friction between the soil and the geomembrane during the test. A linear elastic material model is used for the geomembrane and its properties are obtained from Table 1. The full geometry of the geomembrane, consisting of 536 finite elements and 4288 interface elements, is illustrated in Figure 3.

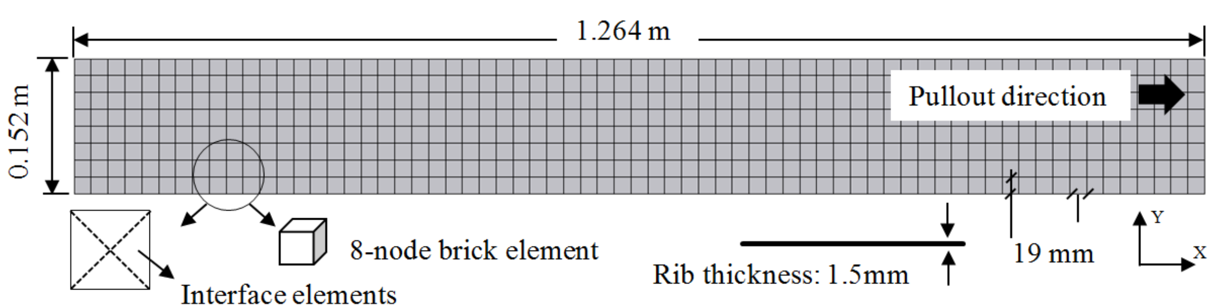

Figure 3 Geometry of the geomembrane

The drainage layer of gravelly soil in the experiment is modeled using spherical particles. The particle size distribution is the same as that used in the experiments as presented in Figure 1b. To generate this layer, a set of non-contacting particles are first generated. Then, all particles are allowed to move under the gravity without compaction. A total of 423 gravel particles are generated with the final thickness similar to that in the experiment: 75mm. The sand used as a subgrade in the experimental test is modeled using spherical particles. Since it is numerically impossible to simulate millions of particles using the actual size distribution, up-scaling is required to keep the duration of the simulation within a reasonable time limit. Among the several packing algorithms developed to generate the discrete element specimen, the radius expansion method is used in this study to generate the pack with specific porosity. A cloud of non-contacting spherical particles is generated, and radii of particles are increased to reach the target porosity of 0.4. Then, the sand specimen is allowed to move under the gravity until the pack reaches the static equilibrium condition. Using a scale factor of 4, a total of over 50,000 particles are generated to replicate the sand subgrade. A partial 3D view of the completely generated sample is shown in Figure 4.

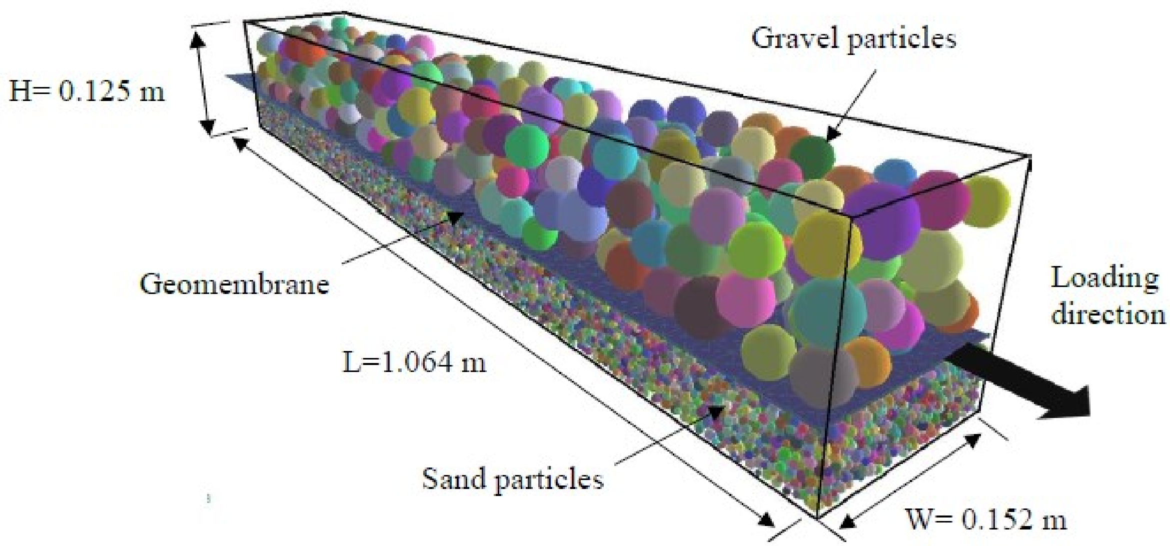

Figure 4 Initial FE-DE specimen

To determine the input parameters of discrete particles, calibration is needed. Since results from laboratory tests (Triaxial and direct shear test) for the drainage layer and the subgrade soil are not available, a parametric study is conducted instead to determine the effect of the input parameters on the shear stresses. The microscopic friction angle of interface elements ($\emptyset_{micro}$), Young's modulus of gravel particles (E_i), the ratio between tangential and normal stiffness of particles

(K_T/K_N), and the rolling resistance coefficient β_r are selected for the parametric study. Table 2 shows the input parameters chosen for the simulation.

After creating the final particle assembly in the box and assigning the input parameters, normal stresses equal to 700 kPa and 1389 kPa are applied on the drainage layer, and the geomembrane is allowed to deform freely. Then, pullout force is applied to the first row of FE nodes of the geomembrane using a displacement control approach with a rate similar to that of the experiment. At each displacement step (0.005 m), movements of the first row of FE nodes are stopped until convergence conditions are satisfied in both DE and FE domains. Additional frontal displacements are then applied in subsequent steps, and the procedure continues until the frontal displacement reaches 50 mm.

Result and discussion

Shear stress-displacement relationship

The relationship between the geomembrane shear stress and its displacement is shown in Figure 5. It can be seen that the FE-DE results for both normal stresses (700 kPa and 1389 kPa) are similar to those of the experimental data. The differences in the maximum shear stress and its location can be attribute to the uncertainty on input parameters for the drainage layer and the subgrade soil. Also, the sandy subgrade porosity and its relative density are needed in the pack generation. As mentioned before, the main objective of this study is to examine the efficiency of the coupled FE-DE framework in modeling soil-GM interaction in shear mode. Hence, considering the simplifications made in the DE simulation, the calculated results are acceptable and useful to understand the behavior of soil-GM interaction.

Figure 6 shows the effect of different input parameters on the shear stress magnitude. Increasing the micro friction angle of the interface elements will increase the maximum shear stress of the geomembrane (Figure 6a). Similarly, increasing the gravel particles modulus (E) increases the shear stress value (Figure 6b). Also, changing in the ratio of the tangential stiffness to the normal stiffness of particles (K_T/K_N) has the same effect on maximum shear stress (Figure 6c). On the other hand, increasing the rolling resistance coefficient (β_r) decreases the maximum shear stress (Figure 6d). It can be seen that changing the input parameters has an effect on the shear stress, and the maximum shear stress is more sensitive to the ratio of the tangential stiffness to the normal stiffness of particles (K_T/K_N) among the different parameters. The main outcome of this parametric study is that calibration is a fundamental step in the DE simulation, and micro parameters have significant effects on the final results.

Table 2 Input parameters of the simulation

Discrete particles	Value
Density of gravel particles (kg/m^3)	2750
Density of sand particles (kg/m^3)	2600
Gravel particle modulus E (MPa)	200
Sand particle modulus E (MPa)	60
Ratio K_T/K_N	0.3
Micro friction angle of gravel particles	40^o
Micro friction angle of sand particles	30^o
η_r	1.0
Rolling resistance coefficient (β_r)	0.3
Damping coefficient	0.2
Finite elements (GM)	**Value**
Young's modulus E (MPa)	800
Poisson's ratio ν	0.3
Interface elements	**Value**
Material modulus E (MPa)	100

Ratio K_T/K_N	0.3
Micro friction angle ($\emptyset_{micro}$)	30°

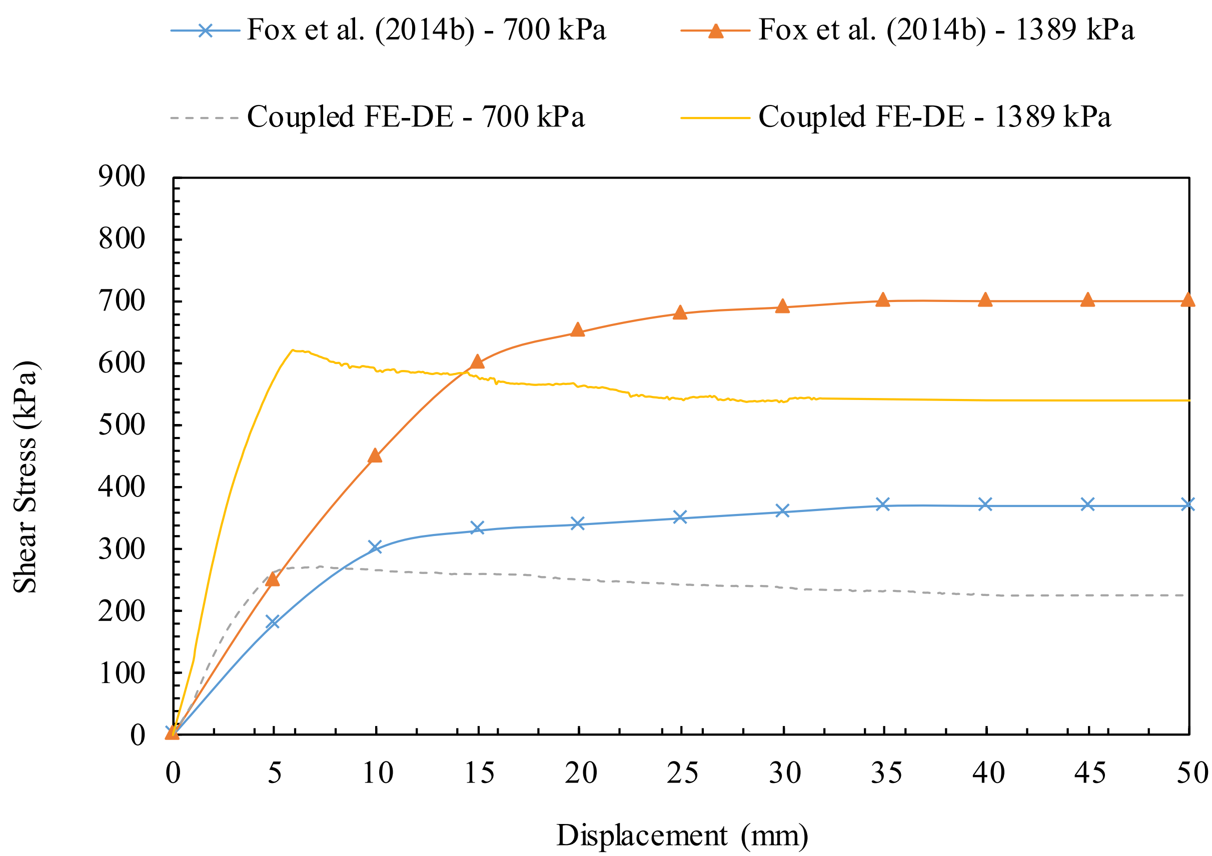

Figure 5 Shear stress-displacement relationship

Response of the geomembrane

The geomembrane vertical deformation (υ_z) for frontal displacements of 0 cm and 20 cm under the vertical stresses of 700 kPa and 1389 kPa are shown in Figure 7 and Figure 8. Before applying the pullout force, the largest deformation of the geomembrane is found to be around 4 mm in the moderate normal stress condition (700 kPa) and around 6 mm under the high normal stress level (1389 kPa). After the shearing stage, vertical deformation increases in both conditions, and the maximum deformation reaches 8 mm in moderate normal stress condition and exceeds 10 mm under the high normal stress level. Hence, prior to the shearing stage, minor indentations occurred in the geomembrane from the stress concentration of the overlaying gravel layer. But, after the shearing displacement to 20 cm, the level of indentation as a damage, and the number of points with significant deformation are increased dramatically. The level of damage due to the indentation is larger in the high normal stress condition than the moderate (Figure 7b .vs. Figure 8b). These results are similar to the observations reported by Fox et al. (2014b). For instance, Figure 9 shows a photograph of a geomembrane under static pressure equal to 1389 kPa (Figure 9a) and after the shearing stage (Figure 9b). It can be seen that major indentation occurred on the geomembrane after applying the shear displacement.

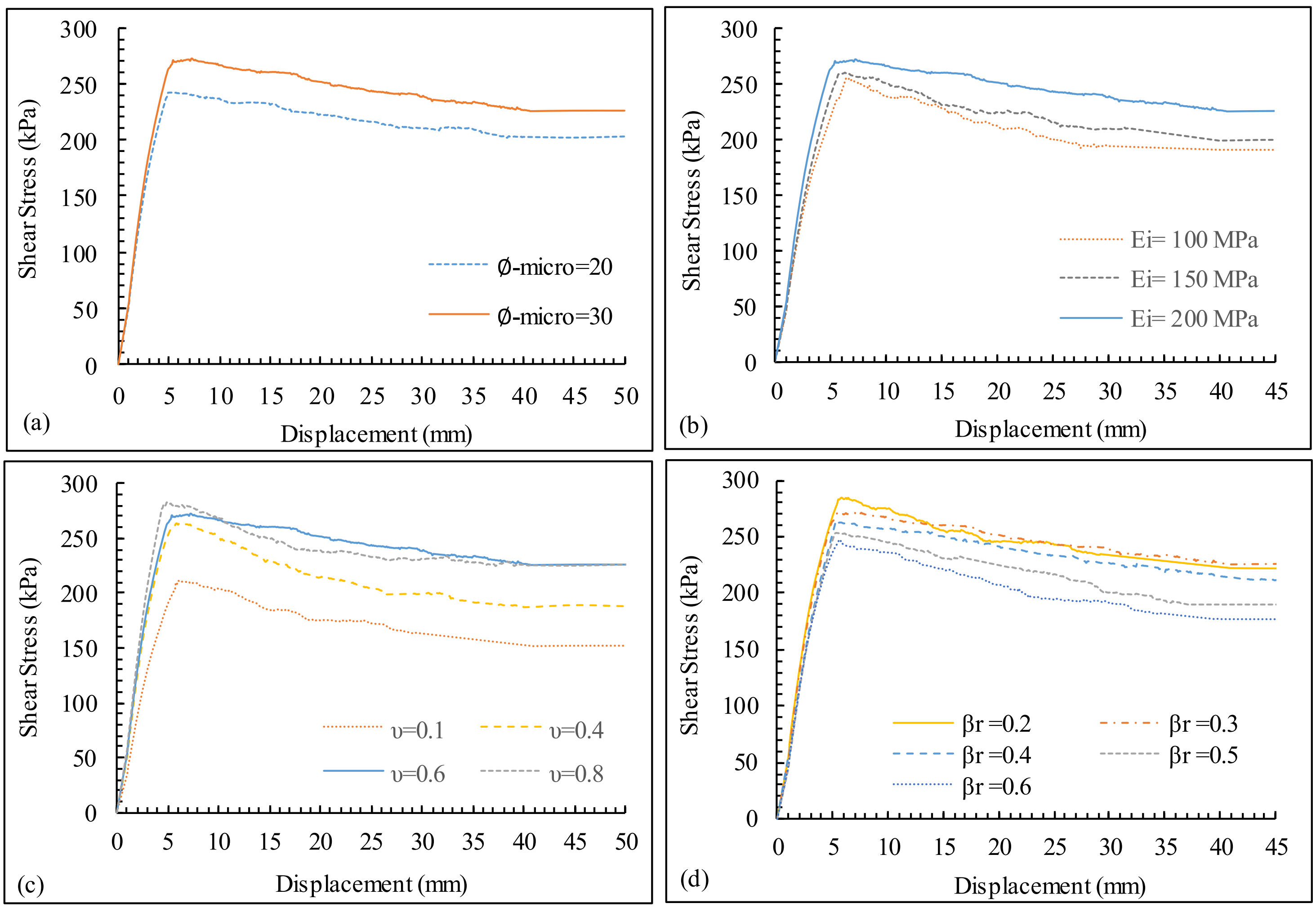

Figure 6 Dependency of shear stress-displacement relationship to different parameters (a) interface friction angle, (b) gravel particle modulus, (c) stiffness ratio, (d) rolling resistance coefficient

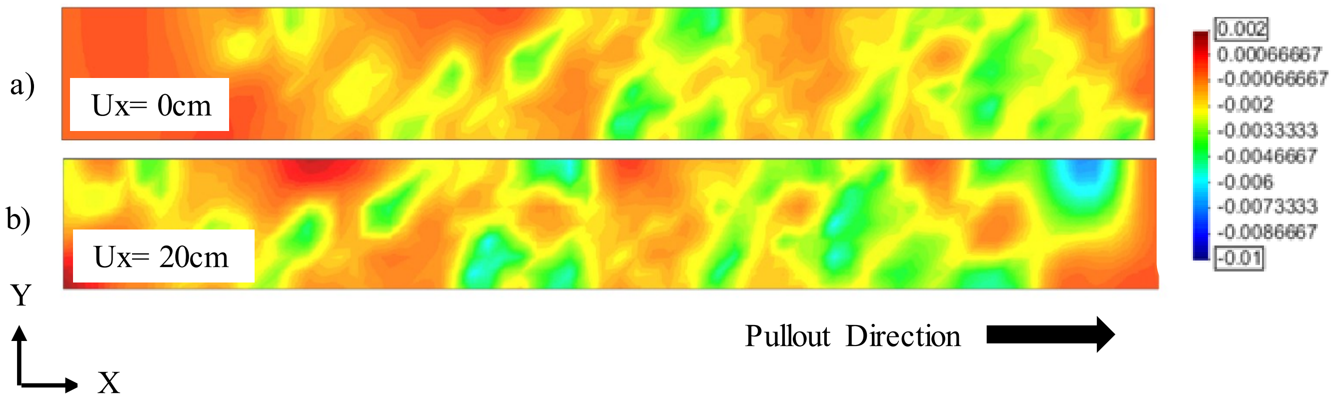

Figure 7 Vertical displacement (m) of the geomembrane (a) before and (b) after the sharing under moderate normal stress level (700 kPa)

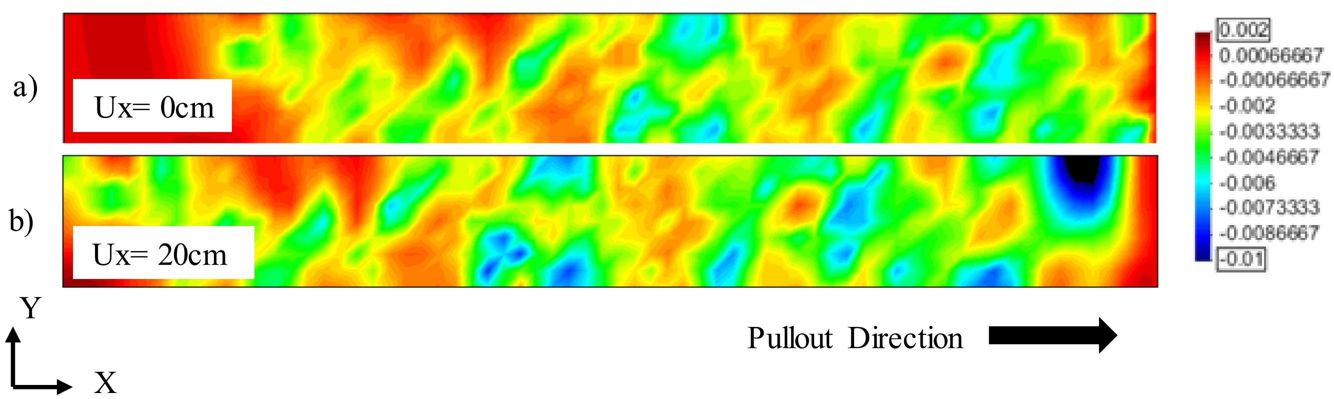

Figure 8 Vertical displacement (m) of the geomembrane (a) before and (b) after the sharing under moderate normal stress level (1389 kPa)

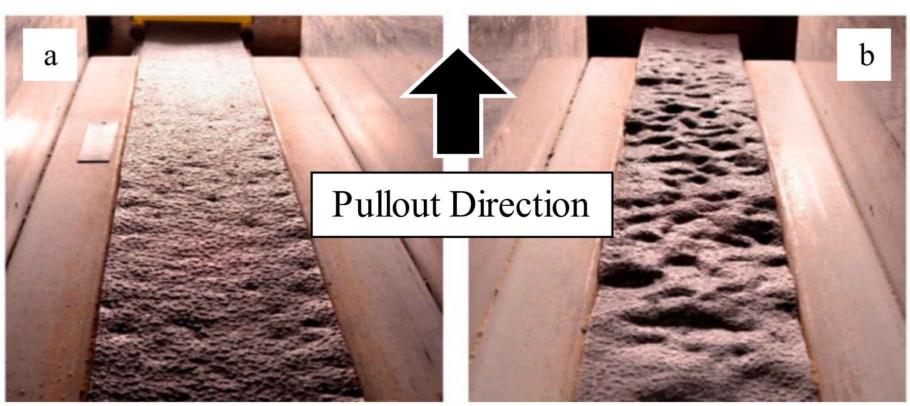

Figure 9 GM after (a) static pressure (1389 kPa) and (b) shearing stage - Fox et al. (2014b)

References

Dang, H.K., Meguid, M.A., 2010a. Algorithm to generate a discrete element specimen with predefined properties. International Journal of Geomechanics 10 (2), 85-91.

Dang, H.K., Meguid, M.A., 2010b. Evaluating the performance of an explicit dynamic relaxation technique in analyzing nonlinear geotechnical engineering problems. Computers and Geotechnics 37 (1), 125-131.

Dang, H.K., Meguid, M.A., 2013. An efficient finite-discrete element method for quasi-static nonlinear soil-structure interaction problems. International Journal for Numerical and Analytical Methods in Geomechanics 37 (2), 130-149.

Fox, P. J., Nye, C. J., Morrison, T. C., Hunter, J. G., and Olsta, J. T., 2006. Large dynamic direct shear machine for geosynthetic clay liners. J. ASTM Geotech. Test., 29(5), 392-400.

Fox, P. J., Thielmann, S. S., Stern, A. N., and Athanassopoulos, C., 2014a. Interface shear damage to a HDPE geomembrane. I: Gravelly compacted clay liner. J. Geotech. Geoenviron. Eng., 10.1061/(ASCE) GT.1943-5606.0001132, 04014039.

Fox, P. J., and Thielmann, S. S., 2014b. Interface shear damage to a HDPE geomembrane. II: Gravel drainage layer. J. Geotech. Geoenviron. Eng., 10.1061/(ASCE)GT.1943-5606.0001120, 04014040.

Kozicki, J., Donze, V.F., 2009. YADE-OPEN DEM: an open-source software using a discrete element method to simulate granular material. Engineering Computations 26 (7), 786e805.

Rowe, R. K., Quigley, R. M., Brachman, R. W. I., and Booker, J. R., 2004. Barrier systems for waste disposal facilities, 2nd Ed., Spon, London.

Smilauer, V., Catalano, E., Chareyre, B., Dorofeenko, S., Duriez, J., Gladky, A., Kozicki, J., Modenese, C., Scholtès, L., Sibille, L., Stránský, J., Thoeni, K., 2010. Yade Documentation. The Yade Project 2010. http://yade-dem.org/doc.

Appendix 2:

A Calibration Procedure for Modeling HDPE Geomembrane Using Discrete Element Method*

Abstract

Geomembranes are geosynthetic impermeable materials used as hydraulic barriers in waste containment facilities. Continuum methods are generally used to analyze the behaviour of geomemberanes and calculate tensile and interface stresses under various loading conditions. However, it is sometimes desired to simulate the interaction behaviour between a geomembrane liner and granular soil subjected to large movements. Discrete element methods have proven to be efficient in modeling granular materials using discrete particles. Using the same procedure to model geomembranes would lead to significant reduction in calculation cost and eliminates the need to use hybrid methods, which require simultaneous use of both continuum and discontinuum modeling approaches. This study presents a procedure to calibrate a discrete element model of a HDPE geomembrane using spherical particles. A constitutive model that takes into account particle normal and shear cohesion is used. Standard index tests used to measure the properties of HDPE geomembrane including tensile and puncture tests are applied to validate the model developed. The effect of microscopic parameters on the overall response is examined and recommendations are made regarding to the optimum approach to simulate continuous geomembrane materials using discrete element method.

***Keywords*:** DEM simulation, HDPE geomembrane, Calibration

* A version of this chapter has been published in the processing of the *GeoVancouver 2016*, October 2016.

Introduction

In the field of solid waste landfill engineering, the use and acceptance of geosynthetics and high-density polyethylene (HDPE) geomembrane (GM) has increased over the past few years. HDPE geomembrane is usually used as a hydraulic barrier in waste containment applications including municipal solid waste facilities.

One of the greatest risk of damage in geomembranes is associated with stress concentrations from direct contact with coarse soil particles (e.g., gravel or stones), which can occur from an underlying soil subgrade or an overlying granular soil layer (Nosko and Touze-Foltz 2000; Giroud and Touze-Foltz 2003). Extensive research has been conducted on granular soil-geomembrane interaction using experimental and numerical methods (Reddy et al. 1996a; Koerner et al. 2010; Hornsey and Wishaw 2012; Brachman and Sabir 2013). Among the different numerical methods that have been developed by researchers to study this interaction, the discrete element method (DEM) has proven to be efficient in modeling granular materials involving large deformations. Also, using the same approach to model geomembrane leads to significant reduction in calculation cost in comparison with other methods such as hybrid procedure that requires simultaneous use of both continuum and discontinuum modeling approaches.

The discrete element method (DEM) has gained popularity in the past few decades among geotechnical engineers and researchers involved in granular soil-structure interaction problems. The method was first proposed by Cundall and Strack (1979) and has been used to analyse geotechnical engineering problems. Laboratory tests such as triaxial and direct shear have been modeled using DEM to investigate the microscopic behavior of soil samples (Cui and O'Sullivan 2006). Also, several researchers applied this method to model soil-geosynthetics problems including elements such as textiles, grids and membranes (McDowell et al. 2006; Effeindzourou et al. 2016). In most of these studies a membrane is modeled using a set of spherical particles bonded together. These bonded particles can simulate the membrane behavior correctly if the input parameters are chosen precisely.

In this work, a calibration procedure is proposed which takes into account the role of each parameter in the macroscopic behavior. Two index tests, namely, tensile and puncture tests are numerically simulated to determine the microscopic parameters of the bonded HDPE geomembrane particles.

Discrete element modeling

General formulation

The discrete element method (DEM) treats the interaction between particles as a dynamic process that reaches static equilibrium when the internal and external forces are balanced. This dynamic process is usually modeled using a time-step algorithm based on an explicit time-difference scheme. Displacement and rotation of each particle are then determined using Newton's and Euler's equations. The DEM simulation in this study is performed using the open source discrete element code YADE (Kozichi and Donze, 2008; Smilauer et al., 2010).

The contact law between particles is briefly described below:

After collision of particles A and B with radii rA and rB, contact penetration depth is defined as

$$\Delta = r_A + r_B - d_0 \quad [1]$$

Where d_0 is the distance between centers of particles *A* and *B*. Interaction between the two particles is represented by the force vector *F*. This vector can be decomposed into normal and tangential forces (Figure 1)

$$F_N = K_N \,.\, \Delta_N \quad [2]$$

$$\delta F_T = -K_T \,.\, \delta\Delta_T \quad [3]$$

Where F_N is the normal force; δF_T is the incremental tangential force; K_N and K_T are the normal and tangential stiffnesses at the contact point; Δ_N is the normal penetration between the two particles and $\delta\Delta_T$ is the incremental tangential displacement between the two particles.

The normal stiffness between particle *A* and *B* at contact point is defined by

$$K_N = \frac{K_N^A \,.\, K_N^B}{K_N^A + K_N^B} \quad [4]$$

Where K_N^A and K_N^B are the particles normal stiffnessess calculated using particle radius r and the particle material modulus E_i.

$$K_N^A = 2E_A r_A \qquad and \qquad K_N^B = 2E_B r_B \quad [5]$$

So the normal stiffness at contact point can be written as:

$$K_N = \frac{2E_A r_A \,.\, 2E_B r_B}{2E_A r_A + 2E_B r_B} \qquad [6]$$

The interaction tangential stiffness K_T is defined as a ratio of the computed K_N as $K_T = \alpha\, K_N$.

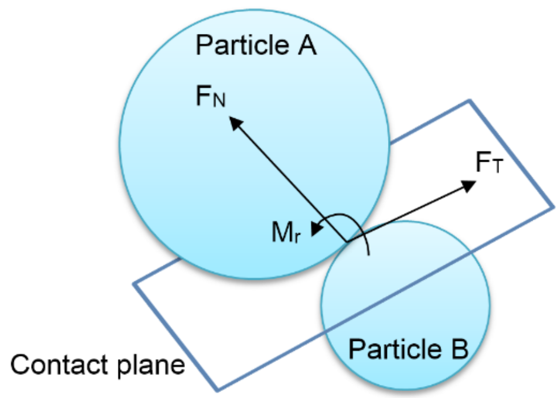

Figure 1. Interaction between two DE particles

Rolling resistance between two particles A and B is determined using a rolling angular vector θ_r. This vector is calculated by summing the angular vector of the incremental rolling (Smilauer et al., 2010)

$$\theta_r = \sum d\,\theta_r \qquad [7]$$

A resistant moment M_r is calculated by

$$M_r = K_r \,.\, \theta_r \qquad [8]$$

Where K_r is the rolling stiffness of the interaction and is defined as

$$K_r = \beta_r \,.\, \left(\frac{r_A + r_B}{2}\right)^2 .\, K_T \qquad [9]$$

Elastic limits can be defined for Eqs. (2) and (3) using shear (C_T) and tensile strength (C_n).

$$F_N \leq C_n \times A \qquad [10]$$

$$F_T \leq F_N \tan \varphi_{micro} + C_T \times A \qquad [11]$$

Where φ_{micro} is the microscopic friction angle between particles and $A = \pi R_C^2$ is the reference surface area (R_C is the reference radius of the contact, R_C= min (R_1 and R_2)). Note that normal force is only limited in traction and it is assumed that compression at contact is always elastic.

Discrete element modeling of a flexible membrane

The developed HDPE geomembrane model consists of an array of bonded spherical particles which are arranged hexagonally. The bonds are defined by shear and normal tensile strength, set high enough that the membrane does not split. Also, rotation of particles and the transmission of moments are restricted to ensure membrane flexibility (De Bono et al. 2012). The main properties of the spherical particles which are needed for the calibration procedure are listed in Table 1. Among these parameters, the value of the micro-friction angle (φ_{micro}) is assigned to zero based on the findings of De Bono et al. (2012) and Bourrier et al. (2013). All four remaining parameters need to be extracted using the calibration method described in the next section.

Tensile test specimen

The tensile test specimen is created based on ASTM D6693 (standard test method for determining tensile properties of flexible geomembranes). The specimen has a dog bone shape and its dimensions are illustrated in Figure. 2.

Table 1 Parameters of the contact model used in the modeling of HDPE geomembrane

Properties
Particle material modulus (E_i)
Density
Micro friction angle (φ_{micro})
$\alpha = \frac{K_T}{K_N}$
Tensile strength (C_n)
Shear strength (C_T)

The test procedure is described below:

1. Measuring the width and thickness of the sample (W=6 mm, t=1.5 mm)
2. Placing the specimen in the grips of the test apparatus (to prevent slippage of the specimen). Grip dimension is 25 mm on each side.
3. Installing the strain gage on the specimen (gage initial length=33 mm).
4. Applying the load at a rate of 50 mm/min on the right side while the left grip is fixed. Then, recording the load-displacement data.

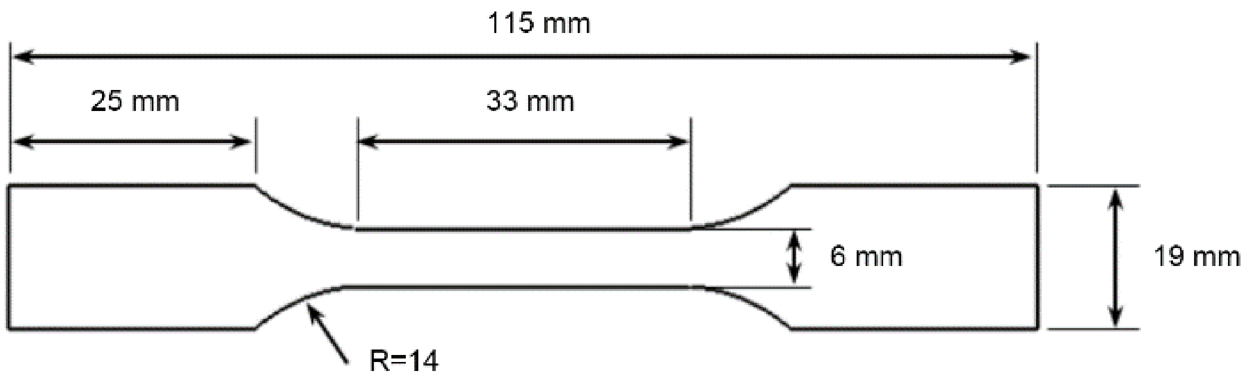

Figure 2 Tensile test specimen dimensions

The diameter of the particles in the discrete element model is chosen considering a balance between simulation time and the geomembrane flexibility. Based on these criteria, spherical particles with diameter of 0.3 mm are created and arranged in hexagonal pattern. Two specimens with different thicknesses are created. First sample with thickness of 0.3 mm consists of 28564 particles arranged in one row. The other sample includes 6 rows of the first specimen with 171,384 particles and final thickness of 1.5 mm. Most of the particles located between the grips do not have interactions with other particles as they have a zero or constant velocity under the specified test condition. Hence, to increase the simulation speed, only 2.5 mm of each grip is modeled. Figure 3 illustrates the final discrete element samples of the tensile test and a close view of the specimen.

Puncture test specimen

The puncture test specimen is created based on ASTM D4833 (standard test method for index puncture resistance of geomembranes). The specimen has a circular shape and its dimensions are illustrated in Figure. 4.

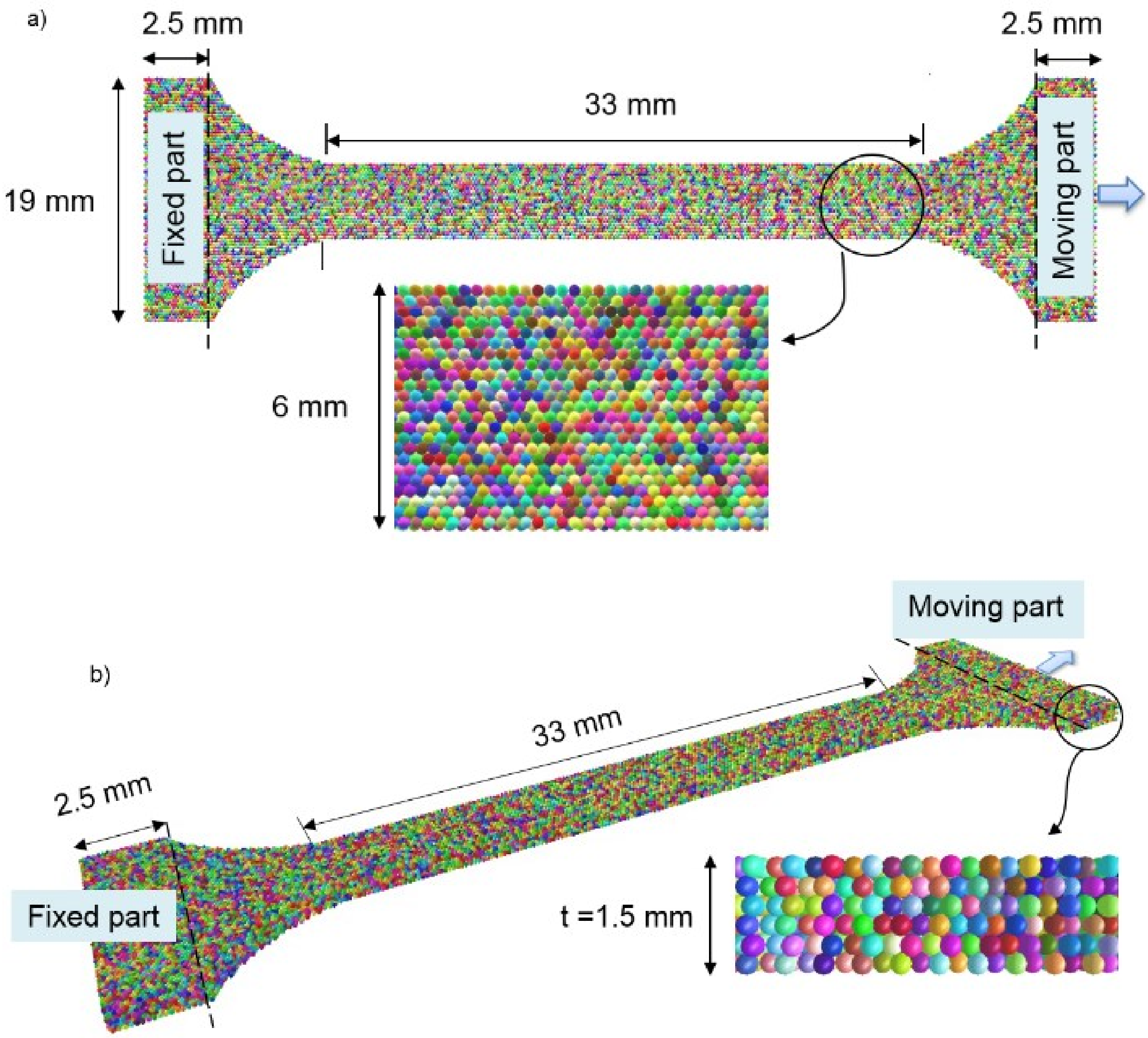

Figure 3 a) Top view of the first test specimen with thickness of 0.3 mm and a partial view of the specimen to illustrate the hexagonal arrangement of particles, b) A 3D view of specimen with a thickness of 1.5 mm.

To perform the puncture test, geomembrane needs to be fixed among an O-ring plate with outer diameter of 100 mm and an open internal diameter of 45 mm. Then a solid steel rod (test probe) is pushed downward with a speed of 300 mm/min towards the center. Probe load (puncture resistance) is recorded until the steel rod completely ruptures the test specimen.

The diameter of the particles in the discrete element model and their arrangement are chosen the same method as the tensile test specimens; and two samples with different thickness are created as well. Particles in the fixed part of the sample don't have any effects on the outcome force. Hence, to decrease the number of particles and duration of the simulation, only 2.5 mm of the fixed part is created. Thus, the diameter of the DE sample is 50 mm. Two samples with thicknesses of 0.3 mm and 1.5 mm and total number of particles of 25,198 and 151,188, respectively, are created. The discrete element model of the puncture test and a partial view of the sample are presented in Figure 5.

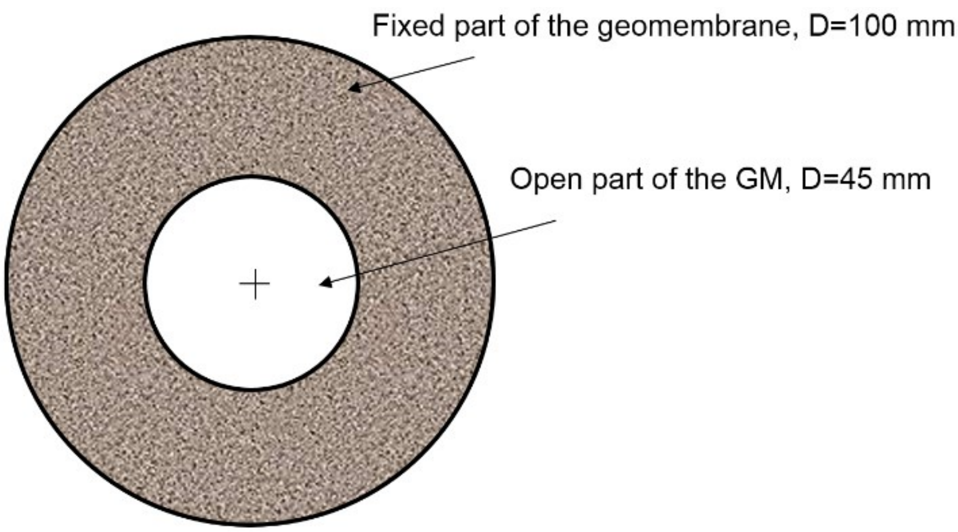

Figure 4 Puncture test details

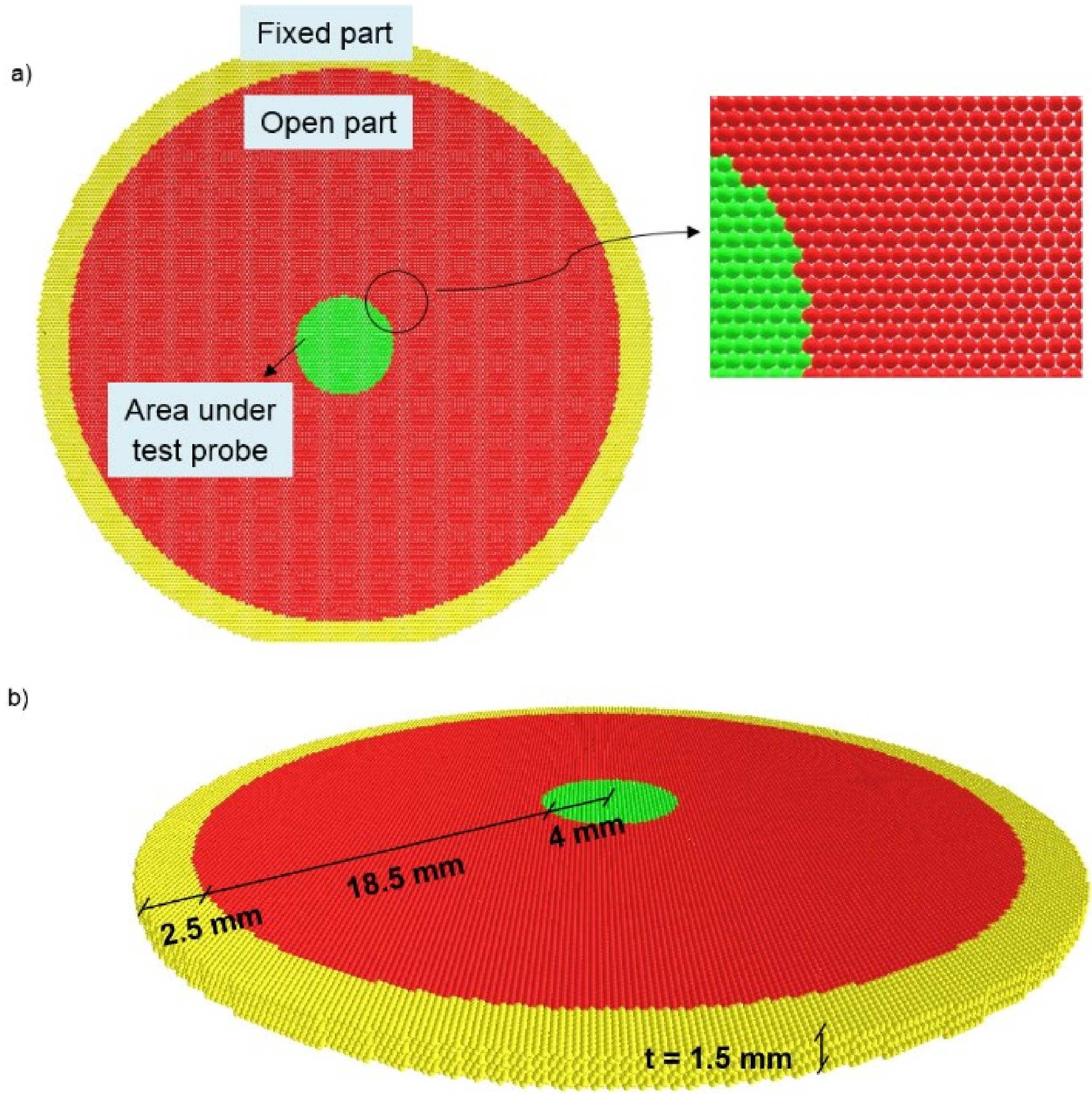

Figure 5. a) Top view of first puncture test specimen with thickness of 0.3 mm and a partial view of the specimen to illustrate the hexagonal arrangement of particles, b) A 3D view of specimen with thickness of 1.5 mm.

Calibration of the local parameters

The calibration of the material properties with respect to the real geomembrane is performed by comparing a simulated and a laboratory test results. Once calibrated, the predictive capabilities of the numerical model is checked and validated by simulating the puncture test. For the calibration step, the selected local parameters include, particle material modulus (E_i), Tensile strength (C_n), Shear strength (C_T) and the ratio between tangential and normal stiffness (α). The choice of these parameters should allow for the correct macroscopic values (Young's modulus E, tensile strength at the yield point, tensile elongation at yield and puncture resistance) to be reproduced. To achieve this objective, the impact of each local parameter on the macroscopic response needs to be identified. Based on the previous studies (Calvetti et al. 2003, Sibille et al. 2006, Plassiard et al. 2009) it was found that elastic parameters (E_i and α) and rupture parameters (C_n, C_T) can be calibrated separately.

The particle modulus (E_i) is known to play an important role in the elastic response whereas, the ratio between tangential and normal stiffness (α) has no significant impact on material Young's modulus E. Therefore, E_i will be used first to calibrate the macroscopic elastic behavior. The value of α is set to 0.3 based on that reported by Effeindzourou et al. (2016) in modeling a deformable structure using DEM. Using this value for α, E_i is set such that the target Young's modulus based on the tensile test results is obtained. As presented in Figure 6, as the particle modulus (E_i) increases, the Young's modulus of the geomembrane increases.

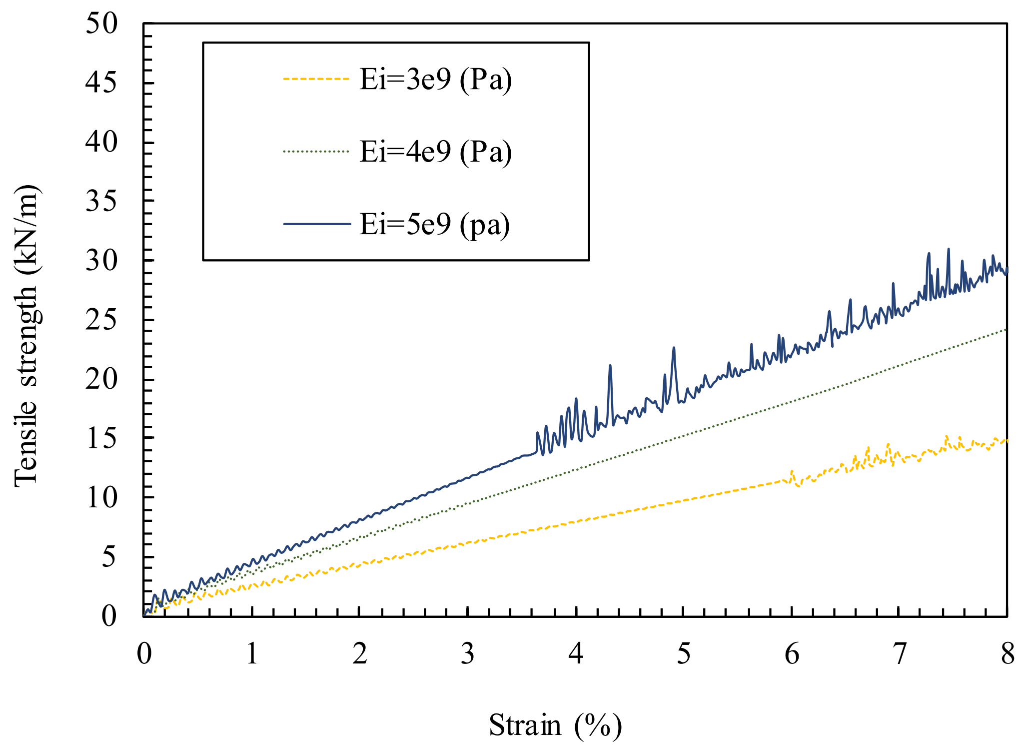

Figure 6 Dependency of Young's modulus on particles material modulus (E_i)

Once the elastic parameters are set, the values of the rupture parameters (C_n, C_T) can be determined. Changing these two parameters separately was found to lead to divergence in the results. Equal values for the two parameters were considered in consistency with De Bono et al. (2012), Bourrier et al. (2013) and Effeindzourou et al. (2016). These two parameters were found to affect the peak stresses with little to no effect on Young's modulus as illustrated in Figure 7.

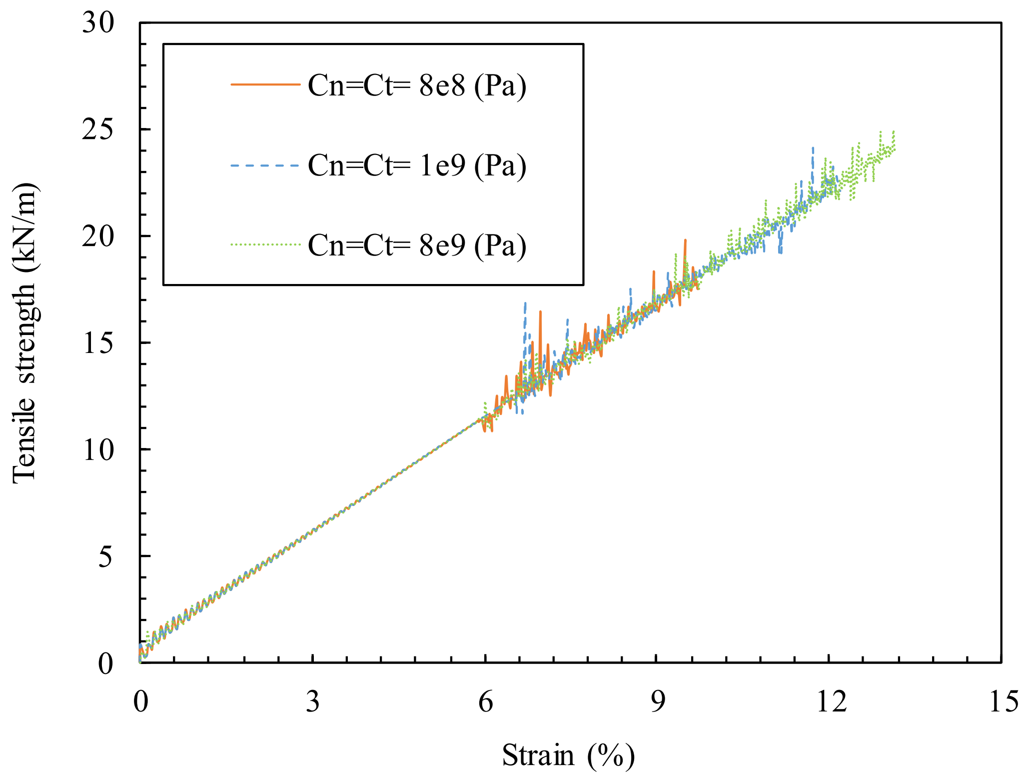

Figure 7 Dependency of peak stress on particles tensile and shear strength

Application of the proposed method to simulate geomembrane response to loading

The selected HDPE GM was manufactured by Layfield Corp. (USA and Canada). Geomembrane specimen has a thickness of 1.5 mm with blown-film texturing on both sides. The GM material properties are given in Table 2.

Following the calibration procedure described in section 2, tensile test is modeled using DEM. At first a specimen with thickness of 0.3 mm is created and the input parameters are determined using the calibration method (see Table 3). To validate these parameters a second tensile test specimen with a thickness of 1.5 mm is created and the micro-parameters are assigned to the particles. Results are summarized in Table 4 which show consistency between the calculated results and the experimental data.

Table 2 Material properties of the selected HDPE geomembrane

Properties	Value
Thickness	1.5 mm
Density	0.94 g/cc
Tensile strength at yield	22 kN/m
Tensile elongation at yield	12 %
Puncture resistance	480 N

The effect of the applied tension force can be further examined by inspecting the contact force distribution within the geomembrane specimen. Figure 8 shows the contact force network in the geomembrane during the test (ε = 6%). Most of the contact forces are directed parallel to the applied external load. In addition, the magnitude of the forces is larger for the narrow section as compared to the rest of sample.

The puncture test was also simulated using two specimens of different thicknesses and the input parameters are assigned to the used particles. Numerical results were found to be in agreement with the experimental data as shown in Table 5. The contact force network distribution during the puncture test before and after failure are illustrated in Figures 9 and 10. As presented in Figure 9 contact forces are higher near the edge and under the test probe in comparison with the rest of the sample. Also, the specimen failure mode is found to be similar to that observed in the experiment. The above results confirm that the proposed DEM based method is acceptable in modeling the response of geomembrane material.

Table 3 Input parameters of the contact model obtained from the selected HDPE geomembrane using the proposed calibration method

Properties	Value (Unit)
Particle material modulus (E_i)	3.0E9 (Pa)
Density	0.94 (g/cc)
Micro friction angle (φ_{micro})	0 (Degree)
$\alpha = \dfrac{K_T}{K_N}$	0.3
Tensile strength (C_n)	1.0E9 (Pa)
Shear strength (C_T)	1.0E9 (Pa)

Table 4 Comparison between calculated and measured tensile strength and Young's modulus of the geomembrane

Properties	Test method	Thickness (mm)	
		0.3	1.5
Tensile strength at yield (kN/m)	Experiment	22	22
	Numerical	23	25
Tensile elongation at yield (%)	Experiment	12	12
	Numerical	12.2	12.5

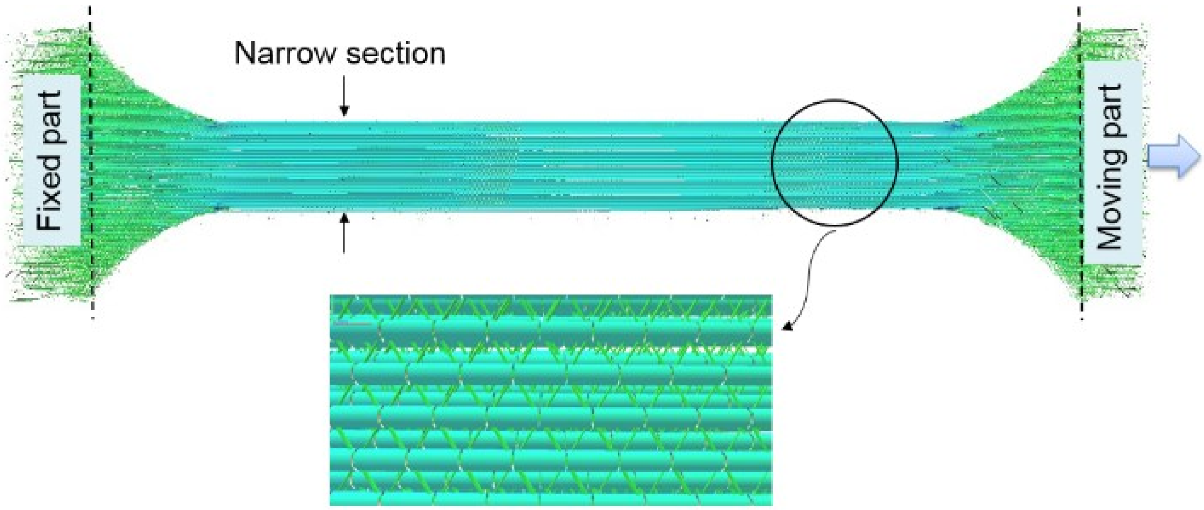

Figure 8 Contact force network in tensile test simulation

Table 5 Comparison between calculated and measured puncture resistance of the geomembrane

Thickness (mm)	Puncture resistance (kN)	
	Experiment	Numerical
1.5	480	505
0.3	96	101

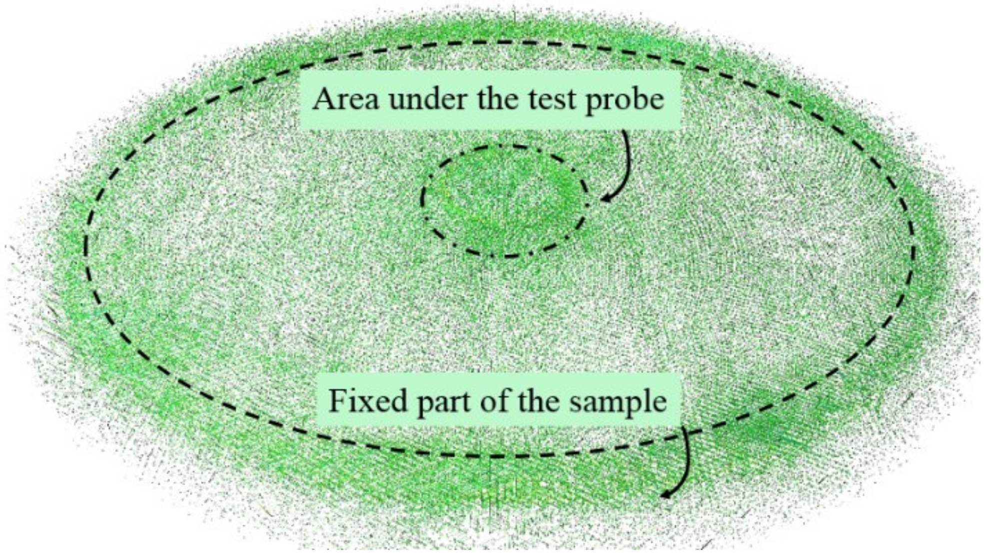

Figure 9 Contact force network in puncture test before the failure

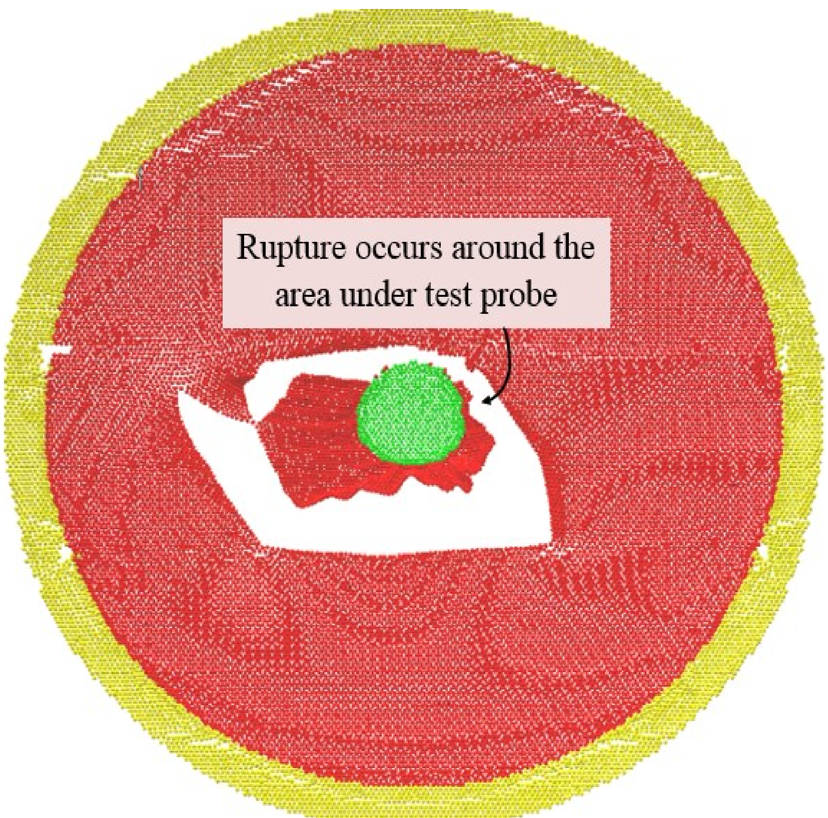

Figure 10 Top view of the puncture test simulation at failure state

Conclusion

A DEM model has been created that can simulates tensile and puncture tests performed on HDPE geomembrane. Bonded spherical particles are used to create a flexible membrane material allowing for the correct deformation pattern to develop. A calibration procedure is proposed which attempts to consider the respective roles of each local parameter on the macroscopic behavior of the material.

Numerical simulations are performed to simulate tensile and puncture tests conducted on a specific HDPE geomembrane to evaluate the applicability of the proposed method. An acceptable agreement between the numerical and experimental results is obtained. In spite of the simplicity of the suggested calibration method, the numerical model was able to reproduce the main features of the tensile and puncture tests up to the yielding point. The calibration method presented in this study and the ability to create a flexible membrane using DEM shows that discontinuous methods are promising in modeling the interaction between granular soil and geomembrane material.

References

ASTM D6693 / D6693M-04(2015)e1, Standard Test Method for Determining Tensile Properties of Nonreinforced Polyethylene and Nonreinforced Flexible Polypropylene Geomembranes, ASTM International, West Conshohocken, PA, 2015, www.astm.org.

ASTM D4833 / D4833M-07(2013)e1, Standard Test Method for Index Puncture Resistance of Geomembranes and Related Products, ASTM International, West Conshohocken, PA, 2013, www.astm.org.

Bourrier, Franck, François Kneib, Bruno Chareyre, and Thierry Fourcaud, 2013. Discrete modeling of granular soils reinforcement by plant roots. Ecological Engineering 61: 646-657.

Brachman, R. W. I., and Sabir, A., 2013. Long-term assessment of a layered-geotextile protection layer for geomembranes. J. Geotech. Geoenviron. Eng., 10.1061, 752-764.

Cui, L, O'Sullivan, C., 2006. Exploring the macro-and micro-scale response of an idealized granular material in the direct shear apparatus, Geotechnique, 56(7), 455-468.

Cundall, P.A, Strack, O.D., 1979. A discrete numerical model for granular assemblies, Geotechnique, 29(1), 47-65.

De Bono, John P., Glenn R. McDowell, and Dariusz Wanatowski, 2012. Discrete element modelling of a flexible membrane for triaxial testing of granular material at high pressures. Géotechnique Letters 2, no. 4 : 199-203.

Effeindzourou, Anna, Bruno Chareyre, Klaus Thoeni, Anna Giacomini, and François Kneib., 2016. Modelling of deformable structures in the general framework of the discrete element method. Geotextiles and Geomembranes. 44 (2): 143-156.

Giroud, J. P., and Touze-Foltz, N. (2003). Geomembranes in landfills: Discussion at the 7th International Conference on Geosynthetics." Geosynthetics Int., 10(4), 124–133.

Hornsey, W. P., and Wishaw, D. M. (2012). "Development of a methodology for the evaluation of geomembrane strain and relative performance of cushion geotextiles." Geotext. Geomembr., 35, 87–99.

Kozicki, J., Donze, V.F., (2008). YADE-OPEN DEM: an open-source software using a discrete element method to simulate granular material. Engineering Computations 26 (7), 786e805.

Koerner, R. M., Hsuan, Y. G., Koerner, G. R., and Gryger, D. (2010). "Ten year creep puncture study of HDPE geomembranes protected by needle-punched nonwoven geotextiles." Geotext. Geomembr., 28(6), 503–513.

Nosko, V., and Touze-Foltz, N. (2000). "Geomembrane liner failure: Modeling of its influence on contaminant transfer." Proc., 2nd European. Conf. On Geosynthetics, A. Cancelli, D. Cazzuffi, and C. Soccodato, eds. Pàtron Editore, Bologna, Italy, 557–560.

Reddy, K. R., Bandi, S. R., Rohr, J. J., Finy, M., and Siebken, J. (1996a). "Field evaluation of protective covers for landfill geomembrane liners under construction loading." Geosynthetics Int., 3(6), 679–700.

Smilauer, V., Catalano, E., Chareyre, B., Dorofeenko, S., Duriez, J., Gladky, A., Kozicki, J., Modenese, C., Scholtès, L., Sibille, L., Stránský, J., Thoeni, K., (2010). Yade Documentation. The Yade Project 2010. http://yade-dem.org/doc/.

Appendix 3:

Analyzing HDPE geomembrane wrinkle overlying sand subgrade using a finite-discrete element framework*

Abstract

High-density polyethylene (HDPE) geomembranes (GM) are commonly used as barrier systems in solid waste landfills as they provide a relatively low hydraulic conductivity. Wrinkles are formed in GM during installation as a result of material expansion due to solar heating or placement of backfill materials. In this research, a coupled finite-discrete element model has been developed to examine the behavior of geomembrane wrinkle placed between firm sand subgrade and gravelly drainage layer. The GM is modeled using finite elements (FE) whereas the drainage layer and the foundation are modeled using discrete elements (DE). To transfer the contact forces and displacements between the DE and FE domains, triangular shaped facet interface elements are adopted. The analysis is performed based on an experimental configuration reported in the literature. The effects of the subgrade properties backfill material and overburden pressure on the wrinkle deformation are investigated. Results show that the presence of wrinkle increases the local strains in the geomembrane right next to the deformed wrinkle. Applying vertical pressure of up to 1100 kPa resulted only in a slight reduction in the size of the gap beneath the geomembrane. Among the different factors, the wrinkle deformation is significantly influenced by the change in subgrade properties and the applied pressure. The numerical results proved the efficiency of the coupled framework in modeling GM-soil interactions problems.

Keywords: FE-DE simulation, HDPE geomembrane, Wrinkle

---

* A version of this chapter has been published in the processing of the *GeoOttawa 2017*, October 2017.

Introduction

High-density polyethylene geomembrane has been widely used in municipal solid waste landfills as a hydraulic barrier system due to the low permeability and ease of installation. Development of holes in the geomembrane can be considered as one of the greatest risks in landfill serviceability. Damage during GM installation; puncture due to placement of overlying drainage layer, and stress-cracking that results from the long-term tensile strains are major factors that lead to the development of holes (Rowe et al., 2004).

Wrinkles in the geomembrane can extend the damage as the gap under the wrinkle prevents contacts between the GM and the underlying material. Redistribution of vertical stresses under the wrinkles induces tensile strains on both sides of the wrinkle. These strains can be compounded by other tensile strains from indentation caused by the drainage layer and increase the potential for stress-related cracking. Wrinkles can also develop in the GM due to the material expansion caused by solar heating or the placement of the overlying drainage layer.

Deformations and strains developing in the wrinkle are functions of the material types below and above the GM. Soong and Koerner (1998) performed a series of experiments to measure the wrinkle deformations for the cases where the GM is placed between two sand layers. The study showed that the height and width of the wrinkle are reduced, but the gap beneath the wrinkle remained. Gudina and Brachman (2006) reported the short-term response of GM wrinkles overlying compacted clays at two different initial water contents. Results showed that the gap was eliminated depending on the vertical pressure and the water content of the clay. Furthermore, Brachman and Gudina (2008) investigated GM strains caused by indentation of coarse gravel and wrinkles in a GM/GCL composite liner. Wrinkle height and width decreased in all tests; however, the gap remained beneath the GM/GCL liner when a firm sand layer was placed as a foundation.

The objective of this research is to present a coupled finite-discrete element framework which is used to evaluate the response of the HDPE geomembrane wrinkles overlying sand subgrade. The numerical model is developed based on the experiments published by Brachman and Gudina (2008). The geomembrane layer is placed between sand foundation and coarse gravel drainage layer. Finite elements (FE) approach is used to model the geomembrane, while the soil domain is created using discrete elements (DE). A brief explanation of the experiments is presented followed by a short description of the numerical framework used in the analysis. Emphasis is placed in this study on the effects of the sand and gravel properties on the wrinkle deformation and geometry. Also, the effect of the overburden pressure on the wrinkle response is evaluated.

Experimental study

The general configuration of the numerical simulation was based on the experimental study by Brachman and Gudina (2008). A cylindrical steel pressure vessel with an inside diameter of 590 mm and a height of 500 mm was used in the experiments. The sample includes 150 mm foundation layer overlain by GM with or without geotextile (GT) sheet as a protection covered with 300 mm coarse gravel and 50 mm of leveling sand. After placing the materials, a vertical pressure is applied in increments. The sample is maintained under the applied pressure for 10 hours. Then a low-shrinkage grout is injected into the GM to maintain the geometry of the gap and the GM. Afterward, pressure is released, and the drainage layer is removed. The final deformation, height and width of the wrinkle are measured.

The foundation layer beneath the GM was dry poorly graded medium-sand (SP). The sand was compacted to reach a density index of 85% corresponding to a dry density of 1.91 g/cm^3. The drainage layer overlying the GM was poorly graded coarse gravel (GP) as per the requirements of Ontario, Canada landfill regulations (MOE, 1998). This layer was placed in a loose condition with a dry density of 1.72 g/cm^3. Grain size distribution curves of these two layers are presented in Figure 1.

The properties of the GM are presented in Table 1. A wrinkle is manually formed in the GM with an initial height of 60 mm and width of 240 mm. The used wrinkle geometry is consistent with Pelte et al. (1994) field observations.

Coupled finite-discrete element framework

The coupled FE-DE framework is a continuation of the work of Dang and Meguid (2010a, 2013). YADE (Kozicki and donze, 2009; Smilauer et al., 2010) open source discrete element code is used as a platform to develop the coupled framework. The algorithm of the coupled numerical simulation is described in sections 2.3 and 2.42.3.

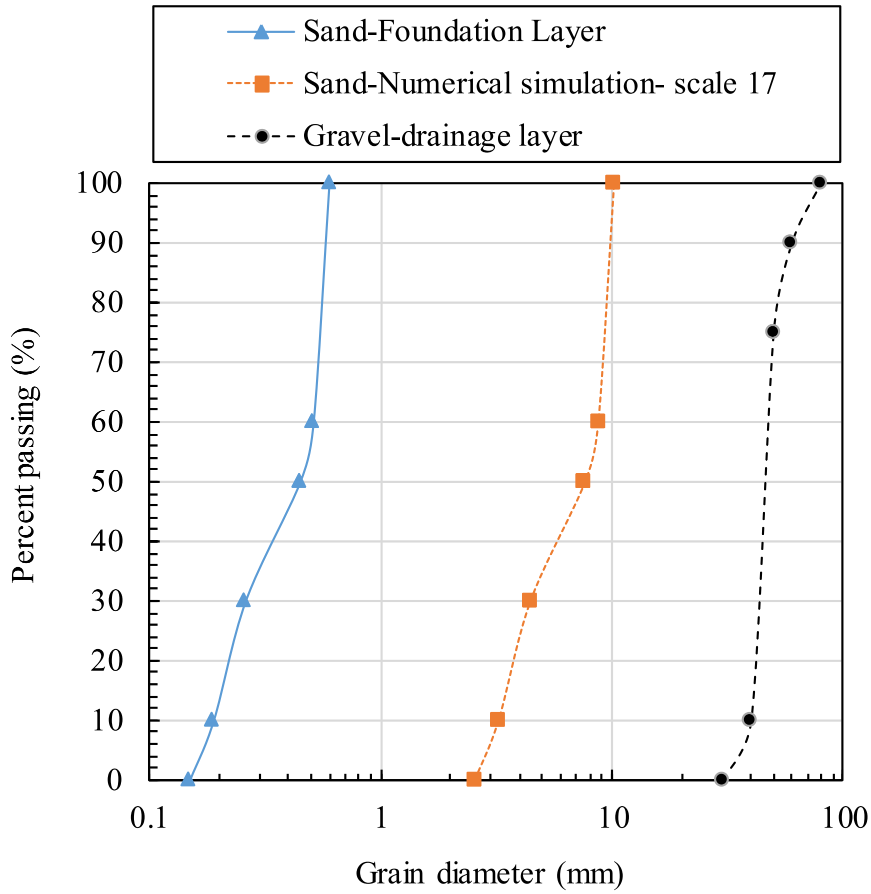

Figure 1 Particle size distribution of the drainage layer and sand subgrade in the experiment and numerical simulation

Table 1 Material properties of HDPE geomembrane

Properties	Value
Thickness (mm)	1.5
Density (g/cc)	0.94
Tensile strength at yield (kN/m)	31
Tensile elongation at yield (%)	18
2% secant modulus (MPa)	300

Model generation

The numerical model is created based on the experiments discussed in previous section. The foundation and drainage layers are modeled using spherical particles. To create these layers, two clouds of non-contacting particles are generated following the particle size distribution presented in Figure 1. Then, for subgrade soil, the radius expansion method is employed to reach the target porosity and density. Since it is numerically impossible to model the exact size of the sand particles, particle up-scaling is required. Considering the minimum *L/d* (Smallest length of the model / median diameter of the simulated particles) ratio of 20 based on the recommendations of Schopfer et al. (2007) and Ding et al. (2014), Scale factor of 17 is chosen for this layer and a total of over 120,000 particles are generated.

For the drainage layer, the generated particles are allowed to move under gravity without any compaction following the same procedure of the experiments. Using scale factor of 1, a total of 1,350 gravel particles are generated with a final thickness of 300 mm. 3D and 2D views of the generated sample are shown in Figure 2.

The GM is modeled using 8-noded hexahedral elements. A linear elastic material model is used following the properties listed in Table 1. The GM sheet is square shaped (590 x 590) with a thickness of 1.5 mm. A total of 900 finite elements and 7200 interface elements are used in this study. The artificial wrinkle is shaped in the model based on the height and width used in the experiments. The geometry of the wrinkled GM sheet is presented in Figure 3.

To determine the input parameters of the spherical particles in the DE simulation, model calibration is needed. This requires triaxial and direct shear test results of the drainage and subgrade layers. As these results are not available, reasonable material parameters are assumed based on previous studies conducted by McGill Geogroup (eg. Tran et al. 2013, Meidani et al. 2017). Table 2 shows the input parameters used in DE simulation. To evaluate the effect of different parameters on the response of the wrinkle, a series of twelve different numerical models are analyzed and the results as well as the input parameters are summarized in Table 3. Simulation 1 is the reference test (test 1) and the highlighted values represent the range of examined parameters.). Hence, tests 2 and 3 focus on the change in subgrade friction angle and tests 4 and 5 evaluate the effect of subgrade Young's modulus. The effect of drainage layer friction angle is investigated in tests 6 and 7; tests 8 and 9 consider a change in the Young's modulus of the drainage layer. Finally, tests 10, 11 and 12 are conducted to assess the effect of overburden pressure on the response of the wrinkle.

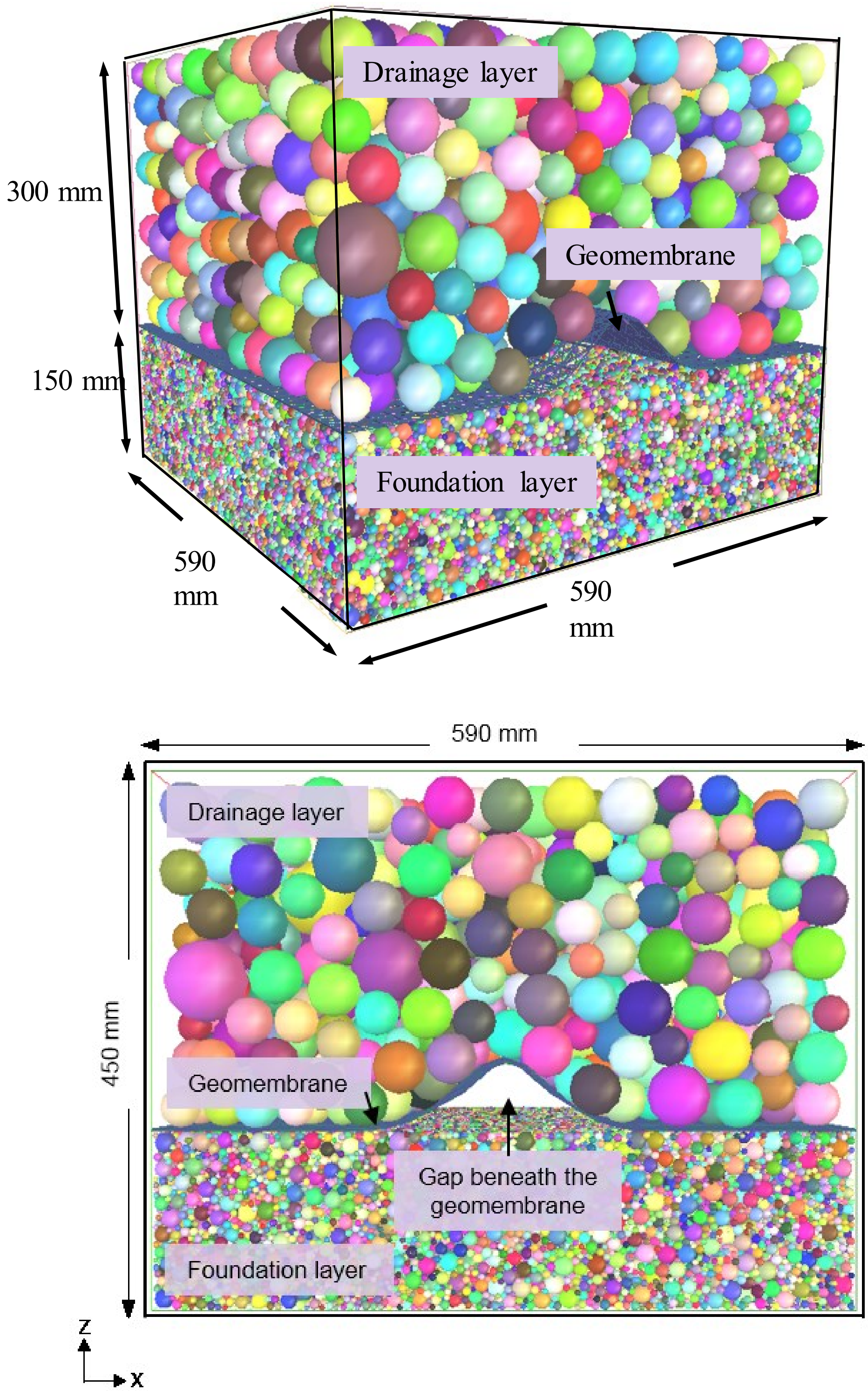

Figure 2 Initial coupled FE-DE specimen

Table 2 Input parameters of the simulation

Discrete particles	Value
Density of gravel particles (kg/m^3)	2750
Density of sand particles (kg/m^3)	2600
Gravel particle modulus E (MPa)	200
Sand particle modulus E (MPa)	150
Ratio K_T/K_N	0.3
Micro friction angle of gravel particles	36^o
Micro friction angle of sand particles	30^o
η_r	1.0
Rolling resistance coefficient (β_r)	0.3
Damping coefficient	0.2
Finite elements (GM)	**Value**
Young's modulus E (MPa)	300
Poisson's ratio v	0.3
Interface elements	**Value**
Material modulus E (MPa)	175
Ratio K_T/K_N	0.3
Micro friction angle ($\emptyset_{micro}$)	30^o

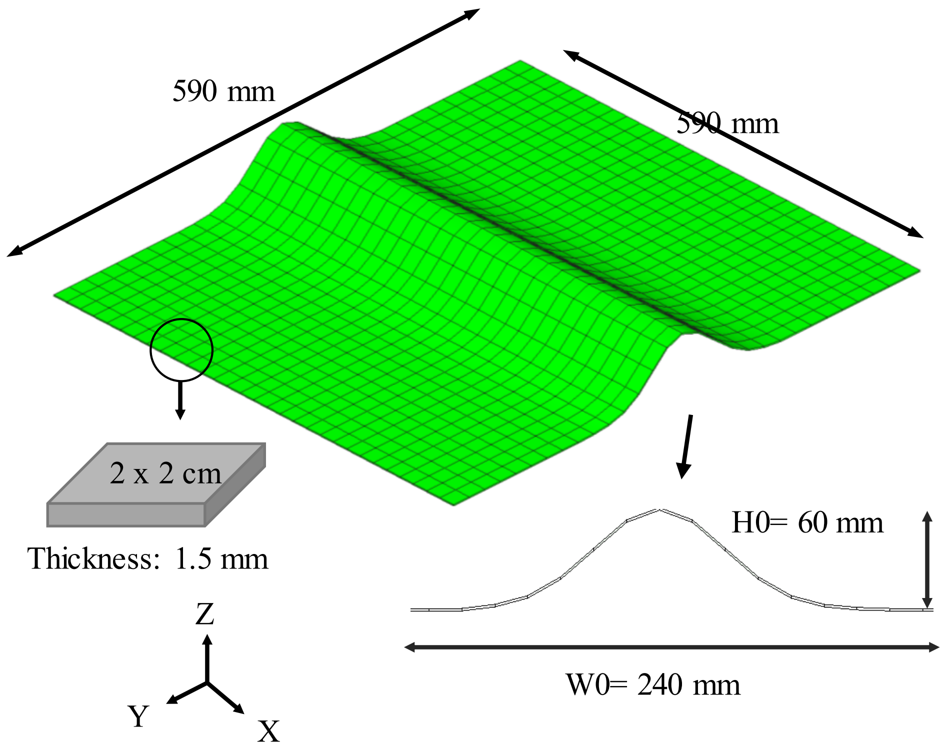

Figure 3 Geometry of the simulated geomembrane sheet

Results and discussion

The result of the reference test (Test 1) is presented first in this section. Figure 4 shows the initial and deformed shape of the GM in test 1 under vertical pressure of 250 kPa. It can be seen that both the wrinkle height and width decreased by 39% and 31% after applying the vertical pressure and the gap became smaller, however, it did not completely disappear. Fig. 5 shows the 2D view of the model used in Test 1 after applying the load. The reduction of the gap size is related to the vertical movement of the drainage layer and the GM sheet, however, due to the stiffness of the foundation layer, no significant upward vertical movement developed in sand. This finding is in agreement with that reported by Brachman and Gudina (2008) who concluded that the physical gap was reduced but remained when the GM was underlain by a firm sand foundation. A summary of the calculated test results with the percentage change in wrinkle height and width are presented in Table 4.

Table 3 Summary of tests configurations

Test	Test conditions				
	Foundation layer		Drainage layer		Pressure (kPa)
	E (Pa)	φ°	*E* (Pa)	φ°	
1	1.50E+08	30	2.00E+08	36	250
2	1.50E+08	25	2.00E+08	36	250
3	1.50E+08	20	2.00E+08	36	250
4	2.00E+08	30	2.00E+08	36	250
5	1.00E+08	30	2.00E+08	36	250
6	1.50E+08	30	2.00E+08	40	250
7	1.50E+08	30	2.00E+08	45	250
8	1.50E+08	30	2.50E+08	36	250
9	1.50E+08	30	1.50E+08	36	250
10	1.50E+08	30	2.00E+08	36	500
11	1.50E+08	30	2.00E+08	36	750
12	1.50E+08	30	2.00E+08	36	1050

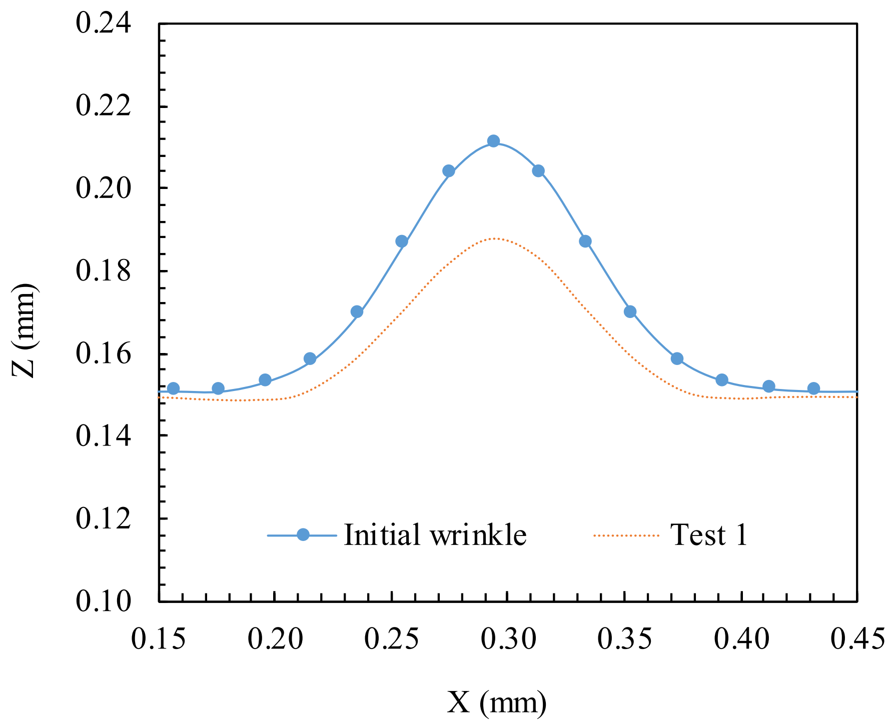

Figure 4 Initial and final shapes of the geomembrane wrinkle subjected to 250 KPa

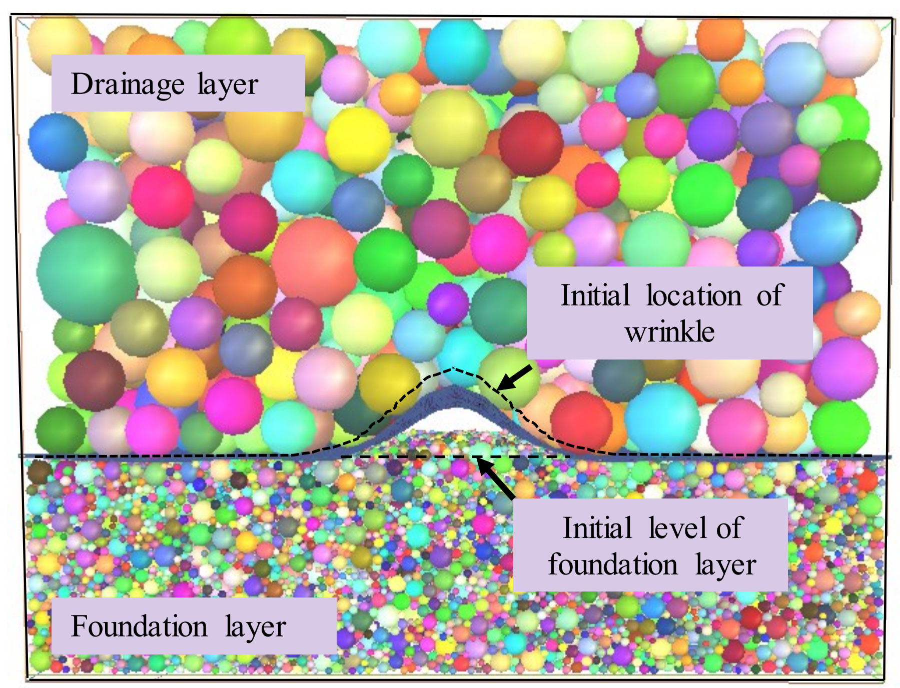

Figure 5 2D view of the model after applying the vertical load in Test 1, initial and final location of the GM wrinkle is illustrated.

Table 4 Summary of the tests results. Wrinkle initial height and width are $H_o = 60$ mm and $W_o = 240$ mm

Test	Final wrinkle geometry					
	H (mm)	ΔH (mm)	ΔH %	w (mm)	Δw (mm)	w %
1	36.7	23.3	39	166	74	31
2	32.3	27.7	46	156	84	35
3	28.1	31.9	53	145	95	40
4	39.6	20.4	34	169	71	30
5	32.5	27.5	46	161	79	33
6	38.2	21.8	36	168	72	30
7	39.2	20.8	35	173	67	28
8	40.7	19.3	32	180	60	25
9	31.0	29.0	48	149	91	38
10	31.9	28.1	47	153	87	36
11	28.8	31.2	52	146	94	39
12	26.2	33.8	56	140	100	42

Tests 2 and 3 are performed to study the effect of the friction angle of the sand layer on the wrinkle deformation. Fig. 6 shows that by decreasing the friction between sand particles, wrinkle deformation increased, and the gap gets smaller. It can be seen from Table 4 that by changing the friction angle from 30° in test 1 to 20° in test 3, the wrinkle height and width decreased by 8 and 21 mm. This response of the GM could be related to the relative movement of sand particles at lower friction angle under vertical load, which allows GM to deform easier.

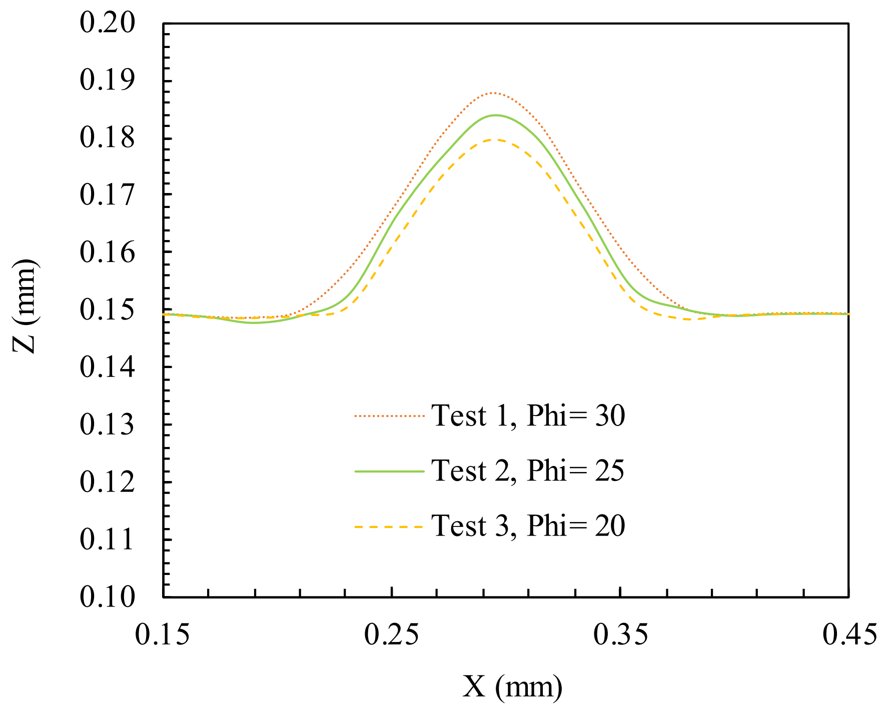

Figure 6 Dependency of wrinkle deformation to foundation layer friction angle

The effect of Young's modulus of the subgrade layer on the wrinkle deformation is evaluated in tests 4 and 5 and the results are presented in Figure 7. By decreasing Young's modulus of the sand layer, the wrinkle deformation increased. Based on the data presented in Table 4, the change in wrinkle height is more significant in comparison with wrinkle width. This response of the wrinkle can be attributed to the higher settlement of the softer foundation under vertical load.

Tests 6 and 7 are performed to evaluate the effect of the friction angle of the drainage layer on the wrinkle deformation. Results of these two simulations with respect to the reference test are presented in Figure 8. It is found that the friction angle of the gravel particles doesn't have a significant effect on the response of the GM and the gap size is similar in all three tests.

Two additional tests are developed to investigate the response of geomembrane wrinkle to the change in Young's modulus of the drainage layer. Figure 9 shows the results of tests 8 and 9 and the reference test. It is concluded that by decreasing the gravel particles Young's modulus, the wrinkle deformation increased and the gap size became smaller. Detailed results of these two tests are presented in Table 4. It can be seen that increasing the *E* value by 40%, the wrinkle height and width decreased 16% and 13%, respectively.

The response of the GM wrinkle to the vertical pressure are evaluated by performing three Tests (Tests 10, 11 and 12) and the results are plotted in Figure 10 and presented in Table 4. Data shows that the vertical pressure and wrinkle deformation are proportional and at higher applied load, a smaller gap is expected. It is interesting to note that even at applied pressure of up to 1,100 kPa the gap was reduced but still remained. This is consistent with the observations of Gudina and Brachman (2006). In addition, the vertical displacement of the geomembrane in test 12 is plotted in Figure 11. It can be seen that most of the vertical movement occurred at the crown of the wrinkle. Displacement in the flat areas of the GM sheet could be related to the indentation made by the course gravel backfill above the GM.

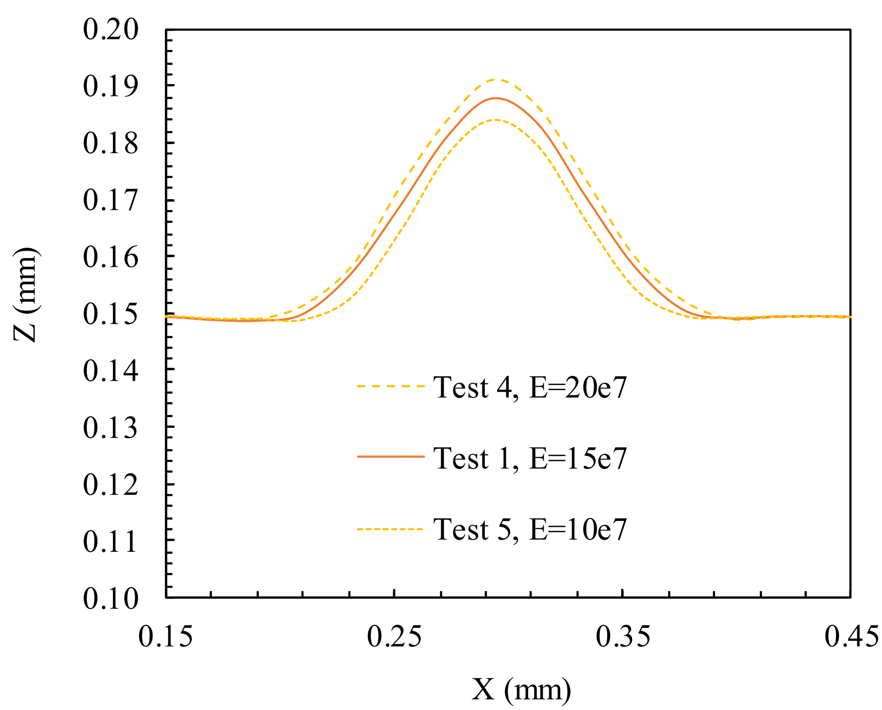

Figure 7 Dependency of wrinkle deformation to foundation layer Young's modulus

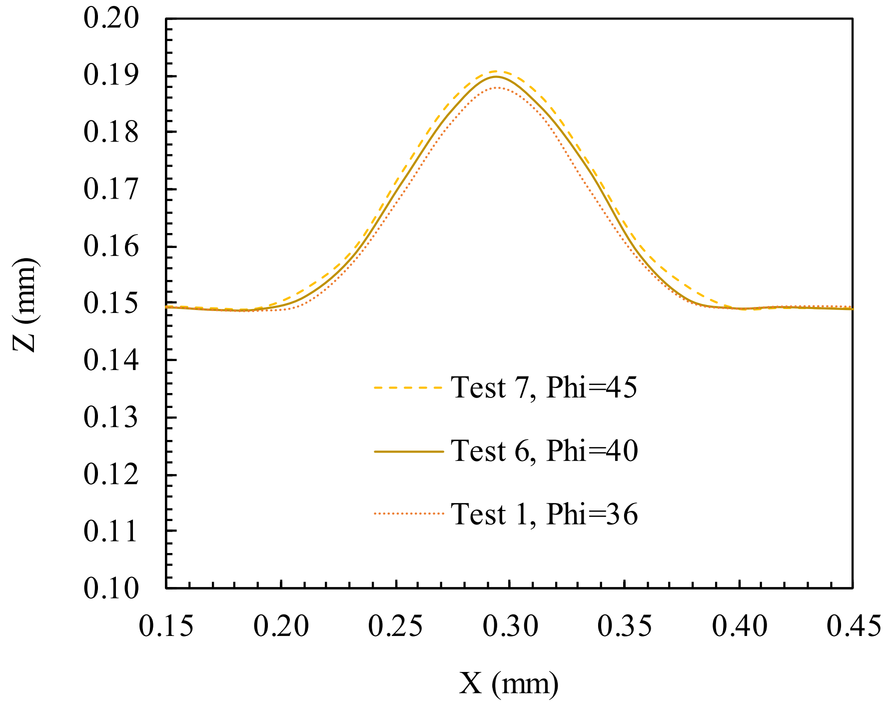

Figure 8 Dependency of wrinkle deformation to drainage layer friction angle

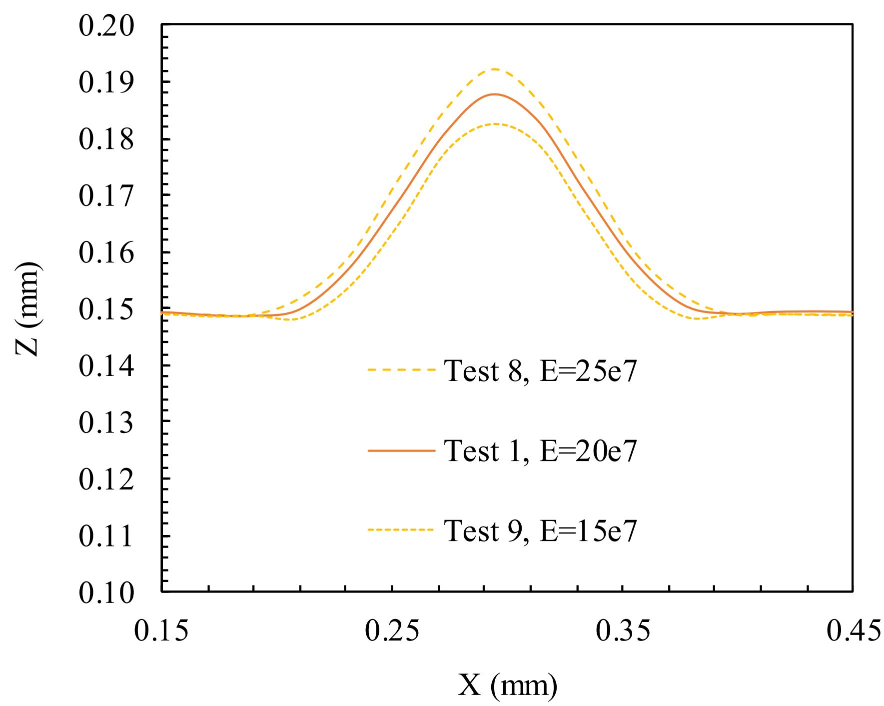

Figure 9 Dependency of wrinkle deformation to drainage layer Young's modulus

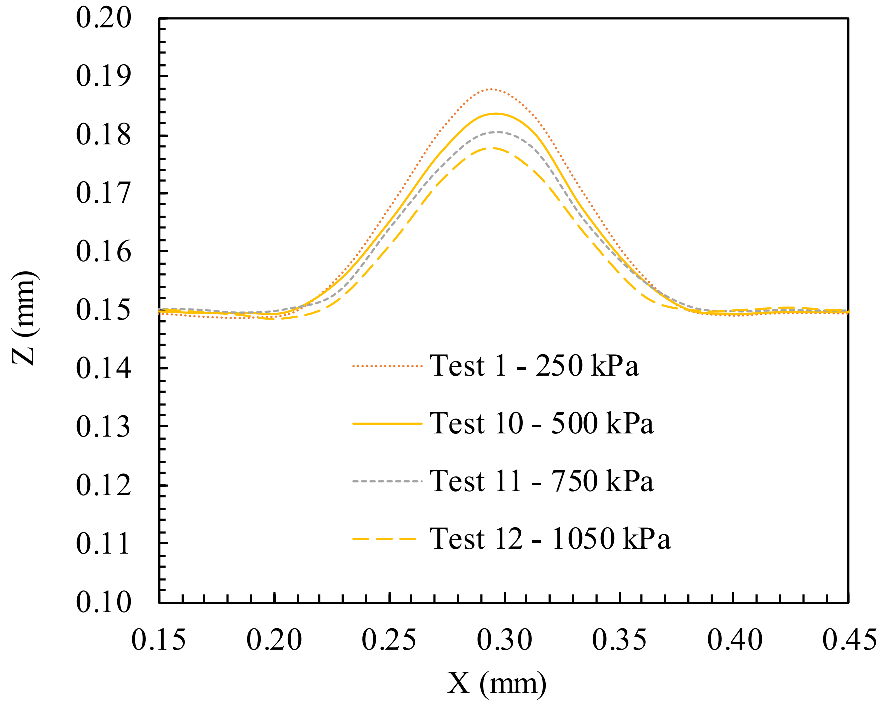

Figure 10 Dependency of wrinkle deformation to vertical pressure

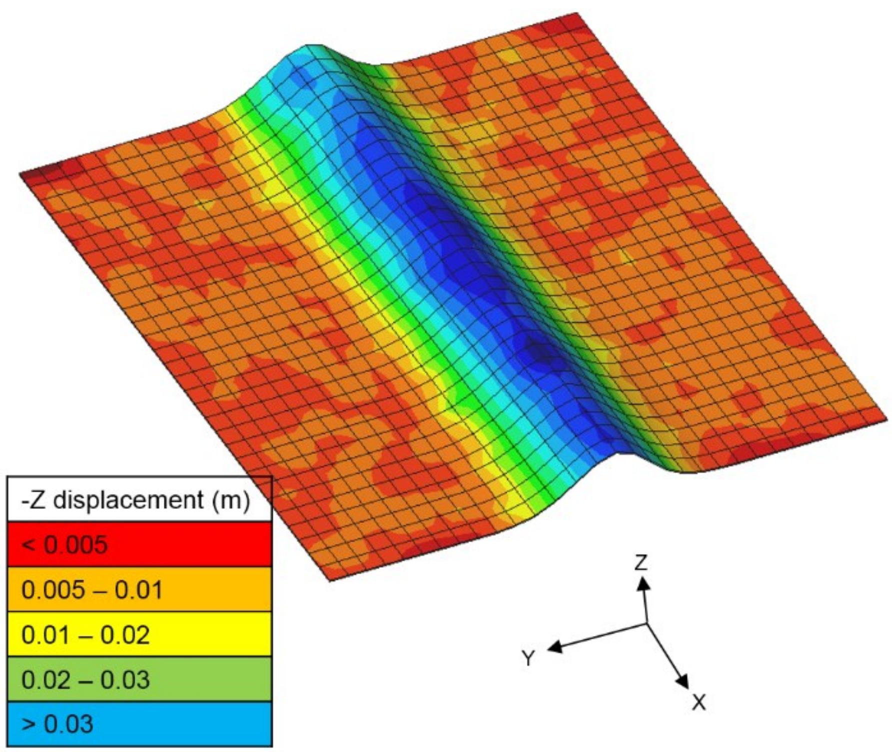

Figure 11 Geomembrane wrinkle vertical displacement at vertical pressure 1,100 kPa

Conclusion

This study has investigated the response of GM wrinkle using coupled finite-discrete element framework. The geomembrane is placed between compacted sand foundation and gravely drainage layer. Effect of different parameters such as sand and gravel friction angle and Young's modulus and the applied vertical pressure on the wrinkle deformation are investigated. The main conclusions are:

The wrinkle moved downwards and inwards (toward the center) in all tests under vertical pressure. Hence, the gap size gets smaller, but the gap remains under the geomembrane.

Increasing the sand layer friction angle and Young's modulus decreases the wrinkle deformation.

Changing the drainage layer friction angle doesn't have a significant effect on wrinkle shape but increasing the Young's modulus affects the height and width of the wrinkle with bigger gap remains beneath the geomembrane.

The wrinkle height and width decrease when subjected to vertical pressure. Increasing the pressure makes the gap between the GM and the foundation smaller but remained as the firm sand foundation layer doesn't fill in the gap.

It should be noted that the reported values for wrinkle height and width are based on numerical simulations using coupled model that has not been properly calibrated. However, the parametric study illustrated the pattern of the wrinkle deformation under different conditions. Finally, the finite-discrete element framework has proven to be efficient in capturing the response of the GM and the surrounding soils.

References

Brachman, R. W. I., & Gudina, S., 2008. Geomembrane strains from coarse gravel and wrinkles in a GM/GCL composite liner. Geotextiles and Geomembranes, 26, 6, 488-497.

Dang, H.K., Meguid, M.A., 2010. Algorithm to generate a discrete element specimen with predefined properties. International Journal of Geomechanics 10 (2), 85-91.

Dang, H.K., Meguid, M.A., 2013. An efficient finite-discrete element method for quasi-static nonlinear soil-structure interaction problems. International Journal for Numerical and Analytical Methods in Geomechanics 37 (2), 130-149.

Ding, X., Zhang, L., Zhu, H., & Zhang, Q., 2014. Effect of Model Scale and Particle Size Distribution on PFC3D Simulation Results. Rock Mechanics and Rock Engineering. 47, 2139-2156.

Gudina, S., & Brachman, R. W. I., 2006. Physical Response of Geomembrane Wrinkles Overlying Compacted Clay. Journal of Geotechnical and Geoenvironmental Engineering, 132, 10, 1346-1353.

Meidani, M., Meguid, M. A., & Chouinard, L. E., 2017. Evaluation of Soil‑Pipe Interaction under Relative Axial Ground Movement. Journal of Pipeline Systems Engineering and Practice, 4, 4017009.

Pelte, T., Pierson, P., and Gourc, J. P., 1994. Thermal analysis of geomembrane exposed to solar radiation. Geosynthet. Int., 1(1), 21–44.

Rowe, R. K., Quigley, R. M., Brachman, R. W. I., Booker, J. R., 2004. Barrier systems for waste disposal facilities, E&FN Spon, London.

Schöpfer, MPJ., Childs, C., Walsh, JJ., 2007. Two-dimensional distinct element modeling of the structure and growth of normal faults in multilayer sequences: 1. Model calibration, boundary conditions, and selected results. Journal of Geophysics Res 112(B10):B10401. doi:10.1029/2006jb004902.

Soong, T.-Y., and Koerner, R. M., 1998. Laboratory study of high density polyethylene waves. Proc., 6th Int. Conf. on Industrial Fabrics Association International, Geosynthetics, St. Paul, Minn., 301–306.

Tran, V. D. H., Meguid, M. A., and Chouinard, L. E., 2013. A finite-discrete element framework for the 3D modeling of geogrid-soil interaction under pullout loading conditions. Geotext. Geomembrane. 37(1-9).

THESIS NON-EXCLUSIVE LICENSE

AUTHOR'S NAME: ____________________ ____________________ ____________________
LAST NAME ***FIRST NAME*** ***INITIALS***

AUTHOR'S DATE OF BIRTH: ________ /______/_______
MONTH / DAY / YEAR

MCGILL EMAIL ADDRESS: ________________________ **STUDENT NUMBER:** ______________________

PERMANENT ADDRESS: ____
COUNTRY

MCGILL UNIT: ____________________________________

FACULTY: ______________________________

DEGREE SOUGHT: ____

TITLE OF THESIS: ____

____

I hereby promise that I am author of the thesis above cited.

I confirm that my thesis is my original work, does not infringe any rights of others, and that I have the right to make the grant conferred by this non-exclusive license. I also confirm that if third party copyrighted material was included in my thesis for which, under the terms of the Copyright Act, written permission from the copyright owners is required, I have obtained such permission from the copyright owners and may grant such permission for the full term of copyright protection.

I hereby grant to McGill University a non-exclusive, worldwide, irrevocable, royalty free license, in respect of my thesis, to reproduce, convert, publish, archive, preserve, conserve, communicate and distribute, and loan, in paper form, in microform, electronically by telecommunication or on the internet, and/or any other formats as may be adopted for such use from time to time. I also authorize McGill University to sub-license, sub-contract for any of the acts mentioned.

I hereby grant permission and authorize McGill University to permit access to my thesis and make it available to interested persons in paper or electronic form, through the library, interlibrary and public loan.

I understand that I retain copyright ownership and moral rights in my thesis, and that I may deal with the copyright in my thesis consistent with these rights. I promise to inform any person to whom I may hereafter assign or license my copyright in my thesis of the rights granted by me to **McGill University** and to **Library and Archives Canada.**

I confirm that I have executed a **Non-exclusive license with the Library and Archives Canada** and hereby grant permission to McGill University to submit the abstract and my thesis to the **Library and Archives Canada** in full compliance with these non-exclusive licenses.

The authorization contained in these non-exclusive licenses are to have effect on the date given below (**Effective Date**) unless a deferral of one year from the date has been expressly requested by me, the author, on submitting the thesis, and acknowledged by McGill University **GRADUATE AND POSTDOCTORAL STUDIES OFFICE.**

I agree to indemnify and hold McGill University harmless against any claim and any loss, damage, settlement cost or expense (including legal fees) incurred by McGill University and arising out of, or in connection with, my statements and representations or this license.

SIGNATURE OF AUTHOR: ____________________________________ **EFFECTIVE DATE:** ______________

Library and Archives Canada | Bibliothèque et Archives Canada

Canada

THESES NON-EXCLUSIVE LICENSE

Surname:	Given Names:
Full Name of University:	
Faculty, Department, School:	
Degree for which thesis was presented:	Date Degree Awarded:
Thesis Title:	
Supervisor:	
Date of Birth. It is **optional** to supply your date of birth. If you choose to do so please note that the information will be included in the bibliographic record for your thesis.	
E-mail: please provide your e-mail address if you are interested in receiving royalties on sales of your thesis.	
Permanent Address: please provide your permanent address if you are interested in receiving royalties on sales of your thesis.	

In consideration of Library and Archives Canada making my thesis available to interested persons, I,

____

hereby grant a non-exclusive, for the full term of copyright protection, license to Library and Archives Canada:

(a) to reproduce, publish, archive, preserve, conserve, communicate to the public by telecommunication or on the Internet, loan, distribute and sell my thesis (the title of which is set forth above) worldwide, for commercial or non-commercial purposes, in microform, paper, electronic and/or any other formats;

(b) to authorize, sub-license, sub-contract or procure any of the acts mentioned in paragraph (a).

I undertake to submit my thesis, through my university, to Library and Archives Canada. Any abstract submitted with the thesis will be considered to form part of the thesis.

I represent and promise that my thesis is my original work, does not infringe any rights of others, and that I have the right to make the grant conferred by this non-exclusive license.

If third party copyrighted material was included in my thesis for which, under the terms of the Copyright Act, written permission from the copyright owners is required I have obtained such permission from the copyright owners to do the acts mentioned in paragraph (a) above for the full term of copyright protection

I retain copyright ownership and moral rights in my thesis, and may deal with the copyright in my thesis, in any way consistent with rights granted by me to Library and Archives Canada in this non-exclusive license.

I further promise to inform any person to whom I may hereafter assign or license my copyright in my thesis of the rights granted by me to Library and Archives Canada in this non-exclusive license.

Signature	**Date**